

Fingerprints of Geometry and Topology on Low Dimensional Mesoscopic Systems

Dissertation zur Erlangung des
naturwissenschaftlichen Doktorgrades der
Bayerischen Julius-Maximilians-Universität Würzburg



Jan Carl Budich

Würzburg 2012

Eingereicht am:.....

bei der Fakultät für Physik und Astronomie

1. Gutachter:.....

2. Gutachter:.....

3. Gutachter:.....

der Dissertation

1. Prüfer:.....

2. Prüfer:.....

3. Prüfer:.....

4. Prüfer:.....

im Promotionskolloquium

Tag des Promotionskolloquiums:.....

Doktorurkunde ausgehändigt am:.....

Zusammenfassung

In dieser Doktorarbeit wird der Zusammenhang zwischen den mathematischen Bereichen der modernen Differentialgeometrie sowie der Topologie und den physikalischen Eigenschaften niedrigdimensionaler mesoskopischer Systeme erläutert. Insbesondere werden Phänomene des holographischen Quantentransportes in Quanten Spin Hall Systemen fernab des thermodynamischen Gleichgewichtes untersucht. Die Quanten Spin Hall Phase ist ein zweidimensionaler, zeitumkehrsymmetrischer elektrisch isolierender Zustand, dessen charakteristische Eigenschaft eindimensionale metallische Randzustände sind. Diese im Englischen als “helical edge states” bezeichneten Randkanäle zeichnen sich dadurch aus, dass Spin und Bewegungsrichtung der Ladungsträger fest miteinander verknüpft sind und zwei Zustände mit gleicher Energie aber unterschiedlicher Bewegungsrichtung stets durch die Symmetrieoperation der Zeitumkehr zusammenhängen. Diese Phänomenologie bedingt einen sogenannten topologischen Schutz durch Zeitumkehrsymmetrie gegen elastische Einteilchenrückstreuung. Wir beschäftigen uns mit den Grenzen dieses Schutzes, indem wir inelastische Rückstreuprozesse in Betracht ziehen, wie sie etwa durch das Wechselspiel von extrinsischer Spin-Bahn Kopplung und Gitterschwingungen induziert werden können, oder aber indem wir Mehrteilchen-Streuprozesse untersuchen, welche die Coulomb-Wechselwirkung ermöglicht. Desweiteren werden Anwendungen aus dem Gebiet der Spintronik vorgeschlagen, welche auf einer dem Quanten Spin Hall Effekt eigenen Dualität zwischen dem Spin und dem Ladungsfreiheitsgrad beruhen. Diese Dualität existiert in einem aus zwei Randzuständen mit entgegengesetzter Helizität zusammengesetzten System, wie etwa durch zwei gegenüberliegende Ränder einer streifenförmigen Probe im Quanten Spin Hall Zustand realisiert.

Konzeptionell gesehen ist der Quanten Spin Hall Zustand das erste experimentell nachgewiesene Beispiel eines symmetriegeschützten topologischen Zustandes nichtwechselwirkender Materie, also eines Bandisolators, welcher eine antiunitäre Symmetrie besitzt und sich von einem trivialen Isolator mit gleicher Symmetrie aber ausschliesslich lokalisierten und daher voneinander unabhängigen atomaren Orbitalen topologisch unterscheidet. Im ersten Teil dieser Dissertation geben wir eine Einführung in die theoretischen Konzepte, welche dem Forschungsgebiet der nichtwechselwirkenden topologischen Zustände zugrunde liegen. In diesem Zusammenhang werden die topologischen Invarianten, welche diese neuartigen Zustände charakterisieren, als globales Analogon zur lokalen geometrischen Phase dargestellt, welche mit einer zyklischen adiabatischen Entwicklung eines physikalischen Systems verknüpft ist. Während die ausführliche Diskussion der globalen Invarianten einem tieferen Verständnis des Quanten Spin Hall Effektes und damit verwandten physikalischen Phänomenen dienen soll, wird die nicht-Abelsche Variante der lokalen geometrischen Phase für einen Vorschlag zur Realisierung von holonomiebasierter Quanteninformationsverarbeitung genutzt. Das Quantenbit der von uns vorgeschlagenen Architektur ist ein in einem Quantenpunkt eingesperrter Spinfreiheitsgrad.

Summary

In this PhD thesis, the fingerprints of geometry and topology on low dimensional mesoscopic systems are investigated. In particular, holographic non-equilibrium transport properties of the quantum spin Hall phase, a two dimensional time reversal symmetric bulk insulating phase featuring one dimensional gapless helical edge modes are studied. In these metallic helical edge states, the spin and the direction of motion of the charge carriers are locked to each other and counter-propagating states at the same energy are conjugated by time reversal symmetry. This phenomenology entails a so called topological protection against elastic single particle backscattering by time reversal symmetry. We investigate the limitations of this topological protection by studying the influence of inelastic processes as induced by the interplay of phonons and extrinsic spin orbit interaction and by taking into account multi electron processes due to electron-electron interaction, respectively. Furthermore, we propose possible spintronics applications that rely on a spin charge duality that is uniquely associated with the quantum spin Hall phase. This duality is present in the composite system of two helical edge states with opposite helicity as realized on the two opposite edges of a quantum spin Hall sample with ribbon geometry.

More conceptually speaking, the quantum spin Hall phase is the first experimentally realized example of a symmetry protected topological state of matter, a non-interacting insulating band structure which preserves an anti-unitary symmetry and is topologically distinct from a trivial insulator in the same symmetry class with totally localized and hence independent atomic orbitals. In the first part of this thesis, the reader is provided with a fairly self-contained introduction into the theoretical concepts underlying the timely research field of topological states of matter. In this context, the topological invariants characterizing these novel states are viewed as global analogues of the geometric phase associated with a cyclic adiabatic evolution. Whereas the detailed discussion of the topological invariants is necessary to gain deeper insight into the nature of the quantum spin Hall effect and related physical phenomena, the non-Abelian version of the local geometric phase is employed in a proposal for holonomic quantum computing with spin qubits in quantum dots.

Contents

Introduction	1
I Theory of topological states of matter and their nonequilibrium transport properties	3
1 Adiabatic time evolution and geometric phases	7
1.1 Adiabatic time evolution in quantum mechanics	7
1.1.1 General outline	7
1.1.2 The adiabatic theorem	8
1.2 Geometric interpretation of adiabatic phases	12
1.2.1 Adiabatic time evolution and parallel transport	12
1.2.2 Gauge dependence and physical observability	16
2 Topological states of matter	17
2.1 From geometry to topology	17
2.1.1 Gauss-Bonnet theorem	18
2.1.2 From adiabatic pumping to Chern numbers	18
2.1.3 Bulk boundary correspondence	22
2.1.4 Symmetry protected topological states of matter	23
2.1.5 Local topological quantum phase transitions	24
2.2 Bulk classification of all possible non-interacting TSM	24
2.2.1 Cartan-Altland-Zirnbauer symmetry classes	25
2.2.2 Definition of the classification problem for continuum models and periodic systems	27
2.2.3 Topological classification of unitary vector bundles	29
2.2.4 K-Theory approach to a complete classification	30
2.3 Calculation of topological invariants of individual systems	35
2.3.1 Systems without anti-unitary symmetries	36
2.3.2 Dimensional reduction and real symmetry classes	38
2.3.3 Bulk invariants of disordered systems and twisted boundary conditions	40
2.3.4 Taking into account interactions	42
2.4 Examples of TSM	49
2.4.1 The QSH state	49
2.4.2 The Majorana wire	53
2.5 Limitations of the framework of TSM	59

3	Non-equilibrium quantum transport in interacting 1D systems	61
3.1	Electron-electron interaction in one spatial dimension	61
3.1.1	Spatial dimension and transmutation statistics	62
3.1.2	Bosonization and the Tomonaga Luttinger Liquid	62
3.2	Non-equilibrium perturbation theory	65
3.2.1	From equilibrium to non-equilibrium	66
3.2.2	Keldysh perturbation theory of the Tomonaga Luttinger Liquid	68
3.3	Peculiarities of the helical Tomonaga Luttinger Liquid	72
3.3.1	A composite spinful TLL consisting of two hTLLs	72
3.3.2	Peculiarities of a single hTLL	74
II	Application to low dimensional mesoscopic systems	77
4	All-electric qubit control via non-Abelian geometric phases	79
4.1	Motivation	79
4.2	Qubit control via quadrupole fields	82
4.3	Estimation of experimental parameters	85
4.3.1	Quadrupole induced HH/LH splitting in strained GaAs quantum dots	87
4.3.2	Stability of the quantum dot setup against perturbing potentials	90
4.4	Summary and outlook	92
5	Transport properties of helical edge states	95
5.1	Charge-spin duality in non-equilibrium transport of helical liquids	95
5.1.1	Motivation and outline	95
5.1.2	Model and spin-charge duality	96
5.1.3	Short junction case	99
5.1.4	Long junction case	102
5.1.5	Summary and outlook	104
5.2	Phonon-Induced Backscattering in Helical Edge States	105
5.2.1	Motivation	105
5.2.2	Topological protection against backscattering and its limitations	105
5.2.3	Model without Coulomb interaction	106
5.2.4	Inelastic backscattering	107
5.2.5	hTLL with Coulomb interaction	110
5.2.6	Summary and outlook	112
5.3	RG approach for the scattering off a single Rashba impurity in a helical liquid	113
5.3.1	Motivation	113
5.3.2	Model	115
5.3.3	RG for interacting fermions	115
5.3.4	Bosonization	117
5.3.5	Transport	118
5.3.6	Summary and outlook	120
6	Conclusion	121

Bibliography	125
Acknowledgments	139
List of publications	141
Curriculum Vitae	143
Erklärung	145

Introduction

Throughout the history of science, a main pursuit has been the understanding of nature via identifying its elementary building blocks and studying their interplay to explain the phenomenology of composite objects. Nowadays, this line of reasoning is at the heart of elementary particle physics. For a long time, this approach has been considered the only fundamental route towards a better understanding of the laws of the universe, rendering every less microscopic ansatz derivative.

A key incentive to change this way of thinking was provided by P.W. Anderson's seminal article "More Is Different" in 1972 [Anderson72]: At every level of complexity, there is emergent phenomenology due to the interplay of a large number of constituents which is not readily derived from the microscopic theory of these building blocks. In some sense, the more microscopic theory can hence be disconnected from the complex phenomenology of a composite system. In practice, this means that the crucial ingredients guiding the derivation of an effective theory for a complex system are often times symmetry arguments and physical input rather than an approximate solution of the microscopic laws governing the interaction of a few elementary constituents. The standard model of elementary particle physics for example predicts accurately the experimentally observed interaction of quarks and leptons through different types of gauge bosons at very high energies. Since all matter a condensed matter physicist will ever work with is made of these building blocks, one could naively expect any solid state system to be at least in principle readily derived from these "fundamental laws". However, in reality, even the mechanism which stably binds three quarks to a proton is not conclusively understood at the level of these microscopic interactions. From a more critical point of view, one could hence consider Quantum Electrodynamics (QED), the microscopic parent theory of condensed matter physics, already as an effective theory which has not been proven fully consistent with the standard model from first principles. Even then, the emergence of say a phonon, one of the key ingredients of many phenomena in solid state physics, could not be readily derived from the two particle Coulomb interaction. As a matter of fact, a phonon is the fingerprint of the spontaneous breaking of translation symmetry, a symmetry which is present in QED but is broken when a gas condenses into a crystalline structure at low temperatures. The acoustic phonons then play the role of Goldstone bosons, where each branch is associated with a generator of the broken continuous translation symmetry of the crystal that has only a discrete residual translation symmetry.

Another example of emergent behavior is the existence of quasi-particles which are the microscopic building blocks of an effective low energy theory, but behave fundamentally different from all elementary particles. In particular, all elementary particles are either fermions or bosons. In two dimensional condensed matter systems, quasi-particles which are neither fermions nor bosons, namely so called anyons [Leinaas77] can occur. Thus, there is

fundamentally more to condensed matter physics than solving the many body problem from first principles, because a complex system can be more than a collection of building blocks the interaction of which is governed by microscopic laws.

From the above motivation, it is evident that identifying possible states of matter which show interesting novel phenomenology is among the fundamental problems in condensed matter physics. Until the discovery of the quantum Hall effect of a two dimensional electron gas subjected to a strong perpendicular magnetic field in 1980 [Klitzing80], it had been believed that all states of matter can be classified in terms of their broken symmetries which give rise to characteristic local order parameters. However, this classification fails for the quantum Hall state which is classified by a global topological invariant [Thouless82, Niu85]. States with different values of this topological invariant concur in all conventional symmetries. Topologically distinct systems cannot be adiabatically, i.e., without closing the bulk energy gap, deformed into each other as long as their fundamental symmetries are preserved. This phenomenology is manifestly macroscopic which is also reflected in the fact that the topological classification becomes mathematically rigorous in the thermodynamic limit.

The main focus of this thesis is precisely on such topological phenomena which go beyond the mechanism of local order parameters associated with spontaneous symmetry breaking. Interestingly, these global topological features are not always immediately visible in the microscopic equations of motion. However, the bulk topology leads to unique finite size effects at the boundary of a finite sample which has been coined bulk boundary correspondence. This general mechanism gives rise to peculiar holographic transport properties of topologically non-trivial systems. Predicting and probing the rich phenomenology of these topological boundary effects in mesoscopic samples has become one of the most rapidly growing fields in condensed matter physics in recent years.

More specifically, we concentrate on topological effects which can be constructed at the level of non-interacting insulating band structures and mean field superconducting models. In Part I, we discuss the classification and phenomenology of such systems in great detail working out the close geometrical relation between adiabatic quantum dynamics and band structure topology. In this context, gapped single particle Hamiltonians are divided into ten symmetry classes reflecting their behavior under time reversal, particle hole conjugation, and the combination of these two operations. While the mentioned quantum Hall state has none of these symmetries, the first symmetry protected topologically nontrivial insulator is the quantum spin Hall state [Kane05a, Kane05b, Bernevig06a, König07] which relies on the presence of time reversal symmetry. The holographic transport properties of the quantum spin Hall state are the main subject of the more applied Part II of this thesis.

Part I

Theory of topological states of matter and their nonequilibrium transport properties

In this first part, we introduce the general concepts which are at the heart of the more applied discussion presented in Part II of this thesis. Owing to the enormous interest the rapidly growing field of topological states of matter (TSM) has attracted in recent years, the main focus of our discussion is to shed some light on the theoretical foundations of TSM. Starting from the adiabatic theorem of quantum mechanics [Born28, Kato50] which we present from a geometrical perspective in Chapter 1, the concept of TSM is introduced in Chapter 2 to distinguish gapped many body ground states of non-interacting systems and mean field superconductors, respectively, regarding their global geometrical features. These classifying features are topological invariants defined in terms of the adiabatic curvature of these bulk insulating systems. Having introduced the general notion of TSM we will focus on the quantum anomalous Hall (QAH) effect [Haldane88], the quantum spin Hall (QSH) effect [Kane05a, Kane05b, Bernevig06a, König07], and the one dimensional (1D) topological superconductor (TSC) [Kitaev01] as concrete examples of TSM which will be of particular relevance for the remainder of this thesis. Furthermore, we outline how interactions and disorder, which will be to some extent present in any realistic system, can be included into the theoretical framework of TSM by reformulating the relevant topological invariants in terms of the single particle Green's function and by introducing twisted boundary conditions, respectively. We integrate the field of TSM into a broader context by distinguishing TSM from the concept of topological order [Wen90] which has been introduced to study fractional quantum Hall (FQH) [Stormer83, Laughlin83, Zee95] systems. Most of our discussion reviews recent developments in the field of TSM. However, even this first part contains a substantial amount of original work which has been done in the context of this PhD project and will be cited during the discussion.

Finally, in Chapter 3, we introduce the essential elements of non-equilibrium quantum transport in interacting one dimensional systems which are excessively used in Part II. Many of those concepts are rather standard tools of condensed matter theory by now and are hence only briefly reviewed to establish our notation and to systematically refer the reader not acquainted with quantum transport theory of low dimensional systems to the relevant references. However, the application of these methods to holographic transport in TSM entails some intriguing peculiarities which are less known and are hence discussed in greater detail for the QSH state which will be the main focus of the more applied Part II.

Chapter 1

Adiabatic time evolution and geometric phases

We review the adiabatic theorem of quantum mechanics and discuss the geometric character of cyclic adiabatic evolutions. We demonstrate how the structure of a classical gauge theory emerges in this framework. Interestingly, the non-Abelian version of this gauge theory affords a global gauge invariant formulation [Kato50] which has interesting consequences as to the experimental observability of its predictions (see Section 1.2.2). Throughout this chapter, we refer the reader to the mathematical literature for a rigorous definition of technical terms from the mathematical fields of differential geometry and topology (see, e.g., Refs. [Choquet-Bruhat82, Kobayashi96, Nakahara03, Nash11] for excellent introductions) which will not be repeated explicitly here for the sake of readability.

1.1 Adiabatic time evolution in quantum mechanics

1.1.1 General outline

The Hamiltonian $\mathcal{H}(R)$ of a physical system often times depends on a set of control parameters, here denoted by $R \in \mathcal{R}$. For concreteness, the reader might think of external electric or magnetic fields which enter the Hamiltonian of a charged particle. In the following, we will implicitly assume \mathcal{R} to have the mathematical structure of a smooth manifold. If we consider a Hamiltonian $\mathcal{H}(R(t))$ which depends on time via the time dependence of its parameters $R(t)$, the time dependent Schrödinger equation reads

$$i \frac{d}{dt} |\Psi(t)\rangle = \mathcal{H}(R(t)) |\Psi(t)\rangle, \quad (1.1)$$

where we have set $\hbar = 1$. Eq. (1.1) is formally solved by $|\Psi(t)\rangle = \mathcal{U}(t, t_0) |\Psi(t_0)\rangle$ where the Dyson time evolution operator $\mathcal{U}(t, t_0)$ is defined as

$$\mathcal{U}(t, t_0) = \mathcal{T} e^{-i \int_{t_0}^t \mathcal{H}(R(\tau)) d\tau} \quad (1.2)$$

with the time ordering operator \mathcal{T} . Eq. (1.1) is in general very hard to solve for an arbitrary time dependence $R(t)$. In contrast, for a time independent Hamiltonian $\mathcal{H}(R)$, Eq. (1.2) boils down to $\mathcal{U}(t, t_0) = e^{-i(t-t_0)\mathcal{H}(R)}$ which is readily calculated once the spectral problem of $\mathcal{H}(R)$ is solved.

The notion of adiabatic time evolution is an intermediate case where the time dependence of \mathcal{H} is sufficiently slow so that the system state $|\Psi(t)\rangle$ stays in the eigenspace of the same instantaneous eigenvalue of the Hamiltonian and its dynamics is determined solely by the geometrical relation between neighboring instantaneous eigenspaces. In the remainder of this section, we will explain what sufficiently slow means and what the adiabatic dynamics in terms of this purely geometric connection looks like. We will use the shorthand notation $\mathcal{H}(t) = \mathcal{H}(R(t))$ unless in cases where suppressing the parameter coordinates R might cause confusion.

1.1.2 The adiabatic theorem

The gist of the adiabatic assumption can be understood at a very intuitive level: Once prepared in an instantaneous eigenstate with an eigenvalue which is separated from the neighboring states by a finite energy gap Δ , the system can only leave this state via a transition which costs a finite excitation energy Δ . A simple way to estimate whether such a transition is possible is to look at the Fourier transform $\tilde{\mathcal{H}}(\omega)$ of the time dependent Hamiltonian $\mathcal{H}(t)$. If the time dependence of \mathcal{H} is made sufficiently slow, $\tilde{\mathcal{H}}(\omega)$ will only have finite matrix elements for $\omega \ll \Delta$. In this regime the system will stick to the same instantaneous eigenstate. This behavior is known as the adiabatic assumption.

Proof due to Born and Fock

The latter rather intuitive argument is at the heart of the adiabatic theorem of quantum mechanics which has been first proven by Born and Fock in 1928 [Born28] for non-degenerate systems. Let $\{|n(t)\rangle\}_n$ be an orthonormal set of instantaneous eigenstates of $\mathcal{H}(t)$ with eigenvalues $\{E_n(t)\}_n$. The exact solution of Eq. (1.1) can be generally expressed as

$$|\Psi(t)\rangle = \sum_n c_n(t) |n(t)\rangle e^{-i\phi_D^n(t)}, \quad (1.3)$$

where the dynamical phase $\phi_D^n(t) = \int_{t_0}^t E_n(\tau) d\tau$ has been separated from the coefficients $c_n(t)$ for later convenience. Plugging Eq. (1.3) into Eq. (1.1) yields

$$\dot{c}_n = -c_n \langle n | \frac{d}{dt} | n \rangle - \sum_{m \neq n} c_m \frac{\langle n | \left(\frac{d}{dt} \mathcal{H} \right) | m \rangle}{E_m - E_n} e^{i(\phi_D^n(t) - \phi_D^m(t))}. \quad (1.4)$$

The salient consequence of the adiabatic theorem is that the last term in Eq. (1.4) can be neglected in the adiabatic limit since its denominator $|E_n - E_m| \geq \Delta$ is finite whereas the matrix elements of $\frac{d}{dt} \mathcal{H}$ become arbitrarily small. More precisely, if we represent the physical time as $t = Ts$, where s is of order 1 for a change in the Hamiltonian of order Δ and T is the large adiabatic timescale, then $\frac{d}{dt} = \frac{1}{T} \frac{d}{ds}$. Now, $\frac{d}{ds} \mathcal{H}(t(s))$ is by construction of order Δ . The entire last term in Eq. (1.4) is thus of order $\frac{1}{T}$. Under these conditions¹, Born and Fock [Born28] showed that the contribution of this second term vanishes in the adiabatic limit

¹As a minor technical point, we note that the proof by Born and Fock [Born28] also takes into account level crossings at isolated points. These slightly more general conditions are not of relevance for our purposes as we will only discuss fully gapped systems. More recent work by Avron and coworkers [Avron99] reported

$T \rightarrow \infty$. Note that this is not a trivial result since the differential equation (1.4) is supposed to be integrated from $t = 0$ to $t \sim T$, so that one could naively expect a contribution of order 1 from a coefficient that scales like $1/T$. The coefficient of c_n in the first term on the right hand side of Eq. (1.4) is purely imaginary since $0 = \frac{d}{dt} \langle n|n \rangle = \left(\frac{d}{dt} \langle n| \right) |n \rangle + \langle n| \frac{d}{dt} |n \rangle$ and hence doesn't change the modulus of c_n when the differential equation $\dot{c}_n = -c_n \langle n| \frac{d}{dt} |n \rangle$ is solved as

$$c_n(t) = c_n(t_0) e^{-\int_{t_0}^t \langle n| \frac{d}{d\tau} |n \rangle d\tau} \quad (1.5)$$

Born and Fock [Born28] argue that $\langle n| \frac{d}{dt} |n \rangle = 0 \forall t$ amounts to a choice of phase for the eigenstates and therefore neglect also the first term on the right hand side of Eq. (1.4).

This thesis is mainly concerned with physical phenomena associated with corrections to this in general unjustified assumption.

Notion of the geometric phase

By the latter assumption, Ref. [Born28] overlooks the potentially nontrivial adiabatic evolution, known as Berry's phase [Berry84], associated with a cyclic time dependence of \mathcal{H} . After a period $[0, T]$ of such a cyclic evolution, Eq. (1.5) yields

$$c_n(T) = c_n(0) e^{-\oint_0^T \langle n| \frac{d}{d\tau} |n \rangle d\tau} \quad (1.6)$$

To understand why the phase factor $e^{-\oint_0^T \langle n| \frac{d}{d\tau} |n \rangle d\tau}$ can in general not be gauged away, we remember that the Hamiltonian depends on time via the time dependence $R(t)$ of some external control parameters. Hence, $\langle n| \frac{d}{dt} |n \rangle = \langle n| \partial_\mu |n \rangle \dot{R}^\mu$, where $\partial_\mu = \frac{\partial}{\partial R^\mu}$. To reveal the mathematical structure of the latter expression, we define

$$\mathcal{A}^B \left(\frac{d}{dt} \right) = \mathcal{A}_\mu^B \dot{R}^\mu = -i \langle n| \partial_\mu |n \rangle \dot{R}^\mu, \quad (1.7)$$

where $\mathcal{A}^B = A_\mu^B dR^\mu$ is called Berry's connection. \mathcal{A}^B clearly has the structure of a gauge field: Under the local gauge transformation $|n \rangle \rightarrow e^{i\xi} |n \rangle$ with a smooth function $R \mapsto \xi(R)$, Berry's connection transforms like

$$\mathcal{A}^B \rightarrow \mathcal{A}^B + d\xi.$$

Furthermore, the cyclic evolution defines a loop $\gamma : t \mapsto R(t)$, $t \in [0, T]$, $R(0) = R(T)$ in the parameter manifold \mathcal{R} . γ can be expressed as the boundary of some piece of surface $\mathcal{S} \subset \mathcal{R}$. Using the theorem of Stokes, we can now calculate

$$-i \oint_0^T \langle n| \frac{d}{d\tau} |n \rangle d\tau = \int_\gamma \mathcal{A}^B = \int_{\mathcal{S}} d\mathcal{A}^B = \int_{\mathcal{S}} \mathcal{F}^B, \quad (1.8)$$

a proof of the adiabatic theorem which, under certain conditions on the level spectrum, works without any gap condition.

where in the last step Berry's curvature $\mathcal{F}^B = \mathcal{F}_{\mu\nu}^B dR^\mu \wedge dR^\nu$ is defined as

$$\mathcal{F}_{\mu\nu}^B = -i(\langle \partial_\mu n | \partial_\nu n \rangle - \langle \partial_\nu n | \partial_\mu n \rangle) = 2\text{Im} \{ \langle \partial_\mu n | \partial_\nu n \rangle \}$$

with the shorthand notation $|\partial_\mu n\rangle = \partial_\mu |n\rangle$. Note that \mathcal{F}^B is a gauge invariant quantity that is analogous to the field strength tensor in electrodynamics. Defining the Berry phase associated with the loop γ as $\varphi_\gamma^B = \int_\gamma \mathcal{A}^B = \int_S \mathcal{F}^B$ we can rewrite Eq. (1.6) as

$$c_n(T) = c_n(0)e^{-i\varphi_\gamma^B}. \quad (1.9)$$

The manifestly gauge invariant Berry phase φ_γ^B can have observable consequences due to interference effects between coherent superpositions that undergo different adiabatic evolutions. The analogue of this phenomenology due to an ordinary electromagnetic vector potential is known as the Aharonov-Bohm effect [Aharonov61]. The geometrical reason why Berry's connection \mathcal{A}^B cannot be gauged away all the way along a cyclic adiabatic evolution is the same as why a vector potential cannot be gauged away along a closed path that encloses magnetic flux, namely the notion of holonomy on a curved manifold. We will come back to the concept of holonomy shortly from a more mathematical point of view. For now we only comment that the Berry phase φ_γ^B is a purely geometrical quantity which only depends on the inner-geometrical relation of the family of states $|n(R)\rangle$ along the loop γ and reflects an abstract notion of curvature in Hilbert space which has been defined as Berry's curvature \mathcal{F}^B .

Proof due to Kato

For a degenerate eigenvalue, Berry's phase is promoted to a unitary matrix acting on the corresponding degenerate eigenspace [Wilczek84]. The first proof of the adiabatic theorem of quantum mechanics that overcomes both the limitation to non-degenerate Hamiltonians and the assumption of an explicit phase gauge for the instantaneous eigenstates was reported in the seminal work by Tosio Kato [Kato50] in 1950. We will review Kato's results briefly for the reader's convenience and use his ideas to illustrate the geometrical origin of the adiabatic phase. The explicit proofs are presented at a very elementary and self contained level in Ref. [Kato50]. Our notation follows Ref. [Avron89] which is convenient to relate the physical quantities to elementary concepts of differential geometry.

Let us assume without loss of generality that the system is at time $t_0 = 0$ in its instantaneous ground state $|\Psi_0(0)\rangle$ or, more generally, since the ground state might be degenerate, in a state $|\Psi\rangle$ satisfying

$$P(0)|\Psi\rangle = |\Psi\rangle, \quad (1.10)$$

where $P(t)$ is the projector onto the eigenspace associated with the instantaneous ground state energy $E_0(t)$ which is defined as

$$P(t) = \frac{1}{2\pi i} \oint_c \frac{dz}{z - \mathcal{H}(t)},$$

where the complex contour c encloses $E_0(t)$ which is again assumed to be separated from the spectrum of excitations by a finite energy gap $\Delta > 0$. To understand the adiabatic evolution, we are not interested in the dynamical phase $\phi_D(t) = \int_0^t E_0(\tau) d\tau$. We thus define a new time evolution operator $\tilde{\mathcal{U}}(t, 0) = e^{i\phi_D(t)} \mathcal{U}(t, 0)$. Clearly, \mathcal{U} represents the exact time evolution operator of a system which has the same eigenstates as the original system but has been subjected to a time dependent energy shift that transforms $E_0(t) \rightarrow \tilde{E}_0(t) = 0 \forall t$. Kato proved the adiabatic theorem in a very constructive way by writing down explicitly the generator \mathcal{A} of the adiabatic evolution:

$$\mathcal{A} \left(\frac{d}{dt} \right) = - [\dot{P}, P]. \quad (1.11)$$

In the adiabatic limit, $\tilde{\mathcal{U}}(t, 0)P(0)$ was shown [Kato50] to converge against the adiabatic Kato propagator \mathcal{K} , i.e.,

$$\tilde{\mathcal{U}}(t, 0)P(0) \xrightarrow{\text{adiabatic limit}} \mathcal{K}(t, 0) = \mathcal{T} e^{-\int_0^t \mathcal{A}(\frac{d}{d\tau}) d\tau}. \quad (1.12)$$

The adiabatic assumption is now a direct corollary from Eq. (1.12) and can be elegantly expressed as [Avron89]

$$P(t)\mathcal{K}(t, 0) = \mathcal{K}(t, 0)P(0), \quad (1.13)$$

implying that a system, which is prepared in an instantaneous ground state at $t_0 = 0$, will be propagated to a state in the subspace of instantaneous ground states at t by virtue of Kato's propagator \mathcal{K} . Note that \mathcal{K} is a completely gauge invariant quantity, i.e., independent of the choice of basis in the possibly degenerate subspace of ground states. The Kato propagator $\mathcal{K}(T, 0)$ associated with a cyclic evolution in parameter space thus yields the Berry phase [Berry84] and its non-Abelian generalization [Wilczek84], respectively. We will call this general adiabatic phase the geometric phase (GP) in the following. The GP \mathcal{K}_γ representing the adiabatic evolution along a loop γ in parameter space can be expressed in a manifestly gauge invariant way as

$$\mathcal{K}_\gamma = \mathcal{T} e^{-\int_\gamma \mathcal{A}}. \quad (1.14)$$

Kato's propagator is the solution of an adiabatic analogue of the Schrödinger equation (1.1), an adiabatic equation of motion that can be written as

$$\left(\frac{d}{dt} + \mathcal{A} \left(\frac{d}{dt} \right) \right) |\Psi(t)\rangle = 0, \quad (1.15)$$

for states satisfying $P(t)|\Psi(t)\rangle = |\Psi(t)\rangle$, i.e., states in the subspace of instantaneous groundstates. Before closing the section, we give a general and at least numerically always viable recipe to calculate the Kato propagator $\mathcal{K}(t, 0)$. We first discretize the time interval $[0, t]$ into n steps by defining $t_i = i\frac{t}{n}$. The discrete version of Eq. (1.15) for the Kato

propagator reads (see Eq. (1.11))

$$\mathcal{K}(t_i, 0) - \mathcal{K}(t_{i-1}, 0) = \{(P(t_i) - P(t_{i-1})) P(t_{i-1}) - P(t_i) (P(t_i) - P(t_{i-1}))\} \mathcal{K}(t_{i-1}, 0). \quad (1.16)$$

Using $P(t_{i-1})\mathcal{K}(t_{i-1}, 0) = \mathcal{K}(t_{i-1}, 0)$ and $P^2 = P$, Eq. (1.16) can be simplified to

$$\mathcal{K}(t_i, 0) = P(t_i)\mathcal{K}(t_{i-1}, 0),$$

which is readily solved by $K(t_i, 0) = \prod_{j=0}^i P(t_j)$. Taking the continuum limit yields [Simon83, Wilczek84, Avron89]

$$\mathcal{K}(t, 0) = \lim_{n \rightarrow \infty} \prod_{i=0}^n P(t_i), \quad (1.17)$$

which is a valuable formula for the practical calculation of the Kato propagator.

1.2 Geometric interpretation of adiabatic phases

In this section, we analyze the GP from a viewpoint of differential geometry. In particular, we view the adiabatic time evolution as an abstract notion of parallel transport in Hilbert space and reveal the GP associated with a cyclic evolution as the phenomenon of holonomy due to the presence of curvature in the vector bundle of ground state subspaces over the manifold \mathcal{R} of control parameters. Interestingly, Kato's approach to the problem provides a gauge invariant, i.e., a global definition of the geometrical entities connection and curvature, whereas standard gauge theories are defined in terms of a complete set of local gauge fields along with their transition functions defined in the overlap of their domains. This difference has an interesting physical ramification: Quantities that are gauge dependent in an ordinary gauge theory like quantum chromodynamics (QCD) are physical observables in the theory of adiabatic time evolution. To name a concrete example, only gauge invariant quantities like the trace of the holonomy, also known as the Wilson loop, are observable in QCD whereas the holonomy itself, in other words the GP defined in Eq.(1.14), is a physical observable in Kato's theory. This subtle difference has been overlooked in standard literature on this subject [Zee88, Bohm03] which we interpreted as an incentive to clarify this point below in greater detail.

1.2.1 Adiabatic time evolution and parallel transport

To get accustomed to parallel transport, we first explain the general concept with the help of a very elementary example, namely a smooth piece of two dimensional surface embedded in \mathbb{R}^3 (see Ref. [Kuehnel05] for rigorous definitions). If the surface is flat, there is a trivial notion of parallel transport of tangent vectors, namely shifting the same vector in the embedding space from one point to another. However, on a curved surface, this program is ill-defined, since a tangent vector at one point might be the normal vector at another point of the surface. Put shortly, a tangent vector can only be transported as parallel

as the curvature of the surface admits. On a curved surface, parallel transport along a curve is thus defined as a vanishing in-plane component of the directional derivative, i.e., a vanishing covariant derivative of a vector field along a curve. The normal component of the directional derivative reflects the rotation of the entire tangent plane in the embedding space and is not an inner-geometric quantity of the surface as a two dimensional manifold.

The analogue of the curved surface in the context of adiabatic time evolution is the manifold of control parameters \mathcal{R} , parameterizing for example external magnetic and electric fields. The analogue of the tangent plane at each point of the surface is the subspace of degenerate ground states of the Hamiltonian $\mathcal{H}(R)$ at each point R in parameter space. An adiabatic time dependence of \mathcal{H} amounts to traversing a curve $t \mapsto R(t)$ in \mathcal{R} at adiabatically slow velocity. A cyclic evolution is uniquely associated with a loop γ in \mathcal{R} . We will now explicitly show that the adiabatic equation of motion (1.15) defines a notion of parallel transport in the fiber bundle of ground state subspaces over \mathcal{R} in a completely analogous way as the ordinary covariant derivative ∇ on a smooth surface defines parallel transport in the tangent bundle of the smooth surface. We first note that $\frac{d}{dt} = \dot{R}^\mu \partial_\mu$ is referring to a particular direction \dot{R}^μ in parameter space, which depends on the choice of the adiabatic time dependence of \mathcal{H} . We can get rid of this dependence by rephrasing Eq. (1.15) as

$$(d + \mathcal{A})|\Psi\rangle = 0, \quad (1.18)$$

where $\mathcal{A} = -[(dP), P]$ and here as in the following $P|\Psi\rangle = |\Psi\rangle$ and the R -dependence has been dropped for notational convenience. The adiabatic derivative $D = d + \mathcal{A}$ takes a tangent vector, e.g., $\frac{d}{dt}$, as an argument to boil down to the directional adiabatic derivative $\frac{d}{dt} + \mathcal{A}\left(\frac{d}{dt}\right)$ appearing in Eq. (1.15). For the following analysis the identities $P^2 = P$ and $P|\Psi\rangle = |\Psi\rangle$ are of key importance. It is now elementary algebra to show

$$P(dP)P = 0. \quad (1.19)$$

Eq. (1.19) has a simple analogue in elementary geometry: Consider the family of normal vectors $\{n(t)\}_t$ where t parameterizes a curve on a smooth surface. Then, since $1 = \langle n|n\rangle$, we get $0 = \frac{d}{dt}\langle n|n\rangle = 2\langle n|\dot{n}\rangle$, i.e., the change of a unit vector is perpendicular to the unit vector itself. Using Eq. (1.19), we immediately derive $P\mathcal{A}|\Psi\rangle = 0$ and with that

$$D|\Psi\rangle = 0 \Leftrightarrow Pd|\Psi\rangle = 0. \quad (1.20)$$

This makes the analogy of our adiabatic derivative $D = d + \mathcal{A}$ to the ordinary notion of parallel transport manifest: $|\Psi\rangle$ is parallel-transported if the in-plane component of its derivative vanishes.

Curvature and holonomy

Let us again start with a very simple example of a curved manifold, a two dimensional sphere S^2 , which has constant Gaussian curvature. Parallel-transporting a tangent vector around a geodesic triangle, say the boundary of an octant of the sphere gives a defect angle which is proportional to the area of the triangle or, more precisely, the integral of the Gaussian

curvature over the enclosed area. This defect angle is called the holonomy of the traversed closed path. This elementary example suggests that the presence of curvature is in some sense probed by the concept of holonomy. This intuition is absolutely right. As a matter of fact, the generalized curvature at a given point x of the base manifold of a fiber bundle is defined as the holonomy associated with an infinitesimal loop at x . More concretely, the curvature Ω is usually defined as $\Omega_{\mu\nu} = [\nabla_\mu, \nabla_\nu]$ which represents an infinitesimal parallel transport around a parallelogram in the $\mu\nu$ -plane.

In total analogy, we define

$$\mathcal{F}_{\mu\nu}|\Psi\rangle = [D_\mu, D_\nu]|\Psi\rangle = P[P_\mu, P_\nu]P|\Psi\rangle, \quad (1.21)$$

with the shorthand notation $P_\mu = \partial_\mu P$. Restricting the domain of \mathcal{F} to states which are in the projection P , we can rewrite Eq. (1.21) as the operator identity

$$\mathcal{F} = \mathcal{F}_{\mu\nu}dR^\mu \wedge dR^\nu = P[(dP), (dP)]P, \quad (1.22)$$

where the product of the two differential forms dP in the commutator is to be understood as the usual exterior \wedge -product.

In the general case of a non-Abelian adiabatic connection, i.e., if the dimension of P is larger than 1, we cannot simply use Stokes theorem to reduce the evaluation of Eq. (1.14) to a surface integral of \mathcal{F} over the surface bounded by γ , as has been done in the case of the Abelian Berry curvature in Eq. (1.8). However, the global one to one correspondence between curvature and holonomy still exists and is the subject of the Ambrose-Singer theorem [Nakahara03].

Relation between Kato's and Berry's language

In order to make contact to the more standard language of gauge theory, we will now express Kato's manifestly gauge invariant formulation [Kato50] in local coordinates thereby recovering Berry's connection \mathcal{A}^B [Berry84, Simon83] and its non-Abelian generalization [Wilczek84], respectively. For this purpose, let us fix a concrete basis $\{|\alpha(R)\rangle\}_\alpha$, $R \in O \subset \mathcal{R}$ in an open subset O of the parameter manifold. We assume the loop γ to lie inside of O . Otherwise we would have to switch the gauge while traversing the loop. We will drop the R -dependence of $|\alpha\rangle$ right away for notational convenience. The projector P can then be represented as $P = \sum_\alpha |\alpha\rangle\langle\alpha|$. Let us start the cyclic evolution without loss of generality with $|\Psi(0)\rangle = |\alpha(0)\rangle$. From Eq. (1.13) we know that the solution $|\Psi(t)\rangle = \mathcal{K}(t, 0)|\alpha(0)\rangle$ of Eq. (1.15) satisfies $P(t)|\Psi(t)\rangle = |\Psi(t)\rangle$ at every point in time during the cyclic evolution. Hence, we can represent $|\Psi(t)\rangle$ in our gauge as

$$|\Psi\rangle = \sum_\beta \langle\beta|\Psi\rangle|\beta\rangle = U_{\beta\alpha}^B|\beta\rangle, \quad (1.23)$$

where the t -dependence has been dropped for brevity. From Eq. (1.20), we know that $P \frac{d}{dt} |\Psi\rangle = 0$ which implies $\langle \gamma | \frac{d}{dt} |\Psi\rangle = 0$. Plugging this into Eq. (1.23) yields

$$\frac{d}{dt} U_{\gamma\alpha}^B = - \sum_{\beta} \langle \gamma | \frac{d}{dt} |\beta\rangle U_{\beta\alpha}^B. \quad (1.24)$$

Redefining \mathcal{A}^B for the non-Abelian case as a matrix valued gauge field through $\mathcal{A}_{\alpha\beta}^B = -i \langle \alpha | \partial_{\mu} | \beta \rangle dR^{\mu}$, Eq. (1.24) is readily solved as

$$U^B(t) = \mathcal{T} e^{-i \int_0^t \mathcal{A}^B(\frac{d}{d\tau}) d\tau}.$$

The representation matrix of the GP associated with the loop γ then reads

$$U_{\gamma}^B = \mathcal{T} e^{-i \int_{\gamma} \mathcal{A}^B}. \quad (1.25)$$

By construction, U_{γ}^B is the representation matrix of the GP \mathcal{K}_{γ} , i.e.,

$$\left(U_{\gamma}^B \right)_{\alpha,\beta} = \langle \alpha(0) | \mathcal{K}_{\gamma} | \beta(0) \rangle,$$

or, more general, for any point in time along the path

$$\left(U^B(t) \right)_{\alpha,\beta} = \langle \alpha(t) | \mathcal{K}(t, 0) | \beta(0) \rangle. \quad (1.26)$$

Eq. (1.26) makes the relation between Kato's formulation of adiabatic time evolution and the non-Abelian Berry phase manifest. In contrast to the gauge independence of Kato's global connection \mathcal{A} , \mathcal{A}^B behaves like a local connection (see Ref. [Choquet-Bruhat82] for rigorous mathematical definitions) and depends on the gauge, i.e., on our choice of the family $\{ |\alpha(R)\rangle \}_{\alpha}$ of basis states. Under a smooth family of basis transformations $\{ U(R) \}_R$ acting on the local coordinates \mathcal{A}^B transforms like [Choquet-Bruhat82, Nakahara03]

$$\mathcal{A}^B \rightarrow \tilde{\mathcal{A}}^B = U^{-1} \mathcal{A}^B U + U^{-1} dU \quad (1.27)$$

resulting in the following gauge dependence of Eq. (1.25),

$$U_{\gamma}^B \rightarrow \tilde{U}_{\gamma}^B = U^{-1} U_{\gamma}^B U, \quad (1.28)$$

which only depends on the basis choice $U = U(R(0))$ at the starting point of the loop γ .

Inserting our representation $P = \sum_{\alpha} |\alpha\rangle \langle \alpha|$ into the gauge independent form of the curvature, Eq.(1.22), we readily derive

$$\mathcal{F}_{\mu\nu,\alpha\beta}^B = \langle \alpha | [P_{\mu}, P_{\nu}] | \beta \rangle = (d\mathcal{A}^B)_{\mu\nu,\alpha\beta} + (\mathcal{A}^B \wedge \mathcal{A}^B)_{\mu\nu,\alpha\beta},$$

which defines \mathcal{F}^B as the usual curvature of a non-Abelian gauge field [Nakahara03], i.e.,

$$\mathcal{F}^B = d\mathcal{A}^B + \mathcal{A}^B \wedge \mathcal{A}^B, \quad (1.29)$$

which transforms under a local gauge transformation U like

$$\mathcal{F}^B \rightarrow U^{-1}\mathcal{F}^B U.$$

1.2.2 Gauge dependence and physical observability

The gauge dependence of the non-Abelian Berry phase U_γ^B (see Eq. (1.28)) has led several prominent authors [Zee88, Bohm03] to the conclusion that only gauge independent features like the trace and the determinant of U_γ^B can have physical meaning. However, working with Kato's manifestly gauge invariant formulation, it is understood that the entire GP \mathcal{K}_γ is experimentally observable. In the remainder of this section we will try to shed some light on this ostensible controversy.

In gauge theory, it goes without saying that explicitly gauge dependent phenomena are not immediately physically observable and that only the gauge invariant information resulting from a calculation performed in a special gauge can be of physical significance. At a formal level this is a direct consequence of the fact that the Lagrangian of a gauge theory is constructed in a manifestly gauge invariant way by tracing over the gauge space indices. The physical reason for this is quite simple: A concrete gauge amounts to a local choice of the coordinate system in the gauge space. Under a local change of basis, a non-abelian gauge field A transforms like (see also Eq. (1.27))

$$A \rightarrow \tilde{A} = U^{-1}AU + U^{-1}dU$$

where $U(x)$ is a smooth family of basis transformations, with x labeling points in the base space of the theory, e.g., in Minkowski space. Now, since the gauge space is an internal degree of freedom, the basis vectors in this space are not associated with physical observables. This situation is fundamentally changed in Kato's adiabatic analogue of a gauge theory. Here, the non-Abelian structure is associated with a degeneracy of the Hamiltonian, e.g., Kramers degeneracy in the presence of time reversal symmetry (TRS). For a system in which spin is a good quantum number, Kramers degeneracy is just spin degeneracy, which makes the spin the analogue of the gauge degree of freedom in an ordinary gauge theory. However, the magnetic moment associated with a spin is a physical observable which can be measured. The basis vectors, e.g., $|\uparrow\rangle, |\downarrow\rangle$ have an objective meaning for the experimentalist (a magnetic moment that points from the lab-floor to the sky which we call z - direction). For concreteness, let us assume that we have calculated a GP $\mathcal{K}_\gamma = |\uparrow\rangle\langle\downarrow| + |\downarrow\rangle\langle\uparrow|$. The representation matrix of \mathcal{K}_γ in this basis of S_z eigenstates is clearly the Pauli matrix σ_x . Choosing a different gauge, i.e., a different basis for the gauge degree of freedom at the starting point of the cyclic adiabatic evolution, we of course would have obtained a different representation matrix U_γ^B for \mathcal{K}_γ , e.g., σ_z , had we chosen the basis as eigenstates of S_x (see Eq. (1.28)). However, the fact that \mathcal{K}_γ rotates a spin which is initially pointing to the lab-ceiling upside down is gauge independent physical reality.

Chapter 2

Topological states of matter

In this chapter, we discuss how insulating ground states can be distinguished by their topological features that are formulated in terms of their adiabatic curvature \mathcal{F} . These topological features are bulk quantities of the gapped ground state of an infinite system. Interestingly, the so called bulk boundary correspondence [Halperin82, Volovik03] generically leads to experimentally observable boundary effects which are uniquely associated with the respective bulk topological properties. Very generally speaking, the understanding of TSM can be divided into two subproblems. First, finding the group that represents the topological invariant for a class of systems characterized by their fundamental symmetries and spatial dimension. Second, assigning the value of the topological invariant to a representative of such a symmetry class, i.e., measuring to which topological equivalence class a given system belongs. We will address the first problem in Section 2.2 and the second problem in Section 2.3. Furthermore, we discuss generalizations for the practical calculation of the topological invariants for interacting and disordered systems. In Section 2.1, we give an accessible introduction to the phenomenology of TSM establishing the relation between TSM and adiabatic pumping processes. The purpose of our analysis is not to give a broad overview over all possible TSM which has been presented from different perspectives in several research papers [Qi08a, Schnyder08, Kitaev09, Ryu10] and review articles [Hasan10, Qi11]. We rather motivate the general concept of topologically classifying band insulators and elaborate on a few examples in greater detail. Finally, we point out the limitations of our construction by distinguishing the field of TSM from the phenomenon of topological order [Wen90].

2.1 From geometry to topology

In Section 1.2, we worked out the relation between the GP and the notion of curvature as a local geometric quantity. The topological invariants introduced in this section are in some sense global GPs. They measure global properties which cannot be altered by virtue of local continuous changes of the physical system. Continuous is at this stage of the analysis synonymous with adiabatic, i.e., happening at energies below the bulk gap. Later on, we will additionally require local continuous changes to respect the fundamental symmetries of the physical system, e.g., particle hole symmetry (PHS) or time reversal symmetry (TRS). We will illustrate some fundamental working principles in the field of TSM with the help of a minimal toy model for the QAH state.

2.1.1 Gauss-Bonnet theorem

Let us illustrate the correspondence between local curvature and global topology of a manifold with the help of the simplest possible example. We consider a two dimensional sphere S^2 with radius r . This manifold has a constant Gaussian curvature of $\kappa = \frac{1}{r^2}$. The integral of κ over the entire sphere obviously gives 4π , independent of r . The Gauss-Bonnet theorem in its classical form (see, e.g., Ref. [Kuehnel05]) relates precisely this integral of the Gaussian curvature of a closed smooth two dimensional manifold \mathcal{M} to its Euler characteristic χ in the following way:

$$\frac{1}{2\pi} \int_{\mathcal{M}} \kappa = \chi(\mathcal{M}) \quad (2.1)$$

Note that χ is a purely algebraic quantity which is defined as the number of vertices minus the number of edges plus the number of faces of a triangulation [Nash11] of \mathcal{M} . χ is by construction of simplicial homology [Nash11] a topological invariant which can only be changed by poking holes into \mathcal{M} and gluing the resulting boundaries together so as to create closed manifolds with different genus. Hence, Eq. (2.1) nicely demonstrates how the integral of the local inner-geometric quantity κ over the entire manifold yields a topological invariant, i.e., a global feature of \mathcal{M} . Concretely, for our example S^2 , a triangulation is provided by continuously deforming the sphere into a tetrahedron. Simple counting of vertices, edges, and faces yields $\chi(S^2) = 4 - 6 + 4 = 2$, in agreement with Eq. (2.1). More generally speaking, $e = \frac{\kappa}{2\pi}$ is our first encounter with a characteristic class [Milnor74], the so called Euler class of \mathcal{M} , which upon integration over \mathcal{M} yields the topological invariant χ . Similar mathematical structures will be ubiquitous when it comes to the classification of TSM.

2.1.2 From adiabatic pumping to Chern numbers

We now establish explicitly the relation between adiabatic evolution and TSM by viewing the integer quantum Hall state [Klitzing80, Laughlin81, Thouless82], the archetype of a TSM as an adiabatic charge pumping process. For pedagogical reasons we discuss the translation-invariant realization of this phase [Haldane88], the QAH state. Our analysis mainly follows Refs. [Zak89, Fu06]. For concreteness, we choose the two band square lattice realization of the QAH effect proposed in Ref. [Qi08a]. The Bloch Hamiltonian of this system with lattice constant $a = 1$ reads

$$\begin{aligned} h(k) &= v^i(k)\sigma_i, \\ v^1 &= \sin k^x, \quad v^2 = \sin k^y, \quad v^3 = m + 4 - 2 \cos k^x - 2 \cos k^y, \end{aligned} \quad (2.2)$$

where σ_i are Pauli matrices in some band pseudo spin space. We will come back to this innocent looking but phenomenologically extremely rich model from various viewpoints in other parts of this thesis. Let us for now consider a tube of unit circumference and infinite length (say in x -direction) of this insulator as a 1D system with one filled and one empty band. For $m = -1$, this insulator is gapped in its entire Brillouin Zone (BZ). k^y now plays the role of a free parameter of our 1D system which we will intermediately call t for reasons that will become obvious shortly. The charge polarization of the Wannier-function $|0\rangle$ localized at

$x = 0$ can be expressed as

$$P(t) = \langle 0(t) | \hat{x} | 0(t) \rangle = \frac{i}{2\pi} \int_0^{2\pi} dk^x \langle u_{k^x}(t) | \partial_x | u_{k^x}(t) \rangle,$$

where $|u_{k^x}(t)\rangle$ are the instantaneous Bloch states of the 1D insulator and $\partial_x = \frac{\partial}{\partial k^x}$. By formal analogy to Eq. (1.7), we define $\mathcal{A}_t^B(\partial_x) = -i \langle u_{k^x}(t) | \partial_x | u_{k^x}(t) \rangle$, which yields

$$P(t) = \frac{-1}{2\pi} \int_0^{2\pi} dk^x \mathcal{A}_t^B(\partial_x), \quad (2.3)$$

Next, we thread a flux through our cylindric 1D system in axial direction. Such a flux ϕ can be generated by applying a vector potential of strength ϕ in the circumferential, i.e., in the y -direction. Physically, this vector potential just shifts k^y by ϕ . Hence, adiabatically threading one quantum of flux 2π through the cylinder amounts to varying t from 0 to 2π in Eq. (2.3). This defines a cyclic adiabatic evolution of the 1D system. We would like to ask by what amount the polarization P changes upon varying t from t_0 to t_1 . The instantaneous BZ of the 1D system has the topology of a circle S^1 . The 1D BZ at t_0 minus the k^x -circle at t_1 can be viewed as the boundary of the cylinder $T_{01} = S^1 \times [t_0, t_1]$. Using the theorem of Stokes we can thus write

$$\int_0^{2\pi} dk^x \mathcal{A}_{t_1}^B(\partial_x) - \int_0^{2\pi} dk^x \mathcal{A}_{t_0}^B(\partial_x) = \int_{T_{01}} \mathcal{F}_{tk^x}^B,$$

where the Berry curvature $\mathcal{F}_{tk^x}^B = 2\text{Im} \{ \langle \partial_t u_{k^x}(t) | \partial_x u_{k^x}(t) \rangle \}$ has been defined. Choosing $t_0 = 0$, $t_1 = 2\pi$, T_{01} becomes the torus T^2 and the change ΔP of the charge polarization during this adiabatic cycle can be expressed as

$$\Delta P = -\frac{1}{2\pi} \int_{T^2} \mathcal{F}^B. \quad (2.4)$$

The formal similarity between Eq. (2.1) and Eq. (2.4) is striking. As a matter of fact, $-\frac{\mathcal{F}^B}{2\pi}$ is again a characteristic class, the so called first Chern character ch_1 [Nakahara03] of the $U(1)$ -bundle of occupied Bloch functions over the 2D (k^x, k^y) -BZ. From a viewpoint of algebraic topology, the integral of ch_1 over the BZ T^2 gives an integer valued topological invariant of the bundle, the so called first Chern number \mathcal{C}_1 . The physical interpretation of the quantized adiabatic observable ΔP as Hall conductivity σ_{xy} in units of the quantum of conductance $G_0 = \frac{e^2}{h} = \frac{1}{2\pi}$ has been first given by Laughlin [Laughlin81] using a similar adiabatic pumping argument as the one just presented. Shortly after Laughlin's explanation, $\frac{\sigma_{xy}}{G_0}$ as resulting from a linear response calculation for a non-interacting insulator was analytically shown to concur with the mentioned Chern number \mathcal{C}_1 [Thouless82, Avron83, Kohmoto85].

Several comments are in order. We have demonstrated that the Hall conductivity of an insulator can be viewed as a quantized global GP of its Bloch Hamiltonian, where the parameter manifold \mathcal{R} introduced in Section 1.1 is represented by the BZ of the 2D system. In Section 1.1.2, we argued that the local GP associated with a loop γ is analogous to a magnetic flux threading the parameter region that is bounded by γ where the role of the

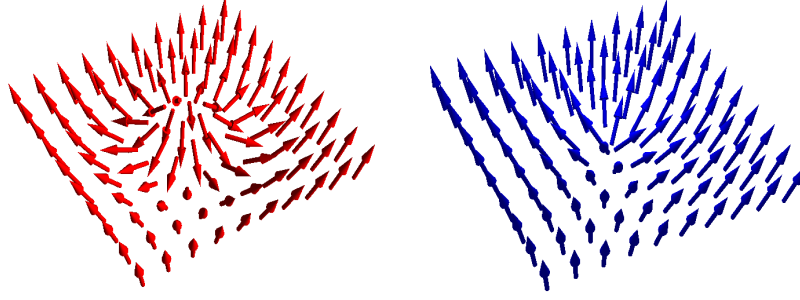


Figure 2.1: Configuration $\hat{v}_c(k)$ for $m = -1$ (red) and $m = 0.2$ (blue).

electromagnetic field-strength tensor is played by Berry's curvature. Along similar lines, the first Chern number \mathcal{C}_1 measures the monopole charge of the k -space Berry curvature appearing in Eq. (2.4) in the entire BZ. The interchangeability of the time variable of an adiabatic evolution and the wave vector has been shown by applying an electric field through adiabatic flux-threading in a cylinder-geometry. Distinguishing periodic 2D insulators without any symmetry except charge conservation by their first Chern number \mathcal{C}_1 is the first example of a topological classification, the QAH state characterized by non-vanishing \mathcal{C}_1 is our first example of a TSM. The topological invariance of \mathcal{C}_1 entails that its value cannot be changed upon variation of the model parameters without closing the bulk gap of the band insulator. However, so far, the advertised robustness of this quantized conductivity against small *physical* perturbations such as impurities has not been established since we explicitly assumed translation invariance and a quadratic Hamiltonian. The classification scheme just presented thus fails to account for interactions and disorder. Hence, \mathcal{C}_1 globally distinguishes insulating band structures of periodic systems but does not at all explain the robustness of topological features of a given band structure against the tiniest of physically relevant perturbations. Interestingly, this additional robustness generically does exist: Physical properties which stem from topological band structure features of the clean system are adiabatically protected by the bulk gap and the fundamental symmetries of the disordered interacting system (see Section 2.2). However, there are certain exceptions to this statement, so called weak TSM, which only exist in the presence of translation-invariance.

Geometric illustration of the topological defect

Following Ref. [Bernevig06a], we illustrate the topologically nontrivial structure of the QAH toy model (2.2). For simplicity, we only consider the corresponding continuum Hamiltonian characterized by $v^i \rightarrow v_c^i$, with $v_c^1 = k^x$, $v_c^2 = k^y$, $v_c^3 = m + k^2$. The configurations of the unit vector $\hat{v}_c(k)$ are shown in Fig. 2.1 for a trivial configuration at $m = 0.2$ and a nontrivial configuration at $m = -1$, respectively. For large values of k , \hat{v}_c always points up. Hence, a one point compactification of the k -space to a sphere S^2 can be performed by identifying $k \rightarrow \infty$ with the north pole of the sphere. It is now clear that the trivial configuration can be combed smooth into a constant configuration $\hat{v}_c(k) = \hat{e}_z$, whereas the nontrivial configuration looks like a hedgehog on alert which cannot be continuously unwound.

Explicit calculation of the topological invariant

Let us explicitly calculate \mathcal{C}_1 starting from the definition of the adiabatic curvature \mathcal{F} in Eq. (1.22). Our toy model (2.2) is non-degenerate and we have $P(k) = |u_-(k)\rangle\langle u_-(k)|$, with the Bloch state $|u_-(k)\rangle$ of the occupied band associated with the lower eigenvalue $\epsilon_-(k) = -|v(k)|$. The matrix structure of the Abelian \mathcal{F} is trivial and can be neglected by identifying \mathcal{F} with its matrix element $\langle u_- | \mathcal{F} | u_- \rangle$. Hence,

$$\mathcal{F}_{\mu\nu} = \langle u_- | [(\partial_\mu P), (\partial_\nu P)] | u_- \rangle = 2i \text{Im} \{ \langle \partial_\mu u_- | \partial_\nu u_- \rangle \}.$$

Using $[\partial_\mu, h(k)] = (\partial_\mu h(k))$ implying $\langle u_\alpha | [\partial_\mu, h] | u_\beta \rangle = (\epsilon_\beta - \epsilon_\alpha) \langle u_\alpha | \partial_\mu u_\beta \rangle = \langle u_\alpha | (\partial_\mu h) | u_\beta \rangle$, we explicitly represent \mathcal{F} as

$$\mathcal{F}_{\mu\nu} = \frac{\langle u_- | (\partial_\mu h) | u_+ \rangle \langle u_+ | (\partial_\nu h) | u_- \rangle - \langle u_- | (\partial_\nu h) | u_+ \rangle \langle u_+ | (\partial_\mu h) | u_- \rangle}{(\epsilon_+ - \epsilon_-)^2}. \quad (2.5)$$

Due to its usefulness for practical calculations we would like to note that the Abelian adiabatic curvature of an insulating model with an arbitrary number of occupied states $|u_\alpha\rangle$ and empty states $|u_\beta\rangle$ reads

$$\mathcal{F}_{\mu\nu} = \sum_{\alpha \text{ occ}, \beta \text{ em}} \frac{\langle u_\alpha | (\partial_\mu h) | u_\beta \rangle \langle u_\beta | (\partial_\nu h) | u_\alpha \rangle - \langle u_\alpha | (\partial_\nu h) | u_\beta \rangle \langle u_\beta | (\partial_\mu h) | u_\alpha \rangle}{(\epsilon_\beta - \epsilon_\alpha)^2}. \quad (2.6)$$

Plugging the general form $h = v^i \sigma_i = |v| \hat{v}^i \sigma_i$ into Eq. (2.5), a straight forward calculation yields

$$\mathcal{F}_{\mu\nu} = \frac{-i}{2} \hat{v} (\hat{v}_\mu \times \hat{v}_\nu) = \frac{-i}{2} \epsilon^{ijk} \hat{v}^i \hat{v}_\mu^j \hat{v}_\nu^k,$$

where $\hat{v}_\mu = \partial_\mu \hat{v}$. The first Chern number \mathcal{C}_1 can now be expressed as

$$\mathcal{C}_1 = \int_{T^2} \frac{i\mathcal{F}}{2\pi} = \frac{\epsilon^{ijk}}{4\pi} \int_{\text{BZ}} d^2k \hat{v}^i \hat{v}_x^j \hat{v}_y^k. \quad (2.7)$$

The integer quantization of Eq. (2.7) can be understood at a very intuitive geometric level. $k \mapsto \hat{v}(k)$ defines a map from the torus T^2 representing the BZ to the unit sphere S^2 [Qi06]. $\hat{v} (\hat{v}_\mu \times \hat{v}_\nu)$ is the oriented Jacobian of this map. Hence, \mathcal{C}_1 measures the surface swept out by \hat{v} on the sphere in units of 4π , i.e., in units of the entire surface of the sphere. To understand the integer quantization, we need to understand why non-integer fractions of surface cannot contribute. To this end, let us vary the map \hat{v} by an infinitesimal k -dependent rotation,

$$\hat{v} \rightarrow \left(1 + \delta^i(k) R_i\right) \hat{v}, \quad (2.8)$$

where $(R_i)_{jk} = \epsilon_{ijk}$ are the generators of $\text{SO}(3)$ rotations. It is straight forward to show [Altland10] that \mathcal{C}_1 is invariant under such an infinitesimal deformation. From the elementary theory of Lie groups it is clear that this manifests the topological invariance of \mathcal{C}_1 as any finite continuous deformation is generated by a transformation of the form (2.8). Geometrically, the integer quantization can be illustrated as follows: An incomplete cover of the unit

sphere looks like a unit sphere with a hole, which is a topologically trivial surface. Upon continuous variation, such an incomplete configuration can be rolled up to the constant map to the north pole which sweeps out zero surface without changing the value of \mathcal{C}_1 . From Fig. 2.1 it is clear that for $m = -1$ the unit sphere is covered once by \hat{v} , whereas the $m = 0.2$ configuration never reaching the south pole only incompletely covers S^2 . Plugging the corresponding functions \hat{v} into Eq. (2.7) indeed yields $\mathcal{C}_1 = 1$ for $m = -1$ and $\mathcal{C}_1 = 0$ for $m = 0.2$, respectively.

2.1.3 Bulk boundary correspondence

The generic experimental fingerprint of a topologically nontrivial band structure in quantum transport is not the bulk invariant itself but a boundary effect appearing in a finite size sample which is uniquely associated with the bulk topology. This so called bulk boundary correspondence has first been explained by Halperin [Halperin82] for the integer quantum Hall effect. A simple phenomenological argument for the existence of gapless boundary modes is the following: The bulk topological invariant cannot change without closing the bulk gap. Hence, at the boundary between a trivial system, e.g., the vacuum, and a nontrivial QAH insulator, there must be a metallic domain wall. This argument has been formalized by Volovik [Volovik03] relating the change in the bulk topological invariant between two domains to the number of zero modes of the Dirac operator in the domain wall. This in turn is a special case of the Atiyah-Singer index theorem [Atiyah63, Nakahara03] which can be considered the mathematical foundation of the bulk boundary correspondence.

We will now explicitly construct the gapless edge modes for our QAH toy model (2.2) in the half space geometry $x > 0$ following a similar analysis as Refs. [Zhou08, Qi11]. For simplicity, we again consider the continuum model $h_c = v_c^i \sigma_i$. On partial Fourier transform in y -direction where the system is still translation-invariant, the full Hamiltonian reads

$$h_c(\hat{k}^x, k^y) = k^y \sigma_y + \hat{k}^x \sigma_x + \left(m + (\hat{k}^x)^2 + (k^y)^2 \right) \sigma_z,$$

with $\hat{k}^x = -i\partial_x$. The time independent Schrödinger equation $h_c \psi = E\psi$ now defines an ordinary differential equation (ODE). We consider $k_y = 0$ for simplicity and search for zeromodes, i.e., we set $E = 0$. Then, using the ansatz $\psi = e^{\lambda x} \phi$, the ODE simplifies to

$$\lambda \phi = (m - \lambda^2) \sigma_y \phi.$$

Expanding the solution in terms of the eigenstates $\phi_{\pm} = \frac{i}{\sqrt{2}} (1, \pm i)^T$ of σ_y , we find that a ϕ_+ solution with parameter λ is automatically a ϕ_- solution with parameter $-\lambda$. Solving the quadratic equation for ϕ_+ we get $\lambda_{1/2} = \frac{1}{2}(-1 \pm \sqrt{1 + 4m})$. Imposing the closed boundary condition $\psi(0) = 0$ along with the normalizability for $x > 0$, yields the constraint $\text{Re}\lambda_{1/2} < 0$ which is satisfied for the ϕ_+ solution precisely for $m < 0$, i.e., for an inverted band structure with $\mathcal{C}_1 = 1$ and cannot be satisfied for the ϕ_- solutions. Hence, for $m < 0$, $k^y = 0$, the zero energy solution reads

$$\psi_0 = N(e^{-|\lambda_1|x} - e^{-|\lambda_2|x})\phi_+, \quad (2.9)$$

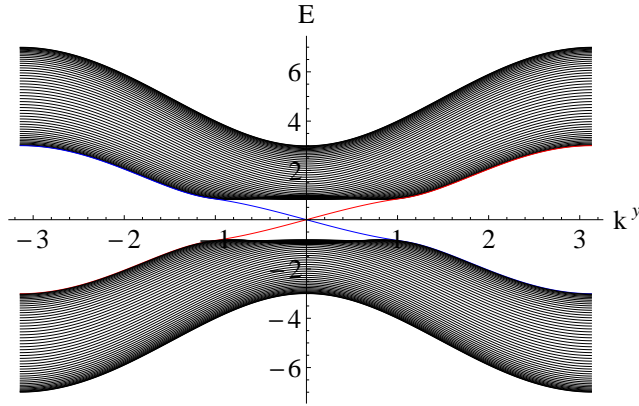


Figure 2.2: Subbands of a QAH ribbon with width 50 sites and $m = -1$. The two chiral subgap modes (blue and red) are exponentially localized at the upper and the lower edge, respectively.

where N is a normalization constant. To illustrate the dispersion of the chiral modes for $k^y \neq 0$, we show the spectrum of a finite width QAH insulator in Fig. 2.2. The crossing point of the two colored subgap modes represents the zero modes at $k^y = 0$ at the two edges of the ribbon which we just obtained by analytical calculation (see Eq. (2.9)).

With that we have demonstrated the one to one correspondence between the non-trivial bulk invariant \mathcal{C}_1 of the QAH insulator and the occurrence of subgap chiral edge modes of a sample of finite size. This bulk boundary correspondence is ubiquitous in the field of TSM. We will later on relate the nature of the surface states directly to the fundamental symmetries of the bulk system.

2.1.4 Symmetry protected topological states of matter

The first Chern number classifying the QAH effect in 2D distinguishes insulating systems which cannot be deformed into each other without closing the insulating gap. This is the strongest notion of a topological protection. If additional symmetry constraints, e.g., TRS or PHS, are imposed on a physical system, the notion of topological protection can be somewhat weakened thereby refining the classification scheme significantly: Two systems can then be considered topologically distinct if they cannot be continuously deformed into each other while neither breaking the protecting symmetry nor closing the gap. Systems which are only non-trivial if certain symmetries are maintained and can be deformed into a trivial system without closing the gap if these symmetries are broken are called topologically protected by these symmetries. The QSH state discussed in some detail in Section 2.4.1 is the first known example of a TSM of this kind: The QSH state is a 2D insulating state which is topologically protected by TRS. The first Chern number of the QSH state is zero which implies that this phase is adiabatically connected to a trivial localized insulator without any hopping. However, such a gapped interpolation crucially relies on the breaking of TRS. Within the class of TRS preserving insulators, the QSH state and the trivial insulator are not adiabatically connected. The systematic classification of TSM in the presence of all

generic additional symmetries is the subject of Section 2.2. Interestingly, also the nature of the bulk boundary correspondence reflects the protecting symmetry. A rough but useful rule of thumb in this context is: If the system preserves TRS with $\mathcal{T}^2 = -1$, the edge modes are helical, i.e., opposite spins have opposite chirality and are degenerate due to the Kramers theorem. If the system has an emergent PHS as for example a mean field superconductor, the protected edge modes are Majorana modes. Combination of both symmetries yields helical Majorana modes.

2.1.5 Local topological quantum phase transitions

From our discussion so far and the explicit calculation of the topological invariant for our toy model (2.2) of the QAH state, it is clear that the topology of a band structure is a global feature which encompasses information about the function $k \mapsto h(k)$ everywhere in the Brillouin zone. However, in reality such a complete information about the physical system is often times lacking. For example, the theoretical prediction of the QSH state in HgTe [Bernevig06a] is based on a perturbative $k.p$ calculation which approximates $h(k)$ as a low order polynomial around the Γ -point $k = 0$. Without further discussion such an approximation seems to be inadequate for the investigation of topological features. However, as the authors of Ref. [Bernevig06a] point out, the gap closing which separates the experimentally observed [König07] QSH phase from the trivial insulating phase happens at the Γ -point and could thus be correctly described by a local theory. Such a singularity changing the topological invariant of the system has been coined topological quantum phase transition (TQPT) [Bernevig06a]. For our toy model (2.2), the TQPT also happens via a gap closing at the Γ -point for $m \rightarrow 0$. This singular point where the Chern number \mathcal{C}_1 is not well defined separates the trivial ($\mathcal{C}_1 = 0$) from a non-trivial ($\mathcal{C}_1 = 1$) QAH phase as is illustrated in Fig. 2.1. An only locally valid theory can thus be suitable for the study of topological features under the following circumstances [Budich12d]: The state to be investigated must be known to concur with a topologically well understood reference state away from the validity regime of the effective theory. A possible transition between the reference state and the state of interest must happen locally at a point within the validity regime of the effective theory. An example where these conditions are not met is the integer quantum Hall effect with degenerate Landau levels. In this case, there is no local gap closing point and the wave functions of all occupied states have to be known to determine the topological invariant [Budich12d]. In Section 2.3.4, we will see that the topology of an interacting system can even change due to dynamical fluctuations which affect the frequency dependence of the single particle Green's function.

2.2 Bulk classification of all possible non-interacting TSM

In this section, we review the general framework for the topological classification of non-interacting systems. This framework does not provide a recipe how to classify an individual system, as we characterized the QAH insulator by calculating its first Chern number in Section 2.1. It rather determines the group of possible topological equivalence classes for a non-interacting system with given spatial dimension and given fundamental symmetries. Regarding the QAH state, the result of this procedure would be: A non-interacting 2D insulator with no fundamental symmetries is characterized by a \mathbb{Z} topological invariant. The

calculation of the value of the respective topological invariants for a given representative of a symmetry class is the subject of Section 2.3.

The general idea that yields the entire table of TSM is quite simple: In addition to requiring a bulk insulating gap, physical systems of a given spatial dimension are divided into 10 symmetry classes distinguished by their fundamental symmetries, i.e., TRS, PHS, and chiral symmetry (CS) [Altland97]. The topological properties of the corresponding Cartan symmetric spaces of quadratic candidate Hamiltonians determine the group of possible topologically inequivalent systems. We outline the mathematical structure behind this general classification scheme in some detail. First, we briefly review the construction of the ten universality classes [Altland97]. Then, we present the associated topological invariants for non-interacting systems of arbitrary spatial dimension giving a complete list of all TSM [Ryu10] that can be distinguished by virtue of this framework. Finally, we discuss in some detail the origin of characteristic patterns appearing in this table using the framework of K-Theory along the lines of the pioneering work by Kitaev [Kitaev09].

2.2.1 Cartan-Altland-Zirnbauer symmetry classes

A physical system can have different types of symmetries. An ordinary symmetry [Ryu10] is characterized by a set of unitary operators representing the symmetry operations that commute with the Hamiltonian. The influence of such a symmetry on the topological classification can be eliminated by transforming the Hamiltonian into a block-diagonal form with symmetry-less blocks. The total system then consists of several uncoupled copies of symmetry-irreducible subsystems which can be classified individually. In contrast, the “extremely generic symmetries” [Ryu10] follow from the anti-unitary operations of TRS and PHS. Involving complex conjugation according to Wigner, they impose certain reality conditions on the system Hamiltonian. In total, the behavior of the system under these operations, and their combination, the CS operation, defines ten universality classes which we call the Cartan-Altland-Zirnbauer (CAZ) classes. For disordered systems, these classes correspond to ten distinct renormalization group (RG) low energy fixed points in random matrix theory [Altland97]. The spaces of candidate Hamiltonians within these symmetry classes correspond to the ten symmetric spaces introduced by Cartan in 1926 [Cartan26] defined in terms of quotients of Lie groups represented in the Hilbert space of the system. For translation-invariant systems, the imposed reality conditions are inherited by the Bloch Hamiltonian $h(k)$.

In the following, the anti-unitary TRS operation will be denoted by \mathcal{T} and the anti-unitary PHS will be denoted by \mathcal{C} . The Hamiltonian \mathcal{H} of a physical system satisfies these symmetries if

$$\mathcal{T}\mathcal{H}\mathcal{T}^{-1} = \mathcal{H}, \tag{2.10}$$

and

$$\mathcal{C}\mathcal{H}\mathcal{C}^{-1} = -\mathcal{H}, \tag{2.11}$$

respectively. According to Wigner’s theorem, these anti-unitary symmetries can be repre-

sented as a unitary operation times the complex conjugation K . We define $\mathcal{T} = TK$, $\mathcal{C} = CK$. Using the unitarity of T, C along with $\mathcal{H} = \mathcal{H}^\dagger$ we can rephrase Eqs. (2.10-2.11) as

$$\begin{aligned} T\mathcal{H}^T T^\dagger &= \mathcal{H} \\ C\mathcal{H}^T C^\dagger &= -\mathcal{H} \end{aligned} \quad (2.12)$$

There are two inequivalent realizations of these anti-unitary operations distinguished by their square which can be plus identity or minus identity. For example, $\mathcal{T}^2 = \pm 1$ for the unfolding of a particle with integer/half-integer spin, respectively. Clearly, $\mathcal{T}^2 = \pm 1 \Leftrightarrow TT^* = \pm 1$ and $\mathcal{C}^2 = \pm 1 \Leftrightarrow CC^* = \pm 1$. In total, there are thus nine possible ways for a system to behave under the two anti-unitary symmetries: each symmetry can be absent, or present with square plus or minus identity. For eight of these nine combinations, the behavior under the combination \mathcal{TC} is fixed. The only exception is the so called unitary class which breaks both PHS and TRS and can either obey or break their combination, the CS. This class hence splits into two universality classes which add up to a grand total of ten classes shown in Tab. 2.1. For a periodic system, symmetry constraints similar to Eq. (2.12) hold for the Bloch

Class	TRS	PHS	CS
A (Unitary)	0	0	0
AI (Orthogonal)	+1	0	0
AII (Symplectic)	-1	0	0
AIII (Chiral Unitary)	0	0	1
BDI (Chiral Orthogonal)	+1	+1	1
CII (Chiral Symplectic)	-1	-1	1
D	0	+1	0
C	0	-1	0
DIII	-1	+1	1
CI	+1	-1	1

Table 2.1: Table of the CAZ universality classes. 0 denotes the absence of a symmetry. For PHS and TRS, ± 1 denotes the square of a present symmetry, the presence of CS is denoted by 1. The last four classes are Bogoliubov deGennes classes of mean field superconductors where the superconducting gap plays the role of the insulating gap.

Hamiltonian $h(k)$, namely

$$\begin{aligned} Th^T(-k)T^\dagger &= h(k) \\ Ch^T(-k)C^\dagger &= -h(k), \end{aligned} \quad (2.13)$$

where T, C now denote the representation of the unitary part of the anti-unitary operations in band space.

For a continuum model, the real space Hamiltonian $H(x)$ is defined through

$$\mathcal{H} = \int d^d x \Psi^\dagger(x) H(x) \Psi(x),$$

where Ψ is a vector/spinor comprising all internal degrees like spin, particle species, etc. The k -space on which the Fourier transform $\tilde{H}(k)$ of $H(x)$ is defined does not have the topology of a torus like the BZ of a periodic system. However, the continuum models one is concerned with in condensed matter physics are effective low energy/large distance theories. For large k , $\tilde{H}(k)$ will thus generically have a trivial structure (c.f. Fig. 2.1), so that the k -space can be endowed with the topology of the sphere S^d by a one point compactification which maps $k \rightarrow \infty$ to a single point (see Section 2.1 for an explicit example of this procedure). The symmetry constraints on $\tilde{H}(k)$ have the same form as those on the Bloch Hamiltonian $h(k)$ shown in Eq. (2.13). By abuse of notation, we will denote both $\tilde{H}(k)$ and $h(k)$ by $h(k)$. Nevertheless, we will point out several differences between periodic systems and continuum models along the way.

2.2.2 Definition of the classification problem for continuum models and periodic systems

For translation-invariant insulating systems with n occupied and m empty bands and continuum models with n occupied and m empty fermion species, respectively, the projection $P(k) = \sum_{\alpha=1}^n |u_{\alpha}(k)\rangle\langle u_{\alpha}(k)|$ onto the occupied states is the relevant quantity for the topological classification. The spectrum of the system is not of interest for adiabatic quantities as long as a bulk gap between the empty and the occupied states is maintained. We thus deform the system adiabatically into a flat band insulator, i.e., a system with eigenenergy $\epsilon_- = -1$ for all occupied states and eigenenergy $\epsilon_+ = +1$ for all empty states. The eigenstates are not changed during this deformation. The Hamiltonian of this flat band system then reads [Qi08a, Schnyder08]

$$Q(k) = (+1)(1 - P(k)) + (-1)P(k) = 1 - 2P(k)$$

Obviously, $Q^2 = 1$, $\text{Tr}[Q] = m - n$. Without further symmetry constraints, Q is an arbitrary $U(n+m)$ matrix which is defined up to a $U(n) \times U(m)$ gauge degree of freedom corresponding to basis transformations within the subspaces of empty and occupied states, respectively. Thus, Q is in the symmetric space

$$G_{n+m,m}(\mathbb{C}) = G_{n+m,n}(\mathbb{C}) = U(n+m)/(U(n) \times U(m)).$$

Geometrically, the complex Grassmannian $G_{k,l}(\mathbb{C})$ is a generalization of the complex projective plane and is defined as the set of l -dimensional planes through the origin of \mathbb{C}^k . The set of topologically different translation-invariant insulators is then given by the group g of homotopically inequivalent maps $k \mapsto Q(k)$ from the BZ T^d of a system of spatial dimension d to the space $G_{n+m,m}(\mathbb{C})$ of possible Bloch Hamiltonians. For continuum models T^d is replaced by S^d and g is by definition given by

$$g = \pi_d(G_{n+m,m}(\mathbb{C})), \tag{2.14}$$

where the n -th homotopy group π_n of a space is by definition the group of homotopically inequivalent maps from S^d to this space. For translation-invariant systems defined on a BZ, the classification can be more complicated than Eq. (2.14) if the lower homotopy groups

π_s , $s = 1, \dots, d - 1$ are nontrivial. For our previous example of the QAH insulator, a 2D translation-invariant state which does not obey any fundamental symmetries, we can infer from $\pi_2(G_{n+m,m}(\mathbb{C})) = \mathbb{Z}$, $\pi_1(G_{n+m,m}(\mathbb{C})) = 0$ that an integer topological invariant must distinguish possible states of matter in this symmetry class, i.e., possible maps $T^2 \rightarrow G_{n+m,m}(\mathbb{C})$. The condition $\pi_1(G_{n+m,m}(\mathbb{C})) = 0$ is necessary because the π_2 classifies maps from S^2 , which is only equivalent to the classification of physical maps from T^2 if the fundamental group π_1 of the target space is trivial. The difference between the base space of a periodic systems which is a torus and of continuum models which has the topology of a sphere has interesting physical ramifications: The so called weak topological insulators are only topologically distinct over a torus but not over a sphere. Physically, this is visible in the lacking robustness of these TSM which break down with the breaking of translation symmetry.

Requiring further symmetries as appropriate for the other nine CAZ universality classes is tantamount to imposing symmetry constraints on the allowed maps $T^d \rightarrow G_{n+m,m}(\mathbb{C})$, $k \mapsto Q(k)$ for translation-invariant systems and $S^d \rightarrow G_{n+m,m}(\mathbb{C})$, $k \mapsto Q(k)$ for continuum models, respectively. The set of topologically distinct physical systems is then still given by the set of homotopically inequivalent maps within this restricted space, i.e., the space of maps which cannot be continuously deformed into each other without breaking a symmetry constraint. For example, for the chiral classes characterized by $\text{CS} = 1$, Q can be brought into the off diagonal form [Schnyder08]

$$Q = \begin{pmatrix} 0 & q \\ q^\dagger & 0 \end{pmatrix},$$

with $qq^\dagger = 1$, which reduces the corresponding target space to $U(n)$. For the chiral unitary class AIII without further symmetry constraints, the calculation of g amounts to calculating $g = \pi_d(U(n)) = \mathbb{Z}$ for odd d and $g = \pi_d(U(n)) = 0$ for even d , respectively. Additional symmetries will again impose additional constraints on the map $T^d \rightarrow U(n)$, $k \mapsto q(k)$.

This procedure rigorously defines the group g of topological equivalence classes for non-interacting translation-invariant insulators in arbitrary spatial dimension and CAZ universality class. However, the practical calculation of g can be highly non-trivial and has been achieved for continuum models via various subtle detours, for example the investigation of surface nonlinear σ -models, in Refs. [Schnyder09, Ryu10]. In the following, we outline a mathematical brute force solution to the classification problem in terms of K-Theory which has been originally introduced in the seminal work by Kitaev in 2009 [Kitaev09]. This method will naturally explain the emergence of weak topological insulators. We will not assume any prior knowledge on K-Theory. In Tab. 2.2, we summarize the resulting groups of topological sectors g for all possible systems [Schnyder09]. We notice an interesting diagonal pattern relating subsequent symmetry classes to neighboring spatial dimensions. Furthermore, the pattern of the two unitary classes shows a periodicity of two in the spatial dimension. If we had shown the classification for higher spatial dimensions, we would have observed a periodicity of eight in the spatial dimension for the eight real classes. The following discussion is dedicated to provide a deeper understanding of these fundamental patterns as pioneered in Ref. [Kitaev09]. The mentioned periodicities have first been pointed

out in Refs. [Qi08a, Schnyder09].

Class	constraint	$d = 1$	$d = 2$	$d = 3$	$d = 4$
A	none	0	\mathbb{Z}	0	\mathbb{Z}
AIII	none on q	\mathbb{Z}	0	\mathbb{Z}	0
AI	$Q^T(k) = Q(-k)$	0	0	0	\mathbb{Z}
BDI	$q^*(k) = q(-k)$	\mathbb{Z}	0	0	0
D	$\tau_x Q^T(k) \tau_x = -Q(-k), m = n$	\mathbb{Z}_2	\mathbb{Z}	0	0
DIII	$q(k)^T = -q(-k), m = n$ even	\mathbb{Z}_2	\mathbb{Z}_2	\mathbb{Z}	0
AII	$i\sigma_y Q^T(k) (-i\sigma_y) = Q(-k), m, n$ even	0	\mathbb{Z}_2	\mathbb{Z}_2	\mathbb{Z}
CII	$i\sigma_y q^*(k) (-i\sigma_y) = q(-k), m = n$ even	\mathbb{Z}	0	\mathbb{Z}_2	\mathbb{Z}_2
C	$\tau_y Q^T(k) \tau_y = -Q(-k), m = n$	0	\mathbb{Z}	0	\mathbb{Z}_2
CI	$q(k)^T = q(-k), m = n$	0	0	\mathbb{Z}	0

Table 2.2: Table of all groups g of topological equivalence classes. The first column denotes the CAZ symmetry class, divided into two unitary classes without anti-unitary symmetry (top) and eight “real” classes with at least one anti-unitary symmetry (bottom). The second column shows the symmetry constraints on the flat band maps, where we have chosen the representation $\mathcal{T} = K$ for $\mathcal{T}^2 = 1$, $\mathcal{T} = i\sigma_y K$ for $\mathcal{T}^2 = -1$, as well as $\mathcal{C} = \tau_x K$ for $\mathcal{C}^2 = 1$, $\mathcal{C} = \tau_y K$ for $\mathcal{C}^2 = -1$. Here, σ_y denotes the Pauli matrix in spin space, τ_x, τ_y denote Pauli matrices in the particle hole pseudo spin space of Bogoliubov deGennes Hilbert spaces. In the last four columns, g is listed for $d = 1, \dots, 4$.

2.2.3 Topological classification of unitary vector bundles

In order to prepare the reader for the application of K-Theory and motivate its usefulness, we first formulate the classification problem in the language of fiber bundles. The mathematical structure of a non-interacting insulator of spatial dimension d is that of a vector bundle $E \xrightarrow{\pi} \mathcal{M}$. The base manifold \mathcal{M} of E is the d dimensional k -space of the system, and the fiber over a point k given by the (projective) space of occupied states $P(k)$. The gauge group of the bundle is $U(n)$, where n is the dimension of P . If no further symmetry conditions are imposed (see class A in Tab. 2.1), the question of how many topologically distinct insulators in a given dimension exist is tantamount to asking how many homotopically different $U(n)$ vector bundles can be constructed over \mathcal{M} . This question can be formally answered for arbitrary smooth manifolds \mathcal{M} as we will outline now. The general idea is the following. There is a universal Bundle $\xi \xrightarrow{\Pi} \mathcal{X}$ into which every bundle E can be embedded through a bundle map [Nakahara03] $\hat{f} : E \rightarrow \xi$ such that

$$f^* \xi = E, \quad (2.15)$$

where $f : \mathcal{M} \rightarrow \mathcal{X}$ is the map between the base manifolds associated with the bundle map \hat{f} . That is to say every bundle can be represented as a pullback bundle [Nakahara03] of the universal bundle ξ by virtue of a suitable bundle map \hat{f} . The key point is now that homotopically different bundles E are distinguished by homotopically distinct maps f . Thus, the set of different TSM is the set $\pi[\mathcal{M}, \mathcal{X}]$ of homotopy classes of maps from the k -space \mathcal{M} to the base manifold \mathcal{X} of the universal bundle. \mathcal{X} is also called the classifying space of

$U(n)$ and is given by the Grassmanian $G_{N,n}(\mathbb{C}) = U(N)/(U(n) \times U(N-n))$ for sufficiently large N , i.e., $N > \lceil \frac{d}{2} + n \rceil$. To be generic in the dimension of the system d , we take the inductive limit $\mathcal{X} = G_n(\mathcal{C}^\infty) = \lim_{N \rightarrow \infty} G_{N,n}(\mathbb{C}) = \lim_{N \rightarrow \infty} U(N)/(U(n) \times U(N-n))$. We thus found for the set $\text{Vect}_n(\mathcal{M}, \mathbb{C})$ of inequivalent $U(n)$ bundles over \mathcal{M} the expression

$$\text{Vect}_n(\mathcal{M}, \mathbb{C}) = \pi[\mathcal{M}, G_n(\mathcal{C}^\infty)],$$

which is known for some rather simple base manifolds. In particular for spheres S^d , there is a trick to calculate $\text{Vect}_n(S^d, \mathbb{C})$: S^d can always be decomposed into two hemispheres which are individually trivial. The homotopy of a bundle over S^d is thus determined by the clutching function f_c defined in the overlap S^{d-1} of the two hemispheres, i.e., along the equator of S^d . Physically, f_c translates a local gauge choice on the upper hemisphere into a local gauge choice on the lower hemisphere and is thus a function $f_c : S^{d-1} \rightarrow U(n)$. The group of homotopy classes of such functions is by definition given $\pi_{d-1}(U(n))$. Interestingly, for $n > \frac{d-1}{2}$, these groups are given by

$$\text{Vect}_n(S^d, \mathbb{C}) = \pi_{d-1}(U(n)) = \begin{cases} \mathbb{Z}, & d-1 \text{ odd} \\ \{0\}, & d-1 \text{ even} \end{cases} \quad (2.16)$$

This periodicity of two in $(d-1)$ is known as the complex Bott periodicity. The physical meaning of Eq. (2.16) is the following: In the unitary universality class A, there is an integer topological invariant in even spatial dimension (QAH in $d=2$) and no TSM in odd spatial dimension.

This classification has two shortcomings. First, it cannot be readily generalized to other CAZ classes at this simple level. Second, only systems with the same number of occupied bands n can be compared. However, adding some trivial bands to the system should yield a system in the same equivalence class. Both shortcomings can be overcome in the framework of K-Theory [Karoubi78, Nash91].

2.2.4 K-Theory approach to a complete classification

K-Theory [Karoubi78, Nash91] is concerned with vector bundles which have a “sufficiently large” fiber dimension. This means, that topological defects which can be unwound by just increasing the fiber dimension are not visible in the resulting classification scheme. This is physically reasonable, as trivial occupied bands from inner localized shells for example increase the number of bands as compared to the effective low energy models under investigation. Models of different number of such trivial bands should be comparable in a robust classification scheme. The use of K-Theory for the classification of TSM has been pioneered in Refs. [Kane05a, Kane05b] and more systematically been discussed in Ref. [Kitaev09].

Crash-course in K-Theory

The direct sum of two vector bundles $E \oplus F$ is the direct sum of their fibers over each point. This addition has only a semi-group structure, since $E \oplus G = F \oplus G \not\Rightarrow E \simeq F$. A minimal

counterexample is given by $E = TS^2$, $F = S^2 \times \mathbb{R}^2$. F is clearly trivial, whereas E , the tangent bundle of S^2 is well known to be non-trivial. However, adding NS^2 , the bundle of normal vectors to S^2 , to both bundles E, F we obtain the same trivial bundle $S^2 \times \mathbb{R}^3$. This motivates the concept of stable equivalence

$$E \stackrel{s}{\simeq} F \Leftrightarrow E \oplus Z^m \simeq F \oplus Z^n, \quad (2.17)$$

where $Z^n = \mathcal{M} \times K^n$, $K = \mathbb{R}, \mathbb{C}$ is the trivial bundle over the fixed base manifold \mathcal{M} , which plays the role of an additive zero as far as stable equivalence is concerned. We denote the set of K -vector bundles over \mathcal{M} by $\mathcal{V}_K(\mathcal{M})$ in the following. Note that stably equivalent bundles can have different fiber dimension, as $m \neq n$ in general in Eq. (2.17). The benefit of this construction is:

$$E \oplus G = F \oplus G \Rightarrow E \stackrel{s}{\simeq} F \quad (2.18)$$

This is because for vector bundles on a smooth manifold every bundle can be augmented to a trivial bundle, i.e.,

$$\forall G \exists H, l \quad G \oplus H = Z^l. \quad (2.19)$$

Eq. (2.18) naturally leads to the notion of a subtraction on $\mathcal{V}_K(\mathcal{M})$ by virtue of the Grothendieck construction: Consider the pairs $(E_1, E_2) \in \mathcal{V}_K(\mathcal{M}) \times \mathcal{V}_K(\mathcal{M})$ and define the equivalence relation

$$(E_1, E_2) \sim (F_1, F_2) \Leftrightarrow \exists H F_1 \oplus E_2 \oplus H \simeq E_1 \oplus F_2 \oplus H. \quad (2.20)$$

Looking at Eq. (2.20), we can intuitively think of the equivalence class $(E_1, E_2)_\sim$ as the formal difference $E_1 - E_2$. We now define the K-group as the quotient

$$K(\mathcal{M}) = (\mathcal{V}_K(\mathcal{M}) \times \mathcal{V}_K(\mathcal{M})) / \sim, \quad (2.21)$$

which identifies all formal differences that are equivalent in the sense of Eq. (2.20). Due to Eq. (2.19), every group element in $K(\mathcal{M})$ can be represented in the form (E, Z^n) . However, $(E, Z^n) \approx (E, Z^m)$ for $n \neq m$. We define the virtual dimension of (E, F) as $d_v = \text{rk}(E) - \text{rk}(F)$, where rk denotes the rank, i.e., the fiber dimension of a vector bundle. By restricting $K(\mathcal{M})$ to elements with $d_v = 0$, we obtain the restricted K-group $\tilde{K}(\mathcal{M}) = \{g \in K(\mathcal{M}) | d_v(g) = 0\}$. $\tilde{K}(\mathcal{M})$ is isomorphic to the set of stable equivalence classes of $\mathcal{V}_K(\mathcal{M})$. Up to now, the construction has been independent of the field over which the vector spaces are defined. In the following, we will distinguish the real and complex K-groups $K_{\mathbb{R}}(\mathcal{M}), K_{\mathbb{C}}(\mathcal{M})$.

A crucial notion in K-Theory which is also our main physical motivation to study it is that of the stable range. The idea is that at sufficiently large fiber dimension n no “new” bundles can be discovered by looking at even larger fiber dimension. Sufficiently large in terms of the dimension d of \mathcal{M} means $n \geq n_{\mathbb{C}} = d/2 + 1$ for the complex case and $n \geq n_{\mathbb{R}} = d + 1$ for the real case, respectively. More formally, every bundle E with $n > n_K$ can be expressed as

a sum

$$E \simeq F \oplus Z^{n-n_K} \quad (2.22)$$

of a bundle F with fiber dimension n_K and a trivial bundle for $K = \mathbb{R}, \mathbb{C}$. Since clearly $E \stackrel{s}{\simeq} F$ (see Eq. (2.18)), this means that all stable equivalence classes have representatives in fiber dimension $n \leq n_K$. Furthermore, a situation like our counterexample above where we augmented two non-isomorphic bundles by the same trivial bundle NS^2 to obtain the same trivial bundle cannot occur in the stable range. That is to say F as appearing in Eq. (2.22) is uniquely defined up to isomorphism. The stable range hence justifies the approach of K -theory of ignoring fiber dimension when defining the stable equivalence. The key result in the stable range which connects K-Theory to our goal of classifying all inequivalent vector bundles with sufficiently large but arbitrary fiber dimension on equal footing reads [Nash91]

$$\tilde{K}_K(\mathcal{M}) = \text{Vect}_n(\mathcal{M}, K) = \pi[\mathcal{M}, G_n(K^\infty)] \quad \forall n \geq n_K. \quad (2.23)$$

The complex Bott periodicity Eq. (2.16) with period $p_{\mathbb{C}} = 2$ has a real analogue concerning the homotopy groups of $O(n)$ with period $p_{\mathbb{R}} = 8$. This immediately implies in the language of K-Theory

$$\tilde{K}_K(S^{d+p_K}) = \tilde{K}_K(S^d), \quad K = \mathbb{R}, \mathbb{C}. \quad (2.24)$$

We define

$$\tilde{K}_K^{-d}(\mathcal{M}) = \tilde{K}_K(S^d \mathcal{M}), \quad (2.25)$$

where S is the reduced suspension [Nash91] which for a sphere S^k indeed satisfies $SS^k = S^{k+1}$. The stronger version of the Bott periodicity in K-Theory now reads [Nash91]

$$\tilde{K}_K^{-d-p_K}(\mathcal{M}) = \tilde{K}_K^{-d}(\mathcal{M}), \quad K = \mathbb{R}, \mathbb{C} \quad (2.26)$$

which only for $\mathcal{M} = S^l$ trivially follows from Eq. (2.24). Using this periodicity, the definition of \tilde{K}_K^{-d} in Eq. (2.25) can be formally extended to $d \in \mathbb{Z}$.

The Bott clock

From the very basic construction of homotopy groups the following identities for the homotopy of a topological space X are evident:

$$\pi_d(X) = \pi[S^d, X] = \pi[SS^{d-1}, X] = \pi[S^{d-1}, \Omega X],$$

where ΩX denotes the loop space [Nash91] of X , i.e., the space of maps from S^1 to X . Iterating this identity gives $\pi_d(X) = \pi_0(\Omega^n X)$ using the complex Bott periodicity (2.16), we immediately see that counting the connected components $\pi_0(U(n)), \pi_1(U(n)) = \pi_0(\Omega U(n))$ of the unitary group and its first loop space, we can classify all $U(n)$ vector bundles over S^d in the stable range, i.e., with $n > \frac{d}{2}$. The real analogue of the Bott periodicity with period $p_{\mathbb{R}} = 8$ leads to analogous statements for $O(n)$ bundles over S^d which depend

Class	Classifying Space
A	$C_0 = U(n+m)/(U(n) \times U(m))$
AIII	$C_1 = U(n)$
AI	$R_0 = O(n+m)/(O(n) \times O(m))$
BDI	$R_1 = O(n)$
D	$R_2 = U(2n)/U(n)$
DIII	$R_3 = U(2n)/Sp(2n)$
AII	$R_4 = Sp(n+m)/(Sp(n) \times Sp(m))$
CII	$R_5 = Sp(n)$
C	$R_6 = Sp(2n)/U(n)$
CI	$R_7 = U(n)/O(n)$

Table 2.3: Table of all classifying spaces C_q , R_q of complex and real K-Theory, respectively. The first column denotes the CAZ symmetry class. From top to bottom, the next complex/real classifying space is the loop space of its predecessor, i.e., $C_{q+1} = \Omega C_q \pmod{2}$, $R_{q+1} = \Omega R_q \pmod{8}$

only on the connected components of $O(n)$ and its first seven loop spaces $\Omega^i O(n)$, $i = 1, \dots, 7$ (see Tab. 2.3). This defines a Bott clock with two ticks for the complex case and eight ticks for the real case, respectively. Interestingly, these ten spaces, for the complex and real case together, are precisely the ten Cartan symmetric spaces in which the time evolution operators associated with Hamiltonians in the ten CAZ classes lie. After this observation, only two points are missing until a complete classification of all TSM of continuum models can be achieved. The first point is a subtlety related to the interdependence of the two wave vectors k and $-k$ as shown in Eq. (2.13), which makes the real Bott clock tick counter clockwise. The second point is the inclusion of symmetry constraints into the scheme which leads to the clockwise ticking Clifford clock (see Eq. (2.30) below). The combination of both implies that the topological invariant of a continuum model of dimension d in the CAZ class q only depends on the difference $q - d \pmod{8}$ for the eight real classes and on $q - d \pmod{2}$ for the two complex classes A and AIII, respectively.

Reality and k-space topology

For systems which obey anti-unitary symmetries the real structure of the Hamiltonian $H(x)$ is most conveniently accounted for in its Majorana representation. $H(x)$ can in this representation be expressed in terms of a real antisymmetric $2n \times 2n$ -matrix B ,

$$\Psi^\dagger(x)H(x)\Psi(x) = \frac{i}{4}B^{ij}c_{x,i}c_{x,j}, \quad (2.27)$$

where $c_{x,i}$, $i = 1, \dots, 2n$ are the Majorana operators representing the n fermion species at x . On Fourier transform, $\mathcal{H} = \int \Psi^\dagger H \Psi$ can be written as [Kitaev09]

$$\mathcal{H} = \frac{i}{4} \int d^d k A^{ij}(k) c_{-k,i} c_{k,j}, \quad (2.28)$$

where A is skew hermitian and satisfies

$$A^*(k) = A(-k). \quad (2.29)$$

Eq. (2.29) naturally leads to a real vector bundle structure as defined in Ref. [Atiyah66] for the bundle of eligible A -matrices over the k -space (\mathbb{R}^d, τ) , where the involution τ (see Ref. [Atiyah66]) is given by $k \mapsto -k$. On one-point compactification, this real k -space becomes a sphere $\bar{S}^d = (S^d, \tau)$ with the same involution [Kitaev09]. Whereas the ordinary sphere S^d can be viewed as a reduced suspension S of S^{d-1} over the real axis, \bar{S}^d can be understood as the reduced suspension \bar{S} of \bar{S}^{d-1} over the imaginary axis. This picture is algebraically motivated by comparing the involution τ to the ordinary complex conjugation which, restricted to the imaginary axis of the complex plane is of the same form. Interestingly, in the language of definition (2.25), \bar{S} plays the role of an inverse to S [Atiyah66, Kitaev09], i.e.,

$$\tilde{K}_{\mathbb{R}}(\mathcal{M}) = \tilde{K}_{\mathbb{R}}^{-1}(\bar{S}\mathcal{M}) = \tilde{K}_{\mathbb{R}}(S\bar{S}\mathcal{M}).$$

This means that the Bott clock over \bar{S}^d is reversed as compared to its analogue over S^d .

Real K-theory and the Clifford clock

The main reason for the real construction of Eq. (2.28) is that the anti-unitary symmetry constraints yielding the eight real CAZ classes (all except A and AIII) can be distinguished in terms of anti-commutation relations of the A -matrix with real Clifford generators [Karoubi78, Kitaev09]. At a purely algebraic level, these constraints can be transformed so as to be expressed only in terms of positive Clifford generators [Kitaev09], i.e., generators that square to plus identity. We call the restricted K-group of a vector bundle of A -matrices over \mathcal{M} that anti-commute with q positive Clifford generators $\hat{K}_{\mathbb{R}}^q(\mathcal{M})$. Interestingly [Karoubi78, Kitaev09],

$$\hat{K}_{\mathbb{R}}^q(\mathcal{M}) \simeq \tilde{K}_{\mathbb{R}}^{-q}(\mathcal{M}). \quad (2.30)$$

Eq. (2.30) defines a Clifford clock that runs in the opposite direction as the \bar{S}^d Bott clock. This algebraic phenomenon explains the full periodic structure of the table of TSM of continuum models (see Tab. 2.2). The classifying spaces of A -matrices for systems that anti-commute with q Clifford generators are shown in Tab. 2.3.

Periodic systems

The classification of periodic systems is much more complicated from a mathematical point of view. Their base space is the real Brillouin zone $\bar{T}^d = (T^d, \tau)$, where the involution τ giving rise to the real structure is again given by $k \mapsto -k$. For \bar{T}^d the reduced suspension does not provide a trivial relation between the K-Theory of different spatial dimension like $\bar{S}\bar{S}^d = \bar{S}^{d+1}$ for the base space of continuum models. The general calculation of all relevant K-groups over \bar{T}^d has been reported in Ref. [Kitaev09]. Interestingly, the resulting groups always contain the respective classification of continuum models in the same symmetry class

as an additive component. Additionally, the topological invariants of weak TSM, i.e., TSM which are only present in translation-invariant systems, can be inferred. The Clifford clock defined in Eq. (2.30) is independent of the base space and hence still applicable. Here, we only review the general result calculated in Ref. [Kitaev09]

$$K_{\mathbb{R}}^{-q}(\bar{T}^d) \simeq K_{\mathbb{R}}^{-q}(\bar{S}^d) \oplus \left(\bigoplus_{s=0}^{d-1} \binom{d}{s} K_{\mathbb{R}}^{-q}(\bar{S}^s) \right). \quad (2.31)$$

The second term on the right hand side of Eq. (2.31) entails the notion of so called weak topological insulators which are obviously due to TSM in lower dimensions. To name the most prominent example, the \mathbb{Z}_2 invariant characterizing the QSH insulator in $d = 2$ in the presence of TRS, CAZ class AII, yields a $3\mathbb{Z}_2$ topological invariant characterizing the weak topological insulators with the same symmetry in $d = 3$.

Lattice systems with disorder

In a continuum model, disorder that is not too short ranged so as to keep the k -space compactification for large k valid, can be included into the model system without changing the classification scheme. However, perturbing a translation-invariant lattice system with disorder also gives its k -space a discrete lattice structure which is not directly amenable to investigation in the framework of K-Theory which we only defined over smooth base-manifolds. Ref. [Kitaev09] shows that a Hamiltonian featuring localized states in the energy gap can be transformed into a gapped Hamiltonian upon renormalization of parameters. The physical consequence of this statement is that only a mobility gap is needed for the classification of a TSM and no energy gap in the density of states. Furthermore, Ref. [Kitaev09] argues without explicit proof that the classification problem of gapped lattice systems without translation invariance is equivalent to the classification problem of continuum models. This statement agrees with the physical intuition that the breaking of translation-invariance must remove the additional structure of weak TSM as described for periodic systems by Eq. (2.31).

2.3 Calculation of topological invariants of individual systems

In Section 2.2, we have shown how many different TSM can be expected in a given spatial dimension and CAZ class. Now, we outline how insulating systems within the same CAZ class and dimension can be assigned a topological equivalence class in terms of their adiabatic connection defined in Eq. (1.11) and their adiabatic curvature defined in Eq. (1.22), respectively. A complete case by case study in terms of Dirac Hamiltonian representatives of all universality classes of this problem has been reported in Ref. [Ryu10]. In this thesis, we outline the general patterns relating the classification of neighboring (see Tab. 2.2) universality classes following the analysis in Refs. [Qi08a, Schnyder08, Ryu10]. Interestingly, all topological invariants can be calculated using only complex invariants, namely Chern numbers and chiral unitary winding numbers. The anti-unitary symmetries are accounted for by the construction of a dimensional hierarchy in Section 2.3.2 starting from a so called parent state in each symmetry class for which the complex classification concurs with the real classification. In Section 2.3.3, we show how the topological invariants can be defined for

disordered systems with the help of twisted boundary conditions. Furthermore, we discuss a generalization of the non-interacting topological invariants to interacting systems in Section 2.3.4.

2.3.1 Systems without anti-unitary symmetries

Chern numbers of unitary vector bundles

Eq. (2.15) shows that every $U(n)$ bundle $E \rightarrow \mathcal{M}$ can be represented as a pullback from the universal bundle $\xi \rightarrow G_n(\mathbb{C}^\infty)$ by some map bundle map \hat{f} . Chern classes are de Rham cohomology classes, i.e., topological invariants [Bott82] that are defined as the pullback of certain cohomology classes of the classifying space $G_n(\mathbb{C}^\infty)$. The cohomology ring $H^*(G_n(\mathbb{C}^\infty))$ consists only of even classes and is generated by the single generator $\tilde{c}_j \in H^{2j}(G_n(\mathbb{C}^\infty))$, $j = 1, \dots, n$ for every even cohomology group [Sato96]. The Chern classes c_i of E are defined as the pullback $c_i = f^* \tilde{c}_i$ from the classifying space by the map $f : \mathcal{M} \rightarrow G_n(\mathbb{C}^\infty)$ associated with the bundle map \hat{f} . Due to the Chern-Weyl theorem [Nakahara03], Chern classes can be expressed in terms of the curvature, i.e., in our case, the adiabatic curvature \mathcal{F} defined in Eq. (1.22) of E . Explicitly, the total Chern class c can be expressed as [Nakahara03]

$$c = \det \left(1 + \frac{i\mathcal{F}}{2\pi} \right) = 1 + c_1(\mathcal{F}) + c_2(\mathcal{F}) \dots \quad (2.32)$$

The determinant is evaluated in gauge space and products of \mathcal{F} are understood to be wedge products. c_j is the monomial of order j in \mathcal{F} . Obviously, c_j is a $2j$ -form and can only be non-vanishing for $2j \leq d$, where d is the dimension of the base manifold \mathcal{M} , i.e., the spatial dimension of the physical system. Another characteristic class which generates all Chern classes is the Chern character [Nakahara03]

$$\text{ch} = \text{Tr} \left[e^{\frac{i\mathcal{F}}{2\pi}} \right] = 1 + \text{ch}_1(\mathcal{F}) + \text{ch}_2(\mathcal{F}) + \dots \quad (2.33)$$

Due to their importance for later calculations, we explicitly spell out the first two Chern characters $\text{ch}_1 = \text{Tr} \left[\frac{i\mathcal{F}}{2\pi} \right]$, $\text{ch}_2 = -\frac{1}{8\pi^2} \text{Tr} [\mathcal{F} \wedge \mathcal{F}]$. Importantly, for even $d = 2p$, the integral

$$\mathcal{C}_p = \int_{\mathcal{M}} \text{ch}_p$$

yields an integer, the so called p -th Chern number [Choquet-Bruhat82]. These Chern numbers characterize systems in the unitary symmetry class A which can only be non-trivial in even spatial dimension (see Tab. 2.2).

Winding numbers of chiral unitary vector bundles

In Section 2.2, we have shown that the classifying space for a chiral unitary (AIII) system is given by $U(n)$ and that the topological sectors are defined by homotopically distinct maps $k \mapsto q(k) \in U(n)$. Now, we discuss how to assign a given map q to an equivalence class by calculating its winding number [Redlich84, Volovik88, Golterman93] following Ref. [Ryu10].

From Tab. 2.2 it is clear that only in odd spatial dimension $d = 2j - 1$ there can be a non-trivial winding number. We define

$$w_{2j-1}^q = \frac{(-(j-1)!)}{(2j-1)!(2\pi i)^j} \text{Tr} \left[(q^{-1}dq)^{2j-1} \right], \quad (2.34)$$

which has been dubbed winding number density [Ryu10]. Integrating this density over the odd-dimensional base manifold \mathcal{M} representing the k -space of the physical system, we get the integral winding number ν_{2j-1}

$$\nu_{2j-1} = \int_{\mathcal{M}} w_{2j-1}^q, \quad (2.35)$$

which is well known to measure the homotopy of the map $k \mapsto q(k)$.

Relation between chiral winding number and Chern Simons form

So far, the relation between the adiabatic connection of a chiral system and its topological invariant has not been made explicit. Since characteristic classes like Chern characters are closed $2j$ -forms, they can locally be expressed as exterior derivatives of a $(2j - 1)$ -forms. These odd forms are called the Chern Simons forms associated with the even characteristic class [Chern74, Nakahara03]. For the j -th Chern character ch_j , which is a $2j$ form, the associated Chern Simons form \mathcal{Q}_{2j-1} reads [Nakahara03]

$$\mathcal{Q}_{2j-1}(\mathcal{A}, \mathcal{F}_t) = \frac{1}{(j-1)!} \left(\frac{i}{2\pi} \right)^j \int_0^1 dt \text{STr} \left[\mathcal{A}, \mathcal{F}_t^{j-1} \right], \quad (2.36)$$

where $\mathcal{F}_t = t\mathcal{F} + (t^2 - t)\mathcal{A} \wedge \mathcal{A}$ is the curvature of the interpolation $t\mathcal{A}$ between the zero connection and \mathcal{A} and STr denotes the symmetrized trace. Explicitly, we have $\mathcal{Q}_1 = \frac{i}{2\pi} \text{Tr} [\mathcal{A}]$, $\mathcal{Q}_3 = -\frac{1}{8\pi^2} \text{Tr} \left[\mathcal{A}d\mathcal{A} + \frac{2}{3}\mathcal{A}^3 \right]$.

It is straightforward to show [Ryu10], that in a suitable gauge, the Berry connection of a chiral bundle yields $\mathcal{A}^B = \frac{1}{2}qdq^\dagger$, where $q \in U(n)$ is again the chiral map characterizing the system. This is not a pure gauge due to the factor $\frac{1}{2}$ which entails that the associated curvature \mathcal{F}^B does not vanish. Plugging \mathcal{A}^B and \mathcal{F}^B into Eq. (2.36) immediately yields [Ryu10]

$$\mathcal{Q}_{2j-1}(\mathcal{A}^B, \mathcal{F}_t^B) = \frac{1}{2}w_{2j-1}^q. \quad (2.37)$$

Eq. (2.37) directly relates the winding number density to the Chern Simons form. We define the Chern Simons invariant of an odd dimensional system as

$$\text{CS}_{2j-1} = \int_{\mathcal{M}} \mathcal{Q}_{2j-1} \pmod{1},$$

where $\pmod{1}$ accounts for the fact that $\int_{\mathcal{M}} \mathcal{Q}_{2j-1}$ has an integer gauge dependence due to

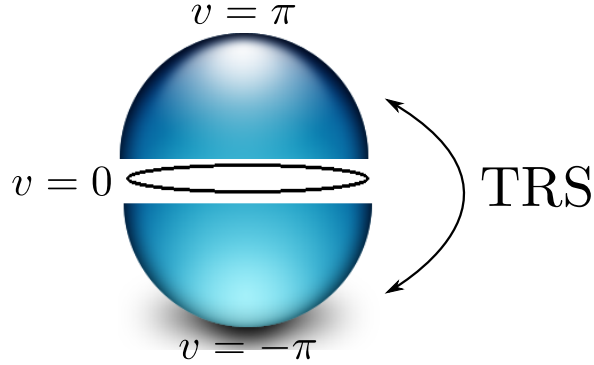


Figure 2.3: Illustration of the WZW dimensional extension. The circle at $v = 0$ represents the physical system. The poles at $v = \pm\pi$ represent the trivial reference system without k -dependence. The two interpolations are conjugated by an anti-unitary symmetry, here exemplarily denoted by TRS.

$\pi_{2j-1}(U(n)) = \mathbb{Z}$ for $n > j$. Looking back at Eq. (2.35), we immediately get

$$\nu_{2j-1}(\text{mod } 2) = 2\text{CS}_{2j-1}(\text{mod } 2).$$

We note that the $(\text{mod } 2)$ can be dropped if we fix the gauge as described above to $\mathcal{A}^B = \frac{1}{2}qdq^{-1}$. This establishes the desired relation between the winding number of a chiral unitary system and its adiabatic curvature.

2.3.2 Dimensional reduction and real symmetry classes

Until now, we have only discussed how to calculate topological invariants of systems in the complex symmetry classes A and AIII. Interestingly, for some real universality classes, the classification in the presence of anti-unitary symmetries concurs with the unitary classification (see Tab. 2.4). The first known example of this type is in the symplectic class AII in $d = 4$ which is characterized by the second Chern number of the corresponding complex bundle [Avron88, Zhang01]. Another example of this kind is the $p + ip$ superconductor in $d = 2$ and symmetry class D which is characterized by its first Chern number, i.e., in the same way as the QAH effect in class A. In odd dimensions similar examples exist for real chiral classes, e.g., for DIII in $d = 3$, where the winding number is calculated using Eq. (2.34) in the same way as for the chiral unitary class AIII in the same dimension. All the topological invariants just mentioned are integer invariants. In some universality classes, these integers can only assume even values (see Tab. 2.4). For physically relevant dimensions, i.e., $d = 1, 2, 3$, these exceptions are CII in $d = 1$, C in $d = 2$, and CI in $d = 3$. All other states where the complex and the real classification concur, can be viewed as parent states of a dimensional hierarchy within the same symmetry class from which all \mathbb{Z}_2 invariants appearing in Tab. 2.4 can be obtained by dimensional reduction. This approach was pioneered in the seminal work by Qi, Hughes, and Zhang [Qi08a].

The general idea is more intuitive if we consider the parent state as a Wess-Zumino-Witten (WZW) dimensional extension [Witten83, Wang10] of the lower dimensional descendants

Class	$d = 1$	$d = 2$	$d = 3$	$d = 4$	$d = 5$	$d = 6$	$d = 7$	$d = 8$
A	0	\mathbb{Z}	0	\mathbb{Z}	0	\mathbb{Z}	0	\mathbb{Z}
AIII	\mathbb{Z}	0	\mathbb{Z}	0	\mathbb{Z}	0	\mathbb{Z}	0
AI	0	0	0	$2\mathbb{Z}$	0	\mathbb{Z}_2	\mathbb{Z}_2	$\boxed{\mathbb{Z}}$
BDI	$\boxed{\mathbb{Z}}$	0	0	0	$2\mathbb{Z}$	0	\mathbb{Z}_2	\mathbb{Z}_2
D	\mathbb{Z}_2	$\boxed{\mathbb{Z}}$	0	0	0	$2\mathbb{Z}$	0	\mathbb{Z}_2
DIII	\mathbb{Z}_2	\mathbb{Z}_2	$\boxed{\mathbb{Z}}$	0	0	0	$2\mathbb{Z}$	0
AII	0	\mathbb{Z}_2	\mathbb{Z}_2	$\boxed{\mathbb{Z}}$	0	0	0	$2\mathbb{Z}$
CII	$2\mathbb{Z}$	0	\mathbb{Z}_2	\mathbb{Z}_2	$\boxed{\mathbb{Z}}$	0	0	0
C	0	$2\mathbb{Z}$	0	\mathbb{Z}_2	\mathbb{Z}_2	$\boxed{\mathbb{Z}}$	0	0
CI	0	0	$2\mathbb{Z}$	0	\mathbb{Z}_2	\mathbb{Z}_2	$\boxed{\mathbb{Z}}$	0

Table 2.4: Table of all groups of topological equivalence classes. The first column denotes the symmetry class, divided into two complex classes without any anti-unitary symmetry (top) and eight real classes with at least one anti-unitary symmetry (bottom). Chiral classes are denoted by bold letters. The parent states of dimensional hierarchies are boxed. For all non-chiral boxed states, the classification concurs with that of class A in the same dimension. For all chiral boxed states, the classification concurs with that of class AIII in the same dimension. $2\mathbb{Z}$ indicates that the topological integer can only assume even values in some cases. Such states are never parent states.

instead of thinking of a dimensional reduction from the d -dimensional parent state to its descendants. This works as follows: We fix a localized $(d - 1)$ -dimensional insulator without any hopping that satisfies the required anti-unitary symmetries as a trivial reference state. This reference state is described by the k -independent Bloch Hamiltonian h_0 . The $(d - 1)$ -dimensional physical system of interest is characterized by the Bloch Hamiltonian $h(k)$. Then, we interpolate by varying the parameter v between the $(d - 1)$ -dimensional physical system ($v = 0$) and the trivial state ($v = \pi$) without closing the insulating gap. However, the intermediate $(d - 1)$ -dimensional system at fixed $v \neq 0, \pi$ might well break the required anti-unitary symmetries. The crucial step is now to do the interpolation for $v \in [0, \pi]$ and $v \in [-\pi, 0]$ in a symmetry conjugated way (see Fig. 2.3). That is to say, we require our $(d - 1)$ -dimensional system of interest and the resulting d -dimensional extended system to be in the same CAZ class. This d -dimensional system is characterized by the Bloch Hamiltonian $h(k, v)$. The $v \in [-\pi, 0]$ and the $v \in [0, \pi]$ half of the extended k -space then are not independent of each other but give equal contributions to the integer topological invariant of the d -dimensional extended system [Qi08a, Ryu10]. One might now ask to which extend the resulting integer invariant of the extended system depends on our choice of the interpolation $h(k, v)$ between $h(k) = h(k, v = 0)$ and $h_0 = h(k, v = \pm\pi)$. To answer this question, one considers two interpolations $h(k, v), \tilde{h}(k, v)$. It is then elementary to show [Qi08a] that the difference between the integer invariants of these two d -dimensional systems is an even integer. This implies that a \mathbb{Z}_2 information, namely the parity of the integer invariant associated with the extended system, is well defined only in terms of the physical system with spatial dimension $(d - 1)$.

A similar procedure can be repeated a second time to obtain a \mathbb{Z}_2 invariant for a $(d -$

2) dimensional second descendant [Qi08a]. From the procedure just sketched, it is obvious why the exceptional phases which are characterized by an even integer are not parent states of such a dimensional hierarchy. The generic constructions for all possible classes can be found in Refs. [Qi08a, Ryu10]. With that, we are provided with a general and fairly explicit recipe for the practical calculation of the topological invariants for all possible CAZ classes in all spatial dimensions. We will work out the dimensional extension explicitly in Section 2.4 for a model of the 1D TSC state which has recently received enormous attention due to its experimental relevance.

2.3.3 Bulk invariants of disordered systems and twisted boundary conditions

Our practical calculation of topological invariants so far has been focused on periodic systems with a BZ, i.e., $\mathcal{M} = T^d$ and continuum models where the k -space can be compactified to a sphere, i.e., $\mathcal{M} = S^d$. As already pointed out in Section 2.2, the situation is more complicated for disordered lattice models. Seminal progress along these lines was reported for the quantum Hall state by Niu *et al.* in 1985 [Niu85]. These authors use twisted boundary conditions (TBC) to define the quantized Hall conductivity σ_{xy} for a 2D system as a topological invariant only requiring a bulk mobility gap. We briefly review their analysis and propose the framework of TBC as a general recipe to calculate topological invariants for disordered systems.

The Hall conductivity σ_{xy} resulting from a linear response calculation at zero temperature yields

$$\sigma_{xy} = \frac{-2}{A} \text{Im} \sum_{n \neq 0} \frac{\langle 0 | \mathcal{H}_x | n \rangle \langle n | \mathcal{H}_y | 0 \rangle}{(E_n - E_0)^2},$$

where $|0\rangle$ is the many body ground state, A is the area of the system, and $\mathcal{H}_i = \frac{\partial \mathcal{H}}{\partial k^i}$. In the presence of a magnetic field, translation-invariance is defined in terms of the magnetic translation operator T_B [Kohmoto85] which concurs with the ordinary translation operator $T(a) = e^{ia\hat{k}}$ in the absence of a magnetic field. TBC now simply mean that a (magnetic) translation by the system length L_j in j -direction gives an additional phase factor $e^{i\phi_j}$. ϕ_j is called the twisting angle in j -direction. Gauging away this additional phase to obtain a wave function with periodic boundaries amounts to a gauge transformation of the Hamiltonian which shifts the momentum operator like

$$-i\partial_j \rightarrow -i\partial_j + \phi_j \tag{2.38}$$

This demonstrates the close relation between the flux threading arguments employed in Section 2.1 and TBC. Using $\mathcal{H}_i = \mathcal{H}_{\phi_i} = [\partial_{\phi_i}, \mathcal{H}]$ the Hall conductivity can be expressed as the sensitivity of the ground state wave function to TBC.

$$\sigma_{xy} = \frac{2}{A} \text{Im} \langle \partial_{\phi_x} 0 | \partial_{\phi_y} 0 \rangle,$$

or, defining $\theta = L_x\phi_x$, $\varphi = L_y\phi_y$

$$\sigma_{xy} = 2\text{Im}\langle\partial_\theta 0|\partial_\varphi 0\rangle = i\mathcal{F}_{\theta\varphi}. \quad (2.39)$$

The main merit of Ref. [Niu85] is to show that this expression actually does not depend on the value of (θ, φ) as long as the single particle Green's function of the system is exponentially decaying in real space. This condition is met if the Fermi energy lies in a mobility gap. Hence, a trivial integration can be introduced as follows:

$$\sigma_{xy} = \frac{i}{4\pi^2} \int_0^{2\pi} d\theta \int_0^{2\pi} d\varphi \mathcal{F}_{\theta\varphi} = G_0 \int_{T^2} \frac{i\mathcal{F}}{2\pi} = G_0\mathcal{C}_1, \quad (2.40)$$

where $G_0 = \frac{e^2}{h} = \frac{1}{2\pi}$ and the integer \mathcal{C}_1 is by definition the first Chern number of the ground state line bundle over the torus of twisting angles. This construction makes the topological quantization of the Hall conductivity manifest.

Eq. (2.38) shows the close relation between momentum and twisting angles. One is thus tempted to just replace the BZ of each periodic system by the torus of twisting angles for the corresponding disordered system which is topologically equivalent to a fictitious periodic system with the physical system as single lattice site [Fu07, Leung12]. We will proceed along these lines below but would like to comment briefly on the special role played by the quantum Hall phase first. Eq. (2.39) represents the physical observable σ_{xy} in terms of the twisting angles. Niu *et al.* argued rigorously [Niu85] that σ_{xy} of a bulk insulating system can actually not depend on the value of these twisting angles which allows them to express σ_{xy} as a manifestly quantized topological invariant in Eq. (2.40). For a generic TSM, the topological invariant of the clean system does in general not represent a physical observable. Furthermore, the integration over the twisting angles will not be trivial, i.e., the function to be integrated will actually depend on the twisting angles. Employing the picture of a periodic system with the physical system as a single site is problematic inasmuch as the bulk boundary correspondence at the ‘‘boundary’’ of a single site is hard to define mathematically rigorously. In the quantum Hall regime for example, it is well known that in disordered systems a complicated landscape of localized states and current carrying regions produces the unchanged topologically quantized Hall conductivity [Halperin82]. However, as opposed to the clean QAH insulator discussed in Section 2.1, the edge states of the disordered quantum Hall state are in general not strictly localized at the boundary.

Replacing the BZ of a translation-invariant system by the torus of twisting angles in the disordered case yields a well defined topological invariant which adiabatically connects to the topological invariant of the clean system where the relation

$$\partial_{k^j} = \partial_{\phi_j} \quad (2.41)$$

follows from Eq. (2.38). This is because from a purely mathematical perspective it cannot matter which torus we consider as the base space of our system. In this sense, the framework of TBC is as good as it gets concerning the definition of topological invariants for disordered systems. The fact that in some symmetry protected topological phases the topological

invariants are not directly representing physical observables is not a problem of the approach of TBC but is a remarkable difference between these TSM and the quantum Hall state at a more fundamental level.

2.3.4 Taking into account interactions

Up to now, this entire thesis has only been concerned with non-interacting systems. As a matter of fact, the entire classification scheme discussed in Sec. 2.2 massively relies on the prerequisite that the Hamiltonian is a quadratic form in the field operators. The violation of this classification scheme for systems with two particle interactions has been explicitly demonstrated in Ref. [Fidkowski10].

As we are not able to give a general classification of TSM for interacting systems, we search for an adiabatic continuation of the non-interacting topological invariants to interacting systems. This procedure does from its outset impose certain adiabaticity constraints on the interactions that can be taken into account. The topological invariants for non-interacting systems are defined in terms of the projection P on the occupied single particle states defining the ground state of the system. The main assumption is thus that the gapped ground state of the non-interacting system is adiabatically connected to the gapped ground state of the interacting system. A counter-example of this phenomenology is the fractional quantum Hall state, where a gap due to non-adiabatic interactions emerges in a system which is gapless without interactions. However, it is clear that the phase space for low energy interactions will be much larger in a gapless than in a gapped non-interacting system. We thus generically expect the classification scheme at hand to be robust against moderate interactions. However, beyond mean field interactions, the Hamiltonian cannot be expressed as an effective single particle operator. Hence, we need to find a formulation of the topological invariants that adiabatically connects to the non-interacting language and is well defined for general gapped interacting systems. The key to achieving this goal is to look at the single particle Green's function G instead of the system Hamiltonian. This approach has been pioneered in the field of TSM by Qi, Hughes, and Zhang [Qi08a] who formulated a topological field theory for TSM in the CAZ class AII.

Chern numbers and Green's function winding numbers

The role model for this construction is again the Hall conductivity σ_{xy} of a gapped 2D system. In Ref. [Redlich84], σ_{xy} has been expressed in terms of G by perturbative expansion of the effective action of a gauge field A that is coupled to the gapped fermionic system. The leading contribution stemming from a vacuum polarization diagram yields the Chern Simons action

$$S_{\text{CS}} = \frac{\sigma_{xy}}{2} \int d^2x dt \epsilon^{\mu\nu\sigma} A_\mu \partial_\nu A_\sigma = \frac{\sigma_{xy}}{2} \int A \wedge dA.$$

The prefactor σ_{xy} in units of the quantum of conductance assumes the form

$$\sigma_{xy} = \frac{1}{24\pi^2} \int d^2k d\omega \text{Tr} \left[(GdG^{-1})^3 \right], \quad (2.42)$$

where d now denotes the exterior derivative in combined frequency-momentum space and G is the time ordered Green's function, or, equivalently as far as the calculation of topological invariants is concerned, the continuous imaginary frequency Green's function as used in zero temperature perturbation theory. An analogous expression has been derived by Volovik using a semi-classical gradient expansion [Volovik88]. The similarity between Eq. (2.34) and the integrand of Eq. (2.42) is striking. Obviously, Eq. (2.42) represents σ_{xy} as a winding number in 3D frequency-momentum space. If this construction makes sense, we should by integration of Eq. (2.42) over ω recover the representation of σ_{xy} as the first Chern number in the 2D BZ for the special case of the non-interacting Green's function $G_0(\omega, k) = (i\omega - h(k))^{-1}$. Due to its importance and generic relevance, we explicitly perform the calculation. For a gapped band structure the spectrum can be deformed into a gapped flat band spectrum without changing the Bloch-eigenstates [Qi08a]. The resulting Hamiltonian

$$h(k) = \epsilon_c P_c(k) + \epsilon_v P_v(k), \quad \epsilon_v < 0 < \epsilon_c,$$

where $P_v = \sum_{\alpha \text{ occ}} |u_k^\alpha\rangle \langle u_k^\alpha|$, $P_c = \sum_{\beta \text{ empty}} |u_k^\beta\rangle \langle u_k^\beta|$ are the projectors on the occupied and the empty states, respectively, then has the same topology as the original model. For this topologically equivalent model, the time ordered Green function can be readily expressed as

$$G(\omega, k) = (\omega + i \text{sgn}(\omega)\delta - H(k))^{-1} = \frac{P_v(k)}{\omega + i\delta - \epsilon_v} + \frac{P_c(k)}{\omega + i\delta - \epsilon_c}.$$

In the last expression the sign dependence of the regularization δ is suppressed for notational convenience. In the derivative of $G(\omega, k)$ with respect to ω , this dependence is also neglected since we do by construction not have zero modes here. Using $\partial_\omega G^{-1} = 1$; $\partial_{k^i} G^{-1} = (\epsilon_c - \epsilon_v)\partial_i P_v$ we get

$$\sigma_{xy} = \frac{1}{8\pi^2} \lim_{\delta \rightarrow 0} \int d^2k d\omega \epsilon^{\nu\rho} \sum_{n,m} \frac{\text{Tr} [P_n(\partial_\nu P_v) P_m(\partial_\rho P_v)] (\epsilon_c - \epsilon_v)^2}{(\omega + i\delta - \epsilon_n)^2 (\omega + i\delta - \epsilon_m)}, \quad n, m = v, c. \quad (2.43)$$

Using $P_v + P_c = 1$ as well as $P_v P_c = 0$, the following identities [Qi08a] are readily derived

$$\begin{aligned} P_c \partial_i P_v &= -(\partial_i P_c) P_v = (\partial_i P_v) P_v, \\ P_v \partial_i P_v &= -P_v \partial_i P_c = (\partial_i P_v) P_c. \end{aligned} \quad (2.44)$$

With the help of these two equations it is obvious that non-vanishing contributions to Eq. (2.43) require $n \neq m$. For the two relevant terms, the integration over ω can be readily

performed using the residue theorem. We get

$$\begin{aligned}\sigma_{xy} &= \frac{i}{4\pi} \int_{T^2} d^2k \epsilon^{\nu\rho} \text{Tr} [P_v(\partial_\nu P_v) P_c(\partial_\rho P_v)] - \text{Tr} [P_c(\partial_\nu P_v) P_v(\partial_\rho P_v)] = \\ &= \frac{i}{2\pi} \int_{T^2} d^2k \epsilon^{\nu\rho} \text{Tr} [(\partial_\nu P_v) P_c(\partial_\rho P_v)],\end{aligned}$$

where in the last equality Eq. (2.44) has again been used. Inserting $P_v = \sum_{\alpha \text{ occ}} |u_k^\alpha\rangle \langle u_k^\alpha|$, $P_c = \sum_{\beta \text{ empty}} |u_k^\beta\rangle \langle u_k^\beta|$ into the latter equation it is straight forward to show that

$$\begin{aligned}\sigma_{xy} &= \frac{i}{2\pi} \int_{T^2} d^2k \epsilon^{\nu\rho} \text{Tr} [(\partial_\nu P_v) P_c(\partial_\rho P_v)] = \\ &= \frac{-i}{2\pi} \sum_{\alpha \text{ occ}} \int_{T^2} d^2k ((\partial_1 \langle u_k^\alpha |) (\partial_2 |u_k^\alpha\rangle) - (\partial_2 \langle u_k^\alpha |) (\partial_1 |u_k^\alpha\rangle)) = \\ &= \frac{i}{2\pi} \int_{T^2} \mathcal{F}_{12} dk^1 dk^2 = \frac{i}{2\pi} \int_{T^2} \mathcal{F} = \mathcal{C}_1.\end{aligned}\tag{2.45}$$

With that we have shown explicitly that the representation of σ_{xy} in terms of the single particle Green's function, Eq. (2.42), is in the non-interacting case equal to the first Chern number \mathcal{C}_1 associated with the Bloch Hamiltonian $k \mapsto h(k)$. This result can be readily generalized to higher even spatial dimensions and higher Chern numbers, respectively. In Ref. [Golterman93], a perturbative expansion similar to Ref. [Redlich84] has been presented for fermions coupled to a gauge field in arbitrary even spatial dimension $2n$. The resulting analogue of the Hall conductivity, i.e., the prefactor of the Chern Simons form in $(2n + 1)\text{D}$ (see Eq. (2.36)) can be expressed as [Golterman93, Volovik03, Qi08a]

$$N_{2r+1} [G] = \frac{-r!}{(2r+1)!(2\pi i)^{r+1}} \int_{\text{BZ} \times \mathbb{R}_\omega} \text{Tr} \left[(G dG^{-1})^{2r+1} \right].\tag{2.46}$$

A similar calculation [Qi08a] to the one just presented shows that $N_5 [G_0] = \mathcal{C}_2$ for the second Chern number \mathcal{C}_2 characterizing the TRS preserving $(4 + 1)\text{D}$ analogue of the quantum Hall effect [Zhang01]. Along similar lines it is now straightforward to generally show

$$N_{2r+1} [G_0] = \mathcal{C}_r.\tag{2.47}$$

Eq. (2.47) makes manifest that we have exactly found what we were looking for, namely a topological invariant $N_{2r+1} [G]$ that can be formulated for an interacting system and which reproduces the non-interacting classification for the free Green's function G_0 of the non-interacting system. The topological invariance of $N_{2r+1} [G]$ is clear by analogy with Eq. (2.35): Whereas the winding number ν_{2j-1} measures the homotopy of the chiral map $k \mapsto q(k) \in U(n)$ which, properly normalized, yields an integer due to $\pi_{2j-1}(U(n)) = \mathbb{Z}$, $n > j$, Eq. (2.46) measures the homotopy of $G \in GL(n + m, \mathbb{C})$ in the $(2r + 1)\text{D}$ frequency-momentum space which is also integer due to $\pi_{2r+1}(GL(n + m, \mathbb{C})) = \mathbb{Z}$, $n + m > r$.

The dimensional hierarchy for symmetry protected descendants of a parent state which is characterized by a Chern number (see Section 2.3.2) can be constructed in a completely

analogous way for the interacting generalization N_{2r+1} of the Chern number \mathcal{C}_r [Wang10]. The resulting topological invariants for the descendant states have been coined topological order parameters in Ref. [Wang10]. Disorder can again be accounted for by imposing TBC and replacing the k -space of the system by the torus of twisting angles (see Section 2.3.3).

Interacting chiral systems

The integer invariant of chiral unitary systems (class AIII) in odd spatial dimension $2r - 1$ is not a Chern number but a winding number (see Section 2.3.1). For all these systems and dimensional hierarchies with a chiral parent state, i.e., all chiral TSM (see Tab. 2.4), a similar interacting extension of the definition of the invariants in terms of $G(i\omega, k)$ has been reported in Ref. [Gurarie11]:

$$I_{2r}[G] = n(r) \int_{\text{BZ} \times \mathbb{R}_\omega} \text{Tr} \left[Q (dQ)^{2r} \right], \quad (2.48)$$

where $n(r)$ is a normalization constant, and $Q(i\omega, k) = G^{-1}(i\omega)U_{\text{CH}}G(i\omega, k)$, with the unitary representation matrix U_{CH} of the chiral symmetry operation. In the non-interacting limit, I_{2r} reduces to ν_{2r-1} as defined in Eq. (2.35) [Gurarie11].

Fluctuation driven topological transitions

Thus far, we have shown that for a non-interacting system the integration over ω reproduces the band structure classification scheme formulated in terms of the adiabatic curvature. However, the additional frequency dependence of the single particle Green's function can cause phenomena without non-interacting counterpart. To see this, we represent the single particle Green's function of an interacting system as

$$G(\omega, k) = (i\omega - h(k) - \Sigma(\omega, k))^{-1},$$

where Σ is the self-energy of the interacting system. In Ref. [Gurarie11], it has been pointed out, that the value of $N_{2r+1}[G]$ cannot only change due to gap closings in the energy spectrum as in the case of the Chern number \mathcal{C}_r . This is due to the possibility of poles in the ω -dependence of the self-energy which give rise to zeros of the Green's function, whereas gap closings correspond to poles of G . From the analytical form of N_1 it is immediately clear that both poles and zeros of G can change the value of N_1 . More generally, the $G \leftrightarrow G^{-1}$ symmetry of N_{2r+1} makes clear that poles of G can be seen as zeros of G^{-1} and vice versa on an equal footing. In Ref. [Wang11a], it has been demonstrated that the ω -dependence of Σ can change a non-trivial winding number into a trivial one. The emergence of a topologically nontrivial phase due to dynamical fluctuations which has no non-interacting counterpart has been presented in Ref. [Budich12c]. We would like to review this new phenomenology in some detail.

To this end, let us consider a local self energy $\Sigma = \Sigma_1(k) + \Sigma_2(\omega)$ consisting of the Hartree Fock part $\Sigma_1(k)$ and the local dynamical self energy $\Sigma_2(\omega)$. The latter can be represented as

a pole expansion [Wang11b]

$$\Sigma_2(\omega) = V^\dagger(i\omega - P)^{-1}V$$

with a frequency independent Hermitian $N \times N$ matrix P , where N is the number of poles of $\Sigma_2(\omega)$ on the imaginary axis. V is an $N \times n$ matrix, where n denotes the number of bands. It has been shown [Wang11b] that N_{2r+1} of the single particle Green's function $G(k, \omega) = (i\omega + \mu - h(k) - \Sigma(k, \omega))^{-1}$ with the single particle Bloch Hamiltonian $h(k)$ can be calculated by introducing an effective extended $(n + N) \times (n + N)$ single particle Hamiltonian

$$H(k) = \begin{pmatrix} h(k) + \Sigma_1(k) - \mu & V^\dagger \\ V & P \end{pmatrix}, \quad (2.49)$$

and then calculating N_3 of the single particle Green's function $\tilde{G}(k, \omega) = (i\omega - H(k))^{-1}$. We now show that a transition from trivial to nontrivial can in principle be driven by means of local fluctuations as described by a non-scalar local self energy. While our idea is very general, let us for concreteness explicitly construct a minimal toy model for such a type of transition. Consider the two band model of the QAH insulator [Qi08a]

$$h(k) = v^i(k)\sigma_i, \quad (2.50)$$

where $v^1 = \sin(k_x)$, $v^2 = \sin(k_y)$, $v^3 = (m + \cos(k_x) + \cos(k_y))$ and m is a real parameter which tunes the sign of the band gap. Assuming an interaction which brings about two poles in the self energy, we make the following ansatz for the parameters V, P of the pole expansion

$$V = \mu\sigma_x, \quad P = \lambda\sigma_z$$

which, for the effective extended Hamiltonian, yields

$$H(k) = \begin{pmatrix} h(k) & \mu\sigma_x \\ \mu\sigma_x & \lambda\sigma_z \end{pmatrix}. \quad (2.51)$$

For $m = -2.5$, the two band model is located in its trivial regime. A two dimensional phase diagram of the single particle Hamiltonian defined in Eq. (2.51) is shown in Fig. 2.4. We find that local fluctuations can drive a system into a topologically nontrivial phase in this model. Note that $\Sigma_1(k) = 0$ in our case. Hence, exclusively $\Sigma_2(\omega)$ causes a transition which has no band structure analogue due to a gap closing in the two band Hamiltonian (2.50), and is a purely fluctuation-induced phase transition that does not connect to a static mean field ansatz.

Chern numbers of effective single particle Hamiltonians

Due to its additional ω -integration, the practical calculation of N_{2r+1} can be numerically very challenging once the single particle Green's function of the interacting system has been calculated. A major breakthrough along these lines has been reported in Ref. [Wang12d]. These authors show using the spectral representation of the Green's function that one can

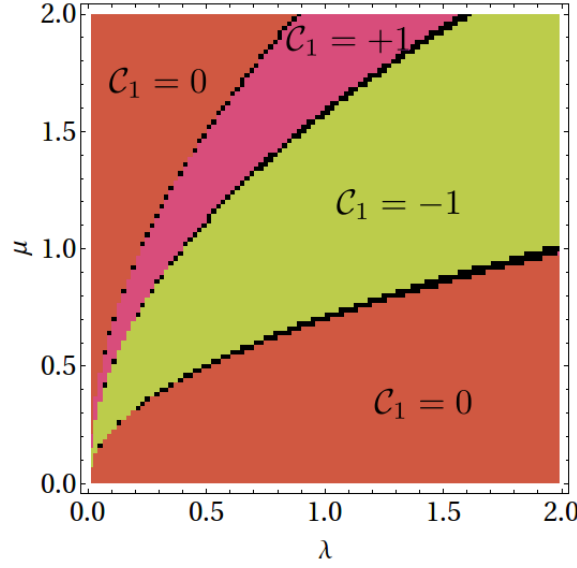


Figure 2.4: Phase diagram of the QAH insulator with local fluctuations. $m = -2.5$ is fixed. The pole structure of the local self energy encoded in λ, μ is varied. The Chern numbers \mathcal{C}_1 of the different phase domains are indicated.

always get rid of the ω -dependence of G . We only review the physical results of this analysis. The both accessible and explicit proof can be found in Ref. [Wang12d]. The physical conclusion is as elegant as simple: Instead of calculating N_{2r+1} we can just calculate the Chern number \mathcal{C}_r associated with the fictitious Hamiltonian

$$\tilde{h}(k) = -G^{-1}(0, k), \quad (2.52)$$

the occupied states of which are just its eigenstates with negative eigenvalues which have been dubbed R -zeros [Wang12d] since they are positive energy eigenstates of $G^{-1}(0, k)$. Obviously, $-G_0^{-1}(0, k) = h(k)$ for the non-interacting Green's function. Hence, $\tilde{h}(k)$, which has recently been coined topological Hamiltonian [Wang12b], adiabatically connects to $h(k)$ in the non-interacting limit. Note that the possibility of eliminating the ω -dependence is not in contradiction to the relevance of this ω -dependence for the topology of the interacting system. All it shows is that the relevant changes due to a different pole structure of G as a function of ω can be inferred from its value at $\omega = 0$. We will use the method of the fictitious Hamiltonian $\tilde{h}(k)$ in Section 2.4.2 to formulate the topological invariant of an interacting 1D TSC.

Topological Hamiltonian for chiral interacting systems

Obviously, this classification scheme just presented only pertains to non-chiral systems, the classification of which can be reduced to the Chern number classifying a unitary bundle in the same dimension (see Section 2.3). In principle, the construction of the topological Hamiltonian $\tilde{h}(k)$ can be readily generalized to chiral interacting systems. To see this, we note that the crucial argument for the construction of the topological Hamiltonian brought

forward in Ref. [Wang12d] is the following: The continuous interpolation

$$G(i\omega, k, \lambda) = (1 - \lambda)G(i\omega, k) + \lambda \left[i\omega + G^{-1}(0, k) \right]^{-1}$$

does not contain any singularities or gap closings. Thus, as long as the calculation of a topological invariant in terms of $G(i\omega, k)$ is concerned, we can also use $\tilde{G}(i\omega, k) = G(i\omega, k, \lambda = 1) = [i\omega + G^{-1}(0, k)]^{-1}$. Obviously, $\tilde{G}(i\omega, k) = [i\omega - \tilde{h}(k)]^{-1}$ is the Green's function of a fictitious non-interacting system which is governed by the topological Hamiltonian $\tilde{h}(k)$. The mere existence of the topological invariant for chiral systems in terms of $G(i\omega, k)$ as presented in Ref. [Gurarie11] (see also Eq. (2.48)) hence suffices to argue that one can equally well investigate the topology of $\tilde{h}(k)$ and its symmetry protected descendants (see Section 2.3.2) instead of directly evaluating Eq. (2.48). Since the single particle Green's function inherits the fundamental symmetries from the Hamiltonian [Gurarie11], $\tilde{h}(k)$ will also obey these symmetries. In particular, for an interacting system with chiral symmetry, the topological Hamiltonian can be brought into the flat band off-diagonal form

$$\tilde{h}(k) \simeq \begin{pmatrix} 0 & \tilde{q}(k) \\ \tilde{q}^\dagger(k) & 0 \end{pmatrix}, \quad (2.53)$$

where $\tilde{q}(k) \in U(n)$ for the topologically equivalent flat-band system. This construction generically defines a topological invariant for the chiral interacting system which adiabatically concurs with the non-interacting system: The winding number $\tilde{\nu}$ associated with the fictitious Hamiltonian $\tilde{h}(k)$. A similar construction for a chiral 1D system has been presented in Ref. [Manmana12].

Discussion of the topological Hamiltonian and practical consequences

As already mentioned above, our construction cannot be valid for arbitrary interacting systems. In particular in 1D, the breakdown of the \mathbb{Z} classification in the presence of general interactions has been investigated in Ref. [Fidkowski10]. However, this problem does not pertain to the concept of the topological Hamiltonian itself but rather reflects the limited validity of the adiabatic continuation of the non-interacting invariants in terms of the single particle Green's function, i.e., the limited validity of Eq. (2.46) and Eq. (2.48). In the validity regime of these equations, we have just shown that we can equivalently use the topological Hamiltonian $\tilde{h}(k) = -G^{-1}(0, k)$ to classify an interacting system in any symmetry class. This is of enormous practical usefulness for at least two reasons. First, we get rid of the ω -integration appearing in Eq. (2.46) and Eq. (2.48) which is cumbersome to evaluate. Second, the method of dimensional extension, though generally valid, is not always the most convenient way to calculate the topological invariant of a symmetry protected descendant state. Provided with the formal equivalence between the non-interacting classification problem of the topological Hamiltonian and the Green's function topology, we can directly apply all simplified schemes that have been introduced to directly calculate non-interacting invariants of symmetry protected states (see, e.g., Refs. [Kitaev01, Fu06, Fu07, Prodan11, Wang12a]) to the topological Hamiltonian. The framework of dimensional extension and Eq. (2.46) or

Eq. (2.48) for the parent state are, with the benefit of hindsight, only needed to justify the validity of the topological Hamiltonian.

Before closing the section, we would like to discuss the role of the bulk boundary correspondence, as introduced for non-interacting systems in Section 2.1.3, in the presence of interactions. In general, interactions can spontaneously break the protecting symmetry of a symmetry protected TSM (see Section 2.1.4) locally at the boundary thus gapping out the characteristic metallic surface states. Importantly, this spontaneous symmetry breaking at the gapless surface will typically happen at a lower critical interaction strength than in the gapped bulk. This is because the gapless surface modes offer more phase space for interactions. A generally valid bulk boundary correspondence is hence absent in the interacting case. Within the validity regime of Eq. (2.46) and Eq. (2.48) for chiral TSM, respectively, an interacting analogue of the bulk boundary correspondence has been reported in Refs. [Gurarie11, Essin11]. The main difference to the non-interacting case is that boundary zero-modes, which represent poles of the Green's function can be canceled by zeros of the Green's function as far as the calculation of topological invariants is concerned. Note that the Green's function of a non-interacting system does not have zeros.

2.4 Examples of TSM

Having analyzed the general framework for the classification and identification of TSM in the last two sections, we now turn to a more phenomenological physical discussion of two examples of TSM: The QSH state (CAZ class AII in 2D) and in particular its holographic subgap states, will be of great relevance for the more applied Part II of this thesis. The 1D TSC state (CAZ class D or BDI) is presented in more detail to practically illustrate at an accessible level virtually all concepts for the calculation of topological invariants that have been introduced in Section 2.3.

2.4.1 The QSH state

The QSH state [Kane05a, Kane05b, Bernevig06a] is, historically speaking, the first symmetry protected TSM. By symmetry protected, we here mean that upon breaking of TRS, the QSH state can be adiabatically deformed to a trivial localized insulator without any hopping (see Section 2.1.4). The QSH state is a 2D phase which preserves TRS with $\mathcal{T}^2 = -1$ and is thus located in the CAZ class AII (see Tab. 2.1). According to Tab. 2.2, the QSH phase is characterized by a \mathbb{Z}_2 invariant which has been originally identified in the framework of K-Theory and explicitly been calculated by Kane and Mele in 2005 [Kane05a, Kane05b]. These authors proposed a realization of the QSH phase in graphene with intrinsic spin orbit interaction (SOI). However, the bulk gap defining the adiabatic energy scale in this material system is only of the order $20\mu\text{eV}$ [Gmitra09] which considerably limits its experimental relevance. Shortly after this discovery, an experimentally much more promising realization of the QSH state in HgTe/CdTe quantum wells (QW) was proposed in 2006 by Bernevig, Hughes, and Zhang [Bernevig06a] and experimentally discovered in 2007 by König *et al.* [König07] in the Molenkamp lab at the University of Würzburg. In this system, the bulk band gap is tunable via the thickness t of the QW and can assume values of tens of meV [König07].

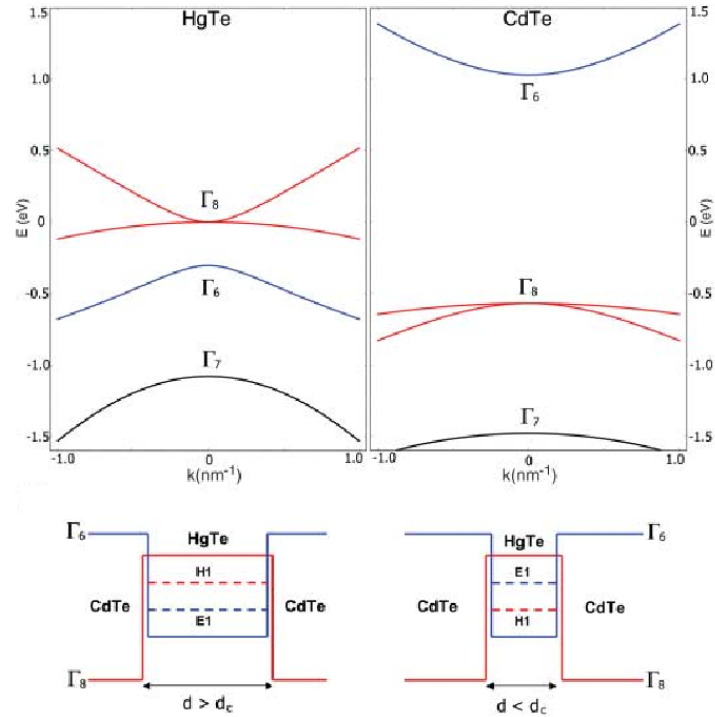


Figure 2.5: Comparison of the inverted band structure of HgTe (left) and the non-inverted band structure of CdTe (right) in the bulk (top) and in a QW geometry (bottom) [Bernevig06a].

Basic phenomenology of the QSH state in HgTe/CdTe quantum wells

The guiding idea behind the search for the QSH phase in material systems based on heavy elements such as Hg is the following: The QSH phase in graphene relies on intrinsic SOI. SOI in atoms goes with the fourth power of the proton number Z . In the II-VI semiconductor HgTe, SOI in the valence bands with orbital p -symmetry and the relativistic Darwin term shifting the conduction band electrons are so strong that the bandgap is inverted. This means that the hole-like $J = \frac{3}{2}$ bands with Γ_8 symmetry are energetically above the electron-like $J = \frac{1}{2}$ bands with Γ_6 symmetry. In contrast, the band structure in CdTe is non-inverted (see Fig. 2.5). The heterostructure proposed in Ref. [Bernevig06a] consists of a HgTe QW sandwiched between two layers of CdTe. For sufficiently large thickness of the HgTe QW, its effective 2D band structure will be inverted, i.e., the first Γ_8 2D sub-band H1 will be energetically above the first Γ_6 sub-band E1. For a very thin QW, however, the effective 2D band structure will be inherited from the surrounding CdTe, i.e., it will be non-inverted. At a critical thickness $t_c \approx 6.4\text{nm}$ of the QW, the 2D bulk gap closes. This critical Dirac point has been identified as a TQPT (see Section 2.1.5) from a trivially insulating quantum well for $t < t_c$ to the QSH state for $t > t_c$ [Bernevig06a]. The topology of this transition can be understood in a geometrically simple way: Without Rashba SOI and neglecting the rather weak bulk inversion asymmetry (BIA) term, there is a fixed spin quantization axis and the QSH effect can be decomposed into two TRS conjugated copies of the QAH state.

In the E1/ H1 basis of one spin projection the two band model for this QAH insulator reads [Bernevig06a]

$$\begin{aligned} h(k) &= \epsilon_0 \sigma_0 + d^i \sigma_i \\ d^1 &= Ak^x, \quad d^2 = -Ak^y, \quad d^3 = M - Bk^2, \quad \epsilon_0 = C - Dk^2, \end{aligned} \quad (2.54)$$

where $B < 0$. Eq. (2.54) is referred to as the Bernevig-Hughes-Zhang (BHZ) model. As long as the spectrum remains fully gapped, the gapless part ϵ_0 is irrelevant for the topological classification of the model. The total Hamiltonian $H(k)$ is given by $H(k) = \text{diag}(h(k), h^*(-k))$ where the diagonal structure is in spin space. The band gap at the Γ -point ($k = 0$) is $2M$. At $t = t_c$ the gap closing entails $M = 0$. For negative M , the unit vector \hat{d} points in the negative z -direction, for positive M , \hat{d} points in the positive z -direction at the Γ -point. Hence, the band inversion can be visualized as a pseudo spin flip of the E1/H1 pseudo spin at the Γ -point. This spin flip is exactly what distinguishes a non-trivial from a trivial QAH state since for large k , the $-Bk^2$ term dominates and tilts the spin upwards no matter what sign M has (see Fig. 2.1). By comparison with Eq. (2.7), we immediately see that the Chern number \mathcal{C}_1^+ of this QAH block can be expressed as

$$\mathcal{C}_1^+ = \frac{i}{2\pi} \int_{S^2} \mathcal{F}_+ = \frac{\epsilon^{ijk}}{4\pi} \int_{S^2} \hat{d}^i \hat{d}_x^j \hat{d}_y^k = \delta_{1, \text{sgn}(\frac{M}{B})},$$

where S^2 denotes the compactified spherical k -space. It is straightforward to show that the adiabatic curvature \mathcal{F}_- of the TRS conjugated block satisfies $\mathcal{F}_-(-k) = -\mathcal{F}_+(k)$. Thus the Chern number \mathcal{C}_1^- of the conjugated block satisfies $\mathcal{C}_1^- = -\mathcal{C}_1^+$. This relation holds generally for a TRS preserving 2D insulator which has an additional $U(1)$ spin rotation symmetry, i.e., a fixed spin quantization axis. Under these conditions the \mathbb{Z}_2 invariant ν characterizing the QSH effect can be expressed as

$$\nu = \mathcal{C}_1^+ \pmod{2} = \mathcal{C}_1^- \pmod{2}. \quad (2.55)$$

General calculation of the \mathbb{Z}_2 invariant characterizing the QSH state

As already mentioned, Eq. (2.55) is only valid in the presence of a fixed spin quantization axis. However, the notion of the QSH state is much more general as it only requires the presence of TRS with $\mathcal{T}^2 = -1$. It is hence of great practical interest to have a general recipe how to calculate ν without the assumption of additional symmetries. Such a calculation has first been presented in Ref. [Kane05b] and in a more pedagogical way in Ref. [Fu06]. Of course, we could also use the general framework outlined in Section 2.3 viewing the QSH state as a second descendant of its 4D parent state, as has been done in Ref. [Qi08a]. For pedagogical reasons, we would like to review a more recent method due to Prodan [Prodan11] which has the practical advantage of being manifestly gauge invariant and which makes the relation to our discussion of adiabatic time evolution in Section 1.2 manifest.

Let $\hat{\theta}_{\alpha\beta}(k) = \langle u_\alpha(k) | \mathcal{T} | u_\beta(k) \rangle$ be the (gauge dependent) representation matrix of the TRS operation \mathcal{T} in the subspace of occupied states at wave vector k . We assume a square lattice with unit lattice constant. The straight line $(k^x, \pi) \rightarrow (k^x, -\pi)$ is then a closed loop which we call γ_{k^x} . We denote by $\mathcal{K}_{\gamma_{k^x}}$ the non-Abelian GP associated with γ_{k^x} (see Eq. (1.14)).

Since $\mathcal{T}P(k)\mathcal{T}^{-1} = P(-k)$ it is clear that any adiabatic evolution along a not necessarily closed path in k -space maps to a TRS conjugated evolution by simply mapping $k \rightarrow -k$. With that, we decompose $\mathcal{K}_{\gamma_{k^x}}$ into two Kato propagators (see Eq. (1.12)) as

$$\mathcal{K}_{\gamma_{k^x}} = \mathcal{K}^{k^x}(\pi, 0)\mathcal{K}^{k^x}(0, -\pi) = \mathcal{K}^{k^x}(\pi, 0)\mathcal{T}\left(\mathcal{K}^{k^x}(\pi, 0)\right)^\dagger\mathcal{T}^{-1}. \quad (2.56)$$

It is elementary to show [Prodan11] that for the representation matrix $(\mathcal{TO}(k))_{\alpha\beta} = \langle u_\alpha(k)|\mathcal{TO}|u_\beta(k)\rangle$, where $O(k)$ is an arbitrary linear operator, the identity

$$(\mathcal{TO}(k))_{\alpha\beta} = \left(\hat{\theta}(k)O^*(k)\right)_{\alpha\beta} \quad (2.57)$$

holds. Plugging Eq. (2.57) into Eq. (2.56) yields

$$\hat{\mathcal{K}}_{\gamma_{k^x}} = \hat{\mathcal{K}}^{k^x}(\pi, 0)\hat{\theta}(k^x, 0)\left(\hat{\mathcal{K}}^{k^x}(\pi, 0)\right)^T\hat{\theta}^{-1}(k^x, \pi),$$

where the hat on the Kato propagators indicates representation matrices in an arbitrary gauge at $(k^x, 0)$ and $(k^y, \pm\pi)$ in which the $\hat{\theta}$ -matrices of the TRS operation are represented. In the following, we are only interested in the gauge independent determinant of the above expression, i.e.,

$$\det\left\{\hat{\mathcal{K}}_{\gamma_{k^x}}\right\} = \det\left\{\hat{\mathcal{K}}^{k^x}(\pi, 0)\right\}^2 \det\left\{\hat{\theta}(k^x, 0)\right\} \det\left\{\hat{\theta}^{-1}(k^x, \pi)\right\}. \quad (2.58)$$

The two loops connecting the four time reversal invariant momenta (TRIM) also used for the classification in Ref. [Fu06] are given by γ_0 and γ_π . At the TRIM, $\hat{\theta}$ is antisymmetric so that its Pfaffian is well defined. Hence, we can take the square-root of Eq. (2.58) which yields

$$\Xi_{k^x} = \frac{\det\left\{\hat{\mathcal{K}}^{k^x}(\pi, 0)\right\} \text{Pf}\left\{\hat{\theta}(k^x, 0)\right\} \text{Pf}\left\{\hat{\theta}^{-1}(k^x, \pi)\right\}}{\sqrt{\det\left\{\hat{\mathcal{K}}_{\gamma_{k^x}}\right\}}} = \pm 1, \quad k^x = 0, \pi. \quad (2.59)$$

For each individual loop, the sign on the right hand side of Eq. (2.59) is arbitrary since it depends on the branch of the square root which is not fixed. However, the sign of the product $\Xi_0\Xi_\pi$ is well defined since the branch of $\sqrt{\det\left\{\hat{\mathcal{K}}_{\gamma_{k^x}}\right\}}$ can be chosen identically for both loops by interpolating continuously between them [Prodan11]. If this common choice of the branch is assured, the sign of $\Xi_0\Xi_\pi$ represents the desired generalization of the \mathbb{Z}_2 invariant defined in Eq. (2.55) to systems without additional unitary symmetries:

$$(-1)^\nu = \Xi_0\Xi_\pi. \quad (2.60)$$

The practical calculation of the Kato propagators entering the definition of Ξ_{k^x} , $k^x = 0, \pi$ is readily achieved at least numerically using Eq. (1.17).

Bulk boundary correspondence and helical edge states

In Section 2.1.3, we explicitly demonstrated the correspondence between the edge states of the QAH state and its bulk Chern number. The phenomenology of the bulk boundary correspondence of the QSH state is most conveniently understood if we begin with a representative with fixed spin quantization axis. As already mentioned, with this additional $U(1)$ -symmetry, the QSH phase can be understood as two uncoupled TRS conjugated copies of the QAH effect. Hence, the bulk boundary correspondence holds for each of the uncoupled QAH blocks separately. Performing an analysis which is completely analogous to the one presented in Section 2.1.3 for the BHZ model of the QSH effect, we find two chiral edge modes with opposite chirality and spin polarization which are TRS conjugated to each other. This characteristic pair of subgap modes has been coined helical edge states [Wu06]. Like the bulk Chern number of a QAH sample counts the number of chiral edge modes, the \mathbb{Z}_2 invariant ν can also be intuitively understood at the level of the bulk boundary correspondence: An even number of Kramers pairs can be gapped out by virtue of local scatterers, whereas an odd number of Kramers pairs is protected by TRS [Wu06, Fu06, Qi11]. Looking at Eq. (2.55) immediately establishes the one to one correspondence between the bulk topological invariant ν and the parity of the number of Kramers pairs at the edge. In the absence of the additional $U(1)$ symmetry, the QSH state cannot simply be represented as two copies of the QAH state but is still adiabatically connected to such a representation without breaking TRS. Since a single Kramers pair of subgap modes at the edge cannot be adiabatically removed from the spectrum of the sample without breaking TRS [Kane05a, Fu06], the helical edge modes are still present in this more general situation. However, the Kramers partners representing the helical pair in general have a spin quantization axis that depends on both position and energy. This limits the physical observability of the QSH effect: Whereas the spin Hall conductivity is topologically quantized in the presence of a fixed spin quantization axis, only a generalized twisted spin [Sugimoto12] is conserved and can be assigned a quantized conductivity in the presence of SOI.

The QSH phase is in principle a promising candidate as to spintronics applications due to its quantized dissipationless edge conductance. However, thus far not many concrete devices have been proposed. For example, it is not immediately clear how to build a transistor, since the QSH phase in a single HgTe well cannot be readily switched on and off by electric means. Recently, several composite realizations of the QSH phase have been predicted [Liu08, Michetti12] which resolve this problem: In these setups, the QSH phase and with that the existence of edge channels can be locally tuned by virtue of a gate voltage.

2.4.2 The Majorana wire

The key feature of a 1D TSC [Kitaev01, Lutchyn10, Oreg10, Beenakker11], also known as the Majorana wire, is a holographic single Majorana bound state (MBS) associated with each of its ends which is topologically protected by PHS. The recently proposed realization of the 1D TSC in an InSb nanowire with strong SOI and proximity induced s-wave superconductivity [Lutchyn10, Oreg10] is so far the most promising candidate as to its experimental feasibility. Very recently, first experimental signatures of MBS have been reported by several experi-

mental groups [Mourik12, Deng12, Das12], however, it should be mentioned that alternative explanations for robust zero bias resonances not owing to Majorana zeromodes have been brought forward [Bagrets12, Liu12].

Note that PHS in this class of systems does not imply a true limitation on the band structure of the normal-conducting spin orbit coupled quantum wire but is emergent from the Bogoliubov-deGennes (BdG) mean field description of superconductivity. Without additional symmetries, the 1D TSC generically belongs to the CAZ class D and is characterized by a \mathbb{Z}_2 topological invariant (see Tab. 2.2). An additional chiral symmetry present in the ideal model systems proposed in Refs. [Lutchyn10, Oreg10] promotes the \mathbb{Z}_2 invariant characterizing the presence of an unpaired MBS to a \mathbb{Z} invariant [Ryu02, Tewari11] counting the number of zeromodes at each edge. However, perturbations modifying the SOI as well as magnetic impurities can break the chiral symmetry and gap out paired MBS.

In this section, we demonstrate the concepts introduced in Sections 2.3.3 and 2.3.4 to include disorder and adiabatic interactions into the classification scheme. We present the \mathbb{Z}_2 -classification of the 1D TSC phase in terms of its single particle Green's function along the lines of Section 2.3.4 and Ref. [Budich12e], respectively. In a first step, we work out explicitly a dimensional extension procedure (see Section 2.3.2) for a realization of the 1D TSC in a nanowire with strong SOI and proximity induced s-wave superconductivity [Lutchyn10, Oreg10]. This allows us to reduce the topological classification of the 1D TSC to the calculation of the first Chern number of its parent state, the $p + ip$ superconductor in 2D, CAZ class D . As explained in Section 2.3.2, this classification of the parent state concurs with that of the unitary (CAZ class A) state in 2D, i.e., the QAH state.

This procedure fits into the general classification framework of topological field theory (TFT) proposed for time reversal invariant topological insulators in Refs. [Qi08a, Wang10] and allows for a reformulation of the invariant in terms of the single particle Green's function (see Section 2.3.4). Upon switching on interactions adiabatically, our classification remains valid for Luttinger liquid like interactions as was argued in Ref. [Volovik03]. Thereafter, we employ the recently proposed topological Hamiltonian [Wang12d, Wang12b] (see Section 2.3.4) showing that the interacting invariant can be expressed in terms of the zero frequency single particle Green's function of the physical 1D system, which is independent of the previously introduced extra dimension (see Section 2.3.4 for the general framework). Finally, we demonstrate how a hybrid approach of TBC [Niu85] (see also Section 2.3.3) in the physical dimension and periodic boundary conditions in the extra dimension can be used to additionally include disorder at the level of the bulk topological invariant, i.e., without probing the presence of unpaired MBS, quantized zero bias resonances, or other finite size effects. The topological invariants of TSC in 2D and 3D have been discussed in Ref. [Wang12c].

Model of the 1D TSC

A lattice model of the 1D TSC [Lutchyn10, Tewari11] can be cast into the form $H = \int \Psi^\dagger \mathcal{H}_{\text{BdG}} \Psi$, where the basis is chosen such that $\Psi = (\psi_\uparrow, \psi_\downarrow, \psi_\uparrow^\dagger, \psi_\downarrow^\dagger)$. In this basis,

$$\mathcal{H}_{\text{BdG}} = \begin{pmatrix} H_0 & \delta \\ \delta^\dagger & -H_0^* \end{pmatrix}.$$

For the 1D TSC, $H_0(k) = \xi_k + B\sigma_x + u \sin(k)\sigma_y$ is the Hamiltonian of a single channel quantum wire in the presence of a B -field induced Zeeman splitting and Rashba SOI. The proximity induced s-wave superconducting gap is of the form $\delta = \begin{pmatrix} 0 & -\Delta \\ \Delta & 0 \end{pmatrix}$ and $\xi_k = 1 - \cos k - \mu$. Introducing the set of Pauli-matrices τ_i for the particle hole pseudo spin, the BdG Bloch Hamiltonian reads

$$H_{\text{BdG}}(k) = (\xi_k + B\sigma_x + u \sin(k)\sigma_y) \tau_z + \Delta \sigma_y \tau_y. \quad (2.61)$$

In this representation, the PHS operation has the intuitive form

$$C = \tau_x K, \quad (2.62)$$

where K denotes complex conjugation. Let us very briefly review the salient physics starting from the continuum model obtained from Eq. (2.61) by substituting $\sin(k) \rightarrow k$, $\cos(k) \mapsto 1 - \frac{k^2}{2}$. For $B = \Delta = 0 \neq u$, the band structure consists of two particle hole symmetric copies (emergent from the BdG picture) of the shifted Rashba parabolae. The lattice regularization in Eq. (2.61) is introduced to make the topological invariants well defined. $\Delta \neq 0$ gaps out the system in its entire Brillouin zone (BZ). For small k this gap competes with a Zeeman gap due to $B \neq 0$ leading to a band inversion at $B^2 = \mu^2 + \Delta^2$. For $B^2 > \mu^2 + \Delta^2$ we have a TSC with a single MBS associated with each end of a finite wire.

Dimensional extension

Following the general outline in Section 2.3.2, we explicitly perform a dimensional extension introducing an extra coordinate v , thus reducing the topological classification of the non-interacting model to the analysis of the QAH effect of the extended 2D system. The idea is quite simple: Our system cannot be deformed into a trivial 1D superconductor without breaking PHS which provides the topological protection of the TSC phase. However, breaking this symmetry we can deform the TSC, say upon varying v from 0 to π , into a trivial 1D superconductor without ever closing the bulk gap of the instantaneous system. As pointed out in Section 2.3.2, it is crucial to perform the particle hole conjugated interpolation to the same trivial state for $v \in [-\pi, 0]$ in such a way that the resulting 2D system is 2π -periodic in v . Then, the extended 2D system is again in the CAZ class D and its first Chern number \mathcal{C}_1 , is well defined up to even integers. This means that a \mathbb{Z}_2 information $\nu = \mathcal{C}_1 \pmod{2}$ is well defined and only depends on the physical 1D system. It is worth noting that finding a suitable interpolation is nontrivial and requires some insight into the physical mecha-

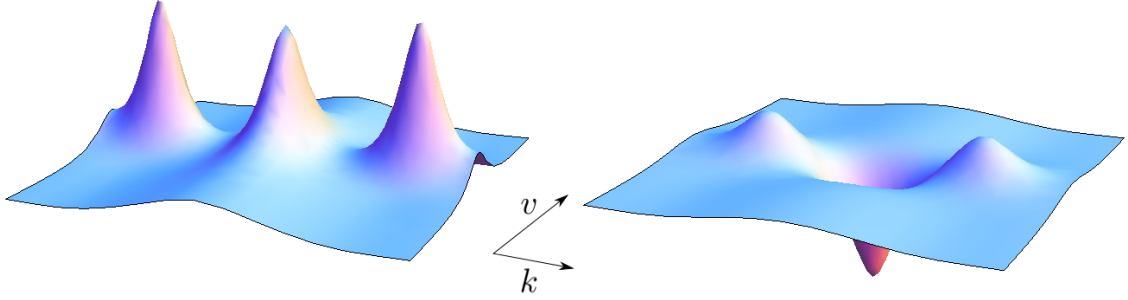


Figure 2.6: 3D plot of the Berry curvature $\mathcal{F}(k, v)$ for nontrivial parameters ($B = 1.5$) (left) and trivial parameters ($B = 0.4$) (right). $u = \Delta = 2\beta = 1$, $\mu = 0$ in both plots.

nisms underlying the model. In the following, we will explicitly present an extension which works for a generic 1D TSC and can also be used later on for the disordered interacting system.

The guiding physical idea is as follows: Switch on a particle hole breaking gap $\sim \sin(v)\tau_x$ which will keep the gap open for $v \neq 0, \pi \pmod{2\pi}$. Destroy the band inversion by a term $\sim \beta(2 - 2\cos v)\sigma_y\tau_y$ which vanishes for the physical model ($v = 0$) and will for sufficiently large β produce a trivial superconducting phase for $v = \pm\pi$ where it enhances the superconducting gap by 4β . In summary, the Wess-Zumino-Witten (WZW) [Witten83] extended Hamiltonian reads

$$\mathcal{H}_{\text{WZW}}(k, v) = H_{\text{BdG}}(k) + \sin(v)\tau_x + \beta(2 - 2\cos v)\sigma_y\tau_y.$$

Integrating the Berry curvature \mathcal{F} of this Hamiltonian over the (k, v) BZ indeed yields

$$\mathcal{C}_1 = \frac{1}{2\pi} \int_{\text{BZ}} \mathcal{F} = \theta(B^2 - \Delta^2 - \mu^2),$$

valid for parameters close enough to the band inversion that no artificial level crossings which depend on the details of the lattice regularization occur.

In Fig. 2.6, we compare the Berry curvature of an extension of a nontrivial 1D TSC with that of a trivial superconducting wire. In the extra dimension v , the modulus of the curvature is smoothly decaying without any notable difference between the trivial and the nontrivial case. This is reflected in our derivation below, which shows that the topological invariant of the translation-invariant system can be defined in terms of its single particle Green's function without reference to the extra dimension. Note that this picture changes in the framework of TBC as introduced to account for the presence of disorder as is discussed below and shown in Fig. 2.7.

Single particle Green's function topology

We now consider the possibility of including interactions into the proposed classification scheme by generalizing the Chern number of the non-interacting system to a topological

invariant of the single particle Green's function in combined frequency-momentum space, as has been proposed for time reversal invariant topological insulators in 2D and 3D [Wang10] (see also Section 2.3.4).

In 1D, interactions play a peculiar role generically leading to non-Fermi-liquid behavior. From a viewpoint of perturbation theory interactions are therefore considered to be non-adiabatic in 1D, as no meaningful quasiparticles can be defined (see Section 3.1). However, it has been argued [Volovik03] that the Fermi surface properties as described by the momentum space topology of the single particle Green's function are still adiabatically connected to those of the non-interacting system. Hence, the framework discussed Section 2.3.4 should be applicable for this kind of interactions.

Rewritten in terms of the single particle Green's function $G(\omega, p)$ of the extended system, i.e., $G_0(\omega, p) = (i\omega - \mathcal{H}_{\text{WZW}}(p))^{-1}$ for the special case of the non-interacting system, the \mathbb{Z}_2 invariant ν reads (see also Eq. (2.46))

$$\nu = \frac{\epsilon^{\mu\nu\rho}}{24\pi^2} \int_{BZ \times \mathbb{R}_\omega} \text{Tr} \left[G G_\mu^{-1} G G_\nu^{-1} G G_\rho^{-1} \right] \pmod{2},$$

where $G_\mu^{-1} = \partial_\mu G^{-1}$, $\mu = 0, 1, 2 = \omega, k, v$. As discussed in Section 2.3.4, an invariant of this form can be simplified by introducing a generalized Berry curvature $\tilde{\mathcal{F}} = -i \sum_{R\text{-zeros}} (d\langle p, \alpha | \wedge d|p, \alpha \rangle)$ associated with the topological Hamiltonian $\tilde{h} = -G^{-1}(0, p)$, which takes into account the eigenvectors $|p, \alpha\rangle$ of $G^{-1}(0, p)$ with positive eigenvalues, the so called R-zeros [Wang12d] (see also Section 2.3.4). The \mathbb{Z}_2 invariant then takes the form of a Chern number, i.e.

$$\nu = \frac{1}{2\pi} \int_{BZ} \tilde{\mathcal{F}} \pmod{2}.$$

As has been shown for the non-interacting case in Ref. [Qi08a], the \mathbb{Z}_2 classification of the particle hole symmetric 1D system can then be further simplified to

$$\nu = 2P(0) \pmod{2} = \frac{1}{\pi} \int_0^{2\pi} dk \tilde{\mathcal{A}}(k) \pmod{2}, \quad (2.63)$$

where $P(0)$ is the charge polarization of the physical 1D system and

$$\tilde{\mathcal{A}}(k) = -i \sum_{R\text{-zeros}} \langle k, \alpha | d|k, \alpha \rangle$$

is the generalized Berry connection restricted to the physical system at $v = 0$, i.e., at $p = (k, 0)$. Note that this general form does no longer depend on the dimensional extension procedure and can be calculated once the zero frequency single particle Green's function $G(0, k)$ is known. Finally, the \mathbb{Z}_2 -invariant can be practically calculated by formal analogy to the non-interacting case by calculating the Majorana number [Kitaev01] defined in terms of the Pfaffian of the topological Hamiltonian \tilde{h} in Majorana representation.

Disorder and Twisted Boundary Conditions

Our formulation so far has been relying on translation-invariance which implies the existence of a BZ. This description will thus no longer be applicable in the presence of disorder. To this end, the concept of TBC has been introduced to topologically classify quantum Hall systems in the absence of translation-invariance [Niu85]. As long as a bulk mobility gap is present, the Green's function is exponentially bounded in real space for energies in this gap. Under these conditions, Niu *et al.* [Niu85] showed that the Hall conductivity can be represented as a constant ground state Berry curvature with the wave vector replaced by the twisting angles θ, ϕ of the TBC (see also Section 2.3.3). In this formalism, the Hall conductivity σ_{xy} reads

$$\sigma_{xy} = 2\pi i G_0 \left(\left\langle \frac{\partial \psi_0}{\partial \theta} \middle| \frac{\partial \psi_0}{\partial \phi} \right\rangle - \left\langle \frac{\partial \psi_0}{\partial \phi} \middle| \frac{\partial \psi_0}{\partial \theta} \right\rangle \right) = 2\pi i G_0 \mathcal{F}_{\theta\phi} = G_0 \int_{T^2} \frac{i\mathcal{F}_{\theta\phi}}{2\pi}, \quad (2.64)$$

where ψ_0 denotes the ground state wave function and $G_0 = \frac{e^2}{h} = \frac{1}{2\pi}$ is the quantum of conductance. In the last equality of Eq. (2.64), the independence of $\mathcal{F}_{\theta\phi}$ on the twisting angles [Niu85] has been used to make the topological quantization of σ_{xy} manifest by representing it as G_0 times the Chern number of the $U(1)$ -bundle over the torus T^2 of the twisting angles (θ, ϕ) . Since in this example, we consider a disordered 1D system, we can without loss of generality assume translation-invariance in the extra dimension. Integrating over the momentum v associated with the direction of translational invariance is equivalent to evaluating Eq. (2.64) for $\theta = 0$ for the special case of a system with translational invariance in x -direction. Within this hybrid approach of twisted boundary conditions in the physical dimension and v -momentum integration in the extra dimension, the Chern number of the extended 2D system in the presence of this stripe-like disorder can be expressed as

$$C_1 = \int_{-\pi}^{\pi} dv \int_{-\pi}^{\pi} d\phi \frac{\hat{\mathcal{F}}_{v\phi}}{2\pi} = \int_{-\pi}^{\pi} dv \hat{\mathcal{F}}_{v\phi} \quad (2.65)$$

where $\hat{\mathcal{F}}$ is the Berry curvature on the “mixed” torus defined by the wave vector in v -direction and the twisting angle ϕ of the TBC imposed in the physical direction. The first equality sign in Eq. (2.65) makes the integer quantization of our topological invariant manifest, whereas the second equality sign follows from the independence of $\int_{-\pi}^{\pi} dv \hat{\mathcal{F}}_{v\phi} = \mathcal{F}_{\theta\phi}|_{\theta=0}$ of the twisting angle ϕ . The main advantage of Eq. (2.65) as compared to the general 2D case (see Eq. (2.64)) is that only the eigenstates of a 1D system have to be calculated to evaluate the topological invariant which is numerically less costly. This program allows for a topological classification of disordered systems with periodic boundaries, i.e., without explicitly probing the presence of unpaired MBS. For non-interacting systems with closed boundary conditions, the influence of disorder on the 1D TSC phase has been studied using a scattering matrix approach [Akhmerov11, Brouwer11a, Brouwer11b].

In Fig. 2.7, we show the mixed Berry curvature $\hat{\mathcal{F}}_{v,\phi}|_{\phi=0}$ for a weakly disordered system ($\gamma = 1$) in the topologically nontrivial phase and a strongly disordered trivial system ($\gamma = 5$). Here, γ is the strength of a scalar Gaussian onsite potential. Note that in contrast to the

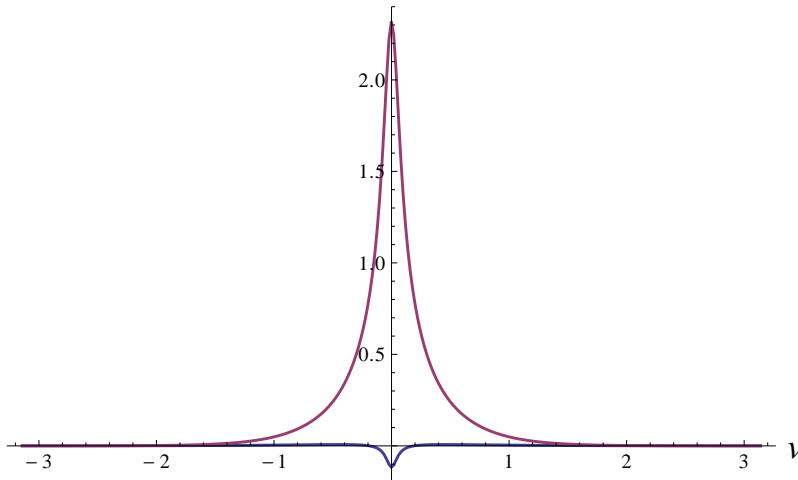


Figure 2.7: Plot of the Berry curvature $\hat{\mathcal{F}}_{v,\phi}\big|_{\phi=0}$, for nontrivial parameters ($\Delta = 0.7$, $\gamma = u = B = \beta = 1$, $\mu = 0$) (purple) and trivial parameters ($\Delta = 0.7$, $\gamma = 5$, $u = B = \beta = 1$, $\mu = 0$) (blue). Wire length 100 sites in both plots.

translation-invariant case (see Eq. (2.63)) the topology is determined by the ν -dependence of the mixed Berry curvature. Finally, we would like to point out that even for $\gamma = 1$, the onsite potential fluctuations significantly exceed the bulk insulating gap of the 1D TSC. The disorder-induced transition from nontrivial to trivial takes place at disorder strengths which are, depending on the other model parameters typically three to five times larger than the bulk gap which is in agreement with recent results obtained from level spectroscopy of a 1D TSC with closed boundary conditions [Cook12]. Note however, that we only consider short ranged disorder, short ranged as measured by the Fermi wavelength. The wave-function can self-average on the length scale of the Fermi wavelength which considerably weakens the effect of disorder on the level spectrum.

2.5 Limitations of the framework of TSM

Before closing the chapter we would like to point out some limitations of the concept of TSM. The two main aspects that one could see critical in the field of TSM are outlined in the following.

First, whereas the topologically quantized Hall conductivity in the integer quantum Hall state, the historical role model of all TSM, is a physical observable, the topological invariants of symmetry protected TSM like the QSH state (see Section 2.4.1) are not directly physically observable without additional unitary symmetries. The quantum Hall effect can be understood in terms of the spectral flow associated with the threading of a flux tube [Avron90]. Along similar lines, the QSH effect can be understood in terms of a spin charge separation associated with the threading of a spin flux [Qi08b]. However, this spin flux, as opposed to an ordinary magnetic flux tube, has no known experimental realization.

Second, the entire construction and classification of TSM is based on single particle Hamiltonians. In Section 2.3.4, we discussed how adiabatic interactions can be taken into account and argued that interactions of moderate strength are not likely to destroy the phenomenology of TSM. In order to position the field of TSM in a broader context, we would like to point out that there are also phenomena of topological origin which emerge only due to the presence of interactions. The historically first phenomenon is the $\frac{1}{\nu}$ FQH effect [Stormer83, Laughlin83] which cannot be adiabatically connected to an insulating non-interacting state. The non-interacting state is in this case a partially filled Landau level which provides an enormous density of states at the Fermi energy. In a system with periodic boundaries, the $\frac{1}{\nu}$ FQH has a characteristic ν -fold ground state degeneracy. Interestingly, this simplest FQH state can still be analyzed in the framework of TBC [Niu85]. For more general FQH systems the concept of topological order has been introduced by Wen [Wen90]. A crucial notion in this framework is the quantum dimension of the topologically ordered system which can be viewed as the ground state degeneracy of the system on a torus, i.e., with periodic boundary conditions. All TSM have quantum dimension one, like a trivial insulator. From the vantage point of topological order, all states discussed in this chapter are thus trivial. Recently, the concepts of TSM and topological order have been combined to the definition of the fractional Chern insulator [Tang11, Sun11, Neupert11] and the fractional topological insulator [Bernevig06b, Levin09, Maciejko10, Swingle11], a translation-invariant realization of the FQH and its symmetry protected analogues, respectively.

Chapter 3

Non-equilibrium quantum transport in interacting 1D systems

This chapter is dedicated to the discussion of some elementary elements of non-equilibrium quantum transport in interacting 1D systems. We first very briefly review the method of Abelian bosonization and its application to Tomonaga Luttinger liquids, mainly to establish our notation. Thereafter, we introduce the Keldysh formalism as the non-equilibrium analogue of zero-temperature perturbation theory. This formalism is readily made for perturbative quantum transport calculations at finite bias voltage. Interestingly, this non-equilibrium theory can be used for finite temperature calculations under fairly general conditions without a construction that corresponds to the Matsubara formalism in equilibrium perturbation theory. Since our main application of this transport theory in Part II will be dealing with the helical edge states realized at the boundary of a QSH sample (see Section 2.4.1), we finally point out some peculiarities of the so called helical Tomonaga Luttinger liquid (hTLL) [Wu06] representing a single pair of helical edge states in the presence of Coulomb interaction.

3.1 Electron-electron interaction in one spatial dimension

In a system with spatial dimension larger than one, repulsive Coulomb interaction can be switched on adiabatically in a broad class of systems which leads to the notion of the Fermi liquid [Landau57]. The quasiparticles of this Fermi liquid have well defined momentum and are characterized by their effective mass and charge just like electrons in a free Fermi gas but with renormalized effective parameters. Close to the Fermi surface, the lifetime of these quasi-particles diverges, which renders them well defined excitations as far as the physics at sufficiently low energy scales is concerned. In 1D, the phenomenology is fundamentally changed since no fermionic quasi-particles that adiabatically connect the non-interacting electrons can be defined [Voit95]. Instead, bosonic electron-hole excitations are the elementary excitations of the electron gas in 1D. In this section, we outline how this observation can be used to construct an effective bosonic low energy theory of the interacting fermionic 1D system, the so called Tomonaga Luttinger liquid (TLL) [Tomonaga50, Luttinger63, Mattis65, Haldane81], see Refs. [Schönhammer97, Voit95, von Delft98, Grabert01, Giamarchi04] for excellent review articles and textbooks. The low energy fixed point theory of the TLL remains quadratic in the bosonic fields and thus exactly solvable in the presence of interactions [Haldane81]. We first motivate phenomenologically why a bosonic description of a fermionic system in 1D is possible and thereafter review very briefly the procedure of Abelian algebraic bosonization.

3.1.1 Spatial dimension and transmutation statistics

Let us think of indistinguishable particles as hard balls which cannot penetrate each other. Since the particles are indistinguishable, the proper configuration space \tilde{X}_N of N indistinguishable particles is a quotient space of the N -fold direct product of the single particle spaces X modulo the symmetric group S_N of permutations, i.e., $\tilde{X}_N = X^N/S_N$ [Laidlaw71, Dowker72, Leinaas77]. In this space, points which can be obtained by exchanging particle labels are identified. In spatial dimension $d = 3$ this space for $N = 2$ has only two connected components. This can be intuitively understood if one considers that in the unrestricted configuration space every closed loop of a particle can be contracted to a point without penetrating the second particle. However, there are loops in \tilde{X}_2 which interchange the particle coordinates and are not contractible. This \mathbb{Z}_2 topology of \tilde{X}_2 with $X = \mathbb{R}^3$ leads to the conclusion that there can only be two types of particles, namely fermions and bosons in 3D [Laidlaw71, Leinaas77]. In 2D, the situation is more complicated. The difference can again be understood at a very intuitive level: Loops of one particle which have a different winding number around the position of the other particle cannot be deformed into each other as long as the two particles cannot penetrate each other. This gives rise to a configuration space of two indistinguishable particles which has an infinite number of connected components. As a consequence, there are infinitely many types of particles, so called anyons, in 2D [Laidlaw71, Leinaas77]. In a 1D world, particles cannot be exchanged at all without penetrating each other. This illustrates why particles in 1D will behave collectively and why it should be in principle possible to switch between a fermionic and a bosonic description of a 1D system of indistinguishable particles.

3.1.2 Bosonization and the Tomonaga Luttinger Liquid

We consider a 1D lattice of spinless free fermions with unit lattice constant and L sites. Close to the Fermi energy E_F , the spectrum can be linearized. This gives rise to two branches, with opposite constant slope v_F , called the left-moving and the right-moving branch which are denoted by $p = \pm$ (see Fig. 3.1). As long as only the physical properties of the model at energies close to the Fermi energy are concerned, this linearization is a reasonable approximation. When extending the linearized model to states with negative energy, only inert states that do not affect the low energy physics are added. As already mentioned, the elementary excitations of the 1D electron gas can be represented as particle hole excitations which are closely related to the Fourier components of the density operator

$$\rho_p(q) = \sum_k c_p^\dagger(k) c_p(k+q), \quad p = \pm$$

where $c_p(k)$ is the electronic annihilation operator for a p -mover with wave vector k of the extended linearized model. These Fourier components satisfy the commutation relations [Giamarchi04]

$$[\rho_p(q), \rho_{p'}(q')] = \frac{pqL}{2\pi} \delta_{p,p'} \delta_{q,-q'} \quad (3.1)$$

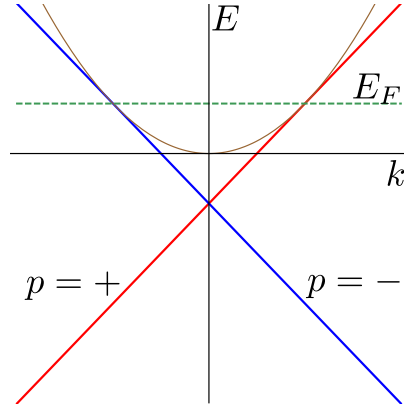


Figure 3.1: Spectrum of the free electron gas (brown) with linear approximation around the Fermi energy E_F that is continued to negative energies yielding a branch of right-movers (red) and left-movers (blue).

which is at the heart of the bosonization procedure. From Eq. (3.1) the construction of the operators

$$b_q = -i\sqrt{\frac{2\pi}{L|q|}} \sum_{p=\pm} \theta(pq)\rho_p(q) \quad (3.2)$$

with the Heaviside step-function θ , that satisfy the bosonic algebra

$$[b_q, b_{q'}^\dagger] = \delta_{q,q'}$$

is straight-forward. In Ref. [Haldane81], Haldane proved that the states

$$|N_+, N_-, \{m_q\}_{q \neq 0}\rangle = \left(\prod_{q \neq 0} \frac{(b_q^\dagger)^{m_q}}{\sqrt{m_q!}} \right) |N_+, N_-\rangle_0$$

form a basis of the Fock space of our linear 1D model. Here, $|N_+, N_-\rangle_0$ is the fermionic ground state of a system with $N_p \in \mathbb{Z}$ excess p -movers as compared to the Fermi sea. To represent the entire model in bosonic language we would like to express the fermionic field operators $\psi_p(x)$ in terms of the b_q operators. Obviously, the b_q operators conserve the number of fermions whereas $\psi_p(x)$ annihilates a fermion. Therefore, we need an operator η_p which commutes with the b_q but changes the number of p -movers by one. Such an operator can be defined by

$$\eta_p |N_p, N_{-p}\rangle = p^{N_p} |N_p - 1, N_{-p}\rangle.$$

The operators are called Klein factors and obey the algebra,

$$\{\eta_p, \eta_{p'}^\dagger\} = 2\delta_{p,p'}$$

with all other anti-commutators vanishing. We define the so called bosonic phase fields as

$$\phi_p(x) = \frac{p}{\sqrt{2L}} \sum_{q \neq 0} \theta(pq) \frac{e^{iqx} e^{-a|q|/2}}{\sqrt{|q|}} b_q,$$

where a is a short distance cutoff regularizing the divergence in the commutators of the bosonic phase fields for equal points in space. The chiral hermitian fields are the linear combinations

$$\Phi_p(x) = \phi_p(x) + \phi_p^\dagger(x). \quad (3.3)$$

With these definitions, the fermionic field operator can be represented as (see [Grabert01] for a step by step derivation)

$$\psi_p(x) = \frac{\eta_p}{\sqrt{2\pi a}} e^{ip(k_F + 2\pi \hat{N}_p/L)x + \sqrt{4\pi} ip \Phi_p(x)}, \quad (3.4)$$

where \hat{N}_p is the number operator of the p -moving electrons. The $\frac{\hat{N}_p}{L}$ term in the exponent on the right hand side of Eq. (3.4) is a $q = 0$ contribution which can be neglected in the limit $L \rightarrow \infty$. Throughout this thesis, the influence of these so called zero-modes will always be neglected which we will make manifest by dropping the mentioned $1/L$ -term from now on. For $|x - x'| \gg a$, the commutator of the chiral hermitian fields reads

$$[\Phi_p(x), \Phi_{p'}(x')] = \frac{ip\delta_{p,p'}}{4} \text{sgn}(x - x'). \quad (3.5)$$

The chiral hermitian field Φ_p is directly related to the density $\rho_p(x)$ of p -moving electronic excitations via the relation [Grabert01]

$$\partial_x \Phi_p(x) = \sqrt{\pi} \rho_p(x).$$

For practical calculations, we will often times use the non-chiral fields

$$\begin{aligned} \varphi &= \Phi_+ + \Phi_-, \\ \theta &= \Phi_+ - \Phi_-. \end{aligned} \quad (3.6)$$

The total density ρ and the current density j can be readily expressed in terms of these fields as

$$\begin{aligned} \rho(x) &= \rho_+(x) + \rho_-(x) = \frac{1}{\sqrt{\pi}} \partial_x \varphi(x), \\ j(x) &= ev_F(\rho_+(x) - \rho_-(x)) = \frac{ev_F}{\sqrt{\pi}} \partial_x \theta. \end{aligned} \quad (3.7)$$

From Eq. (3.5) and Eq. (3.6) it is immediately clear that $\Pi_\varphi(x) = -\partial_x \theta(x)$ is the conjugate momentum of φ , i.e.,

$$[\varphi(x), \Pi_\varphi(y)] = i\delta(x - y). \quad (3.8)$$

The free Hamiltonian H_0 of the non-interacting 1D model with linear dispersion can then be expressed as

$$H_0 = \frac{v_F}{2} \int_{-\frac{L}{2}}^{+\frac{L}{2}} dx \left[\Pi_\varphi^2(x) + (\partial_x \varphi(x))^2 \right].$$

The main advantage of this bosonic representation is that the Hamiltonian remains quadratic if one includes Coulomb interaction into the picture: Forward-scattering terms due to local Coulomb interaction only renormalize the model parameters and the backscattering term can in the spinless case be viewed as a Pauli exchange term of the forward scattering (see [Grabert01] for a more detailed discussion). At this level of rigor, short ranged Coulomb interaction enters the low energy fixed point theory only through a single parameter g , where $g = 1$ is the non-interacting case, $g < 1$ indicates repulsive interaction, and $g > 1$ in the case of attractive interaction. The Hamiltonian H_{TLL} of the interacting Tomonaga Luttinger Liquid then reads [Grabert01]

$$H_{\text{TLL}} = \frac{v_F}{2} \int_{-\frac{L}{2}}^{+\frac{L}{2}} dx \left[\Pi_\varphi^2(x) + \frac{1}{g^2} (\partial_x \varphi(x))^2 \right]. \quad (3.9)$$

Note that v_F here is an effective Fermi velocity which can be renormalized from its bare non-interacting value when high energy modes that are also affected by the Coulomb interaction are integrated out to obtain the effective low energy theory [Grabert01]. Using the Heisenberg equation of motion

$$\partial_t \varphi = i [H_{\text{TLL}}, \varphi] = v_F \Pi_\varphi, \quad (3.10)$$

the current operator j defined in Eq. (3.7) can be expressed as

$$j(x, t) = -\frac{e}{\sqrt{\pi}} \partial_t \varphi(x, t). \quad (3.11)$$

3.2 Non-equilibrium perturbation theory

Applying a finite bias voltage can drive a physical system out of thermal equilibrium. Hence, a non-equilibrium theory is needed in order to describe quantum transport phenomena beyond the level of linear response theory. In this section, we review the construction of a non-equilibrium theory which is ready made for transport calculations in helical edge states. In Section 3.2.1, we follow the construction by Schwinger [Schwinger61] and Keldysh [Keldysh65] to generally formulate a non-equilibrium perturbation theory. In Section 3.2.2, we apply this formalism to the TLL and show how non-equilibrium expectation values of crucial physical observables like the current operator can be calculated in this framework.

3.2.1 From equilibrium to non-equilibrium

Validity of equilibrium zero temperature perturbation theory and its limitations

Assuming that the reader is familiar with equilibrium perturbation theory in many body physics, we now outline how the absence of thermal equilibrium changes the perturbative approach. In thermal equilibrium at zero temperature, the time ordered Green's function $G_{\mathcal{T}}(x, t; x', t') = -i\langle \mathcal{T}(\psi(x, t)\psi^\dagger(x', t')) \rangle$ of an interacting many body system with physical Hamiltonian $H = H_0 + V$ can in a broad class of cases be represented as

$$G_{\mathcal{T}}(x, t; x', t') = -i \frac{\langle 0 | \mathcal{T} \left(\mathcal{S}(\infty, -\infty) \psi_I(x, t) \psi_I^\dagger(x', t') \right) | 0 \rangle}{\langle 0 | \mathcal{S}(-\infty, \infty) | 0 \rangle}, \quad (3.12)$$

where $|0\rangle$ denotes the unique ground state of the **non**-interacting system, $\mathcal{S}(t, t')$ denotes the time evolution operator in the interaction picture, and ψ_I denotes the field operator in the interaction picture. The key assumptions under which Eq. (3.12) is valid are the following ones: If the interaction term is switched on and off adiabatically as $V(t) = \lim_{\eta \rightarrow 0^+} V e^{-|t|\eta}$, $\mathcal{S}(0, -\infty)$ evolves the ground state $|0\rangle$ of the non-interacting system adiabatically into the ground state of the interacting system. The formal conditions entering this assumption are the Gell-Mann and Low theorem [Gell-Mann51, Nozieres97] and the Luttinger theorem [Luttinger60a]: The Gell-Mann and Low theorem states that if the adiabatic limit of $|\psi_0\rangle = \frac{\mathcal{S}(0, -\infty)|0\rangle}{\langle 0 | \mathcal{S}(0, -\infty) | 0 \rangle}$ exists, it corresponds to an eigenstate of the interacting system with the ground state energy of the non-interacting system [Nozieres97]. However, this state does not have to be the ground state of the interacting system. For interactions that can be represented as a power series, the Luttinger theorem shows that the volume enclosed by the Fermi surface and for isotropic interaction also the spherical shape of the Fermi surface [Luttinger60b] are preserved. Under these conditions, $|\psi_0\rangle$ is indeed the interacting ground state and the adiabatic switching procedure makes sense as the interacting system then has evolved to its physical ground state by the time the field operators $\psi(x, t)$, $\psi^\dagger(x', t')$ are acting. There is one additional assumption entering Eq. (3.12), namely that $\mathcal{S}(\infty, -\infty)|0\rangle$ differs from $|0\rangle$ only by a phase factor. This amounts to assuming thermal equilibrium at zero temperature for each point in time since the system is assumed to relax to its non-interacting ground-state during the adiabatic switching-off of interactions.

The mentioned assumptions of equilibrium zero temperature perturbation theory fail under the following physical circumstances. First, the interactions might not be representable as a power series, i.e., the iterative expansion of the full time evolution operator as a von Neumann series fails to converge or does not represent the time evolution operator. An example for this scenario is a superconducting ground state consisting of a condensate of Cooper pairs. This class of problems can only be treated by non-perturbative methods. Second, the von Neumann series represents the time evolution operator but the physical ground state does not evolve adiabatically from the non-interacting one. In this case, the Matsubara method [Matsubara55] which works in thermal equilibrium at arbitrary temperature and does not rely on an adiabatic switching procedure can be used. The difference between the zero temperature limit of the Matsubara approach and the above ground state formalism has been demonstrated by Kohn and Luttinger [Kohn60]. Third, if a system which is coupled to an

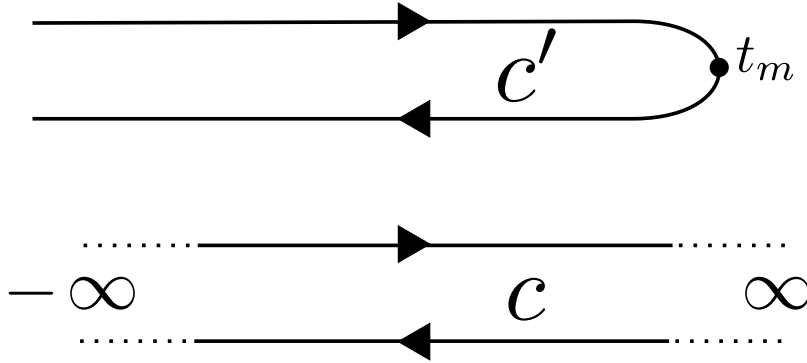


Figure 3.2: Time contour c' and extended time contour c . The arrows indicate the time ordering enacted by the operators $\mathcal{T}_{c'}$ and \mathcal{T}_c , respectively.

external time dependent field is out of thermal equilibrium, it might be dynamically pumped to a different state than its equilibrium ground state even if the time dependent perturbation is switched off adiabatically for $t \rightarrow \infty$. Then, $\mathcal{S}(\infty, -\infty)|0\rangle$ differs from $|0\rangle$ by more than a simple phase factor. This scenario is only problematic in that it precludes the picture of an instantaneous thermal equilibrium but does not pertain to the perturbative ansatz itself. Hence, this issue can be overcome by a non-equilibrium construction of perturbation theory which we review now.

The non-equilibrium construction

We consider a physical system with the Hamiltonian $H(t) = H_0 + V + F(t)$, where H_0 is a quadratic non-interacting Hamiltonian, V represents the time independent many body interactions and $F(t)$ is a coupling induced by a time dependent external field which vanishes as $t \rightarrow -\infty$. For $t \rightarrow -\infty$, the system is assumed to be in a **non**-interacting thermal state with density matrix $\rho_0 = \frac{1}{Z_0} e^{-\beta(H_0 - \mu N)}$, where $Z_0 = \text{Tr} [e^{-\beta(H_0 - \mu N)}]$. This assumption amounts to neglecting initial correlations [Rammer86]. The time ordered Green's function can then be represented in a straightforward way as [Rammer07]

$$G_{\mathcal{T}}(x, t; x', t') = -i \text{Tr} \left[\rho_0 \mathcal{S}(-\infty, t_m) \mathcal{T} \left(\psi_I(x, t) \psi_I^\dagger(x', t') \mathcal{S}(t_m, -\infty) \right) \right], \quad t_m = \max(t, t'). \quad (3.13)$$

Obviously, we can represent the order of operators in Eq. (3.13) by a generalized time ordering $\mathcal{T}_{c'}$ along the time contour c' shown in Fig. 3.2. Noting that $\mathcal{S}(t_m, \infty) \mathcal{S}(\infty, t_m) = 1$, we can extend the time contour c' to c (see Fig. 3.2) which stretches from $-\infty$ to ∞ (forward branch) and back (backward branch). The external times t, t' then always lie on the forward branch of the contour where the ordering operator \mathcal{T}_c concurs with the ordinary time-ordering \mathcal{T} . The time-ordered Green's function can then be represented as

$$G_{\mathcal{T}}(x, t; x', t') = -i \text{Tr} \left[\rho_0 \mathcal{T}_c \left(e^{-i \int_c d\tau H_I(\tau)} \psi_I(x, t) \psi_I^\dagger(x', t') \right) \right].$$

Later on, we would like to do perturbation theory which amounts to an expansion of the time evolution operator on the contour c as a von Neumann series. This expansion will of course produce operators $H_I(\tau)$, the time argument of which is integrated over the entire contour c . A straight-forward non-equilibrium generalization of Wick's theorem [Rammer07] will then produce contour-ordered pairwise contractions of the field operators appearing in these $H_I(\tau)$. In order to represent the perturbation series in a closed form, we thus introduce the contour ordered Green's function

$$G_c(x_1, \tau_1; x_2, \tau_2) = -i \text{Tr} \left[\rho_0 \mathcal{T}_c \left(e^{-i \int_c d\tau H_I(\tau)} \psi_I(x_1, \tau_1) \psi_I^\dagger(x_2, \tau_2) \right) \right],$$

the time arguments τ_1, τ_2 of which can lie anywhere on the contour c . Obviously, G_c concurs with $G_{\mathcal{T}}$ if both arguments are located on the forward branch of c . Denoting the branches of c by $+$ (forward) and $-$ (backward), G_c affords a representation as a 2×2 matrix in the so called Keldysh space of branches:

$$G_c = \begin{pmatrix} G_{++} & G_{+-} \\ G_{-+} & G_{--} \end{pmatrix} \quad (3.14)$$

As already mentioned, $G_{++} = G_{\mathcal{T}}$. Furthermore $G_{--} = G_{\bar{\mathcal{T}}}$ is the anti-time-ordered Green's function, $G_{-+}(x_1, \tau_1; x_2, \tau_2) = -i \text{Tr} \left[\rho_0 \psi(x_1, \tau_1) \psi^\dagger(x_2, \tau_2) \right]$, and $G_{+-}(x_1, \tau_1; x_2, \tau_2) = i \text{Tr} \left[\rho_0 \psi^\dagger(x_2, \tau_2) \psi(x_1, \tau_1) \right]$. Note that the extra minus sign in the definition of G_{+-} is due to the Grassman algebra that the fermionic field operators satisfy under the time/contour ordering operator.

By now, we have formulated the non-equilibrium problem in a strikingly similar way to its equilibrium counterpart. The salient new element in the non-equilibrium theory is the backward branch of the contour c which allows us to drop any assumptions as to the relation between the system state at $t \rightarrow -\infty$ and $t \rightarrow \infty$. This construction comes at a price: The Green's function naturally appearing in the perturbation series is the contour ordered Green's function G_c which can be represented as a 2×2 matrix of Green's functions with an ordinary real time argument (see Eq. (3.14)). Once this complication has been digested, practical perturbative calculations work fairly analogous to the ordinary equilibrium case (see Ref. [Rammer07] for a detailed elementary discussion). Hence, instead of reviewing more details of the general construction, we would here like to focus on the bosonic non-equilibrium perturbation theory in the TLL which will be of crucial relevance for Chapter 5.

3.2.2 Keldysh perturbation theory of the Tomonaga Luttinger Liquid

In Section 3.1 we constructed the translation-invariant TLL which is even in the presence of Coulomb interaction quadratic in the bosonic field operators. A bias voltage can be modeled [Dolcini05] by adding the following perturbation to the Hamiltonian:

$$H_V^\varphi(t) = -\frac{e}{\sqrt{\pi}} \int dx E(x, t) \varphi(x). \quad (3.15)$$

For our purposes, we can think of the bias term as induced by the gradient of a chemical potential, i.e., $-eE = \partial_x \mu^\varphi$. The simplest perturbation which makes the TLL non-quadratic in the bosonic fields is a single impurity with strength λ at $x = 0$ which is described by the model Hamiltonian [Kane92a, Dolcini05]

$$H_S = \lambda \cos(\sqrt{4\pi}\varphi(x=0)). \quad (3.16)$$

Obviously, this perturbation is of infinite order in the bosonic field operator φ which precludes the efficient application of Wick's theorem in the non-equilibrium perturbative expansion. Our general strategy will thus be as follows: We first perform a unitary operation thus representing the bias term Eq. (3.15) as a shift in the field φ appearing in the impurity Hamiltonian (3.16). Using $2 \cos(x) = e^{ix} + e^{-ix}$, we note that the impurity can be represented as a sum of so called vertex operators, i.e., operators of the form $e^{i\alpha\varphi}$, $\alpha \in \mathbb{R}$. For the free expectation value of such an operator, we can use the crucial identity

$$\langle e^{\alpha\varphi} \rangle_0 = e^{\alpha^2 \frac{\langle \varphi^2 \rangle_0}{2}}, \quad \alpha \in \mathbb{C}. \quad (3.17)$$

However, the current operator (see Eq. (3.7)) is not a vertex operator but is linear in φ . We thus need a vertex operator which generates expectation values of φ , a source term like $e^{iJ\varphi}$ which satisfies $-i\partial_{J\varphi} \langle e^{iJ\varphi} \rangle \Big|_{J\varphi=0} = \langle \varphi \rangle$. This naturally leads us to the construction of a generating functional.

Let us now follow the program just outlined in more detail. Since our impurity Hamiltonian H_S will later on in general depend on both φ and θ , we generalize the analysis in Ref. [Dolcini05] meaning that $\Pi_\varphi = -\partial_x \theta$ is not integrated out. We follow Ref. [Liu11] but for the spinless TLL for simplicity. First, we combine the two bosonic fields to the vector $\Phi^\eta = (\varphi^\eta, \theta^\eta)^T$, where η is the index in Keldysh space, i.e., $\eta = \pm$ on the forward/backward branch of the contour c . For later convenience, we would like to generalize the bias Hamiltonian (3.15) so as to include a generalized chemical potential μ^θ which couples to the dual field θ . This gives rise to the additional term

$$H_V^\theta = \frac{1}{\sqrt{\pi}} \int dx \left(\partial_x \mu^\theta(x, t) \right) \theta(x).$$

Furthermore, we also introduce a source-term J^θ which generates expectation values of the dual field θ . Let us compactify our notation by the following definitions

$$\Phi(\mathbf{r}) = \begin{pmatrix} \varphi^+(\mathbf{r}) \\ \varphi^-(\mathbf{r}) \\ \theta^+(\mathbf{r}) \\ \theta^-(\mathbf{r}) \end{pmatrix},$$

$$J(\mathbf{r}) = \begin{pmatrix} -\sqrt{\frac{1}{\pi}}\partial_x\mu^\varphi(\mathbf{r}) \\ \sqrt{2}J^\varphi(\mathbf{r}) \\ -\sqrt{\frac{1}{\pi}}\partial_x\mu^\theta(\mathbf{r}) \\ \sqrt{2}J^\theta(\mathbf{r}) \end{pmatrix},$$

$$Q(\mathbf{r}, \mathbf{r}') = \frac{1}{\sqrt{2}}\delta(\mathbf{r} - \mathbf{r}') \begin{pmatrix} 1 & -1 & 0 & 0 \\ 1 & 1 & 0 & 0 \\ 0 & 0 & 1 & -1 \\ 0 & 0 & 1 & 1 \end{pmatrix},$$

$$\mathbf{C}(r, r') = \begin{pmatrix} \mathcal{C}^{++}(\mathbf{r}, \mathbf{r}') & \mathcal{C}^{+-}(\mathbf{r}, \mathbf{r}') & \mathcal{F}^{++}(\mathbf{r}, \mathbf{r}') & \mathcal{F}^{+-}(\mathbf{r}, \mathbf{r}') \\ \mathcal{C}^{-+}(\mathbf{r}, \mathbf{r}') & \mathcal{C}^{--}(\mathbf{r}, \mathbf{r}') & \mathcal{F}^{-+}(\mathbf{r}, \mathbf{r}') & \mathcal{F}^{--}(\mathbf{r}, \mathbf{r}') \\ \mathcal{Q}^{++}(\mathbf{r}, \mathbf{r}') & \mathcal{Q}^{+-}(\mathbf{r}, \mathbf{r}') & \mathcal{D}^{++}(\mathbf{r}, \mathbf{r}') & \mathcal{D}^{+-}(\mathbf{r}, \mathbf{r}') \\ \mathcal{Q}^{-+}(\mathbf{r}, \mathbf{r}') & \mathcal{Q}^{--}(\mathbf{r}, \mathbf{r}') & \mathcal{D}^{-+}(\mathbf{r}, \mathbf{r}') & \mathcal{D}^{--}(\mathbf{r}, \mathbf{r}') \end{pmatrix},$$

where $\mathbf{r} = (x, t)$, and $\varphi(\mathbf{r}), \theta(\mathbf{r})$ are the bosonic fields in the interaction picture, i.e., in the Heisenberg picture with respect to H_{TLL} (see Eq. (3.9)). Furthermore,

$$\begin{aligned} \mathcal{C}^{\eta\eta'}(\mathbf{r}, \mathbf{r}') &= \langle \varphi^\eta(\mathbf{r})\varphi^{\eta'}(\mathbf{r}') \rangle_0, \\ \mathcal{D}^{\eta\eta'}(\mathbf{r}, \mathbf{r}') &= \langle \theta^\eta(\mathbf{r})\theta^{\eta'}(\mathbf{r}') \rangle_0, \\ \mathcal{F}^{\eta\eta'}(\mathbf{r}, \mathbf{r}') &= \langle \varphi^\eta(\mathbf{r})\theta^{\eta'}(\mathbf{r}') \rangle_0, \\ \mathcal{Q}^{\eta\eta'}(\mathbf{r}, \mathbf{r}') &= \langle \theta^\eta(\mathbf{r})\varphi^{\eta'}(\mathbf{r}') \rangle_0 = (\mathcal{F}^{\eta',\eta}(\mathbf{r}', \mathbf{r}))^\dagger \end{aligned} \quad (3.18)$$

are the free correlation functions. With the compact definitions above, the generating functional which is the starting point for all practical calculations can be written as

$$Z[J] = \int \frac{\mathcal{D}\Phi}{N_Z} e^{-\frac{1}{2}\Phi^T \mathbf{C}^{-1} \Phi + i\mathbf{J}^T Q \Phi} e^{-i\sum_\eta \eta \int_{-\infty}^{\infty} dt H_S[\Phi^\eta]}. \quad (3.19)$$

Here, the superscript T denotes matrix transpose. Note that the matrix product in the above equations includes an integration over space and time. In order to separate the free part of the generating functional from the terms to be treated perturbatively, we apply the following shift to the vector of boson fields

$$\tilde{\Phi} = \Phi - \mathbf{A}[J], \quad \mathbf{A}[J] = i\mathbf{C}Q^T \mathbf{J},$$

and explicitly $\mathbf{A}[J] = (A^{+, \varphi}, A^{-, \varphi}, A^{+, \theta}, A^{-, \theta})^T$ with

$$\begin{aligned} A^{\eta, \varphi}[J] &= -\frac{i}{\sqrt{2\pi}} \int d\mathbf{r}' \left(\mathcal{C}^R(\mathbf{r}, \mathbf{r}') \partial_x \mu^\varphi(\mathbf{r}') \right. \\ &\quad \left. + \mathcal{F}^R(\mathbf{r}, \mathbf{r}') \partial_x \mu^\theta(\mathbf{r}') \right) + i \int d\mathbf{r}' (\mathcal{C}^K(\mathbf{r}, \mathbf{r}') + \eta \mathcal{C}^A(\mathbf{r}, \mathbf{r}')) J^\varphi(\mathbf{r}') \\ &\quad + i \int d\mathbf{r}' (\mathcal{F}^K(\mathbf{r}, \mathbf{r}') + \eta \mathcal{F}^A(\mathbf{r}, \mathbf{r}')) J^\theta(\mathbf{r}'), \end{aligned}$$

$$\begin{aligned} A^{\eta, \theta}[J] &= -\frac{i}{\sqrt{2\pi}} \int d\mathbf{r}' \left(\mathcal{Q}^R(\mathbf{r}, \mathbf{r}') \partial_x \mu^\varphi(\mathbf{r}') \right. \\ &\quad \left. + \mathcal{D}^R(\mathbf{r}, \mathbf{r}') \partial_x \mu^\theta(\mathbf{r}') \right) + i \int d\mathbf{r}' (\mathcal{Q}^K(\mathbf{r}, \mathbf{r}') + \eta \mathcal{Q}^A(\mathbf{r}, \mathbf{r}')) J^\varphi(\mathbf{r}') \\ &\quad + i \int d\mathbf{r}' (\mathcal{D}^K(\mathbf{r}, \mathbf{r}') + \eta \mathcal{D}^A(\mathbf{r}, \mathbf{r}')) J^\theta(\mathbf{r}'). \end{aligned}$$

The generating functional then factorizes as follows

$$Z[J] = Z_0[J_c] Z_S[J] \quad (3.20)$$

where

$$Z_0[\mathbf{J}] = e^{-\frac{1}{2} \mathbf{J}^T \tilde{\mathbf{C}} \mathbf{J}},$$

and

$$\tilde{\mathbf{C}} = \mathbf{Q} \mathbf{C} \mathbf{Q}^T = \begin{pmatrix} 0 & \mathcal{C}^A(\mathbf{r}, \mathbf{r}') & 0 & \mathcal{F}^A(\mathbf{r}, \mathbf{r}') \\ \mathcal{C}^R(\mathbf{r}, \mathbf{r}') & \mathcal{C}^K(\mathbf{r}, \mathbf{r}') & \mathcal{F}^R(\mathbf{r}, \mathbf{r}') & \mathcal{F}^K(\mathbf{r}, \mathbf{r}') \\ 0 & \mathcal{Q}^A(\mathbf{r}, \mathbf{r}') & 0 & \mathcal{D}^A(\mathbf{r}, \mathbf{r}') \\ \mathcal{Q}^R(\mathbf{r}, \mathbf{r}') & \mathcal{Q}^K(\mathbf{r}, \mathbf{r}') & \mathcal{D}^R(\mathbf{r}, \mathbf{r}') & \mathcal{D}^K(\mathbf{r}, \mathbf{r}') \end{pmatrix}$$

with

$$\begin{aligned} \mathcal{C}^R(\mathbf{r}, \mathbf{r}') &= \theta(t - t') \langle [\varphi(\mathbf{r}), \varphi(\mathbf{r}')] \rangle_0, \\ \mathcal{C}^A(\mathbf{r}, \mathbf{r}') &= -\theta(t' - t) \langle [\varphi(\mathbf{r}), \varphi(\mathbf{r}')] \rangle_0, \\ \mathcal{C}^K(\mathbf{r}, \mathbf{r}') &= \langle \{\varphi(\mathbf{r}), \varphi(\mathbf{r}')\} \rangle_0 \end{aligned}$$

and similar definitions for the other correlation functions \mathcal{D} , \mathcal{F} and \mathcal{Q} . $Z_S[J]$ is given by

$$Z_S[J] = \int \frac{\mathcal{D}\tilde{\Phi}}{N_Z} e^{-\frac{1}{2} \tilde{\Phi}^T \mathbf{C}^{-1} \tilde{\Phi}} e^{-i \sum_\eta \eta \int_{-\infty}^{\infty} dt H_S[\tilde{\Phi}^\eta + \mathbf{A}^\eta]} = \langle e^{-i \int_c d\tau H_S[\tilde{\Phi} + \mathbf{A}]} \rangle_0. \quad (3.21)$$

Next, we need to relate the physical quantities to the generating functional. From Eq. (3.7), it is clear that we need to calculate expectation values like $\langle \varphi \rangle$ and $\langle \theta \rangle$ which can be

conveniently evaluated from the functional derivatives of the generating functional $Z[J]$ with respect to J^φ and J^θ . A direct calculation shows that

$$\langle \varphi(\mathbf{r}) \rangle = \frac{1}{2} \sum_{\eta} \langle \varphi^{\eta}(\mathbf{r}) \rangle = -\frac{i}{2} \frac{1}{Z[0]} \left. \frac{\delta Z[J]}{\delta J^{\varphi}(\mathbf{r})} \right|_{J=0} = -\frac{i}{2} \left[\frac{\delta Z_0[J]}{\delta J^{\varphi}(\mathbf{r})} + \frac{1}{Z_S[0]} \frac{\delta Z_S[J]}{\delta J^{\varphi}(\mathbf{r})} \right] \Big|_{J=0} \quad (3.22)$$

with a similar expression holding for $\langle \theta \rangle$. From Eq. (3.22), we find that $\langle \varphi \rangle$ can be decomposed into two parts: one is the zero order term coming from $Z_0[J]$, and the other one is the scattering term coming from $Z_S[J]$. Consequently, any physical quantity \hat{O} can also be divided into two parts $\langle \hat{O} \rangle = \langle \hat{O}_0 \rangle + \langle \hat{O}_2 \rangle$. All transport calculations in this thesis will be based on a perturbative evaluation of Eq. (3.22) and its analogue for the dual field θ , respectively.

3.3 Peculiarities of the helical Tomonaga Luttinger Liquid

In this section, we briefly would like to point out some peculiarities of the helical TLL (hTLL) as realized on the edge of a QSH sample. Our at this stage rather general discussion is meant to give a short overview over the unique features of the hTLL which motivate the more detailed transport studies presented in Chapter 5. The hTLL consists of one left and on right moving channel which have opposite spin polarization. Hence, ignoring the spin polarization, a single hTLL has the same number of degrees of freedom as the spinless TLL. However, the counter-propagating states at a given energy are conjugated by TRS, i.e., they are so called Kramers partners. This imposes serious constrictions on possible scatterers in the hTLL as long as TRS is conserved as we will detail in Section 3.3.2. If we consider two hTLLs with opposite helicity, e.g., the two parallel edges of a QSH ribbon, we recover the degrees of freedom of a spinful TLL (sTLL). In Section 3.3.1, we will discuss the phase space constraints on the Coulomb interaction imposed by the nonlocal nature of this composite realization of the sTLL.

3.3.1 A composite spinful TLL consisting of two hTLLs

The spinful TLL

We consider a model with linear dispersion as in the construction of the spinless TLL with the sole difference that there are two species $s = \uparrow, \downarrow$ for each direction of motion $p = \pm$. The fermionic operators $\psi_{p,s}(x)$ can then be represented in terms of bosonic fields in total analogy to the spinless case, Eq. (3.4):

$$\psi_{p,s}(x) = \frac{\eta_{p,s}}{\sqrt{2\pi a}} e^{ip(k_F + 2\pi \hat{N}_{p,s}/L)x + \sqrt{4\pi} ip \Phi_{p,s}(x)}, \quad (3.23)$$

where $\Phi_{p,s}$ are the spinful chiral hermitian fields which are defined by Eq. (3.3) for each spin species separately and the $1/L$ terms will be neglected from now on following the same argumentation as for the spinless case above. Let us define a non-chiral bosonic field and its

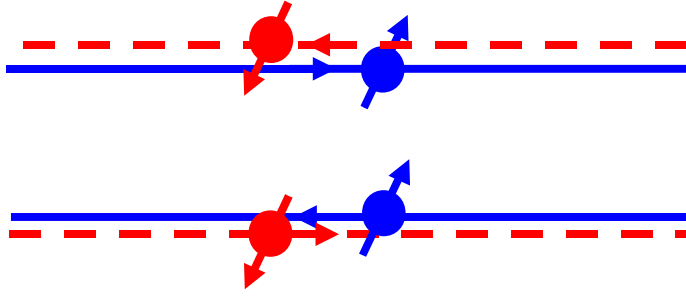


Figure 3.3: Composite sTLL consisting of two hTLLs with opposite helicity as realized at the two parallel edges of a QSH ribbon.

dual also for the spinful case as

$$\begin{aligned}\varphi_s &= \Phi_{+,s} + \Phi_{-,s}, \\ \theta_s &= \Phi_{+,s} - \Phi_{-,s}.\end{aligned}\quad (3.24)$$

It is often times convenient to work in the so called spin-charge (σ - ρ) basis, where charge (ρ) represents the sum of the two spin species and spin (σ) represents their difference. This basis is hence defined by the unitary transformation

$$\begin{aligned}\varphi_\rho &= \frac{1}{\sqrt{2}}(\varphi_\uparrow + \varphi_\downarrow), \\ \varphi_\sigma &= \frac{1}{\sqrt{2}}(\varphi_\uparrow - \varphi_\downarrow), \\ \theta_\rho &= \frac{1}{\sqrt{2}}(\theta_\uparrow + \theta_\downarrow), \\ \theta_\sigma &= \frac{1}{\sqrt{2}}(\theta_\uparrow - \theta_\downarrow).\end{aligned}\quad (3.25)$$

In the presence of short ranged Coulomb interaction, the low energy fixed point theory of the translation-invariant sTLL can be written as (see Ref.[Grabert01] for a more detailed discussion)

$$H_{s\text{TLL}} = \frac{v_F}{2} \sum_{\nu=\rho,\sigma} \int_{-\infty}^{\infty} dx \left[(\partial_x \theta_\nu)^2 + \frac{1}{g_\nu^2} (\partial_x \varphi_\nu)^2 \right], \quad (3.26)$$

where the interaction parameters g_ρ and g_σ and with them the associated group velocities $v_\rho = v_F/g_\rho$ and $v_\sigma = v_F/g_\sigma$ for the charge and spin excitations of the sTLL can be different. This phenomenon is known as spin charge separation in 1D.

The composite sTLL

As already mentioned we can recover the degrees of freedom of an sTLL by considering two hTLLs with opposite helicity which are realized at two parallel edges of a QSH bar (see Fig. 3.3). For concreteness, we assume that the upper edge features the fields $(\Phi_{+,\uparrow}, \Phi_{-,\downarrow}) =$

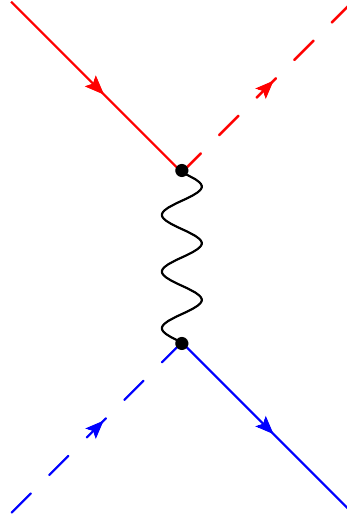


Figure 3.4: Coulomb-backscattering process that gives a non-quadratic contribution to the sTLL. Red denotes spin up, blue denotes spin down. Solid lines represent right movers and dashed lines represent left movers.

(Φ_+^u, Φ_-^u) , whereas the lower edge features the fields $(\Phi_{+,\downarrow}, \Phi_{-,\uparrow}) = (\Phi_+^l, \Phi_-^l)$. The two edges u, l are assumed to have identical interaction strength g and can be represented as two spinless TLL with the Hamiltonian

$$H_{\text{hTLL}}^\mu = \frac{v_F}{2} \int_{-\infty}^{\infty} dx \left[(\partial_x \theta^\mu)^2 + \frac{1}{g^2} (\partial_x \varphi^\mu)^2 \right], \quad \mu = u, l. \quad (3.27)$$

If we ignore the u, l -labels on the bosonic fields, we can rewrite the total Hamiltonian $H_{2\text{Edge}} = H_{\text{hTLL}}^u + H_{\text{hTLL}}^l$ of the two independent edges in the language of an sTLL as defined in Eq. (3.26) and find by simple comparison of coefficients [Hou09, Teo09]

$$g_c = g, \quad g_s = \frac{1}{g_c} = \frac{1}{g}. \quad (3.28)$$

As we will work out in Section 5.1, this constraint is at the heart of a duality between the charge and spin degree of freedom which even survives in a non-equilibrium setup.

3.3.2 Peculiarities of a single hTLL

Let us now focus on a single hTLL. Instead of ignoring the spin degree of freedom, one might ask what kind of interesting consequences the locking between spin and direction of motion might bring about.

Vanishing Coulomb backscattering

The first point worth mentioning is that the hTLL is in some sense a better TLL than the ordinary sTLL. Let us explain what we mean by this argument. To derive Eq. (3.26) for the interacting sTLL, a non-quadratic term stemming from a spin conserving backscattering

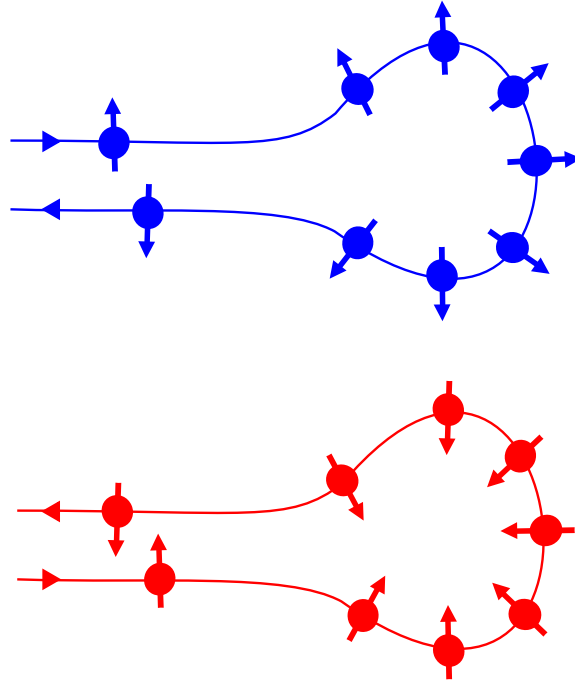


Figure 3.5: Two backscattering trajectories conjugated by TRS. The blue trajectory amounts to a clockwise spin rotation by π whereas the red trajectory amounts to a counter-clockwise rotation by π .

process (see Fig. 3.4) which has a non-vanishing matrix element in the sTLL needs to be neglected. This is justified exactly at the low energy fixed-point because the mentioned term is not relevant in RG sense. However, at finite bias this becomes an approximation. For the ideal hTLL, neglecting the diagram shown in Fig. 3.4 becomes exact since there is no phase space for spin-conserving backscattering: States moving in opposite direction always have opposite spin, whereas the mentioned process involves all four species of the sTLL. This argument supports the quantized conductance of the hTLL.

Kramers degeneracy and topological protection

The next peculiarity of the hTLL is closely related to our discussion of topological protection by an anti-unitary symmetry (see Section 2.1.4 and Section 2.4.1). The opposite spin of counter-propagating states precludes a local scalar backscattering term analogous to Eq. (3.16) for the hTLL directly from simple phase space arguments. Interestingly, the robustness against backscattering is much stronger than this obvious phase space constraint as we will outline now. In the bulk of a QSH sample, TRS prevents us from deforming the QSH phase adiabatically into a trivial insulating phase. On the edge, the two counter-propagating channels forming the hTLL are conjugated to each other by TRS. This implies that the degenerate pair of counter-propagating states at a given energy are Kramers partners. This phenomenology entails a new ramification of topological protection as has been discussed in Refs. [Wu06, Qi11], namely that elastic single particle backscattering is forbidden as long as TRS is conserved. Here, we only give an illustrative argument following [Qi11] which views

the protection as a weak anti-localization with perfect efficiency. Let us assume that we put an impurity that can rotate spin but does preserve TRS in a clean hTLL. Such an imperfection could be realized by locally induced extrinsic SOI. Fig. 3.5 shows two backscattering paths which are conjugated by TRS. Obviously, the two paths differ by a spin rotation of 2π which, for half-integer fermions, entails a relative phase factor of -1 , i.e., destructive interference. Since all possible trajectories have a conjugated counterpart canceling their contribution, there is no backscattering provided that the range of the scattering potential is smaller than the phase coherence length. In Section 5.2, we will discuss this protection more formally and investigate its limitations in great detail in Sections 5.2-5.3.

Part II

Application to low dimensional mesoscopic systems

Chapter 4

All-electric qubit control in heavy hole quantum dots via non-Abelian geometric phases

In this chapter, we demonstrate how non-Abelian geometric phases (see Section 1.1.2) can be used to universally process spin qubits [Loss98] in heavy hole quantum dots in the absence of magnetic fields. An adiabatically time dependent electric quadrupole field is used to perform any desired single qubit operation by virtue of non-Abelian holonomy. During the proposed operations, the degeneracy of the time dependent two level system representing the qubit is not split. Since time reversal symmetry is preserved and hyperfine coupling is known to be weak in spin qubits based on heavy holes, we expect very long coherence times in the proposed setup. Our analysis follows closely Ref. [Budich12b]. The theoretical foundations underlying this application are presented in Chapter 1. We will repeat some of the key equations to increase the readability of this chapter.

4.1 Motivation

Coherent spin control by all-electric means (without breaking TRS) is among the major goals of spintronics. One of the reasons why is that the presence of TRS is known to forbid several dephasing mechanisms, for example, in spin qubits [Loss98], due to the interplay of electron phonon coupling and Rashba spin orbit coupling [Bulaev05]. In the original work by Loss and DiVincenzo [Loss98], the proposed scheme for universal quantum computing based on spin qubits in quantum dots (QDs) relied on the one hand on all-electric two qubit operations, but, on the other hand, on single qubit operations based on magnetic fields or ferromagnetic auxiliary devices that both break TRS. A few years later, electric-dipole-induced spin resonance (EDSR) has been proposed [Golovach06] and experimentally realized [Nowack07] as a way to process spins electrically in the presence of a static magnetic field which is still breaking TRS. Rather recently, it has been theoretically shown that in spin qubits based on carbon nanotube QDs it is indeed possible to accomplish all-electric single qubit operations using EDSR [Bulaev08, Klinovaja11]. This is possible because the specific spin orbit interaction in carbon nanotubes provides a way to split spin up and spin down states in the absence of magnetic fields (zero field splitting). However, spin qubits based on carbon nanotubes face other problems related to readout and integrability and it is hence fair to say that all host materials for spin qubits have advantages and disadvantages.

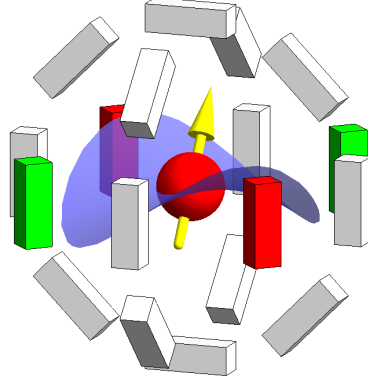


Figure 4.1: Schematic of a single particle (red ball) with a HH (pseudo)spin (yellow arrow) in a $J = \frac{3}{2}$ valence band QD. The three-dimensional QD is surrounded by 18 gates that allow to generate an electrostatic potential with quadrupole symmetry in any direction in real space. The red and green colors on the gates should visualize applied electrostatic potentials with opposite sign that give rise to the quadrupole field shown in light blue.

In this chapter, we are interested in spin qubits based on heavy hole (HH) QDs. We show how universal single qubit operations can be performed by all-electric means in the framework of holonomic quantum computing [Zanardi99] in these systems. The gist of holonomic quantum computing is to employ non-Abelian GPs (see Eq. (1.14)) to perform unitary operations on qubits. In our subsequent proposal, the adiabatic evolution in the presence of a time dependent electric quadrupole field is used as a means to control the HH qubit (see Fig. 4.1 for a schematic). For our purposes, HH spin qubits (composed of $J = \frac{3}{2}$ states) are the simplest two level system that can be manipulated in the desired way. However, HH spin qubits are, of course, a very active research area by itself beyond holonomic quantum computing. Two reasons why HH QDs are promising and interesting candidates for spin qubits are, for instance, the advanced level of optical control [Gerardot08, Eble09, Brunner09, de Greve11] and the predicted long coherence times [Fischer10].

The topological properties of TRS preserving half integer spin systems have been analyzed in a series of seminal papers by Avron and coworkers [Avron88, Avron89]. The case $J = \frac{3}{2}$ is of particular interest both from a theoretical and from a more applied point of view. From the theoretical side, all TRS preserving gapped Hamiltonians are unitarily related due to an $SO(5)$ symmetry [Avron88, Avron89] giving rise to an $SO(5)$ Clifford algebra [Avron89, Demler99] which allows for a simple analytical calculation of the adiabatic time evolution and with that the GP. From the experimental side, the $J = \frac{3}{2}$ system is naturally realized in the p -like valence band of many semiconductors where spin orbit coupling iso-

lates the $J = \frac{3}{2}$ states from the so called split-off band. Interestingly, the fingerprints of $SU(2)$ non-Abelian GPs [Kato50, Wilczek84] (see Eq. (1.14)) could also be identified on several transport properties of this class of semiconducting materials [Arovas98, Murakami04].

The pioneering idea of using non-Abelian holonomy to perform quantum computing tasks in the $J = \frac{3}{2}$ system is due to Bernevig and Zhang [Bernevig05] who proposed the electric Stark effect to process valence band impurities in III-V semiconductors. Their idea works for the light hole (LH) subspace of the $J = \frac{3}{2}$ Hilbert space. However, the resulting holonomy is Abelian on the HH subspace [Zee88] so that the electric Stark-effect cannot be used to process HH qubits. In contrast, the electric quadrupole fields employed in our proposal allow for full adiabatic control over the entire $J = \frac{3}{2}$ Hilbert space. This is a consequence of the topologically nontrivial structure of the accessible parameter space which becomes manifest in the nontrivial second Chern number (see Section 2.3.1) of the associated $SU(2)$ gauge theory over the four dimensional parameter space of quadrupole tensors with unit strength [Avron88].

Holonomic quantum computing with dark exciton states [Solinas03] and due to tunable spin orbit coupling with electron spins in spatially transported quantum dots [San-Jose08, Golovach10], respectively, has been suggested previously. Our idea is conceptually much simpler. We derive below the time dependent electric quadrupole field that realizes any desired single qubit operation

$$\mathcal{U}(\hat{n}, \varphi) = \exp\left(i\varphi \frac{\hat{n}\vec{\sigma}}{2}\right) \quad (4.1)$$

on the HH spin qubit. Here, \hat{n} is a unit vector representing the rotation axis, φ is the angle of the rotation, and $\vec{\sigma}$ denotes the vector of Pauli matrices acting on the qubit space. Two-qubit gates can be performed by all-electric means along the lines of Ref. [Loss98]. To perform universal quantum computing with a device which employs our proposal, initialization and readout tasks have to be implemented without magnetic fields. All-electric spin pumping and spin filtering techniques, respectively [Broscio10], can be used to perform these crucial tasks on the quantum dots without breaking TRS. Alternatively, it is of course also possible to realize initialization and readout of our qubit in a standard way using static magnetic fields [Hanson07]. Then, our proposal would still have the advantage that during the computational steps, the degeneracy of the two-level system is not lifted.

This chapter is organized as follows: In Section 4.2, we derive the time dependent quadrupole field associated with an arbitrary single qubit gate and illustrate our results by discussing an exemplary operation in great detail. In Section 4.3, we discuss the influence of several imperfections, which might be present in an experimental setup, on the working precision of our proposal. By virtue of a detailed numerical calculation, we provide an estimate of the adiabatic time scale which determines the maximum operating frequency of single qubit gates showing that the physics we describe is experimentally feasible. Finally, in Section 4.4, we sum up our findings.

4.2 Qubit control via quadrupole fields

The non-Abelian GP, occurring in a degenerate subspace after an adiabatic cyclic evolution, is readily expressed once the time-dependent projection $P(t)$ onto this degenerate subspace is known. In Section 1.1.2, it has been discussed that the generator of the adiabatic evolution reads [Kato50] (see also Eq. (1.11))

$$\mathcal{A}\left(\frac{d}{dt}\right) = -\left[\frac{dP(t)}{dt}, P(t)\right].$$

On the basis of this generator, the non-Abelian GP [Wilczek84] (see Section 1.2) associated with a loop γ in parameter space is given by the holonomy (see also Eq. (1.14))

$$\mathcal{K}_\gamma = \mathcal{T}e^{-\int_\gamma \mathcal{A}}, \quad (4.2)$$

where \mathcal{T} denotes time-ordering. For the Hilbert space of a $J = \frac{3}{2}$ particle in the presence of TRS, this holonomy is readily calculated analytically as we explicitly demonstrate below.

The Hamiltonian of a spin $\frac{3}{2}$ particle coupled to an electric quadrupole field can be written as [Avron88]

$$H(\mathcal{Q}) = J_i \mathcal{Q}^{ij} J_j, \quad (4.3)$$

where J is the angular momentum operator and \mathcal{Q} is the quadrupole tensor of the applied field. \mathcal{Q} is a real, symmetric, traceless matrix. The space of such matrices is five dimensional. An orthonormal basis of this space is given by the matrices $\{Q_\mu\}_\mu$, $\mu = 0, \dots, 4$ with

$$\begin{aligned} Q_0 &= \frac{1}{3} \begin{pmatrix} -1 & 0 & 0 \\ 0 & -1 & 0 \\ 0 & 0 & 2 \end{pmatrix}, & Q_1 &= \frac{1}{\sqrt{3}} \begin{pmatrix} 0 & 0 & 1 \\ 0 & 0 & 0 \\ 1 & 0 & 0 \end{pmatrix}, \\ Q_2 &= \frac{1}{\sqrt{3}} \begin{pmatrix} 0 & 0 & 0 \\ 0 & 0 & 1 \\ 0 & 1 & 0 \end{pmatrix}, & Q_3 &= \frac{1}{\sqrt{3}} \begin{pmatrix} 1 & 0 & 0 \\ 0 & -1 & 0 \\ 0 & 0 & 0 \end{pmatrix}, \\ Q_4 &= \frac{1}{\sqrt{3}} \begin{pmatrix} 0 & 1 & 0 \\ 1 & 0 & 0 \\ 0 & 0 & 0 \end{pmatrix}, \end{aligned}$$

which satisfy the normalization condition

$$\frac{3}{2} \text{Tr} \{Q_\mu Q_\nu\} = \delta_{\mu\nu}.$$

A general quadrupole field is then of the form $x^\mu Q_\mu$ and the associated Hamiltonian reads

$$H(\mathcal{Q}) = H(x^\mu Q_\mu) = x^\mu J_i Q_\mu^{ij} J_j = x^\mu \Gamma_\mu,$$

where the basis Hamiltonians $\Gamma_\mu = J_i Q_\mu^{ij} J_j$ obey the SO(5) Clifford algebra [Avron89,

Demler99]

$$\{\Gamma_\mu, \Gamma_\nu\} = 2\delta_{\mu\nu}.$$

As far as the geometric phase associated with a cycle in this parameter space is concerned, we can confine our interest to quadrupole fields of constant strength, say $|\mathbf{x}| = 1$. (This is justified because the quadrupole energy is so far the only energy scale of the problem.) Note that the experimentally relevant scale of $|\mathbf{x}|$ defines the splitting between the two Kramers pairs and therefore the adiabatic operating frequencies of the proposed setup. Due to the mentioned SO(5) symmetry in the system [Avron88], all possible quadrupole Hamiltonians $H(\mathcal{Q})$ are unitarily related by a Spin(5) representation of this SO(5) symmetry. The ten generators of this symmetry group of our family of Hamiltonians are given by [Avron89]

$$\{V_i\}_i = \left\{ \frac{1}{2} [\Gamma_\alpha, \Gamma_\beta] = \Gamma_\alpha \Gamma_\beta \right\}_{\alpha < \beta}, \quad i \in 0, \dots, 9,$$

where $\alpha, \beta \in 0, \dots, 4$. A cyclic time evolution $t \mapsto H(t)$ starting from $H(t=0) = \Gamma_0$ is then given by a 2π SO(5) rotation in the space of quadrupole fields which is uniquely associated with a 2π Spin(5) rotation

$$t \mapsto H(t) = e^{t \frac{\hat{a}\vec{V}}{2}} \Gamma_0 e^{-t \frac{\hat{a}\vec{V}}{2}}, \quad t \in [0, 2\pi],$$

in Hilbert space, where \hat{a} is a ten-component unit vector specifying the direction of the rotation in the Lie algebra of SO(5). We call

$$P_0^\pm = \frac{1}{2}(1 \pm \Gamma_0)$$

the projector on the Kramers pair with eigenvalue $\pm|\mathbf{x}|$. In fact, due to our choice of the initial Hamiltonian, P_0^\pm concurs with the projection on the HH/LH subspaces. Starting with a HH state $|\psi(0)\rangle$ satisfying $P_0^+|\psi(0)\rangle = |\psi(0)\rangle$, the Kato propagator $\mathcal{K}(t, 0)$ can be conveniently expressed as [Simon83, Wilczek84, Avron89] (see also Eq. (1.17))

$$\begin{aligned} \mathcal{K}(t, 0) &= \lim_{n \rightarrow \infty} \mathcal{K}_n(t, 0) \text{ with} \\ \mathcal{K}_n(t, 0) &= P^+(t) P^+ \left(\frac{(n-1)t}{n} \right) \dots P^+ \left(\frac{2t}{n} \right) P^+ \left(\frac{t}{n} \right) P_0^+, \end{aligned} \quad (4.4)$$

where the time dependent projector on the Kramers pair with positive eigenvalue is given by $P^+(t) = e^{t \frac{\hat{a}\vec{V}}{2}} P_0^+ e^{-t \frac{\hat{a}\vec{V}}{2}}$.

Along any such loop γ in parameter space the adiabatic evolution is readily computed analytically to yield [Avron89]

$$\mathcal{K}(t, 0) = e^{t \frac{\hat{a}\vec{V}}{2}} e^{-t P_0^+ \frac{\hat{a}\vec{V}}{2} P_0^+}. \quad (4.5)$$

The first factor gives $e^{2\pi \frac{\hat{a}\vec{V}}{2}} = -1$ once the loop is completed. The second factor at $t = 2\pi$ de-

fines an $SU(2)$ transformation on the HH subspace which is the desired holonomy \mathcal{K}_γ (see Eq. (4.2)) up to a sign. As has been shown in Section 1.2, the holonomy associated with a loop γ is a purely geometrical object. It does not depend on the parameterization, i.e., on the time-dependent velocity with which the electric field is ramped, as long as the adiabatic approximation is justified.

We now explicitly construct the direction \hat{a} needed to obtain any holonomy as parameterized in Eq. (4.1). The angle and axis of the rotation can be tuned using the relations

$$P_0^+ \Gamma_0 \Gamma_\mu P_0^+ = 0, \quad \mu \neq 0, \quad (4.6)$$

as well as

$$\begin{aligned} P_0^+ \Gamma_4 \Gamma_1 P_0^+ &= i\sigma_x, & P_0^+ \Gamma_1 \Gamma_3 P_0^+ &= i\sigma_y, \\ P_0^+ \Gamma_1 \Gamma_2 P_0^+ &= i\sigma_z, \end{aligned} \quad (4.7)$$

where σ_i are the Pauli matrices on the HH subspace with eigenvalue $+|\mathbf{x}|$. To see this, let us restrict ourselves to the four generators $\Gamma_1 \Gamma_\mu$, $\mu \neq 1$ and label them $V_0 = \Gamma_0 \Gamma_1$, $V_1 = \Gamma_4 \Gamma_1$, $V_2 = \Gamma_1 \Gamma_3$, $V_3 = \Gamma_1 \Gamma_2$. With this restriction, \hat{a} only has the nonvanishing components a_0, a_1, a_2, a_3 satisfying $\sum_{i=0}^3 a_i^2 = 1$. Using Eqs. (4.5-4.7) we get by comparison to Eq. (4.1)

$$\begin{aligned} \varphi &= 2\pi \left(1 - \sqrt{\sum_{i \neq 0} a_i^2} \right) = 2\pi \left(1 - \sqrt{1 - a_0^2} \right) \in [0, 2\pi], \\ \hat{n} &= \frac{(a_1, a_2, a_3)}{|(a_1, a_2, a_3)|}. \end{aligned} \quad (4.8)$$

Next, we translate the loop associated with the direction \hat{a} into a time dependent quadrupole field. To this end, we write the time dependent Hamiltonian $H(t) = x^\mu(t) \Gamma_\mu$ in two different ways:

$$H(t) = e^{t \frac{\hat{a} \cdot \vec{V}}{2}} x^\mu(0) \Gamma_\mu e^{-t \frac{\hat{a} \cdot \vec{V}}{2}} = \left(e^{t \hat{a} \cdot \vec{W}} \mathbf{x}(0) \right)^\mu \Gamma_\mu, \quad (4.9)$$

Spelling Eq. (4.9) out for infinitesimal transformations and using the independence of the different Γ_μ , i.e., $\frac{1}{4} \text{Tr} \{ \Gamma_\mu \Gamma_\nu \} = \delta_{\mu\nu}$, we obtain the desired real $SO(5)$ generators W_0, \dots, W_3 associated with the $Spin(5)$ generators V_0, \dots, V_3 . Explicitly, the $SO(5)$ defining representation $W_0 \dots W_3$ of the $Spin(5)$ generators $V_0 \dots V_3$ reads

$$W_0 = \begin{pmatrix} 0 & 1 & 0 & 0 & 0 \\ -1 & 0 & 0 & 0 & 0 \\ 0 & 0 & 0 & 0 & 0 \\ 0 & 0 & 0 & 0 & 0 \\ 0 & 0 & 0 & 0 & 0 \end{pmatrix}, \quad W_1 = \begin{pmatrix} 0 & 0 & 0 & 0 & 0 \\ 0 & 0 & 0 & 0 & -1 \\ 0 & 0 & 0 & 0 & 0 \\ 0 & 0 & 0 & 0 & 0 \\ 0 & 1 & 0 & 0 & 0 \end{pmatrix},$$

$$W_2 = \begin{pmatrix} 0 & 0 & 0 & 0 & 0 \\ 0 & 0 & 0 & 1 & 0 \\ 0 & 0 & 0 & 0 & 0 \\ 0 & -1 & 0 & 0 & 0 \\ 0 & 0 & 0 & 0 & 0 \end{pmatrix}, \quad W_3 = \begin{pmatrix} 0 & 0 & 0 & 0 & 0 \\ 0 & 0 & 1 & 0 & 0 \\ 0 & -1 & 0 & 0 & 0 \\ 0 & 0 & 0 & 0 & 0 \\ 0 & 0 & 0 & 0 & 0 \end{pmatrix}.$$

Now, we can define the time dependent quadrupole field associated with the loop in direction \hat{a} :

$$\mathcal{Q}(t) = x^\mu(t)Q_\mu = \left(e^{t\hat{a}\vec{W}} \mathbf{x}(0) \right)^\mu Q_\mu, \quad t \in [0, 2\pi],$$

which needs to be experimentally applied to perform the desired single qubit operation.

Let us give a concrete example. If we were to rotate the HH spin from pointing in z -direction to the x -direction, this would correspond to the operation $\mathcal{U}(-\hat{e}_y, \frac{\pi}{2}) = \frac{1}{\sqrt{2}} \begin{pmatrix} 1 & -1 \\ 1 & 1 \end{pmatrix}$ which is associated with the quadrupole field

$$\mathcal{Q}(t) = \left(e^{t\left(\frac{\sqrt{7}}{4}W_0 - \frac{3}{4}W_2\right)} \mathbf{e}_0 \right)^\mu Q_\mu, \quad t \in [0, 2\pi],$$

i.e., $\hat{a} = (a_0, a_1, a_2, a_3) = (\frac{\sqrt{7}}{4}, 0, -\frac{3}{4}, 0)$ and $\mathbf{x}(t=0) = \mathbf{e}_0 = (1, 0, 0, 0, 0)$ in the language of our general analysis. Indeed, plugging this choice of \hat{a} into Eq. (4.8) yields $\hat{n} = -\hat{e}_y$, $\varphi = \frac{\pi}{2}$. A stroboscopic illustration of a possible electrostatic gating scheme realizing this time-dependent quadrupole field is shown in Fig. 4.2. For this particular example, we only need 10 of the 18 gates illustrated in Fig. 4.1. To perform an arbitrary SU(2) transformation 14 of these 18 gates are needed. We could drop, for instance, the four gates that are colored in red and green in Fig. 4.1 and still would be able to perform any desired single qubit rotation on the HH subspace. This is because only two non-commuting generators need to be realized to represent an arbitrary SU(2) operation as a composite operation.

4.3 Estimation of experimental parameters

Up to now, the energy scale $\Delta E = |\mathcal{Q}| = |\mathbf{x}|$ (see Eq. (4.3)) has been treated as a free parameter. To show that this scale is amenable to state of the art experiments on GaAs quantum dots, we give a numerical estimate for ΔE . To this end, we calculate the HH-LH splitting ΔE associated with an electrostatic potential $e\Phi_4(\vec{r}) = \lambda \vec{r}^T \mathcal{Q} \vec{r}$ with quadrupole symmetry on the basis of a Luttinger four-band model for the valence bands of a GaAs/AlGaAs quantum well [Andreani87, Chuang91]. Here, \vec{r} denotes the real space position vector and the QDs are modeled by a parabolic lateral confinement potential defining the dots on a typical length scale of 50nm. The strength of the potential is determined by the constant λ . For a realistic quadrupole potential $e\Phi_4 \sim 50\text{meV}$ at a distance $r \sim 50\text{nm}$ away from the center of the dot, we obtain a splitting of $\Delta E = 0.57\text{meV}$, which corresponds to a temperature of 6.6 K and an adiabatic frequency of $\omega = 0.87\text{THz}$, respectively (see Section 4.3.1). Therefore, it is easily possible to stay below this frequency such that the adiabatic evolution is justified and at the

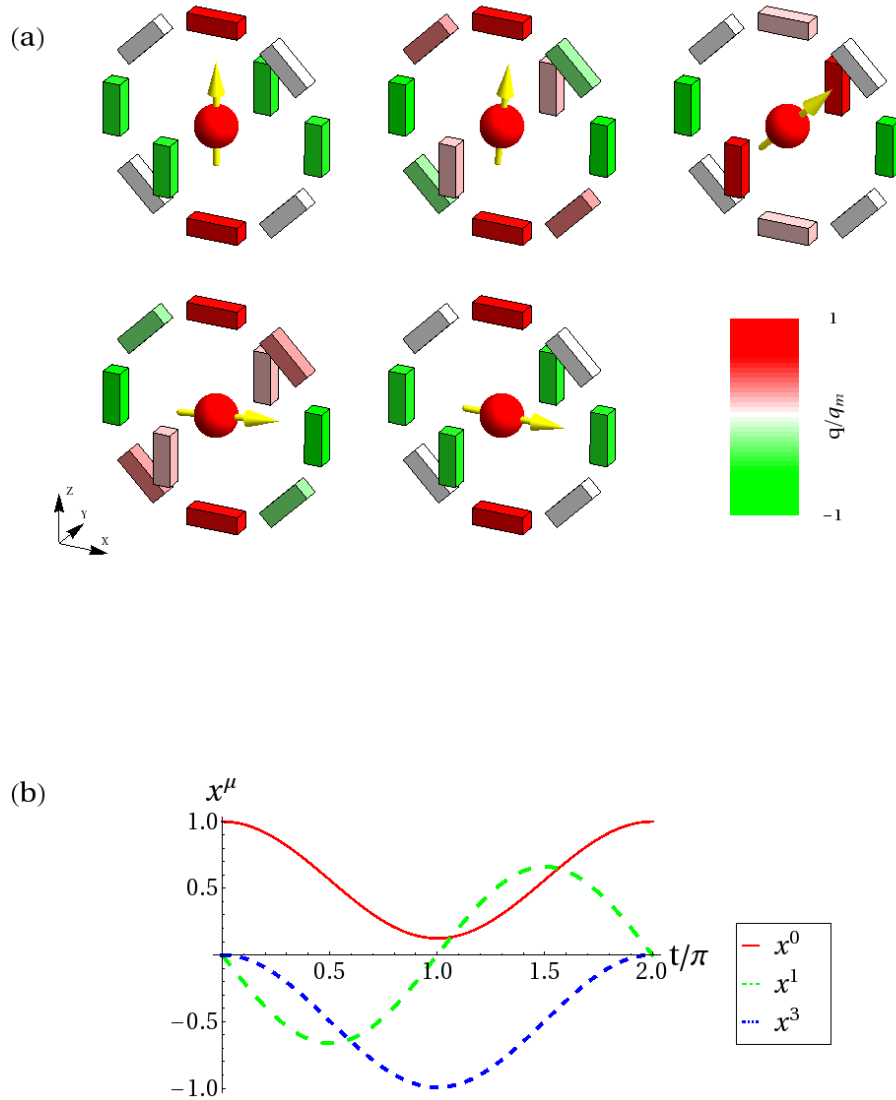


Figure 4.2: (a) A 10-gate setup realizing the operation $\mathcal{U}(-\hat{e}_y, \frac{\pi}{2})$ on the HH spin (yellow arrow). The colors of the schematic gates visualize their time-dependent charge during the loop operation, at times from left to right and top to bottom, $t = 0, \frac{\pi}{2}, \pi, \frac{3\pi}{2},$ and 2π . All charges are normalized to the charge q_m of the topmost gate at $t = 0$. (b) Time-dependence of non-zero components of \mathbf{x} during the operation $\mathcal{U}(-\hat{e}_y, \frac{\pi}{2})$.

same time complete the loop much faster than typical dephasing times in HH spin qubits. (T_2 of the order of μs has been measured in Ref. [de Greve11].)

In real experiments, there will not only be the (wanted) HH-LH splitting ΔE induced by the quadrupole field but also an (unwanted) HH-LH splitting ΔE_0 induced by confinement. For our purposes, the former should be much larger than the latter. We estimate in Section 4.3.1 that often times it is the other way round, i.e. ΔE_0 is much larger than ΔE which is a true problem for our proposal. However, by applying mechanical strain, the splitting of the individual quadruplet subbands on the quantum dot can be engineered significantly [Andreani87, Chuang95]. For the parameters used in our model, the confinement induced splitting ΔE_0 can then be realistically tuned below our estimated value of $\Delta E = 0.57\text{meV}$ (see Section 4.3.1). Hence, strain engineering of the QD is needed to guarantee a reliable performance of our setup. Additionally, we note that our proposal is robust against unwanted residual dipole fields, deviations from a quadrupole potential with only $l = 2$ contributions, and deviations from a quadratic confinement potential. The influence of these perturbations on ΔE are carefully analyzed in the Section 4.3.2 and shown to be harmless.

4.3.1 Quadrupole induced HH/LH splitting in strained GaAs quantum dots

In this section, we give a quantitative estimate of the HH-LH splitting induced by an electric quadrupole field on strained GaAs quantum dots. We model a quantum dot using the effective 2D Hamiltonian of a [001] quantum well [Andreani87] (QW) and add some parabolic confinement $\Phi_1(x, y)$. This reduces the symmetry to D_{2d} and therefore, even without a quadrupole potential, we expect a HH/LH splitting ΔE_0 . We account for this by extending the Hamiltonian $H(Q) = J^T Q J$ to

$$H' = H(Q) + \frac{\Delta E_0}{2} \tau_z$$

with $\tau_z = \text{diag}(1, -1, -1, 1)$ and the Hamiltonian is written in the basis

$$\left\{ \left| \frac{3}{2}, \frac{3}{2} \right\rangle, \left| \frac{3}{2}, \frac{1}{2} \right\rangle, \left| \frac{3}{2}, -\frac{1}{2} \right\rangle, \left| \frac{3}{2}, -\frac{3}{2} \right\rangle \right\}.$$

Without loss of generality, we use a quadrupole potential $e\Phi_4 = \frac{1}{R^2} \vec{r}^T Q \vec{r}$ associated with the quadrupole tensor of four Coulomb charges $\pm q$ at equal radius R in the (x, y) plane (corresponding to $\lambda = \frac{1}{R^2}$ above),

$$Q = \frac{1}{4\pi\epsilon} \frac{6eq}{R} \begin{pmatrix} 1 & 0 & 0 \\ 0 & -1 & 0 \\ 0 & 0 & 0 \end{pmatrix}.$$

Whereas the spectrum of H is $E = \pm|\mathbf{x}|$, where \mathbf{x} is the 5-component vector defined by the expansion $Q = x^\mu Q_\mu$, the spectrum of H' simplifies for our choice of the quadrupole potential to

$$E = \pm \frac{1}{2} \sqrt{\Delta E_0^2 + 4|\mathbf{x}|^2}. \quad (4.10)$$

We will use this relation to fit $|\mathbf{x}|$ as a function of the strength of the quadrupole potential. To obtain an effective Hamiltonian for the QW, we first solve the envelope function $\vec{f}(z)$ where z is the direction of growth. In general, the 4-component envelope function $\vec{f}(z)$ depends on $k_{\parallel} = (k_x, k_y)$. We simplify the problem by performing a $k \cdot p$ calculation with expansion of k_{\parallel} around the Γ point. The Luttinger Hamiltonian $H_L(k_{\parallel} = 0)$ is diagonal and for the i th component f_i of \vec{f} we find

$$\left(k_z \frac{1}{2m_i(z)} k_z + V(z) \right) f_i(z) = E_i f_i(z).$$

Here, $m_i(z)$ is the material dependent bulk effective mass, which is $m_{B,i}$ for the barrier and $m_{W,i}$ for the material of the well and band dependent (index i). Furthermore, $V(z) = V_B$ in the barrier and zero otherwise. We use the symmetric ansatz

$$f_i(z) = \begin{cases} A_i e^{\xi_i(z+W/2)} & z < -W/2, \\ B_i \cos(k_i z) & -W/2 \leq z \leq W/2, \\ A_i e^{-\xi_i(z-W/2)} & z > W/2, \end{cases}$$

where $W = 60\text{nm}$ is the QW width, $k_i = \sqrt{2m_{W,i}E_i}$, and $\xi_i = \sqrt{2m_{B,i}(V_B - E_i)}$. Continuity of $f_i(z)$ and $m_i(z)f_i'(z)$ give the secular equation

$$\sqrt{1 - \frac{1}{\tilde{k}_i^2}} = \left(\frac{m_{B,i}}{m_{W,i}} \right)^{3/2} \tan \left(\tilde{k}_i W \sqrt{\frac{m_{W,i}V_B}{2}} \right)$$

with $\tilde{k}_i \sqrt{2m_{W,i}V_B} = k_i$.

The Luttinger Hamiltonian for Γ_8 bands including corrections due to strain reads

$$H_L = - \begin{pmatrix} P + Q & -S & R & 0 \\ -S^\dagger & P - Q & 0 & R \\ R^\dagger & 0 & P - Q & S \\ 0 & R^\dagger & S^\dagger & P + Q \end{pmatrix}$$

written in the basis $\left\{ \left| \frac{3}{2}, \frac{3}{2} \right\rangle, \left| \frac{3}{2}, \frac{1}{2} \right\rangle, \left| \frac{3}{2}, -\frac{1}{2} \right\rangle, \left| \frac{3}{2}, -\frac{3}{2} \right\rangle \right\}$. The strain tensor ϵ_{ij} gives the displacement of an atom at unit vector \hat{i} along unit vector \hat{j} . We consider only uniaxial strain with $\epsilon_{xx} = \epsilon_{yy} \neq \epsilon_{zz}$ and $\epsilon_{xy} = \epsilon_{xz} = \epsilon_{yz} = 0$. Then, only P and Q include corrections due to strain:

$$\begin{aligned} P &= t_0 \gamma_1 (k_x^2 + k_y^2) + t_0 k_z \gamma_1 k_z + P_\epsilon, \\ Q &= t_0 \gamma_2 (k_x^2 + k_y^2) - 2t_0 k_z \gamma_2 k_z + Q_\epsilon, \\ R &= t_0 \sqrt{3} (-\gamma_2 (k_x^2 - k_y^2) + 2i \gamma_3 k_x k_y), \\ S &= t_0 \sqrt{3} (k_x - ik_y) \{ \gamma_3, k_z \} \end{aligned}$$

with $t_0 = \frac{1}{2m_0}$ and

$$\begin{aligned} P_\epsilon &= -a_v(\epsilon_{xx} + \epsilon_{yy} + \epsilon_{zz}), \\ Q_\epsilon &= -\frac{b}{2}(\epsilon_{xx} + \epsilon_{yy} - 2\epsilon_{zz}). \end{aligned}$$

The GaAs/AlAs lattice constants are almost the same (5.65Å vs. 5.66Å). This is desirable because one needs rather wide quantum wells and intends to avoid uncontrolled relaxation of strain. Here, we assume additional strain due to external pressure τ_{zz} which can be expressed in terms of the stiffness tensor C relating strain and stress. The condition of no transversal stress $\tau_{xx} = \tau_{yy} = 0$ gives

$$\begin{aligned} \epsilon_{xx} = \epsilon_{yy} &= \frac{-C_{12}}{C_{11}^2 + C_{11}C_{12} - 2C_{12}^2} \tau_{zz} \\ \epsilon_{zz} &= \frac{C_{11} + C_{12}}{C_{11}^2 + C_{11}C_{12} - 2C_{12}^2} \tau_{zz}, \end{aligned}$$

where $C_{11} = 11.88 \cdot 10^5 \text{bar}$, $C_{12} = 5.38 \cdot 10^5 \text{bar}$. [Chuang95] We take the same values for barrier and QW for the deformation potentials, $a_v = 1.16 \text{eV}$ and $b = -1.7 \text{eV}$. [Chuang95] The parameter $\zeta := Q_\epsilon$ will be used as strain control. A pressure of 1kbar gives $\zeta = 2.61 \text{meV}$. Note that P_ϵ is an unimportant overall energy shift.

The effective QW Hamiltonian is obtained by integration over envelope functions $f_\alpha(z)$ of the lowest LH and HH QW subbands,

$$H_{\alpha\beta}^{QW} = \int dz f_\alpha^\dagger(z) H_L f_\beta(z).$$

Contributions of higher subbands give quantitative, but not qualitative changes of our estimates, since strain gives a diagonal correction to H^{QW} and can be used to tune ΔE_0 . Together with the in-plane potentials Φ_i , H^{QW} gives our QD model which is numerically diagonalized.

For a quantitative estimate of $|\mathbf{x}|$, we use the same parameters as Ref. [Andreani87]: For GaAs, $\gamma_1 = 6.85$, $\gamma_2 = 2.1$, $\gamma_3 = 2.9$. For AlAs, $\gamma_1 = 3.45$, $\gamma_2 = 0.68$, $\gamma_3 = 1.29$. The barrier material is $\text{Al}_{1-\nu}\text{Ga}_\nu\text{As}$ with $\nu = 0.21$ and the Luttinger parameters are obtained by linear interpolation. The bulk gap difference is $\Delta E_g = (1.04\nu + 0.47\nu^2) \text{eV} = 0.239 \text{eV}$. We assume that the valence band shift from well to barrier is $-0.4\Delta E_g$.

For the in-plane confinement, we use $e\Phi_1 = -0.15 \text{eV}(r/R_{max})^2$ where $r^2 = x^2 + y^2$. $e\Phi_1(R_{max})$ should not exceed ΔE_g . Φ_1 is discretized on a lattice corresponding to $L=100$ nm side length, so $R_{max} = 50 \text{nm}$. By choosing R_{max} and W comparable, we intend to have about the same level spacing due to in-plane and QW confinement. Then, the confinement comes closer to the ideal, fully rotationally symmetric confinement.

With this geometry, a value of $e\Phi_i(R_{max}) = -1 \text{eV}$ gives a field strength of 40 meV/nm

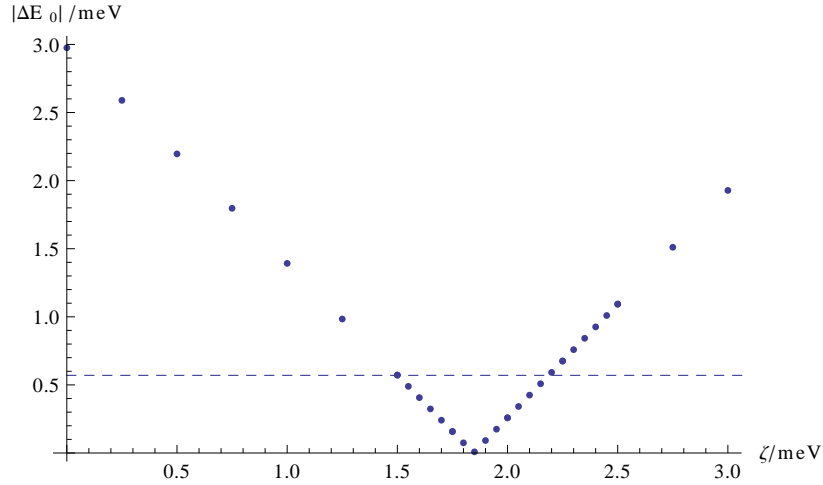


Figure 4.3: HH/LH splitting ΔE_0 (in the absence of a quadrupole field) as a function of the strain-induced subband shift ζ for a QW thickness $W = 60$ nm. Evidently, the (unwanted) HH/LH splitting ΔE_0 can be tuned down to zero by a uniform strain in z direction. The dashed line marks the value of the typical (wanted) HH/LH splitting $\Delta E = 0.57$ meV due to a quadrupole field as discussed in Section 4.2.

at R_{max} . Fig. 4.3 shows the zero-field splitting ΔE_0 as a function of strain, demonstrating that the confinement induced splitting can be tuned down to zero by means of uniaxial strain.

Fig. 4.4 shows fits to the dispersion (4.10) in order to obtain the quadrupole induced splitting $|\mathbf{x}|$. A realistic quadrupole with a maximum potential $e\Phi_4|_{r=50nm}$ of 50 meV gives a quadrupole induced splitting of $2|\mathbf{x}| \approx 0.57$ meV.

4.3.2 Stability of the quantum dot setup against perturbing potentials

The aim of this section is to analyze the stability of the effective quadrupole Hamiltonian H' against deviations from a perfect quadrupole potential with $l = 2$. These deviations include external dipole fields and deviations from the quadratic confinement and will be described as $V(r, \phi)$ in the following. The stability of H' implies the stability of the quadrupole Hamiltonian $H(Q)$ since a change in the unwanted ΔE_0 can be suppressed by adjusting the strain.

We consider the axial multipole expansion of the in-plane potential $V(r, \phi)$ given by a distribution of Coulomb charges $\rho(R, \phi')$. The QD extension is small against the distance to the gates, i.e., $r \ll R$. We expand the potential in the Legendre Polynomials P_l ,

$$V(r, \phi) = \frac{e}{4\pi\epsilon} \sum_{l=0}^{\infty} r^l \int_0^{2\pi} d\phi' P_l(\cos(\phi - \phi')) \int_0^{\infty} dR \frac{1}{R^l} \rho(R, \phi'). \quad (4.11)$$

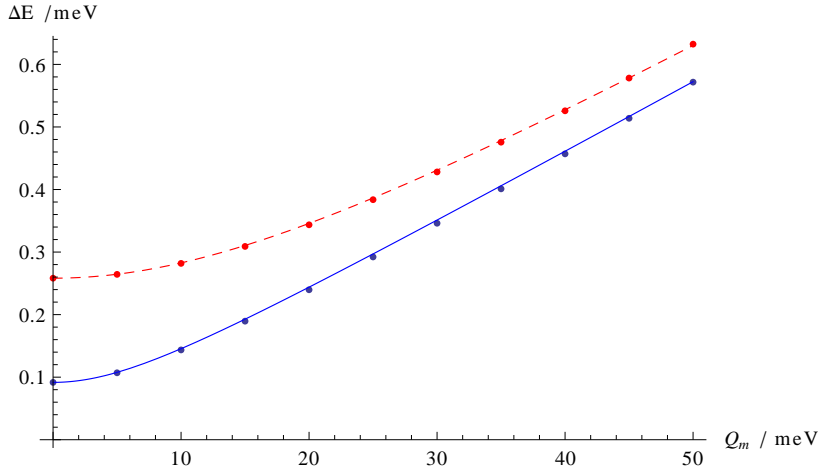


Figure 4.4: HH/LH splitting ΔE as function of the quadrupole potential $Q_m = \max(e\Phi_4)$ at $r = 50nm$. The dots are numerical results and the continuous lines fits to the expected dispersion (4.10) with the quadrupole parameter $|\mathbf{x}| = 0.00575Q_m$ (red dashed) and $|\mathbf{x}| = 0.00565Q_m$ (blue solid). The dashed red line corresponds to a strain energy $\zeta = 2meV$ and the solid blue line to $\zeta = 1.9meV$.

We continue by expanding the P_l as

$$r^l P_l(\cos(\phi - \phi')) = r^l \sum_{j=l, l-2, \dots} \alpha_{l,j} \cos(j(\phi - \phi')). \quad (4.12)$$

For the quadrupole symmetry $V(r, \phi + \frac{\pi}{2}) = -V(r, \phi)$ and upon inserting (4.12) into (4.11), the nonzero coefficients $\alpha_{l,j}$ have $j = 2, 6, 10, \dots$ and $j \leq l$. Similarly, for the dipole symmetry $V(r, \phi + \pi) = -V(r, \phi)$, the nonzero coefficients $\alpha_{l,j}$ fulfill $j = 1, 3, 5, \dots$ and $j \leq l$. Table 4.1 shows how some characteristic terms in the expansion (4.11) enter our model.

Let us now summarize the results included in Table I. The $l = 0$ term induces an uninteresting energy shift. The $l = 1$ term could give rise to a linear or quadratic Stark effect. However, in very good approximation, we may assume that GaAs and AlAs have inversion symmetry and can be described by a Luttinger Hamiltonian. Since the Luttinger Hamiltonian H_L is even under inversion, the lowest bound states have even parity. This excludes the linear Stark effect by symmetry. Further, as long as we model both the confinement and the quadrupole potential as quadratic in r , a linear potential will simply shift the center of the wave function. Thus, the quadratic Stark effect cannot change ΔE either.

For a numerical estimate of higher- l terms, we model the gates by four Coulomb charges at $r = 50nm$. We find that the $l = 3$ and $l = 4$ terms barely change ΔE even if the corresponding charge imbalance at the gates is highly overestimated as compared to a realistic experimental setup, meaning we have chosen them of the order of the quadrupole charges itself. If quadrupole symmetry of the potential holds, the lowest perturbation term is $l = 6$. This term will change depending on the shape of the gates, but, since it contains a small parameter (r^6/R^6), it is negligible.

$l = 0$		Overall shift in energy that does not change ΔE .
$l = 1$	$r \cos \phi$	Shift of the center of the bound state assuming that quadrupole and confining potentials ($\Phi_1 + \Phi_4$) are quadratic in r . ΔE unchanged.
$l = 2$	$r^2, r^2 \cos 2\phi$	Included in the model as $\Phi_1 + \Phi_4$.
$l = 3$	$r^3 P_3 = r^3(\frac{3}{8} \cos \phi + \frac{5}{8} \cos 3\phi)$	Lowest order that appears in dipole expansion and can induce quadratic Stark effect.
$l = 4$	$r^4 \cos 4\phi$ $r^4 \cos 2\phi$ r^4	Deviation from quadrupole symmetry by four equally charged gates. Allowed by quadrupole symmetry leading to the same effective Hamiltonian $H(\mathcal{Q})$ with $J = \frac{3}{2}$ but with the induced value ΔE only a few percent in comparison with $l = 2$ term. Does not influence holonomy operations. Correction to the confinement potential, which removes stability against the $l = 1$ perturbation.
$l = 6$	$r^6 \cos 6\phi$	Lowest order perturbation that appears in quadrupole expansion.

Table 4.1: Characteristic terms of the axial multipole expansion.

Finally, we note that the system is no longer robust against the quadratic Stark effect if the confinement potential behaves other than r^2 . We analyze this case in Fig. 4.5 by changing the in-plane confinement to $e\Phi'_1 = -0.15\text{eV}(r/R_{max})^2(1 + \frac{1}{3}\frac{r^2}{R_{max}^2})$. A residual constant dipole field is modeled by an additional potential $e\Phi_2 = -0.025\text{eV}\frac{r}{R_{max}}\cos(\phi - \pi/3)$ so that it is not aligned with the other potentials, and corresponds to a dipole charging being $\frac{1}{3}$ of the quadrupole charging. This certainly overestimates the error expected in an experiment. Nevertheless, as can be seen in Fig. 4.5, ΔE is barely affected by this perturbation.

Summarizing, we find that the effective Hamiltonian $H(\mathcal{Q})$ remains valid in good approximation. In all cases, the quadrupole splitting dominates the other (disturbing) contributions for realistic parameters.

4.4 Summary and outlook

We have demonstrated that an electric quadrupole field can be used to fully control a HH qubit without breaking TRS. The adiabatic time scale of our proposal is determined by the field induced splitting ΔE between the two Kramers pairs, which we have estimated for GaAs QDs to be on the order of 0.57meV. The maximum operating frequency of the device should be significantly below this energy scale to justify the adiabatic assumption which is understood throughout our analysis. Confinement induced splitting between the two Kramers pairs in the $J = \frac{3}{2}$ quadruplet of levels at the relevant energy in the HH QD impinges on the efficiency of the geometric control over the qubit. The scale of this splitting for a given quadruplet can be tuned/reduced by applying strain. We note that

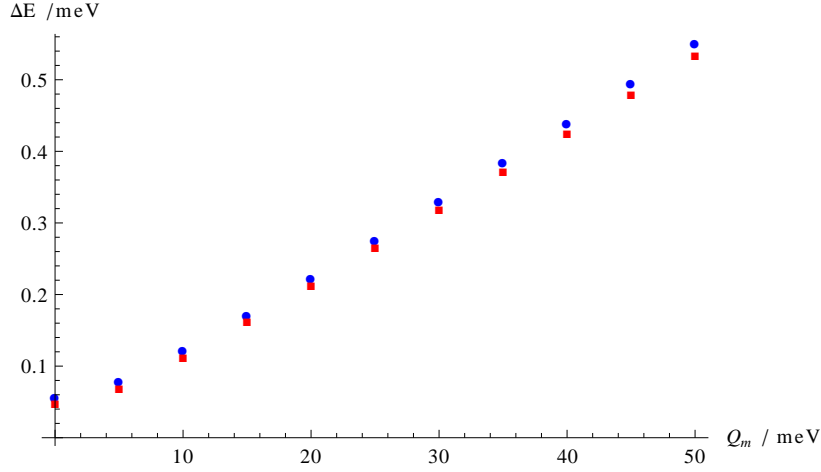


Figure 4.5: Including a r^4 correction to the confinement (Φ'_1 in the text) allows for the quadratic Stark effect by a homogeneous electric field. The plot shows the HH/LH splitting ΔE as function of the quadrupole potential $Q_m = \max(e\Phi_4)$ at $r = 50nm$ with $\zeta = 1.9meV$ and $W = 60nm$. Blue dots are without the dipole potential Φ_2 while red boxes include the Φ_2 , which corresponds to a charging ratio of 1/3 of a dipole vs. quadrupole configuration. This ratio certainly overestimates the error that we expect in the experimental situation.

exact control over the qubit is still possible as long as the quadrupole energy gap is larger than the confinement induced splitting. Our proposal is not limited to HH quantum dots in GaAs quantum wells, but can in principle also be employed to process trapped spin $\frac{3}{2}$ ions or HH-like valence band impurities by means of a quadrupole field. The presence of TRS in combination with suppressed hyperfine coupling in HH systems renders our proposal less prone to decoherence than non-adiabatic processing schemes relying on the presence of a Zeeman splitting due to an external magnetic field. Two-qubit gates can be performed by virtue of electrostatic gates as proposed in Ref. [Loss98]. All-electric spin pumping and spin filtering techniques [Broscio10], respectively, can be used to perform initialization and readout tasks on the quantum dots. Hence, our proposal in principle allows for TRS preserving universal quantum computing.

Chapter 5

Transport properties of helical edge states

This chapter is dedicated to the study of non-equilibrium transport properties of the hTLL. We employ the theory developed in Chapter 3 to investigate several holographic quantum transport peculiarities of the QSH state (see Section 2.4.1). In Section 5.1, we study an sTLL composed of two hTLLs (see Section 3.3.1) under non-equilibrium conditions and investigate the fingerprints of several coupling terms between the two hTLLs on the transport properties in a four terminal setup. In Section 5.2, we discuss the topological protection against elastic single electron backscattering (see also Section 3.3.2) in the hTLL in more detail and show how phonons can induce inelastic backscattering. In contrast, two electron backscattering due to Coulomb interaction has been known in the literature since the discovery of the hTLL [Wu06]. However, more recent literature [Ström10] on the microscopic realization of such interaction induced backscattering terms failed to predict the vanishing of backscattering in the non-interacting limit. We interpreted this as an incentive to resolve this controversy by revisiting the problem of Coulomb induced backscattering from an RG perspective which is the subject of Section 5.3.

5.1 Charge-spin duality in non-equilibrium transport of helical liquids

In this section, we study non-equilibrium transport properties of the charge and spin sectors of two edges of a QSH insulator in a four-terminal configuration following Ref. [Liu11]. A simple duality relation between charge and spin sector is found for two hTLLs (see also Section 3.3.1) connected to non-interacting electron reservoirs. If the hTLLs on opposite edges are coupled locally or non-locally, the mixing between them yields interesting physics where spin information can be easily detected by a charge measurement and vice versa. Particularly, we show how a pure spin density in the absence of charge current can be generated in a setup that contains two hTLLs and one sTLL in between.

5.1.1 Motivation and outline

An important feature of the hTLL is that spin and momentum are locked to each other (see Section 3.3 for a more detailed discussion). Consequently, we can easily manipulate the spin degree of freedom by electric means in an hTLL and vice versa. One hTLL has only half the degrees of freedom of an sTLL. Thus, two hTLLs, which naturally exist at two opposite edges of a QSH insulator, can recover the degrees of freedom of a single sTLL (see Section 3.3.1). It is well known and has even been experimentally confirmed [Auslaender05] that

there is spin-charge separation for a 1D sTLL. Therefore, it is natural and interesting to ask how the spin and the charge sector behave for two uncoupled as well as coupled hTLLs. In this section, we investigate the non-equilibrium transport properties of two hTLLs in a four-terminal configuration. The practical calculation follows closely our general outline in Section 3.2.2 with the minor complication that an additional index ν labeling the two hTLLs at the two edges of the QSH sample appears.

Most interestingly, we find a duality relation between the charge and the spin sector of two hTLLs taking into account the coupling to non-interacting electron reservoirs. As a physical consequence, there is a simple relation between the charge current and spin polarization in the dual voltage configurations of two hTLLs. Importantly, the coupling between the two edges will destroy the simple duality relation. However, we can still manipulate the charge and the spin sector separately only by electric means. To demonstrate this, we study different scattering mechanisms between the two hTLLs within the non-equilibrium Keldysh formalism (see Section 3.2) and bosonization (see Section 3.1). Different bias dependences are found for different scattering mechanisms which can be used to distinguish and identify them in experiments.

5.1.2 Model and spin-charge duality

We consider a QSH insulator in a four-terminal configuration as shown in Fig. 5.1 (a). The two edges are denoted by $\nu = u(l)$ for the upper (lower) edge. On each edge ν , there are two terminals with chemical potentials $\mu_{i,\nu}$ ($i = 1, 2$ means left and right lead, respectively). Two terminals on the same edge are connected by an hTLL of finite length L . As far as the $1/L$ terms appearing in Eq. (3.4) are concerned, we still consider L as infinite. The hTLL states are described by the field operators $\psi_{p,s}$ where $(p, s) = (R, \uparrow)$ or (L, \downarrow) for the upper edge and $(p, s) = (R, \downarrow)$ or (L, \uparrow) for the lower edge. In the middle region of the sample, the hTLLs at the two edges can mix and different types of coupling mechanisms will be discussed below.

As discussed in Section 3.3.1, there are two possibilities for choosing the basis states of the composite sTLL: (i) the helical edge basis and (ii) the spin-charge basis. For the helical edge basis, the nonchiral boson field is defined separately for each edge with $\varphi_{u(l)} = \phi_{R,\uparrow(\downarrow)} + \phi_{L,\downarrow(\uparrow)}$ at the upper (lower) edge and the corresponding dual field $\theta_{u(l)} = \phi_{R,\uparrow(\downarrow)} - \phi_{L,\downarrow(\uparrow)}$. Here, $\phi_{p,s}$ ($p = R, L$ and $s = \uparrow, \downarrow$) is the spinful chiral hermitian field appearing in the bosonization identity, Eq. (3.23). This basis is suitable to study the current at different terminals. However, when we are interested in spin properties, it is more convenient to introduce the spin-charge basis, which ignores the u, l labels and is related to the basis of the spinful bosonic fields defined in Eq. (3.24) by Eq. (3.25) which we repeat here for the reader's

convenience.

$$\begin{aligned}\varphi_\rho &= \frac{1}{\sqrt{2}}(\varphi_\uparrow + \varphi_\downarrow), \\ \varphi_\sigma &= \frac{1}{\sqrt{2}}(\varphi_\uparrow - \varphi_\downarrow), \\ \theta_\rho &= \frac{1}{\sqrt{2}}(\theta_\uparrow + \theta_\downarrow), \\ \theta_\sigma &= \frac{1}{\sqrt{2}}(\theta_\uparrow - \theta_\downarrow).\end{aligned}$$

The Hamiltonian can be written as

$$H = H_0 + H_V + H_t, \quad (5.1)$$

where H_0 describes the hTLLs at two edges, H_V the coupling between the helical liquid and the leads (see Eq. (3.15)), and H_t the scattering region coupling the two hTLLs.

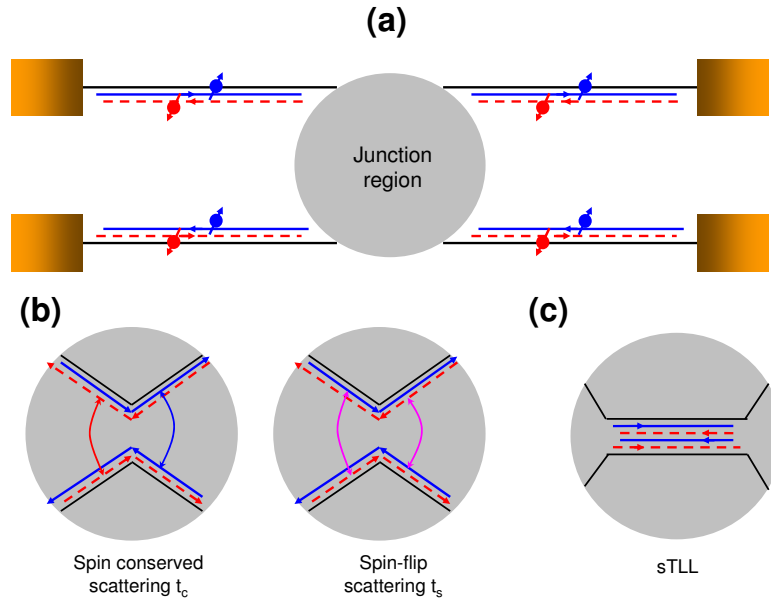


Figure 5.1: (a) Schematic of the four-terminal setup. At each edge, there is a conducting channel of an hTLL (blue line corresponds to spin up; red line to spin down). The two hTLLs are mixed in the junction region and different types of junctions are analyzed: (b) the short junction with two possible single particle scattering terms: (i) spin conserving scattering \tilde{t}_c and (ii) spin-flip scattering \tilde{t}_s and (c) the long junction modeled by an sTLL.

The hTLL coupled to electronic reservoirs can be modeled by the so-called $g(x)$ -model

[Maslov95, Ponomarenko95, Safi95] given by

$$\begin{aligned} H_0^\rho &= \frac{v_F}{2} \int dx \left[(\partial_x \theta_\rho)^2 + \frac{1}{g^2(x)} (\partial_x \varphi_\rho)^2 \right], \\ H_0^\sigma &= \frac{v_F}{2} \int dx \left[\frac{1}{g^2(x)} (\partial_x \theta_\sigma)^2 + (\partial_x \varphi_\sigma)^2 \right] \end{aligned} \quad (5.2)$$

in the spin-charge basis. Here, v_F is the Fermi velocity and $g(x)$ is the hTLL interaction parameter, with $g(x) = g_0 < 1$ for repulsive interactions within the helical edge located at $|x| < L/2$, and $g(x) = 1$ for the non-interacting fermions in the leads with $|x| > L/2$. We assume the same parameters v_F and g_0 at the two edges ($\nu = u, l$). This is reasonable for two edges of the same system. The chemical potentials in the leads are naturally taken into account with the bias Hamiltonian

$$H_V = \int \frac{dx}{\sqrt{2\pi}} [\partial_x \mu_\rho(x) \varphi_\rho + \partial_x \mu_\sigma(x) \theta_\sigma],$$

where

$$\partial_x \mu_{\rho(\sigma)} = -\mu_{1,\rho(\sigma)} \delta(x + L/2) + \mu_{2,\rho(\sigma)} \delta(x - L/2)$$

with $\mu_{i,\rho} = \mu_{i,u} + \mu_{i,l}$ and $\mu_{i,\sigma} = \mu_{i,u} - \mu_{i,l}$ ($i = 1, 2$). Remarkably, μ_ρ couples to φ_ρ while μ_σ couples to θ_σ . Therefore, the electric voltage can couple to both the charge and the spin sector of the composite sTLL. This provides us with a means to control the charge sector and the spin sector separately, in contrast to the usual sTLL where the electric chemical potential only couples to the charge sector. Moreover, we discover that there is a duality relation between the charge sector and the spin sector

$$\varphi_\rho \leftrightarrow \theta_\sigma, \quad \theta_\rho \leftrightarrow \varphi_\sigma. \quad (5.3)$$

For H_0^λ ($\lambda = \rho, \sigma$), the above duality relation is directly related to the constraint $g_c = 1/g_s$ discovered in Ref. [Hou09] before (see also Section 3.3.1). Here, we show that this relation remains valid even if the system is coupled to non-equilibrium electron reservoirs. Thus, it is observable in transport properties of the system.

What is the physical consequence of this duality relation? To answer this question, we investigate the total charge current and the total spin density of the system. The charge current is given by $j_\rho = -e\sqrt{\frac{2}{\pi}}\partial_t\varphi_\rho$, which is the sum of the currents along the two edges $j_\rho = j_u + j_l$, with $j_\nu(x) = -\frac{e}{\sqrt{\pi}}\partial_t\varphi_\nu$ (see Eq. (3.11)). The spin density can be defined as $\rho_\sigma = \sqrt{\frac{2}{\pi}}\partial_x\varphi_\sigma$. Combining Eq. (3.25) and $\partial_t\varphi_\nu = -v_F\partial_x\theta_\nu$ (see Eq. (3.10)), it is evident that the spin density can be directly related to the charge current along the two edges by

$$\rho_s = \frac{1}{ev_F}(j_u - j_l).$$

In the absence of mixing between the two edges, our setup describes the transport through two independent 1D channels. Then, it follows directly from previous work [Maslov95,

Ponomarenko95, Safi95] that

$$\langle j_{0,\nu} \rangle = \frac{e^2}{h} V_\nu,$$

where $-eV_\nu = \mu_{1,\nu} - \mu_{2,\nu}$. Thus, the total charge current is $\langle j_{0,\rho} \rangle = \frac{2e^2}{h} V_\rho$ with $V_\rho = V_u + V_l = -\frac{1}{2e}(\mu_{1,\rho} - \mu_{2,\rho})$, while the total spin density is given by $\langle \rho_{0,\sigma} \rangle = \frac{2e}{h v_F} V_\sigma$ with $V_\sigma = V_u - V_l = -\frac{1}{2e}(\mu_{1,s} - \mu_{2,s})$. Importantly, it is spin density and not spin current that is dual to the charge current, which is a direct consequence of the duality relation (5.3). Physically, V_ρ and V_σ can be easily generated by two different voltage configurations of the four terminal setup, as shown in Fig. 5.2. In Fig. 5.2(a), $\mu_{1,+} = \mu_{1,-} = -\mu_{2,+} = -\mu_{2,-} = -eV_0/2$, which yields $V_\rho = V_0$ and $V_\sigma = 0$; and in Fig. 5.2(b), $\mu_{1,+} = \mu_{2,-} = -\mu_{1,-} = -\mu_{2,+} = -eV_0/2$, resulting in $V_\rho = 0$ and $V_\sigma = V_0$. In these two symmetrical bias configurations, we find either charge current or spin density but no spin current. This is different for unsymmetrical bias configurations where charge current and spin density are usually accompanied by spin current as well.

Thus, in Fig. 5.2(a), there is charge current but no spin density while in Fig. 5.2(b) there is spin density but no charge current. There is a simple physical picture to understand this result. For the upper edge, the right mover has spin up and the left mover has spin down, while for the lower edge the situation is just the other way round. In Fig. 5.2(a), on both edges the left movers have a larger chemical potential than the right movers resulting in total charge current from left to right. However, since now the left movers for the upper edge and lower edge have opposite spin, the spin density at the two different edges will cancel each other. A similar analysis can also be applied to the configuration of Fig. 5.2(b), in which the left movers have higher (lower) Fermi energy than the right movers for the upper (lower) edge. Since both the left movers at the upper edge and the right movers at the lower edge have spin up, the spin density will be finite and maximal in this configuration.

Up to now, we have discussed the transport properties of two hTLLs and shown a simple relation between the charge current and the spin density in two (dual) voltage configurations. In the following, we would like to take into account a junction structure introducing scattering between the two hTLLs within a region of finite length d . We consider two different scenarios: (i) the short junction (SJ) with $d \ll \lambda_F$ and (ii) the long junction (LJ) with $d \gg \lambda_F$, where λ_F is the electron Fermi wave length. For SJ, we can neglect the length of the scattering region and model it as a quantum point contact, while for LJ, we can regard the scattering region as a finite length sTLL.

5.1.3 Short junction case

In the following, we concentrate on the experimentally relevant regime $1/2 < g_0 < 1$ [Teo09]. Then, all the possible one-particle and two-particle scattering terms will be irrelevant [Teo09]. Hence, we can safely treat the scattering Hamiltonian H_t as a perturbation. For the SJ case, two types of one particle scattering terms, which preserve time reversal symmetry, are taken

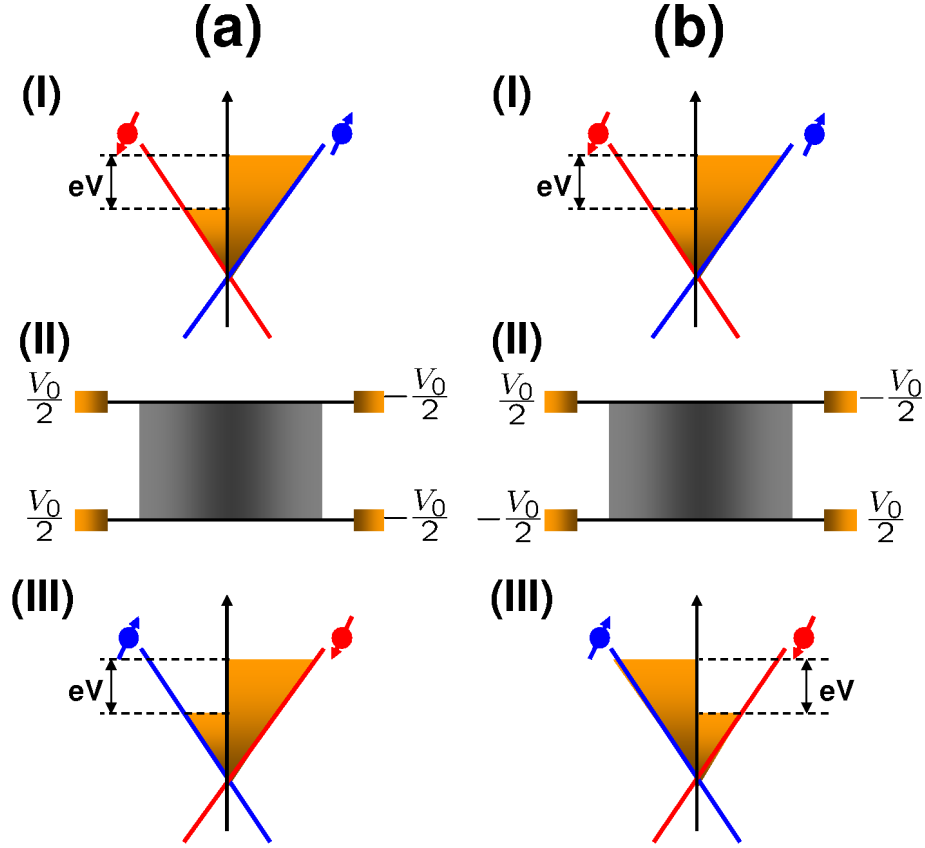


Figure 5.2: (a). (I) and (III) show band dispersions and chemical potentials of the upper edge and the lower edge, respectively. (II) illustrates the voltage configuration $\mu_{1,u} = \mu_{1,l} = eV_0/2$ and $\mu_{2,u} = \mu_{2,l} = -eV_0/2$. (b). Similar to (a) with a different voltage configuration $\mu_{1,u} = \mu_{2,l} = eV_0/2$ and $\mu_{2,u} = \mu_{1,l} = -eV_0/2$.

into account (see Fig. 5.1(b)): the first one is the spin conserving term

$$H_{t1} = t_c(\psi_{R,\uparrow}^\dagger(x_0)\psi_{L,\uparrow}(x_0) + \psi_{L,\downarrow}^\dagger(x_0)\psi_{R,\downarrow}(x_0) + h.c.),$$

and the second one is the spin flip term

$$H_{t2} = t_s(\psi_{R,\uparrow}^\dagger(x_0)\psi_{R,\downarrow}(x_0) - \psi_{L,\downarrow}^\dagger(x_0)\psi_{L,\uparrow}(x_0) + h.c.)$$

with the junction position x_0 . In bosonization,

$$\hat{H}_t = i\tilde{t}_c \sum_s \eta^{R,s} \eta^{L,s} \sin(\sqrt{\pi} \Xi_s) + i\tilde{t}_s \sum_\nu \eta^{\nu,\uparrow} \eta^{\nu,\downarrow} \sin(\sqrt{\pi} \Psi_\nu)$$

with $\Xi_s = \sqrt{2}(\varphi_\rho + s\varphi_\sigma)$ and $\Psi_\nu = \sqrt{2}(\varphi_\sigma + \nu\theta_\sigma)$. Here, $\eta^{\nu,s}$ is the Klein factor and $\tilde{t}_{c(s)} = \frac{t_{c(s)}}{\pi}$. We now perform the perturbative calculation of our four terminal system within the non-equilibrium Keldysh formalism (see Section 3.2.2). All physical quantities can be related to the expectation value of boson fields, which can be obtained from the functional derivatives of the generating function $Z[J]$ which includes the Hamiltonian (5.1) and the additional source term J coupling to the boson field φ_ν or θ_ν . Treating H_t as a perturbation, we can expand any physical quantity \hat{O} in powers of $\tilde{t}_{c(s)}$, e.g., $\langle \hat{O} \rangle = \langle \hat{O}_0 \rangle + \langle \hat{O}_2 \rangle$ up to second order (see Eq. (3.22) and discussion thereafter).

The first corrections to $\langle j_{0,\rho} \rangle$ and $\langle \rho_{0,\sigma} \rangle$ come from one particle scattering and can be expressed as $\langle j_{2,\rho} \rangle = \sum_{s=\pm} J_{\Xi,s}$ and $\langle \hat{\rho}_{2,\sigma} \rangle = \frac{1}{ev_F} \sum_{\nu=\pm} \nu J_{\Psi,\nu}$ with

$$J_{\Xi,s} = \frac{e\tilde{t}_c^2}{4} \int_{-\infty}^{\infty} dt \sum_m m e^{imeV_\rho t} e^{\pi C_s^\Xi(x_0, x_0; t)},$$

$$J_{\Psi,\nu} = \frac{e\tilde{t}_s^2}{4} \int_{-\infty}^{\infty} dt \sum_m m e^{ima_e V_\sigma t} e^{\pi C_\nu^\Psi(x_0, x_0; t)}$$

for the edge $\nu = \pm$. All the information about the detailed sample configuration is now included in the correlators C_s^Ξ and C_ν^Ψ , which are given by $C_s^\Xi = 2(C_\rho + C_\sigma)$ and $C_\nu^\Psi = 2(C_\sigma + \mathcal{D}_\sigma) + 2\nu(\mathcal{F}_\sigma + \mathcal{Q}_\sigma)$ with the correlation functions

$$\begin{aligned} C_\lambda &= \langle \varphi_\lambda \varphi_\lambda \rangle_0, \mathcal{D}_\lambda = \langle \theta_\lambda \theta_\lambda \rangle_0, \\ \mathcal{F}_\lambda &= \langle \varphi_\lambda \theta_\lambda \rangle_0, \mathcal{Q}_\lambda = \langle \theta_\lambda \varphi_\lambda \rangle_0, \quad \lambda = \rho, \sigma, \end{aligned}$$

defined in total analogy to Eq. (3.18) but with an additional spin-charge index λ . We note that the spin conserving scattering \tilde{t}_c can only be induced by a charge voltage V_ρ and, hence, will reduce the total charge current in the voltage configuration of Fig. 5.2(a), while the spin-flip scattering \tilde{t}_s is only driven by the spin voltage V_σ and decreases the spin density in the configuration of Fig. 5.2(b). For clarity, we further divide the operator O_2 into two parts $\langle O_2 \rangle = \langle O_2^{(0)} \rangle + \langle O_2^{(1)} \rangle$, where $\langle O_2^{(0)} \rangle$ is calculated on the basis of $L \rightarrow \infty$ correlation functions, while $\langle O_2^{(1)} \rangle$ contains all finite length corrections. Then, analytical expressions for the charge current and the spin density are readily obtained and given by

$$\begin{aligned} \langle j_{2,\rho}^{(0)} \rangle &= -\frac{e\pi\tilde{t}_c^2\tau_c^{g_0+\frac{1}{g_0}}}{\Gamma\left(g_0+\frac{1}{g_0}\right)} \text{sgn}(V_\rho) |eV_\rho|^{g_0+\frac{1}{g_0}-1}, \\ \langle \rho_{2,\sigma}^{(0)} \rangle &= -\frac{\pi\tilde{t}_s^2\tau_c^{g_0+\frac{1}{g_0}}}{v_F\Gamma\left(g_0+\frac{1}{g_0}\right)} \text{sgn}(V_\sigma) |eV_\sigma|^{g_0+\frac{1}{g_0}-1}. \end{aligned}$$

Here, τ_c is the short time cutoff. Both the charge current and the spin density depend in a power law fashion on the voltage. This coincides with earlier work based on a renormalization group analysis [Hou09, Teo09, Ström09, Tanaka09]. Then, for $V_\rho = V_\sigma$, we find that the ratio between the charge current and spin density in the two different voltage configurations

is

$$\langle j_{2,\rho}^{(0)} \rangle / \langle \rho_{2,\sigma}^{(0)} \rangle = ev_F \frac{\tilde{t}_c^2}{\tilde{t}_s^2},$$

which contains the information about the scattering strength for the different types of scattering. In the finite length case, we use the numerical method of Ref. [Dolcini05] to evaluate $J_{\Xi,s}$ and $J_{\Psi,\nu}$. As shown in Fig. 5.3(a) and (b), the finite length will introduce oscillations in both the backscattering current and the spin density, which originates from Fabry-Perot-type interferences of plasmonic excitations [Safi95]. However, since the power law $g_0 + \frac{1}{g_0} - 1$ is always larger than 1 for positive g_0 , $\langle j_{2,\rho}^{(0)} \rangle$ ($\langle \rho_{2,\sigma}^{(0)} \rangle$) will increase rapidly with V_ρ (V_σ) and dominate the oscillatory corrections for large V_ρ (V_σ). Hence, finite length corrections are not very important in this setup.

5.1.4 Long junction case

Now, we consider the opposite limit $d \gg \lambda_F$ as shown in Fig. 5.1(c). This case could be achieved by gradually narrowing the QSH sample into a 1D wire experimentally. In the following, we analyze finite size effects related to d and assume that $L \gg d$, hence $L \rightarrow \infty$ is a reasonable approximation. For simplicity, we model the LJ as an sTLL described by $H_t = H_{t0} + H_{t2}$ with $H_{t0} = H_{t0}^\rho + H_{t0}^\sigma$ where

$$\begin{aligned} H_{t0}^\rho &= \frac{v_F}{2} \int dx \left[(\partial_x \theta_\rho)^2 + \frac{1}{g_0^2} (\partial_x \varphi_\rho)^2 \right], \\ H_{t0}^\sigma &= \frac{v_F}{2} \int dx \left[(\partial_x \theta_\sigma)^2 + (\partial_x \varphi_\sigma)^2 \right], \end{aligned}$$

for $|x| < d/2$. Compared to Eq. (5.2), we find that the charge sector remains unchanged while the interaction parameter of the spin sector varies from $1/g_0$ to 1. This originates from the SU(2) symmetry of the spin sector of an sTLL. For the charge sector, since the Hamiltonian remains the same, we see that the interaction between two hTLL will not affect the charge current $\langle j_\rho \rangle$ at all. For the spin sector of a 1D sTLL, besides H_{t0}^σ , we consider two additional interaction terms [Gritsev05, Tanaka09]

$$H_{t2} = \int_{-\frac{d}{2}}^{\frac{d}{2}} dx \left[g_{1\perp} \cos(\sqrt{8\pi}\varphi_\sigma) + g_{\text{sf}} \cos(\sqrt{8\pi}\theta_\sigma) \right],$$

where the $g_{1\perp}$ -term is related to spin conserving backscattering $\psi_{L,\uparrow}^\dagger \psi_{R,\downarrow}^\dagger \psi_{L,\downarrow} \psi_{R,\uparrow} + h.c.$ while the g_{sf} -term is related to the spin-flip backscattering process $\psi_{L,\downarrow}^\dagger \psi_{R,\downarrow}^\dagger \psi_{L,\uparrow} \psi_{R,\uparrow} + h.c.$, see Fig. 5.3(c). These are the most important perturbations in the absence of impurity scattering which we assume here. Since the $g_{1\perp}$ -term conserves spin, it will not influence the spin density. Thus, we focus on the g_{sf} -term below. Up to second order perturbation theory, we

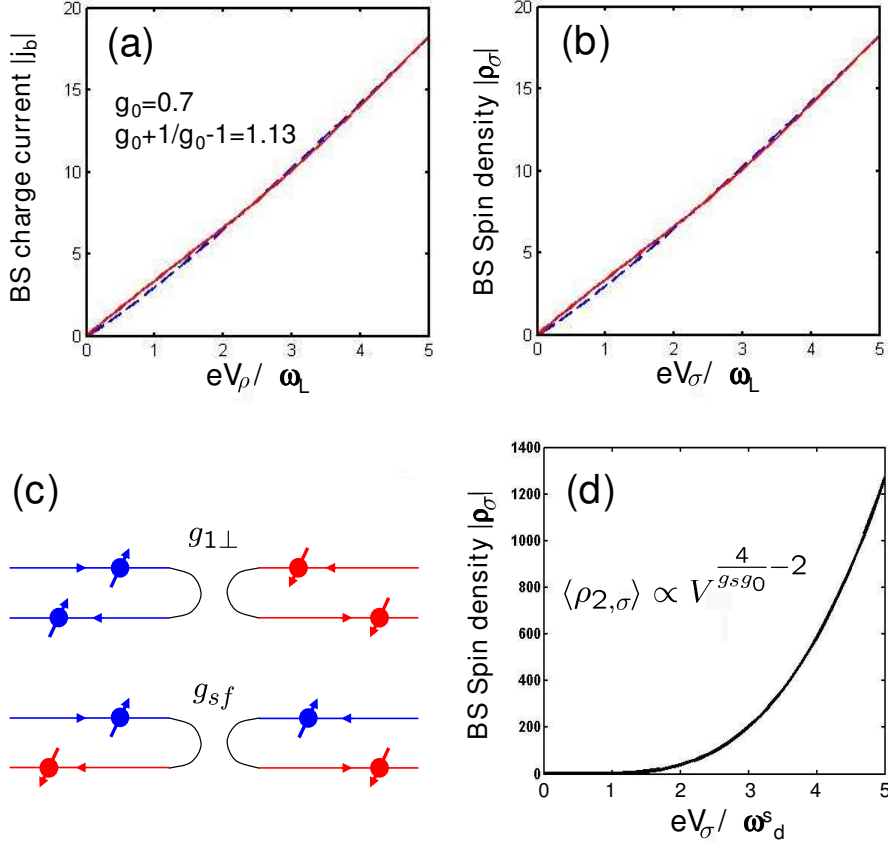


Figure 5.3: (a) The backscattering current as a function of charge bias V_ρ generated by the spin conserving t_c -term for the voltage configuration of Fig. 5.2(a). The blue dashed line corresponds to the charge current $\langle j_{2,\rho}^{(0)} \rangle$, while the red solid line additionally includes the finite length corrections. The current unit is $\frac{2e\tilde{t}_c^2(\tau_c\omega_L)^{g_0+\frac{1}{g_0}}}{\omega_L}$. (b) is similar to (a), except that now we show the spin density $\langle \rho_{2,\sigma}^{(0)} \rangle$ and $\langle \rho_{2,\sigma} \rangle$ as a function of the spin bias V_σ generated by the spin-flip t_s -term for the voltage configuration of Fig. 5.2(b). The spin density unit is $\frac{2\tilde{t}_s^2(\tau_c\omega_L)^{g_0+\frac{1}{g_0}}}{v_F\omega_L}$. (c) Possible two particle backscattering terms: spin conserving backscattering $g_{1\perp}$ and spin-flip backscattering g_{sf} . (d) The voltage dependence of the correction to the spin density $\langle \rho_{2,\sigma} \rangle$ due to the two particle spin-flip term g_{sf} . The spin density unit is $\frac{(g_{sf}d)^2(\tau_c\omega_d)^{4/g_0}}{2v_F\omega_d}$. In all expressions above, we use $\omega_L = \frac{v_F}{g_0L}$, $\omega_d = \frac{v_F}{d}$, and $g_0 = 0.7$.

obtain the following correction to the spin density

$$\langle \rho_{2,\sigma} \rangle = -\frac{g_{\text{sf}}^2 d^2}{v_F} \int_0^1 dR \int_0^{1-|R|} dr f(r, R),$$

$$f(r, R) = \int_{-\infty}^{\infty} dt' \sum_m m e^{i2meV_\sigma t'} e^{8\pi \mathcal{D}_\sigma(x,y,t')},$$

where $r = (x - y)/d$ and $R = (x + y)/d$. The above triple integration can be easily evaluated numerically and the obtained correction to the spin density is shown in Fig. 5.3(d). To make analytical progress, we can again divide the obtained spin density into two parts $\langle \rho_{2,\sigma} \rangle = \langle \rho_{2,\sigma}^{(0)} \rangle + \langle \rho_{2,\sigma}^{(1)} \rangle$ with $\langle \rho_{2,\sigma}^{(0)} \rangle$ for the infinite d contribution and $\langle \rho_{2,\sigma}^{(1)} \rangle$ accounting for finite length corrections. We find that $\langle \rho_{2,\sigma}^{(0)} \rangle$ always dominates over $\langle \rho_{2,\sigma}^{(1)} \rangle$. In the limit $eV_\sigma \omega_d \gg 1$, we obtain

$$\langle \rho_{2,\sigma}^{(0)} \rangle \approx -\text{sgn}(eV_\sigma) \frac{\omega_d g_{\text{sf}}^2 d^2 \pi^2 \tau_c^{4/g_0}}{v_F \Gamma^2(2/g_0)} |eV_\sigma|^{\frac{4}{g_0}-2}$$

with $\omega_d = v_F/d$.

It is important to analyze the validity regime of our perturbation theory. Note that for $g_0 < 1$, the power law exponent $\frac{4}{g_0} - 2$ will always be larger than 2. Thus, the second order correction to the spin density $\langle \rho_{2,\sigma} \rangle$ will increase faster than the zero order term $\langle \rho_{0,\sigma} \rangle$ as a function of bias voltage. Evidently, our perturbation theory is only justified when $(\omega_d \tau_c) (g_{\text{sf}} d \tau_c)^2 |eV_\sigma \tau_c|^{\frac{4}{g_0}-3} \ll 1$.

5.1.5 Summary and outlook

We have analyzed the charge current and the spin density in a four-terminal setup based on two hTLL coupled to non-interacting electron reservoirs. Different types of scattering mechanisms between the edges have been taken into account, particularly short junctions and long junctions. It has been shown that different power law dependencies as a function of bias voltages applied to the four terminals can be used to distinguish the scattering mechanisms. A simple duality relation between charge current and spin density has been discovered. Remarkably, all spin-related observables can be measured by straightforward charge measurements in the four-terminal configuration. It is interesting to ask the question whether the spin density in such a setup can also be measured by other means (e.g., as a test of the model). Taking typical values for $v_F = 3eV \cdot \text{\AA}$ and $eV_\sigma = 5meV$, we find that the zero order spin density is about $\langle \hat{\rho}_{0,\sigma} \rangle \approx 5.3 \mu\text{m}^{-1}$. This may be detected by state-of-the-art local Faraday/Kerr rotation [Kato04]. Furthermore, the possibility of applying a spin dependent bias voltage in the composite sTLL is also interesting in the context of non-equilibrium two channel Kondo physics. Exact results on the non-equilibrium Kondo cloud in a related setup have recently been reported in Ref. [Posske12] demonstrating how such a spin bias can be used to manipulate spin correlations in a way which is not viable by virtue of a conventional bias.

In the next two sections, we focus on a single hTLL. We will take a closer look at the

quantized conductance of a single helical edge state mentioned in Section 3.3.2 and investigate its robustness against phonon-induced and Coulomb interaction induced backscattering, respectively.

5.2 Phonon-Induced Backscattering in Helical Edge States

A single pair of helical edge states as realized at the boundary of a quantum spin Hall insulator is known to be robust against elastic single particle backscattering as long as time reversal symmetry is preserved [Wu06] (see also Section 3.3.2). However, there is no symmetry preventing inelastic backscattering as brought about by phonons in the presence of Rashba spin orbit coupling. In this section, we first review the phenomenon of topological protection by TRS and point out its limitations. We then show that the quantized conductivity of a single channel of helical Dirac electrons is protected even against the mentioned inelastic mechanism to leading order. We further demonstrate that this result remains valid when Coulomb interaction is included in the framework of a helical Tomonaga Luttinger liquid. Our analysis follows closely the original material published in Ref. [Budich12a].

5.2.1 Motivation

During recent years, great interest has been attracted by the theoretical prediction [Kane05a, Bernevig06a] and experimental discovery [König07] of the QSH state (see Section 2.4.1). The QSH phase is a two dimensional TRS preserving TSM that differs essentially from trivial atomic insulators by a \mathbb{Z}_2 topological invariant [Kane05b, Qi11, Hasan10] (see Section 2.4.1 for a detailed discussion). Besides the enormous conceptual depth of TSM, the QSH phase is also considered a promising candidate as to future applications in nanoelectronics. This is due to its topologically protected transport properties which might be exploited for high precision spintronics devices operating at low power consumption. Therefore, modeling the QSH effect under experimentally relevant conditions is crucial to test the practical limitations of these protected features.

5.2.2 Topological protection against backscattering and its limitations

As far as the robustness of the topological protection is concerned, the QSH effect is fundamentally different from the integer quantum Hall (IQH) effect. For the TRS breaking IQH insulator [Klitzing80, Laughlin81, Thouless82], the bulk topology leads to a quantization of conductivity to impressive accuracy. In the IQH regime, edge state transport is chiral, meaning that the density of states for subgap backscattering vanishes. This excludes such processes by simple phase space arguments. In contrast, in the TRS preserving QSH phase a single pair of helical edge states induced by bulk boundary correspondence is supported at the edge of the QSH bar. This means that both right- and leftmovers exist at a single edge. However, states of opposite direction of motion are Kramers partners due to TRS. The well known topological protection of a single pair of helical edge states against backscattering in this scenario can be mathematically illustrated by the following simple argument [Xu06].

Let $|\phi\rangle$ and $|\psi\rangle = T|\phi\rangle$ be Kramers partners. Then, as long as H is a TRS preserving Hamiltonian

$$\begin{aligned}\langle\psi|H|\phi\rangle &= \langle\phi|H|\psi\rangle^* = \langle T\phi|TH|\psi\rangle = \\ &= \langle\psi|HT|\psi\rangle = \langle\psi|HT^2|\phi\rangle = -\langle\psi|H|\phi\rangle,\end{aligned}\tag{5.4}$$

i.e., the matrix element for scattering between the Kramers partners vanishes. Note that the argument (5.4) of protection relies on two fundamental constraints: First, only single electron processes are considered. Second, since Kramers partners are degenerate states, it only precludes elastic backscattering. Within the validity of these restrictions extensive studies of the hTLL [Xu06, Wu06] representing a single pair of helical edge states have shown that Anderson localization is avoided [Kane05a, Ryu10] in the presence of TRS preserving disorder and that TRS breaking magnetic impurities can open a gap in these systems [Maciejko09]. Furthermore, interedge backscattering can occur if the QSH sample is locally narrowed down to a quantum point contact [Ström09, Teo09, Hou09, Liu11, Schmidt11] (see also Section 5.1) or if two QSH bars are brought close to each other [Tanaka09]. In general, backscattering at a single helical edge requires spin flip processes. In realistic setups, these are induced by Rashba SOI originating from unavoidable potential fluctuations. Preserving TRS, Rashba SOI cannot cause *single electron* elastic backscattering, though. However, relaxing the single electron processes constraint by additionally including Coulomb interaction, two electron backscattering processes have been shown to arise in these systems [Ström10]. Such backscattering terms are well known to be allowed by TRS [Wu06].

Under realistic experimental conditions, finite temperature and bias voltage also imply the presence of phonons, i.e., inelastic processes that undermine the second constraint for the validity of the argument (5.4). It is thus of crucial importance to investigate the influence of this dissipative mechanism on the topological protection. Here, we show two important results of the helical edge states in the presence of two TRS preserving perturbations: Rashba SOI and electron phonon coupling. First, we demonstrate that in this scenario there is no strict protection against inelastic *single electron* backscattering. Second, we find that for helical Dirac fermions the leading order contribution of this mechanism vanishes, supporting the protection for practical purposes. We further demonstrate how this additional robustness fully survives in the presence of Coulomb interaction, i.e., in an hTLL with electron phonon coupling and Rashba SOI. In a nonequilibrium transport calculation for the hTLL, we take the electron phonon coupling into account exactly by integrating out the phonons using a Keldysh contour path integral representation of the generating functional (see Section 3.2.2). Our analysis is relevant for any realization of the hTLL as a one dimensional system.

5.2.3 Model without Coulomb interaction

We investigate a single pair of helical Dirac fermions coupled linearly to longitudinal acoustic phonons. The two species of electrons are coupled via Rashba SOI (see Fig. 5.4). In most parts of this work, we will have a sharp impurity-like scattering potential in mind which brings about momentum transfer on the order of $2k_F$, where k_F is the Fermi wave vector. We represent the helical fermionic fields as a spinor $\Psi = (\Psi_{R\uparrow}, \Psi_{L\downarrow})^T = (\Psi_+, \Psi_-)^T$. The

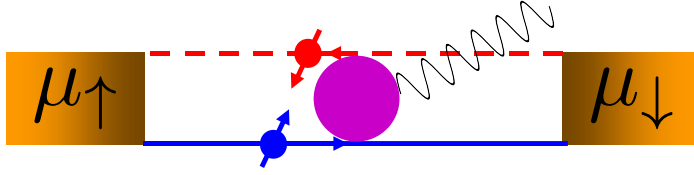


Figure 5.4: Pair of helical edge states with two terminals and a Rashba impurity coupling the two channels. The wavy line illustrates the presence of electron phonon coupling in the system.

free electron Hamiltonian then reads

$$H_{\text{hl}} = \int dx \Psi^\dagger(x) p \sigma_z \Psi(x),$$

where $p = -i\partial_x$ is the momentum operator and σ_z is a Pauli matrix in spin space. The two most relevant Rashba-terms induced by a spatially dependent electric field in z -direction are given by [Ström10, Rothe10]

$$H_R = \frac{1}{2} \int dx \Psi^\dagger(x) \left(\{ \alpha_1(x), p \} + \{ \alpha_3(x), p^3 \} \right) \sigma_y \Psi(x).$$

Note that only odd powers of p are allowed by TRS. Electron phonon coupling to the displacement field d of longitudinal acoustic phonons is modeled by the Hamiltonian [Martin95]

$$H_{\text{ep}} = \lambda \int dx \Psi^\dagger(x) \sigma_0 \Psi(x) \partial_x d(x)$$

with all dimensionful constants absorbed into λ . The free phonon dynamics is governed by

$$H_p = \frac{1}{2} \int dx \left[(\Pi_d(x))^2 + c^2 (\partial_x d(x))^2 \right],$$

where c is the acoustic phonon velocity in units of the electronic Fermi velocity and Π_d is the conjugate momentum of d . We model the phonons for a strictly 1D system which corresponds to an in transverse direction perfectly localized edge state. Later on, we will see that our key results do not critically depend on the details of the phonon model. The total Hamiltonian of our setup is then given by

$$H = H_{\text{hl}} + H_p + H_R + H_{\text{ep}} = H_0 + H_I,$$

where $H_0 = H_{\text{hl}} + H_p$ is the free Hamiltonian whereas $H_I = H_R + H_{\text{ep}}$ encompasses the coupling terms.

5.2.4 Inelastic backscattering

We will now demonstrate how the combination of H_R and H_{ep} will in principle be able to cause *single electron* backscattering at a single edge of a QSH insulator. As observed above, since H_R is TRS preserving, it cannot cause elastic single electron backscattering. Due to its offdiagonal structure in spin space it couples opposite spins though. In contrast, H_{ep} does not

mix different spin species but can bring about energy dissipation by virtue of energy transfer from the electronic degrees of freedom to phonons. Thus, the second order in H_I diagrams shown in Figure 5.5 which are first order in H_{ep} and in H_R cause backscattering at finite bias (see Fig. 5.6) if their contribution does not vanish for momentum transfer $p_i - p_f \approx 2k_F$. We

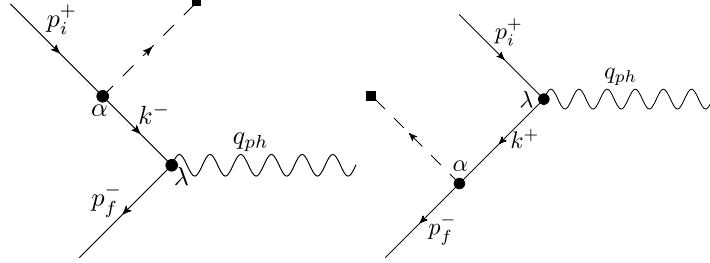


Figure 5.5: Tree diagrams for lowest order backscattering. Dashed line with square represents the external Rashba potential. Wavy line denotes the phonon propagator.

consider scattering between a right mover $|p_i^+\rangle$ and a left mover $|p_f^-, q_{\text{ph}}\rangle$ with an additional phonon. Up to second order, the corresponding scattering matrix element M_{if} can be written as

$$M_{\text{if}} = \langle p_f^-, q_{\text{ph}} | H_I G_0 H_I | p_i^+ \rangle,$$

where G_0 is the free propagator corresponding to H_0 . Interestingly, the lowest order contribution of the Rashba term linear in momentum associated with α_1 vanishes due to a nontrivial destructive quantum interference of the two contributing diagrams which stems from the linearity of both H_{hl} and the α_1 -Rashba term. To show that this is not due to any fundamental symmetry like TRS, we calculate the same matrix element for the Rashba term associated with α_3 which yields

$$|M_{\text{if}}|^2 = \frac{\lambda^2 c}{16\pi} \tilde{\alpha}_3^2 (q_{\text{ph}} + p_f^- - p_i^+) |q_{\text{ph}}|^5$$

where $\tilde{\alpha}_3(k)$ is the Fourier transform of $\alpha_3(x)$. At the level of an analytical Fermi's golden rule calculation for a δ -shaped Rashba impurity $\alpha_3(x) = \alpha_3 \delta(x)$, the backscattering current I_{BS} at zero temperature can be readily expressed as

$$I_{\text{BS}} = 2\pi e \int dp_i^+ \int dp_f^- \int dq_{\text{ph}} \left[f_{\text{FD}}^+(\epsilon_i^+) (1 - f_{\text{FD}}^-(\epsilon_f^-)) |M_{\text{if}}|^2 \delta(\epsilon_i^+ - \epsilon_f^- - \omega_{\text{ph}}) \right], \quad (5.5)$$

where $\epsilon_i^+ = p_i^+ - k_F$ and $\epsilon_f^- = -p_f^- - k_F$ denote the initial and the final energy of the scattered electron, $\omega_{\text{ph}} = c|q_{\text{ph}}|$ is the phonon frequency and f_{FD}^\pm is the Fermi-Dirac distribution function associated with the chemical potential μ_\pm of the branch of right movers (+) and left movers (-), respectively. Using $f_{\text{FD}}^\pm(\epsilon) = \theta(\mu_\pm - \epsilon)$ at zero temperature, we can readily perform the integrals occurring in Eq. (5.5) analytically and obtain

$$I_{\text{BS}} = \frac{\alpha_3^2 \lambda^2 e}{672\pi^2 c^5} V^7. \quad (5.6)$$

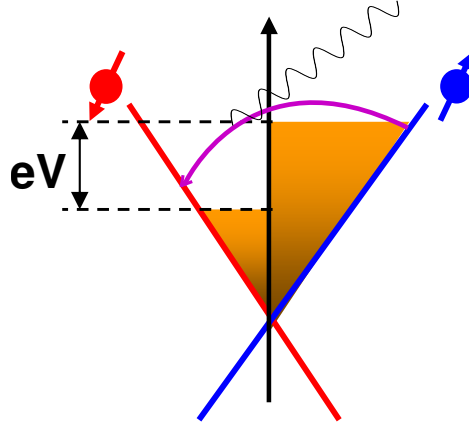


Figure 5.6: Voltage configuration to pass a spin up current from the left to the right. The bias V opens an energy window for inelastic phonon scattering.

This contribution will be negligible at low bias V reflecting the irrelevance of the p^3 -Rashba term. The importance of this non-vanishing result is that it demonstrates how in principle inelastic *single electron* backscattering can occur at finite bias even though the perturbations Rashba SOI and electron phonon coupling preserve TRS. The lowest order nonvanishing matrix element for the α_1 term could be third order in α_1 which has the same relevance as α_3 in renormalization group (RG) sense. Also, quadratic corrections to the linear electronic dispersion which might become relevant at higher energies can give rise to α_1 backscattering.

At finite temperature, there will be additional scattering contributions to the current, e.g., from processes where a phonon is absorbed or where an electron is scattered from a thermally excited state in the branch with the lower chemical potential to an empty state below the chemical potential of the other branch. For finite T , we numerically evaluate the correction ΔG to the conductance by calculating

$$\Delta G = \left. \frac{\partial \Delta I(V, T)}{\partial V} \right|_{V=0},$$

where ΔI contains all perturbative corrections to the current up to second order in H_I . In Fig. 5.7, we show the temperature dependence of the conductance which scales to convincing accuracy with the sixth power of T .

We would again like to point out that the vanishing matrix element M_{if} for the α_1 -Rashba leads to an exactly quantized conductance in the absence of the α_3 -Rashba term also at finite temperature. We hence conclude that for the helical edge state without Coulomb interaction the most relevant inelastic backscattering contributions allowed by TRS and phase space arguments cancel out. This can be interpreted as an enhanced precision of the quantized conductivity of the helical edge states at finite temperature/bias going beyond the topological protection only pertaining to elastic scattering.

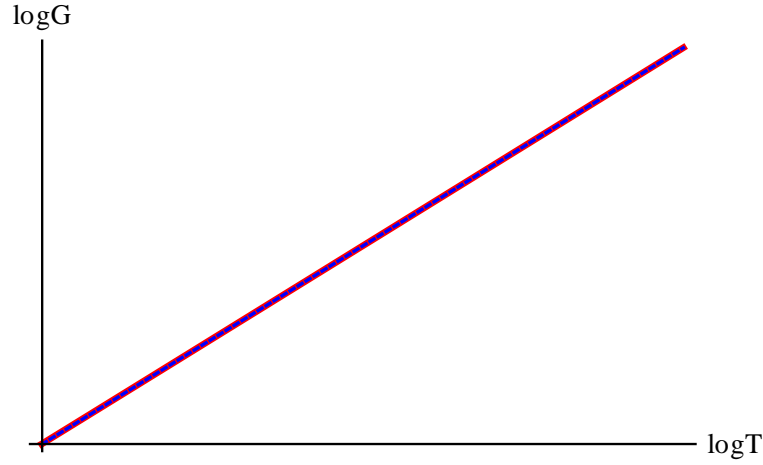


Figure 5.7: Temperature dependence of the conductance G in arbitrary units (red solid). Plot of the power law $\sim T^6$ (blue dashed). Logarithmic scale on both axes.

5.2.5 hTLL with Coulomb interaction

Now, we want to investigate whether the observed robustness of the helical Dirac fermions against inelastic backscattering by virtue of the α_1 -Rashba SOI term, i.e., the most relevant TRS preserving term coupling opposite spins, persists in the presence of Coulomb interaction. In order to account for Coulomb interaction we represent the fermionic degrees of freedom in terms of an hTLL using the bosonization identity (see also Eq. (3.4))

$$\psi_{\pm} = \frac{1}{\sqrt{2\pi a}} \eta^{\pm} e^{i\sqrt{\pi}(\varphi \pm \theta)},$$

where ψ_{\pm} now denote the slowly varying fields with a factor of $e^{\pm ik_F x}$ separated off, a is the high energy cutoff of the model and φ , θ are the bosonic phase field and its dual, respectively. In the thermodynamic limit, the Klein factors η^{\pm} obey the algebra of Majorana fermions. Absorbing a prefactor of $\frac{1}{\pi}$ by redefining λ , the electron phonon coupling can be represented as

$$H_{\text{ep}} = \lambda \int dx \partial_x \varphi(x) \partial_x d(x).$$

The translation invariant hTLL Hamiltonian reads (see also Eq. (3.9))

$$H_{\text{hTLL}} = \frac{1}{2} \int dx \left[\Pi_{\varphi}^2(x) + \frac{1}{g^2} (\partial_x \varphi(x))^2 \right]$$

with the interaction strength parameter $g < 1$ modeling repulsive Coulomb interaction. The α_1 -Rashba Hamiltonian with $\alpha_1(x) = \alpha \delta(x)$ in bosonized form yields

$$H_R = \frac{i\alpha}{\sqrt{\pi a}} \eta^+ \eta^- : (\partial_x \theta(x)) \cos(\sqrt{4\pi} \varphi(x)) : \Big|_{x=0} \quad (5.7)$$

where the dots denote normal ordering.

We want to calculate the average current $I(x, t) = -\frac{e}{\sqrt{\pi}}\partial_t\langle\varphi(x, t)\rangle$ due to an applied bias V . Such expectation values can be most easily represented for practical calculations in terms of a generating functional

$$Z[J] = \int D(\varphi, \theta, d) e^{iS_0 - i \int_c H_R + i \frac{e}{\sqrt{\pi}} E^T \sigma_3 \varphi + \frac{i}{\sqrt{2}} J^T \varphi}, \quad (5.8)$$

where S_0 encompasses the electron phonon system without the Rashba impurity, \int_c denotes the integral along the Keldysh contour, σ_3 is a Pauli matrix in Keldysh space, and scalar products like $J^T \varphi$ involve an integration over real space and time. The applied bias is modeled by $E(x, t)$ along the lines of Ref. [Dolcini05] (see also Eq. (3.15)).

To make further analytical progress we now integrate out the phonons on the Keldysh contour. The part of the Lagrangian involving the phonon field d reads

$$L_d = \frac{1}{2} \left((\partial_t d)^2 - c^2 (\partial_x d)^2 \right) - \lambda (\partial_x \varphi) (\partial_x d).$$

The phonon dependent part of the action can be represented on the Keldysh contour as

$$S_d = \frac{1}{2} d^T G_{\text{ph}}^{-1} d + \lambda d^T \sigma^3 \partial_x^2 \varphi$$

with the phonon propagator G_{ph} . Performing the Gaussian integral

$$\int Dd e^{iS_d(d, \varphi)} = e^{iS_{\text{diss}}(\varphi)}$$

in the rotated Keldysh basis

$$\begin{pmatrix} \varphi^+ \\ \varphi^- \end{pmatrix} \rightarrow \frac{1}{\sqrt{2}} \begin{pmatrix} 1 & 1 \\ 1 & -1 \end{pmatrix} \begin{pmatrix} \varphi^+ \\ \varphi^- \end{pmatrix} = U \varphi$$

yields for the dissipative action

$$S_{\text{diss}} = -\frac{\lambda^2}{2} (\partial_x^2 \varphi)^T \sigma_1 G_{\text{ph}} \sigma_1 \partial_x^2 \varphi, \quad (5.9)$$

where $\sigma_1 G_{\text{ph}} \sigma_1 = \begin{pmatrix} 0 & G_{\text{ph}}^A \\ G_{\text{ph}}^R & G_{\text{ph}}^K \end{pmatrix}$. By this dissipative action, the inverse free electron Green's function in Fourier space is changed to the following dressed version

$$\left(G_e^{-1}(k, \omega) \right)_{\varphi\varphi} \rightarrow \left(G_e^{-1}(k, \omega) \right)_{\varphi\varphi} - \frac{\lambda^2 k^4}{\omega^2 - c^2 k^2}. \quad (5.10)$$

This result generalizes to the Keldysh formalism a similar imaginary time calculation carried out in Ref. [Martin95]. The retarded, advanced and Keldysh part of this Green's function can be calculated exactly. From now on the free action $S_0(\varphi, \theta)$ refers to the effective action

where the phonons have been integrated out. To calculate the current we basically have to evaluate

$$\langle \varphi(x) \rangle = \frac{-i}{\sqrt{2}} \frac{\delta Z[J]}{\delta J(r)} \Big|_{J=0}, \quad (5.11)$$

which can be done along the lines of Ref. [Dolcini05] (see also Section 3.2.2). The equation of motion $\partial_t \varphi = -\partial_x \theta$ (see Eq. 3.10) inside the free correlators averaged with $S_0(\varphi, \theta)$ remains valid for the free action which is dressed by the phonon dissipation. That is because S_{diss} (see Eq. (5.9)) depends only on φ and not on its conjugate momentum $\Pi_\varphi = -\partial_x \theta$ (see Eq. (3.8)). Using only this property of the electron phonon coupling the current to second order in α_1 is readily shown to be zero. This proves that our result for the case without Coulomb interaction persists in the nonequilibrium hTLL.

This result might be understood on more general grounds. The fact that S_0 remains quadratic in $\Pi_\varphi = -\partial_x \theta$ means that the following argument first brought forward in Ref. [Ström10] for an hTLL in equilibrium without electron phonon interaction could be used for our setup as well: Integrating out Π_φ in the path integral representation of the generating functional will produce terms proportional to $(\partial_t \varphi)^2$, $\alpha(\partial_t \varphi) \cos(\sqrt{4\pi}\varphi)$, $\alpha^2 \cos(\sqrt{4\pi}\varphi)^2$ in the action. While the first contribution is the term well known from the free hTLL case, the second one is a pure gauge which can be dropped. The third term can up to a constant be written as $\cos(\sqrt{16\pi}\varphi)$ which is a two electron TRS preserving backscattering term [Wu06]. Note that the presence of the source term $J^T \varphi$ in Eq. (5.8) does not affect this argument. Thus, we have found that the α_1 -Rashba term cannot lead to a single electron backscattering term in the presence of any external spin independent dissipation which couples linearly to the electron density.

One cautious remark is in order: In the non-interacting limit, i.e., for $g \rightarrow 1$, the term $\alpha^2 \cos(\sqrt{4\pi}\varphi)^2$ does not seem to vanish which suggests the presence of two-particle backscattering in the absence of Coulomb interaction. This cannot be true. Since, at this point, it is not clear to us how the physical truth can be reconciled with the argument based on integrating out Π_φ , the latter should be taken with care. However, this does not affect at all our previous discussion of phonon-induced backscattering in helical edge states. We again point out that this result goes beyond the topological protection of the hTLL. It is due to the quadratic form of S_0 in Π_φ , the Luttinger liquid analogue of the linear dispersion of helical Dirac fermions on which our result without Coulomb interaction relied. Bosonizing the α_3 -Rashba term implies terms up to third power in $\partial_x \theta$ thus breaking the quadratic form of S_0 in Π_φ . Furthermore mixed terms like $(\partial_x \varphi)(\partial_x \theta)^2$ will occur which render the modifications of free Green's function (see Eq. (5.10)) by the presence of phonons important. These observations are perfectly compatible with our nonvanishing result for single electron backscattering in the presence of α_3 (see Eq.(5.6)).

5.2.6 Summary and outlook

In summary, we have studied helical Dirac fermions in the presence of electron phonon coupling and Rashba SOI, which both preserve TRS. We have shown that, although TRS

does not provide a protection against inelastic scattering, the current carried by the helical states in the presence of a finite bias is not changed to leading order. Furthermore, we have proven that this result still holds for an hTLL including Coulomb interaction. The linear dispersion of the helical edge states of a QSH bar has been nicely verified experimentally [König07] and is an exact feature of the four band model for inverted HgTe/CdTe quantum wells introduced in Ref. [Bernevig06a]. Therefore, our analysis is not only interesting for the abstract model of an hTLL. It supports the robustness of the quantized subgap conductance of a QSH sample beyond the well known argument (5.4) of topological protection. Our results turn out to be not restricted to the coupling to longitudinal acoustic 1D phonons. In fact, we have shown that any external bath coupling linearly to the electron density cannot give rise to inelastic single electron backscattering in the presence of linear in k spin orbit coupling. In HgTe/CdTe layer structures, external coupling mechanisms, e.g., coupling to charge puddles in the bulk, are likely to cause phase decoherence which gives rise to additional backscattering. However, such effects are not intrinsic features of the hTLL and can in principle be contained by improving the sample quality. In contrast, electron phonon coupling and Coulomb interaction are intrinsic mechanisms the role of which we have investigated for a generic realization of the hTLL. The discussed mechanism of phonon-induced backscattering gives rise to conductance corrections that scale like T^6 . We already pointed out that integrating out Π_φ in the path integral leads to the unphysical result of non-vanishing backscattering in the limit of vanishing Coulomb interaction. In the following section, we resolve this controversy by studying the interplay of the α_1 -Rashba term and Coulomb interaction from an RG perspective.

5.3 Renormalization group approach for the scattering off a single Rashba impurity in a helical liquid

The occurrence of two-particle inelastic backscattering has been conjectured in helical edge states of topological insulators and is expected to alter transport. In this section, by using a renormalization group approach, we provide a microscopic derivation of this process, in the presence of a time-reversal invariant Rashba impurity potential. Unlike previous approaches to the problem, we are able to prove that such an effect only occurs in the presence of electron-electron interaction. Furthermore, we find that the linear conductance as a function of temperature exhibits a crossover between two scaling behaviors: T^{4K} for $K > 1/2$ and T^{8K-2} for $K < 1/2$, with K the Luttinger parameter modeling Coulomb interaction. Here, we choose a notation which is convenient for our RG analysis and which slightly differs from our general presentation in Section 3.1. The relation between the two notations will be established explicitly below. Our presentation follows closely the analysis of Ref. [Crépin12].

5.3.1 Motivation

Since the prediction of the quantum spin Hall phase [Kane05a, Kane05b] (see Section 2.4.1) in HgTe quantum wells [Bernevig06a], transport measurements on these compounds have shown evidence of a quantized edge conductance $G = 2e^2/h$, thereby paving the way for non-local dissipationless transport in semiconductors at zero external magnetic field

[König07, König08, Roth09]. In the simplest case of quantum wells with inversion symmetry, transport occurs through two counter-propagating edge channels that carry opposite spin-1/2 quantum numbers. Such helical liquids form a new class of 1D quantum liquids in the sense that they are protected by time-reversal symmetry against single-particle elastic backscattering [Kane05a, Xu06, Wu06] (see also Section 5.2). However, deviations from the quantized conductance arise in various situations, involving either a breaking of time-reversal symmetry – by a magnetic impurity for instance – or the interplay between a TRS preserving external potential and a source of inelastic scattering. Inelastic single-particle backscattering [Budich12a, Schmidt12] and two-particle backscattering [Kane05a, Xu06, Wu06, Ström10] are two examples of the latter. In this section, we focus on two-particle backscattering off a TRS preserving impurity and report new results regarding the temperature scaling of conductance corrections. Our purpose is to derive the Hamiltonian for such a process starting with a minimal model of an interacting helical liquid coupled to a TRS preserving potential. In particular, we focus on a Rashba spin-orbit potential [Ström10, Budich12a], which can originate from fluctuations of an electric field perpendicular to the 2D electron gas [Rothe10], and acts as a TRS preserving effective magnetic field that couples right and left movers. In the recent literature, inelastic two-particle backscattering off an impurity was mostly studied phenomenologically, by postulating the generic form of the Hamiltonian due to symmetry considerations – namely TRS and Pauli principle [Kane05a, Xu06, Wu06, Lezmy12],

$$H_{2p}^{\text{in}} = \gamma_{2p} \left[(\partial_x \Psi_+^\dagger) \Psi_+^\dagger (\partial_x \Psi_-) \Psi_- \right] (x_0) + \text{H.c.}, \quad (5.12)$$

where \pm designate right and left movers respectively. A straightforward scaling analysis [Kane92a, Kane92b] would lead to a temperature dependence of T^{8K-2} for conductance corrections, with K the Luttinger parameter, implying a T^6 behavior in the limit of weak Coulomb interaction, $K \simeq 1$. These studies, however, do not explain how two-particle backscattering is generated at the microscopic level. To our knowledge, the only microscopic explanation proposed so far is the one by Ström *et al.* [Ström10], already based on Rashba spin-orbit coupling. Their analysis, however, leads to the unphysical conclusion that these processes are present even in the limit of vanishing Coulomb interaction. Indeed, without interaction, two-particle backscattering can always be factorized to two uncorrelated single-particle elastic backscattering processes and does not affect transport. A satisfactory explanation of the effect is therefore still lacking.

Here, we use a renormalization group (RG) approach to show how two-particle inelastic backscattering is generated from Rashba spin-orbit coupling and Coulomb interaction. Upon integrating the flow equations, we are able to demonstrate that the effect only occurs in the presence of electron-electron interaction. Furthermore, we find a K -dependent crossover behavior for the temperature scaling of the conductance corrections, namely

$$\delta G/G_0 \sim \begin{cases} (a_0 T/v)^{4K} & \text{if } K > 1/2, \\ (a_0 T/v)^{8K-2} & \text{if } 1/4 < K < 1/2, \end{cases} \quad (5.13)$$

where a_0 is the inverse bandwidth and v the interaction-renormalized Fermi velocity. Our analysis demonstrates that, in the limit of weak interactions, two-particle inelastic processes,

with a scaling of T^4 , are a more important source of scattering than usually anticipated from phenomenology.

5.3.2 Model

We study an interacting 1D helical liquid in the presence of Rashba spin-orbit coupling. The Hamiltonian of the system is the sum of three terms, $H = H_0 + H_I + H_R$, given by

$$\begin{aligned}
 H_0 &= \int dx \sum_{\eta=\pm} \Psi_{\eta}^{\dagger}(x) (-i\eta v_F \partial_x - E_F) \Psi_{\eta}(x), \\
 H_I &= \iint dx dx' \Psi_{+}^{\dagger}(x) \Psi_{-}^{\dagger}(x') g_2 (x - x') \Psi_{-}(x') \Psi_{+}(x), \\
 H_R &= \int dx \alpha(x) \left[(\partial_x \Psi_{+}^{\dagger}) \Psi_{-} - \Psi_{+}^{\dagger} (\partial_x \Psi_{-}) \right] (x) + \text{H.c.}
 \end{aligned} \tag{5.14}$$

Here, $\Psi_{+}^{\dagger}(x)$ and $\Psi_{-}^{\dagger}(x)$ are creation operators for right and left moving electrons, respectively. Both species carry spin-1/2 opposite quantum numbers and hence transform as $\mathcal{T} \Psi_{\pm}^{\dagger}(x) \mathcal{T}^{-1} = \pm \Psi_{\mp}^{\dagger}(x)$ under time reversal. H_0 entails a strictly linear spectrum, with a finite bandwidth, the size of the bulk band gap. v_F is the Fermi velocity, E_F the Fermi energy. Without loss of generality, we consider in H_I only interaction between electrons moving in opposite directions, since chiral interactions – so-called g_4 terms – only renormalize the Fermi velocity. Finally, H_R describes a linear Rashba spin-orbit potential likely to stem from fluctuations of a transverse electric field [Ström10, Budich12a]. We emphasize that H_R is, in a helical liquid, the time-reversal invariant Hamiltonian with the lowest scaling dimension, able to couple right and left-movers. Nevertheless it has no effect on transport as long as elastic scattering is concerned [Xu06]. In the following, we consider a point-like impurity, that is, $\alpha(x) = \alpha \delta(x)$. We show with a RG calculation how two-particle inelastic backscattering is generated. First, we carry it out on the fermion partition function before treating the Coulomb interaction exactly using bosonization.

5.3.3 RG for interacting fermions

Much insight is gained by first treating, at the fermion level, both Coulomb interaction and the Rashba potential as perturbations to the non-interacting fixed point. We use the path integral representation of the partition function, $\mathcal{Z} = \int D\Psi_{\pm}^* D\Psi_{\pm} e^{-S}$, with an action $S = \int_0^{\beta} d\tau \left[\sum_{\eta=\pm} \int dx \Psi_{\eta}^*(x, \tau) \partial_{\tau} \Psi_{\eta}(x, \tau) + H(\tau) \right]$, and $\Psi_{\pm}(x, \tau)$, $\Psi_{\pm}^*(x, \tau)$ Grassmann fields. We introduce an ultra-violet (UV) cutoff Λ of the order of half the bulk band gap on the dispersion relation of both right and left movers as $v_F |\eta k - k_F| < \Lambda$, with k_F the Fermi momentum. Following Ref. [Shankar94], we then proceed to integrate out the fields living on an infinitesimal momentum shell $\Lambda/s < v_F |\eta k - k_F| < \Lambda$, with $s = 1 + d\ell$. As usual in a 1D quantum liquid, interactions contribute an infinite series of diagrams. However, in the absence of $2k_F$ scattering processes, and the impurity being point-like, g_2 is invariant under RG transformations. The integration of high energy fields also generates new terms. To third order perturbation theory, the diagram (b) depicted in Fig. 5.8 generates an inelastic

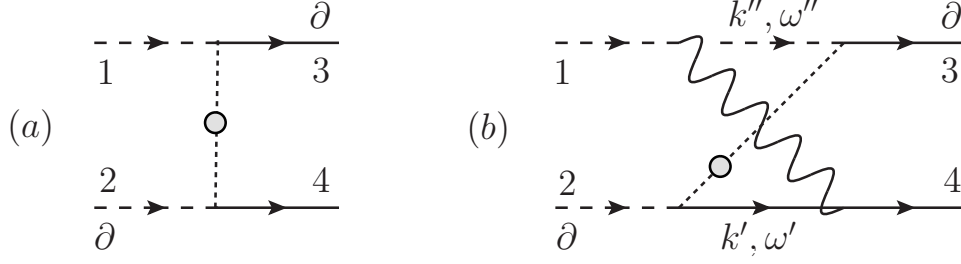


Figure 5.8: Examples of diagrams to order α^2 (a) and $g_2\alpha^2$ (b), in the expansion of the partition function. Partial derivative signs indicate which external lines are differentiated with respect to x . Full (dashed) arrows are for right (left) movers. Wavy lines are for Coulomb interaction, and grey balls denote scattering off the impurity.

two-particle backscattering process whose action is of the form

$$S_{2p} = \gamma_{2p} \int \prod_{i=1}^4 \frac{dk_i}{2\pi} \frac{d\omega_i}{2\pi} 2\pi \delta(\omega_1 + \omega_2 - \omega_3 - \omega_4) \times (-ik_3 \Psi_+^*(3)) \Psi_+^*(4) (ik_2 \Psi_-(2)) \Psi_-(1) + \{+ \leftrightarrow -\}. \quad (5.15)$$

This is precisely the action one would derive from the Hamiltonian of Eq. (5.12) in momentum space. The scaling dimension of γ_{2p} is (-3) by power-counting. We take into account the aforementioned third-order diagram (b) shown in Fig. 5.8, which is of second order in the Rashba coupling constant α and of first order in the Coulomb forward scattering g_2 . Performing the momentum shell integration on the contribution of this diagram, we obtain the flow equation

$$\frac{d\gamma_{2p}}{d\ell} = -3\gamma_{2p}(\ell) + \frac{\alpha(\ell)^2}{v_F \Lambda} \frac{g_2}{2\pi v_F}, \quad (5.16)$$

where the first term on the right hand side stems from the scaling dimension of γ_{2p} and the second term accounts for the perturbative third order correction. Note that the initial condition is $\gamma_{2p}(\ell = 0) = 0$, since two-particle inelastic backscattering is absent from the bare action. Finally, power counting on the Rashba action yields for $\alpha(\ell)$ the flow equation

$$\frac{d\alpha}{d\ell} = -\alpha(\ell). \quad (5.17)$$

This calculation confirms that inelastic two-particle backscattering off a Rashba impurity is only generated in the presence of Coulomb interaction, as it disappears altogether as soon as $g_2 = 0$. We emphasize that to second order in α , diagrams such as (a) in Fig. 5.8 do not generate inelastic processes since Matsubara frequencies are conserved independently at each Rashba scattering vertex; in this example, $\omega_1 = \omega_3$ and $\omega_2 = \omega_4$. Finally, we point out that g_4 (chiral) interactions fail to generate inelastic two-particle backscattering as all diagrams will be suppressed by the Pauli principle.

5.3.4 Bosonization

We refine our analysis by treating interactions exactly, through bosonization of the fermion Hamiltonian. Excitations around the true ground state of the 1D interacting helical liquid are indeed described by the Tomonaga Luttinger liquid Hamiltonian (see also Eq. (3.9))

$$\mathcal{H}_0 = \frac{v}{2} \int dx \left[K(\partial_x \theta)^2 + \frac{1}{K}(\partial_x \varphi)^2 \right], \quad (5.18)$$

where the notation is related to Eq. (3.9) through the identifications $K = g$, and $v = v_F/g$. The present symmetric notation is more convenient for our RG analysis. By using the bosonization identity, Eq. (3.4), the bosonized form of the Rashba Hamiltonian is readily obtained as [Ström10, Budich12a] (see also Eq. (5.7))

$$H_R = i\eta^+ \eta^- \int dx \frac{\alpha(x)}{(\pi)^{\frac{3}{2}} a} \left(\frac{2\pi a}{L} \right)^K : \partial_x \theta(x) \left(: e^{-i2\varphi(x)} : e^{i2k_F x} + : e^{i2\varphi(x)} : e^{-i2k_F x} \right) : \quad (5.19)$$

where $: \dots :$ indicate normal order with respect to boson operators that annihilate the ground state of the helical liquid (see Eq. (3.2)). Here, η^\pm are again the Klein factors, and a is a short-distance cutoff and the running scale in the RG approach. For all purposes here, its bare value a_0 can readily be identified with Λ^{-1} , where Λ is the bandwidth previously introduced in the fermion RG analysis. The total bosonized Hamiltonian of the system is $H = \mathcal{H}_0 + H_R$. We perform an RG transformation in real space [Cardy96], which consists in rescaling first the short distance cutoff, $a \rightarrow a' = (1 + d\ell)a$, and then the couplings in order to keep the low-energy form of the Hamiltonian invariant. We rescale the cutoff order by order in an expansion to order $\mathcal{O}(\alpha^2)$ of the partition function $\mathcal{Z} = \text{Tre}^{-\beta \mathcal{H}_0} \hat{U}(\beta, 0)$, where $\hat{U}(\beta, 0) = \mathcal{T}_\tau e^{-\int_0^\beta d\tau_1 \hat{\mathcal{H}}_R(\tau_1)}$ is the time-evolution operator in the interaction representation. At tree level, we derive the following flow equation for the Rashba coupling

$$\frac{d\tilde{\alpha}}{d\ell} = -K\tilde{\alpha}(\ell), \quad (5.20)$$

in which we have introduced the dimensionless variable $\tilde{\alpha} = \alpha/(\pi v a)$. Bosonization readily takes into account vertex corrections due to interactions and we recover Eq. (5.17) in the limit of weak interactions, $K \rightarrow 1$. Two-particle inelastic backscattering is generated as a second-order perturbation process. Indeed, the expansion to order α^2 of the partition function leads to a term

$$\begin{aligned} & \alpha^2 \left(\frac{2a}{v} \right) \int_0^\beta d\tau_1 \left[(\partial_x \hat{\psi}_+^\dagger) \hat{\psi}_+^\dagger (\partial_x \hat{\psi}_-) \hat{\psi}_- \right] (1) \\ & + \frac{\alpha^2}{2} \int_{v|\tau_1 - \tau_2| > a} d\tau_1 d\tau_2 (\partial_x \hat{\psi}_+^\dagger)(1) \hat{\psi}_+^\dagger(2) (\partial_x \hat{\psi}_-)(1) \hat{\psi}_-(2) + \text{H.c.}, \end{aligned} \quad (5.21)$$

where the UV cutoff is enforced by splitting the double integral over imaginary time into two parts for which $v|\tau_1 - \tau_2| < a$ and $v|\tau_1 - \tau_2| > a$, respectively. The first line, corresponding to short time differences $\tau_1 \simeq \tau_2$, contributes an inelastic scattering process. Importantly, in the limit of vanishing interactions, the first term exactly cancels a similar term generated

by the cutoff rescaling in the second integral, proving that no two-particle backscattering occurs without interactions¹. By writing Eq. (5.21) in terms of the bosonic fields and after normal ordering, we obtain

$$\begin{aligned} & \left(: \partial_x \theta(1) : e^{i2\sqrt{K}\varphi(1)} :: \right) \left(: \partial_x \theta(2) : e^{i2\sqrt{K}\varphi(2)} :: \right) = \\ & \frac{1}{2} \left(\frac{2\pi}{L}(y+a) \right)^{2K} \frac{1-2K}{(y+a)^2} : e^{i2\sqrt{K}\varphi(1)} e^{i2\sqrt{K}\varphi(2)} : + \dots \end{aligned} \quad (5.22)$$

Note that we have rescaled the bosonic fields according to $\sqrt{K\pi}\theta \rightarrow \theta$ and $\sqrt{\frac{\pi}{K}}\varphi \rightarrow \varphi$. Furthermore, $y_{1(2)} = v\tau_{1(2)}$ has dimension of a length and we define $y = y_1 - y_2$. The dots represent extra terms that have a vanishing expectation value. Keeping the lowest order term in an operator product expansion, the rescaling of a generates a new coupling, which we identify with a two-particle inelastic backscattering process. At the end of the RG step, the time-evolution operator $\hat{U}(\beta, 0)$ is corrected by a Hamiltonian

$$\int_0^\beta d\tau_1 \hat{\mathcal{H}}_{2p}(\tau_1) = \frac{\tilde{\gamma}_{2p}}{a} \int_0^{v\beta} dy \left[e^{i4\sqrt{K}\varphi(x_0, y)} + \text{H.c.} \right],$$

where $\tilde{\gamma}_{2p}$ is a dimensionless coupling² given by

$$\tilde{\gamma}_{2p}(\ell) = \tilde{\gamma}_{2p}^{\text{in}}(\ell) - \frac{\tilde{\alpha}(\ell)^2}{2K}(1-2K). \quad (5.23)$$

On the r.h.s of Eq. (5.23), $\tilde{\gamma}_{2p}^{\text{in}}(\ell)$ stands for the true inelastic backscattering processes, which in the present case, has the bare value $\tilde{\gamma}_{2p}^{\text{in}}(\ell=0) = 0$. The second term is the correction arising from the first integral in Eq. (5.21). Using Eq. (5.20), the flow equation for the true inelastic two-particle backscattering reads

$$\frac{d\tilde{\gamma}_{2p}^{\text{in}}}{d\ell} = (1-4K)\tilde{\gamma}_{2p}^{\text{in}}(\ell) + \left(1 - \frac{1}{K}\right)(1-2K)\tilde{\alpha}(\ell)^2. \quad (5.24)$$

In the absence of interactions, $K=1$ and $\tilde{\gamma}_{2p}^{\text{in}}(\ell) = 0$ at any scale ℓ , consistently with the fermionic result of Eq. (5.16).

5.3.5 Transport

We now apply a small voltage bias V to the hTLL. The dc conductance G is then obtained from linear response as the zero-frequency limit of the current-current correlation function [Kane92a, Kane92b]. The latter is evaluated in perturbation theory, and because of TRS, corrections to the quantized conductance $G_0 = e^2/h$ arise only to order $\mathcal{O}(\alpha^4)$. Equivalently here, by letting the system flow to a certain scale ℓ we obtain corrections to the conductance to order $\mathcal{O}(\tilde{\gamma}_{2p}^{\text{in}}(\ell)^2)$ in perturbation theory. Integrating equations (5.20) and (5.24) between

¹This subtlety of the RG procedure for impurity scattering was first noticed by Giamarchi and Schulz in their study of Anderson localization in 1D interacting liquids [Giamarchi88], and recently emphasized by Gornyi et al. [Gornyi07] in their treatment of weak localization.

²Compared to Eq. (5.12), we have $\tilde{\gamma}_{2p} = \gamma_{2p}/(\pi^2 v a^3)$

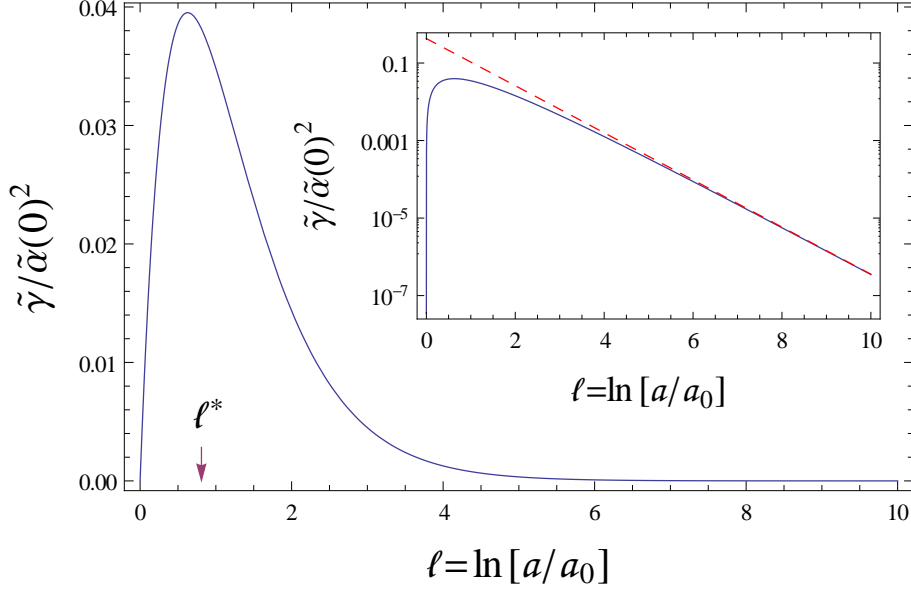


Figure 5.9: Flow of $\tilde{\gamma}_{2p}^{\text{in}}$ as a function of $\ell = \ln[a/a_0]$, for $K = 0.7$. A crossover scale ℓ^* separates a region of linear growth for small $\ell < \ell^*$ from a region of exponential decay at large $\ell > \ell^*$. The inset is the same plot on a semi-logarithmic scale. The asymptote is for $e^{-2K\ell}$.

0 and ℓ we find $\tilde{\alpha}(\ell) = \tilde{\alpha}(0)e^{-K\ell}$ and

$$\tilde{\gamma}_{2p}^{\text{in}}(\ell) = \left(1 - \frac{1}{K}\right) \tilde{\alpha}(0)^2 \left[e^{(1-4K)\ell} - e^{-2K\ell} \right], \quad (5.25)$$

which we plot in Fig. 5.9 for a particular value of K . We find two different asymptotic behaviors, separated by a crossover scale $\ell^* = (2K - 1)^{-1} \ln[(4K - 1)/(2K)]$, independent of $\tilde{\alpha}(0)$, the bare value of the Rashba coupling. For small $\ell \ll \ell^*$, $\tilde{\gamma}_{2p}^{\text{in}}(\ell) \simeq \tilde{\alpha}(0)^2(1 - K^{-1})(1 - 2K)\ell e^{-2K\ell}$ while for $\ell \gg \ell^*$, $\tilde{\gamma}_{2p}^{\text{in}}$ crosses over from

$$\tilde{\gamma}_{2p}^{\text{in}}(\ell) \simeq -\tilde{\alpha}(0)^2(1 - K^{-1})e^{-2K\ell}$$

for $K > 1/2$ to

$$\tilde{\gamma}_{2p}^{\text{in}}(\ell) \simeq \tilde{\alpha}(0)^2(1 - K^{-1})e^{(1-4K)\ell}$$

for $K < 1/2$. As can be seen from Eq. (5.24), $K = 1/2$ is an intermediate fixed point where two-particle inelastic backscattering is not generated, at least not in second order perturbation theory. Integrating out energy scales between the bare cutoff a_0 and the thermal length $a(\ell) = v\beta$, we obtain the temperature scaling of Eq. (5.13) for conductance corrections to order $\mathcal{O}(\tilde{\alpha}^4)$, which we repeat here for the reader's convenience

$$\delta G/G_0 \sim \begin{cases} (a_0 T/v)^{4K} & \text{if } K > 1/2, \\ (a_0 T/v)^{8K-2} & \text{if } 1/4 < K < 1/2. \end{cases}$$

Note that this power-law behavior holds for temperatures lower than the crossover temperature $T^* = (v/a_0)e^{-\ell^*}$ and measures the exponential decay of the flow of $\tilde{\gamma}_{2p}^{\text{in}}(\ell)$ for $\ell \gg \ell^*$ as exemplary shown for $K = 0.7$ in Fig. 5.9. In contrast, for $T > T^*$, i.e., $\ell < \ell^*$, these corrections are logarithmically suppressed as T approaches $T_0 = v/a_0$, i.e.,

$$\delta G/G_0 \sim (a_0 T/v)^{4K} \ln^2(a_0 T/v), \quad (5.26)$$

for all values of K . This behavior reflects the asymptotic temperature dependence of $\tilde{\gamma}_{2p}^{\text{in}}(\ell)^2$ in the regime $\ell < \ell^*$ where the flow of $\tilde{\gamma}_{2p}^{\text{in}}(\ell)$ shown in Fig. 5.9 increases linearly. Note that for $K < 1/4$, two-particle backscattering becomes a relevant perturbation and the Rashba impurity effectively cuts the helical liquid into two separate regions [Kane92a, Kane92b, Wu06]. We emphasize that at low temperatures, $T \ll T^*$, and in the limit of weak interactions, $K \simeq 1$, we predict corrections to the conductance from two-particle backscattering off a Rashba impurity that scale as T^4 instead of T^6 , as one would naively predict from the Hamiltonian of Eq. (5.12).

5.3.6 Summary and outlook

In summary, we have studied the simplest model of a 1D helical liquid in the presence of a TRS preserving impurity and electron-electron interactions, that alters transport. Our approach provides a firm microscopic explanation for the generation of two-particle backscattering in helical liquids and predicts the occurrence of a conductance crossover, which could not be captured by previous approaches. As current estimates for the Luttinger parameter in HgTe quantum wells, ranging between $K \simeq 0.5$ and $K \simeq 1$, show a strong dependence on the geometry of the device [Maciejko09, Teo09, Hou09, Ström10], all regimes presented here could be of experimental relevance in transport measurements. However, a correct path integral formulation of the model studied in this section is still an open question that should definitely be addressed by future work.

It is worth emphasizing the difference with respect to a recent work by Schmidt *et al.* [Schmidt12], where a different model for a helical liquid with broken S_z symmetry was analysed. There, Rashba spin-orbit coupling, by imposing a momentum-dependent rotation of the spin of right and left movers, allows for inelastic single-particle backscattering off a scalar impurity. These processes contribute a T^4 correction to the quantized conductance, in the limit of weak Coulomb repulsion. The fact that in our approach, two-particle backscattering actually leads to the same temperature dependence is a mere coincidence.

Chapter 6

Conclusion

The main focus of this thesis was on signatures of geometry and topology in mesoscopic condensed matter systems which were first investigated from a conceptual perspective and were then applied to non-equilibrium quantum transport phenomena and quantum information processing with spin qubits, respectively. This chapter is intended to provide a concluding presentation of the main points of our analysis and to give a brief outlook as to open questions that could be subject of future work.

In Chapter 1, we elucidated the role of differential geometry in the time evolution of a gapped physical system with an adiabatically time dependent Hamiltonian. A cyclic adiabatic evolution amounts to a unitary transformation within the eigenspace of a single energy eigenvalue, the geometric phase. Most interestingly, this geometric phase turns out to be a physical observable which can be formulated in a manifestly gauge invariant way which is a key difference as compared to analogous geometric effects in conventional gauge theories. In Chapter 2, we viewed the topological invariants characterizing topological states of matter as a global version of the geometric phase where the k -space of the physical system plays the role of the parameter manifold. Non-interacting insulators and mean field superconductors were divided into ten symmetry classes and the classification for all symmetry classes and spatial dimensions was outlined employing the mathematical framework of K-Theory. Furthermore, the practical calculation of all relevant topological invariants was discussed and possible generalizations to interacting and disordered systems were presented. However, the entire notion of topological states of matter is defined for quadratic model Hamiltonians, which limits the validity of interacting generalizations to systems that can be adiabatically connected to a non-interacting gapped phase. In order to prepare the reader for our holographic transport studies in the quantum spin Hall phase in Chapter 5, some basic perturbative techniques of non-equilibrium quantum transport were introduced in Chapter 3 along with the bosonized description of the one-dimensional Fermi system modeling the metallic holographic states of the two dimensional QSH state. In this context, we emphasized some peculiarities of these so called helical edge states, where the word helical stands for the locking of spin and direction of motion. The notion of a non-Abelian geometric phase introduced in Chapter 1 was employed for a proposal realizing holonomic quantum information processing in Chapter 4. The qubit of the studied architecture is given by a heavy hole subband of a valence band quantum dot which is twofold degenerate in the presence of time reversal symmetry. This qubit was demonstrated to be controllable by virtue of adiabatically time dependent electric fields with quadrupole symmetry. In Chapter 5, we took a closer look at the quantum spin Hall phase using a perturbative non-equilibrium

approach to quantum transport. In particular, the mentioned locking of spin and momentum of the helical edge states was shown to entail a spin charge duality which remains valid away from thermal equilibrium. Therefore, both spin and charge properties of a pair of helical edge states can be inferred from charge transport measurements in a four terminal setup, a very promising scenario as to future spintronics applications of the quantum spin Hall insulator. A key feature of a single helical edge state is its quantized conductance which stems from the protection against elastic single electron backscattering. We pointed out that an interacting system at finite bias or finite temperature offers loop holes for both the elasticity and the single particle condition. We investigated inelastic phonon-induced backscattering in the presence of Rashba spin orbit interaction and found a non-trivial robustness of the quantized conductance due to a destructive quantum interference. Owing to two electron backscattering in the presence of both Coulomb interaction and Rashba spin orbit coupling, we found corrections to the conductance that scale with the fourth power of temperature in the weakly interacting limit. All in all, our results of Chapter 5 corroborate the robustness of the peculiar holographic transport properties of the quantum spin Hall phase.

From a conceptual point of view, the entire zoo of topological states of matter can be seen as conclusively understood in the framework outlined in Chapter 2 of this thesis. However, there are at least two general routes to be considerably further explored by future research. First, the precise experimental implications of many topological states of matter have not been fully understood yet. Whereas in the quantum Hall state, the topological invariant directly represents a physical observable, namely the Hall conductivity of the sample, the observability of the topological invariants of several topological states of matter is unknown or still under active debate (see our discussion in Section 2.4.2). This issue is from our point of view closely related to the rather limited number of promising proposals for concrete technological applications based on these novel states of matter. Obviously, successful research in this direction will be of decisive importance for the long term future of the entire field of topological states of matter. Second, the influence of interactions and open quantum system effects on topological states of matter is by no means conclusively understood, let alone an exhaustive topological classification of interacting or dissipative systems. As a first step along these lines, a purely dissipation driven topological state has been reported in Ref. [Bardyn12].

On a more concrete note, there are several natural questions arising from our studies presented in Chapter 4 and Chapter 5, respectively. The quantum information processing architecture presented in Chapter 4 uses the geometric phase only to perform single qubit operations. All-holonomic universal quantum computing would require control over degenerate subspaces of coupled pairs of heavy hole spin qubits which has not been explored in this thesis. For a full theoretical understanding of the role of Rashba spin orbit coupling in helical edge states, a consistent path integral formulation of the problem could be very helpful. As we pointed out in Section 5.3, the path integral analysis presented in Ref. [Ström10] is not careful enough as to the normal ordering of the Rashba Hamiltonian which leads to physical inconsistencies. A resolution of this issue in path integral language would be elucidating but has not been achieved in this thesis. Furthermore, we treated the helical edge states as a pure 1D system throughout this thesis. For a realistic quantum spin Hall insulator, the finite bulk gap entails the influence of the gapped bulk states on the effective theory of spin orbit

coupling on the edge. A microscopic modeling of such effects including the crossover to pure 1D behavior in the limit of an infinite bulk gap would be another crucial step towards the modeling of quantum spin Hall devices under experimentally realistic conditions.

Bibliography

- [Aharonov61] Y. Aharonov and D. Bohm. *Further Considerations on Electromagnetic Potentials in the Quantum Theory*. Phys. Rev. **123**, 1511 (1961).
- [Akhmerov11] A. R. Akhmerov, J. P. Dahlhaus, F. Hassler, M. Wimmer, and C. W. J. Beenakker. *Quantized Conductance at the Majorana Phase Transition in a Disordered Superconducting Wire*. Phys. Rev. Lett. **106**, 057001 (2011).
- [Altland97] A. Altland and M. R. Zirnbauer. *Nonstandard symmetry classes in mesoscopic normal-superconducting hybrid structures*. Phys. Rev. B **55**, 1142 (1997).
- [Altland10] A. Altland and B. Simons. *Condensed matter field theory*. Cambridge University Press, 2010.
- [Anderson72] P. W. Anderson. *More Is Different*. Science **177**, 393 (1972).
- [Andreani87] L. C. Andreani, A. Pasquarello, and F. Bassani. *Hole subbands in strained GaAs-Ga_{1-x}Al_xAs quantum wells: Exact solution of the effective-mass equation*. Phys. Rev. B **36**, 5887 (1987).
- [Arovas98] D. P. Arovas and Y. Lyanda-Geller. *Non-Abelian geometric phases and conductance of spin- $\frac{3}{2}$ holes*. Phys. Rev. B **57**, 12302 (1998).
- [Atiyah63] M. F. Atiyah and I. M. Singer. *The index of elliptic operators on compact manifolds*. Bull. Amer. Math. Soc. **69**, 422 (1963).
- [Atiyah66] M. F. Atiyah. *K-Theory and Reality*. The Quarterly Journal of Mathematics **17**, 367 (1966).
- [Auslaender05] O. M. Auslaender, H. Steinberg, A. Yacoby, Y. Tserkovnyak, B. I. Halperin, K. W. Baldwin, L. N. Pfeiffer, and K. W. West. *Spin-Charge Separation and Localization in One Dimension*. Science **308**, 88 (2005).
- [Avron83] J. E. Avron, R. Seiler, and B. Simon. *Homotopy and Quantization in Condensed Matter Physics*. Phys. Rev. Lett. **51**, 51 (1983).
- [Avron88] J. E. Avron, L. Sadun, J. Segert, and B. Simon. *Topological Invariants in Fermi Systems with Time-Reversal Invariance*. Phys. Rev. Lett. **61**, 1329 (1988).
- [Avron89] J. E. Avron, L. Sadun, J. Segert, and B. Simon. *Chern numbers, quaternions, and Berry's phases in Fermi systems*. Communications in Mathematical Physics **124**, 595 (1989).

- [Avron90] J. E. Avron, R. Seiler, and B. Simon. *Quantum Hall effect and the relative index for projections*. Phys. Rev. Lett. **65**, 2185 (1990).
- [Avron99] J. E. Avron and A. Elgart. *Adiabatic Theorem without a Gap Condition*. Communications in Mathematical Physics **203**, 445 (1999).
- [Bagrets12] D. Bagrets and A. Altland. *Class D spectral peak in Majorana quantum wires*. arXiv:1206.0434 (2012).
- [Bardyn12] C.-E. Bardyn, M. A. Baranov, E. Rico, A. Imamoglu, P. Zoller, and S. Diehl. *Majorana Modes in Driven-Dissipative Atomic Superfluids With Zero Chern Number*. arXiv:1201.2112 (2012).
- [Beenakker11] C. W. J. Beenakker. *Search for Majorana fermions in superconductors*. arXiv:1112.1950 (2011).
- [Bernevig05] B. A. Bernevig and S.-C. Zhang. *Holonomic quantum computing based on the Stark effect*. Phys. Rev. B **71**, 035303 (2005).
- [Bernevig06a] B. A. Bernevig, T. L. Hughes, and S.-C. Zhang. *Quantum Spin Hall Effect and Topological Phase Transition in HgTe Quantum Wells*. Science **314**, 1757 (2006).
- [Bernevig06b] B. A. Bernevig and S. C. Zhang. *Quantum spin Hall effect*. Phys. Rev. Lett. **96**, 106802 (2006).
- [Berry84] M. V. Berry. *Quantal phase factors accompanying adiabatic changes*. Proc. R. Soc. Lond. A **392**, 45 (1984).
- [Bohm03] A. Bohm, A. Mostafazadeh, H. Koizumi, Q. Niu, and J. Zwanziger. *The geometric phase in quantum systems*. Springer, 2003.
- [Born28] M. Born and V. Fock. *Beweis des Adiabatenatzes*. Zeitschrift für Physik A Hadrons and Nuclei **51**, 165 (1928).
- [Bott82] R. Bott and L. W. Tu. *Differential Forms in Algebraic Topology*. Springer, 1982.
- [Brosco10] V. Brosco, M. Jerger, P. San-José, G. Zarand, A. Shnirman, and G. Schön. *Prediction of resonant all-electric spin pumping with spin-orbit coupling*. Phys. Rev. B **82**, 041309 (2010).
- [Brouwer11a] P. W. Brouwer, M. Duckheim, A. Romito, and F. von Oppen. *Probability Distribution of Majorana End-State Energies in Disordered Wires*. Phys. Rev. Lett. **107**, 196804 (2011).
- [Brouwer11b] P. W. Brouwer, M. Duckheim, A. Romito, and F. von Oppen. *Topological superconducting phases in disordered quantum wires with strong spin-orbit coupling*. Phys. Rev. B **84**, 144526 (2011).

-
- [Brunner09] D. Brunner, B. D. Gerardot, P. A. Dalgarno, G. Wüst, K. Karrai, N. G. Stoltz, P. M. Petroff, and R. J. Warburton. *A Coherent Single-Hole Spin in a Semiconductor*. *Science* **325**, 70 (2009).
- [Budich12a] J. C. Budich, F. Dolcini, P. Recher, and B. Trauzettel. *Phonon-Induced Backscattering in Helical Edge States*. *Phys. Rev. Lett.* **108**, 086602 (2012).
- [Budich12b] J. C. Budich, D. G. Rothe, E. M. Hankiewicz, and B. Trauzettel. *All-electric qubit control in heavy hole quantum dots via non-Abelian geometric phases*. *Phys. Rev. B* **85**, 205425 (2012).
- [Budich12c] J. C. Budich, R. Thomale, G. Li, M. Laubach, and S.-C. Zhang. *Fluctuation-induced Topological Quantum Phase Transitions in Quantum Spin Hall and Quantum Anomalous Hall Insulators*. arXiv:1203.2928 (2012).
- [Budich12d] J. C. Budich and B. Trauzettel. *Local topological phase transitions in periodic condensed matter systems*. *Eur. Phys. J. B* **85**, 94 (2012).
- [Budich12e] J. C. Budich and B. Trauzettel. *Z_2 Green's function topology of Majorana wires*. arXiv:1207.1104 (2012).
- [Bulaev05] D. V. Bulaev and D. Loss. *Spin Relaxation and Decoherence of Holes in Quantum Dots*. *Phys. Rev. Lett.* **95**, 076805 (2005).
- [Bulaev08] D. V. Bulaev, B. Trauzettel, and D. Loss. *Spin-orbit interaction and anomalous spin relaxation in carbon nanotube quantum dots*. *Phys. Rev. B* **77**, 235301 (2008).
- [Cardy96] J. Cardy. *Scaling and Renormalization in Statistical Physics*. Cambridge Lecture Notes in Physics. Cambridge University Press, 1996.
- [Cartan26] E. Cartan. *Sur une classe remarquable d'espaces de Riemann*. *Bull. Soc. Math. France* **54**, 214–264 (1926).
- [Chern74] S.-S. Chern and J. Simons. *Characteristic Forms and Geometric Invariants*. *The Annals of Mathematics* **99**, pp. 48 (1974).
- [Choquet-Bruhat82] Y. Choquet-Bruhat and C. deWitt Morette. *Analysis Manifolds and Physics*. Elsevier Science, 1982.
- [Chuang91] S. L. Chuang. *Efficient band-structure calculations of strained quantum wells*. *Phys. Rev. B* **43**, 9649 (1991).
- [Chuang95] S. L. Chuang. *Physics of optoelectronic devices*. Wiley-Interscience, 1995.
- [Cook12] A. M. Cook, M. M. Vazifeh, and M. Franz. *Stability of Majorana Fermions in Proximity-Coupled Topological Insulator Nanowires*. arXiv:1206.3829 (2012).

- [Crépin12] F. Crépin, J. C. Budich, F. Dolcini, P. Recher, and B. Trauzettel. *Renormalization group approach for the scattering off a single Rashba impurity in a helical liquid*. arXiv:1205.0374 (2012).
- [Das12] A. Das, Y. Ronen, Y. Most, Y. Oreg, M. Heiblum, and H. Shtrikman. *Evidence of Majorana fermions in an Al - InAs nanowire topological superconductor*. arXiv:1205.7073 (2012).
- [de Greve11] K. de Greve, P. L. McMahon, D. Press, T. D. Ladd, D. Bisping, C. Schneider, M. Kamp, L. Worschech, S. Höfling, A. Forchel, and Y. Yamamoto. *Ultrafast coherent control and suppressed nuclear feedback of a single quantum dot hole qubit*. Nature Physics **7**, 872 (2011).
- [Demler99] E. Demler and S.-C. Zhang. *Non-Abelian Holonomy of BCS and SDW Quasiparticles*. Annals of Physics **271**, 83 (1999).
- [Deng12] M. T. Deng, C. L. Yu, G. Y. Huang, M. Larsson, P. Caroff, and H. Q. Xu. *Observation of Majorana Fermions in a Nb-InSb Nanowire-Nb Hybrid Quantum Device*. arXiv:1204.4130 (2012).
- [Dolcini05] F. Dolcini, B. Trauzettel, I. Safi, and H. Grabert. *Transport properties of single-channel quantum wires with an impurity: Influence of finite length and temperature on average current and noise*. Phys. Rev. B **71**, 165309 (2005).
- [Dowker72] J. S. Dowker. *Quantum mechanics and field theory on multiply connected and on homogeneous spaces*. Journal of Physics A: General Physics **5**, 936 (1972).
- [Eble09] B. Eble, C. Testelin, P. Desfonds, F. Bernardot, A. Balocchi, T. Amand, A. Miard, A. Lemaitre, X. Marie, and M. Chamarro. *Hole-Nuclear Spin Interaction in Quantum Dots*. Phys. Rev. Lett. **102**, 146601 (2009).
- [Essin11] A. M. Essin and V. Gurarie. *Bulk-boundary correspondence of topological insulators from their respective Green's functions*. Phys. Rev. B **84**, 125132 (2011).
- [Fidkowski10] L. Fidkowski and A. Kitaev. *Effects of interactions on the topological classification of free fermion systems*. Phys. Rev. B **81**, 134509 (2010).
- [Fischer10] J. Fischer and D. Loss. *Hybridization and Spin Decoherence in Heavy-Hole Quantum Dots*. Phys. Rev. Lett. **105**, 266603 (2010).
- [Fu06] L. Fu and C. L. Kane. *Time reversal polarization and a Z_2 adiabatic spin pump*. Phys. Rev. B **74**, 195312 (2006).
- [Fu07] L. Fu and C. L. Kane. *Topological insulators with inversion symmetry*. Phys. Rev. B **76**, 045302 (2007).

-
- [Gell-Mann51] M. Gell-Mann and F. Low. *Bound States in Quantum Field Theory*. Phys. Rev. **84**, 350 (1951).
- [Gerardot08] B. D. Gerardot, D. Brunner, P. A. Dalgarno, P. Öhberg, S. Seidl, M. Kroner, K. Karrai, N. G. Stoltz, P. M. Petroff, and R. J. Warburton. *Optical pumping of a single hole spin in a quantum dot*. Nature **451**, 441 (2008).
- [Giamarchi88] T. Giamarchi and H. J. Schulz. *Anderson localization and interactions in one-dimensional metals*. Phys. Rev. B **37**, 325 (1988).
- [Giamarchi04] T. Giamarchi. *Quantum physics in one dimension*. Oxford University Press, 2004.
- [Gmitra09] M. Gmitra, S. Konschuh, C. Ertler, C. Ambrosch-Draxl, and J. Fabian. *Band-structure topologies of graphene: Spin-orbit coupling effects from first principles*. Phys. Rev. B **80**, 235431 (2009).
- [Golovach06] V. N. Golovach, M. Borhani, and D. Loss. *Electric-dipole-induced spin resonance in quantum dots*. Phys. Rev. B **74**, 165319 (2006).
- [Golovach10] V. N. Golovach, M. Borhani, and D. Loss. *Holonomic quantum computation with electron spins in quantum dots*. Phys. Rev. A **81**, 022315 (2010).
- [Golterman93] M. F. L. Golterman, K. Jansen, and D. B. Kaplan. *Chern-Simons currents and chiral fermions on the lattice*. Physics Letters B **301**, 219 (1993).
- [Gornyi07] I. V. Gornyi, A. D. Mirlin, and D. G. Polyakov. *Electron transport in a disordered Luttinger liquid*. Phys. Rev. B **75**, 085421 (2007).
- [Grabert01] H. Grabert. *Transport in Single Channel Quantum Wires*. arXiv:cond-mat/0107175 (2001).
- [Gritsev05] V. Gritsev, G. Japaridze, M. Pletyukhov, and D. Baeriswyl. *Competing Effects of Interactions and Spin-Orbit Coupling in a Quantum Wire*. Phys. Rev. Lett. **94**, 137207 (2005).
- [Gurarie11] V. Gurarie. *Single-particle Green's functions and interacting topological insulators*. Phys. Rev. B **83**, 085426 (2011).
- [Haldane81] F. D. M. Haldane. *Effective Harmonic-Fluid Approach to Low-Energy Properties of One-Dimensional Quantum Fluids*. Phys. Rev. Lett. **47**, 1840 (1981).
- [Haldane88] F. D. M. Haldane. *Model for a Quantum Hall Effect without Landau Levels: Condensed-Matter Realization of the "Parity Anomaly"*. Phys. Rev. Lett. **61**, 2015 (1988).
- [Halperin82] B. I. Halperin. *Quantized Hall conductance, current-carrying edge states, and the existence of extended states in a two-dimensional disordered potential*. Phys. Rev. B **25**, 2185 (1982).

- [Hanson07] R. Hanson, L. P. Kouwenhoven, J. R. Petta, S. Tarucha, and L. M. K. Vandersypen. *Spins in few-electron quantum dots*. Rev. Mod. Phys. **79**, 1217 (2007).
- [Hasan10] M. Z. Hasan and C. L. Kane. *Colloquium: Topological insulators*. Rev. Mod. Phys. **82**, 3045 (2010).
- [Hou09] C.-Y. Hou, E.-A. Kim, and C. Chamon. *Corner Junction as a Probe of Helical Edge States*. Phys. Rev. Lett. **102**, 076602 (2009).
- [Kane92a] C. L. Kane and M. P. A. Fisher. *Transmission through barriers and resonant tunneling in an interacting one-dimensional electron gas*. Phys. Rev. B **46**, 15233 (1992).
- [Kane92b] C. L. Kane and M. P. A. Fisher. *Transport in a one-channeluttinger liquid*. Phys. Rev. Lett. **68**, 1220 (1992).
- [Kane05a] C. L. Kane and E. J. Mele. *Quantum Spin Hall Effect in Graphene*. Phys. Rev. Lett. **95**, 226801 (2005).
- [Kane05b] C. L. Kane and E. J. Mele. *Z_2 Topological Order and the Quantum Spin Hall Effect*. Phys. Rev. Lett. **95**, 146802 (2005).
- [Karoubi78] M. Karoubi. *K-Theory: An Introduction*. Springer, 1978.
- [Kato50] T. Kato. *On the Adiabatic Theorem of Quantum Mechanics*. Journal of the Physical Society of Japan **5**, 435 (1950).
- [Kato04] Y. K. Kato, R. C. Myers, A. C. Gossard, and D. D. Awschalom. *Current-Induced Spin Polarization in Strained Semiconductors*. Phys. Rev. Lett. **93**, 176601 (2004).
- [Keldysh65] L. V. Keldysh. *Diagram Technique for Nonequilibrium Processes*. Sov. Phys. JETP **20**, 1018 (1965).
- [Kitaev01] A. Kitaev. *Unpaired Majorana fermions in quantum wires*. Physics-Uspokhi **44**, 131 (2001).
- [Kitaev09] A. Kitaev. *Periodic table for topological insulators and superconductors*. AIP Conference Proceedings **1134**, 22 (2009).
- [Klinovaja11] J. Klinovaja, M. J. Schmidt, B. Braunecker, and D. Loss. *Carbon nanotubes in electric and magnetic fields*. Phys. Rev. B **84**, 085452 (2011).
- [Klitzing80] K. v. Klitzing, G. Dorda, and M. Pepper. *New Method for High-Accuracy Determination of the Fine-Structure Constant Based on Quantized Hall Resistance*. Phys. Rev. Lett. **45**, 494 (1980).
- [Kobayashi96] S. Kobayashi and K. Nomizu. *Foundations of Differential Geometry*. Wiley-Interscience, 1996.

- [Kohmoto85] M. Kohmoto. *Topological invariant and the quantization of the Hall conductance*. Annals of Physics **160**, 343 (1985).
- [Kohn60] W. Kohn and J. M. Luttinger. *Ground-State Energy of a Many-Fermion System*. Phys. Rev. **118**, 41 (1960).
- [König07] M. König, S. Wiedmann, C. Brüne, A. Roth, H. Buhmann, L. Molenkamp, X.-L. Qi, and S.-C. Zhang. *Quantum Spin Hall Insulator State in HgTe Quantum Wells*. Science **318**, 766 (2007).
- [König08] M. König, H. Buhmann, L. W. Molenkamp, T. Hughes, C.-X. Liu, X.-L. Qi, and S.-C. Zhang. *The Quantum Spin Hall Effect: Theory and Experiment*. Journal of the Physical Society of Japan **77**, 031007 (2008).
- [Kuehnel05] W. Kuehnel. *Differential Geometry: Curves - Surfaces - Manifolds*. American Mathematical Society, 2005.
- [Laidlaw71] M. G. G. Laidlaw and C. M. DeWitt. *Feynman Functional Integrals for Systems of Indistinguishable Particles*. Phys. Rev. D **3**, 1375 (1971).
- [Landau57] L. D. Landau. *The theory of a Fermi liquid*. Soviet Physics JETP-USSR **3**, 920 (1957).
- [Laughlin81] R. B. Laughlin. *Quantized Hall conductivity in two dimensions*. Phys. Rev. B **23**, 5632 (1981).
- [Laughlin83] R. B. Laughlin. *Anomalous Quantum Hall Effect: An Incompressible Quantum Fluid with Fractionally Charged Excitations*. Phys. Rev. Lett. **50**, 1395 (1983).
- [Leinaas77] J. Leinaas and J. Myrheim. *On the theory of identical particles*. Il Nuovo Cimento B **37**, 1 (1977).
- [Leung12] B. Leung and E. Prodan. *Effect of strong disorder in a three-dimensional topological insulator: Phase diagram and maps of the Z_2 invariant*. Phys. Rev. B **85**, 205136 (2012).
- [Levin09] M. Levin and A. Stern. *Fractional Topological Insulators*. Phys. Rev. Lett. **103**, 196803 (2009).
- [Lezmy12] N. Lezmy, Y. Oreg, and M. Berkooz. *Single and multi-particle scattering in Helical liquid with an impurity*. arXiv:1201.6197 (2012).
- [Liu08] C. Liu, T. L. Hughes, X.-L. Qi, K. Wang, and S.-C. Zhang. *Quantum Spin Hall Effect in Inverted Type-II Semiconductors*. Phys. Rev. Lett. **100**, 236601 (2008).
- [Liu11] C.-X. Liu, J. C. Budich, P. Recher, and B. Trauzettel. *Charge-spin duality in nonequilibrium transport of helical liquids*. Phys. Rev. B **83**, 035407 (2011).

- [Liu12] J. Liu, A. C. Potter, K. T. Law, and P. A. Lee. *Zero-bias peaks in spin-orbit coupled superconducting wires with and without Majorana end-states*. arXiv:1206.1276 (2012).
- [Loss98] D. Loss and D. P. DiVincenzo. *Quantum computation with quantum dots*. Phys. Rev. A **57**, 120 (1998).
- [Lutchyn10] R. M. Lutchyn, J. D. Sau, and S. Das Sarma. *Majorana Fermions and a Topological Phase Transition in Semiconductor-Superconductor Heterostructures*. Phys. Rev. Lett. **105**, 077001 (2010).
- [Luttinger60a] J. M. Luttinger. *Fermi Surface and Some Simple Equilibrium Properties of a System of Interacting Fermions*. Phys. Rev. **119**, 1153 (1960).
- [Luttinger60b] J. M. Luttinger and J. C. Ward. *Ground-State Energy of a Many-Fermion System. II*. Phys. Rev. **118**, 1417 (1960).
- [Luttinger63] J. M. Luttinger. *An Exactly Soluble Model of a Many-Fermion System*. Journal of Mathematical Physics **4**, 1154 (1963).
- [Maciejko09] J. Maciejko, C. Liu, Y. Oreg, X.-L. Qi, C. Wu, and S.-C. Zhang. *Kondo Effect in the Helical Edge Liquid of the Quantum Spin Hall State*. Phys. Rev. Lett. **102**, 256803 (2009).
- [Maciejko10] J. Maciejko, X.-L. Qi, A. Karch, and S.-C. Zhang. *Fractional Topological Insulators in Three Dimensions*. Phys. Rev. Lett. **105**, 246809 (2010).
- [Manmana12] S. R. Manmana, A. M. Essin, R. M. Noack, and V. Gurarie. *Topological invariants and interacting one-dimensional fermionic systems*. arXiv:1205.5095 (2012).
- [Martin95] T. Martin and D. Loss. *Phase Diagram for a Luttinger Liquid Coupled to Phonons in One Dimension*. International Journal of Modern Physics B **9**, 495 (1995).
- [Maslov95] D. L. Maslov and M. Stone. *Landauer conductance of Luttinger liquids with leads*. Phys. Rev. B **52**, R5539 (1995).
- [Matsubara55] T. Matsubara. *A New Approach to Quantum-Statistical Mechanics*. Progress of Theoretical Physics **14**, 351 (1955).
- [Mattis65] D. C. Mattis and E. H. Lieb. *Exact Solution of a Many-Fermion System and Its Associated Boson Field*. J. Math. Phys. **6**, 304 (1965).
- [Michetti12] P. Michetti, J. C. Budich, E. G. Novik, and P. Recher. *Tunable quantum spin Hall effect in double quantum wells*. Phys. Rev. B **85**, 125309 (2012).
- [Milnor74] J. W. Milnor and J. Stasheff. *Characteristic Classes*. Princeton University Press, 1974.

-
- [Mourik12] V. Mourik, K. Zuo, S. M. Frolov, S. R. Plissard, E. P. A. M. Bakkers, and L. P. Kouwenhoven. *Signatures of Majorana Fermions in Hybrid Superconductor-Semiconductor Nanowire Devices*. *Science* **336**, 1003 (2012).
- [Murakami04] S. Murakami, N. Nagosa, and S.-C. Zhang. *Spin-Hall Insulator*. *Phys. Rev. Lett.* **93**, 156804 (2004).
- [Nakahara03] M. Nakahara. *Geometry, Topology and Physics*. Taylor & Francis, 2003.
- [Nash91] C. Nash. *Differential Topology and Quantum Field Theory*. Academic Press, 1991.
- [Nash11] C. Nash and S. Sen. *Topology and Geometry for Physicists*. Dover Publications, 2011.
- [Neupert11] T. Neupert, L. Santos, C. Chamon, and C. Mudry. *Fractional Quantum Hall States at Zero Magnetic Field*. *Phys. Rev. Lett.* **106**, 236804 (2011).
- [Niu85] Q. Niu, D. J. Thouless, and Y.-S. Wu. *Quantized Hall conductance as a topological invariant*. *Phys. Rev. B* **31**, 3372 (1985).
- [Nowack07] K. C. Nowack, F. H. L. Koppens, Y. V. Nazarov, and L. M. K. Vandersypen. *Coherent Control of a Single Electron Spin with Electric Fields*. *Science* **318**, 1430 (2007).
- [Nozieres97] P. Nozieres. *Theory of interacting Fermi systems*. Westview Press, 1997.
- [Oreg10] Y. Oreg, G. Refael, and F. von Oppen. *Helical Liquids and Majorana Bound States in Quantum Wires*. *Phys. Rev. Lett.* **105**, 177002 (2010).
- [Ponomarenko95] V. V. Ponomarenko. *Renormalization of the one-dimensional conductance in the Luttinger-liquid model*. *Phys. Rev. B* **52**, R8666 (1995).
- [Posske12] T. Posske, C.-X. Liu, J. C. Budich, and B. Trauzettel. *Exact results for the Kondo screening cloud of two helical liquids*. arXiv:1207.7081 (2012).
- [Prodan11] E. Prodan. *Manifestly gauge-independent formulations of the Z_2 invariants*. *Phys. Rev. B* **83**, 235115 (2011).
- [Qi06] X.-L. Qi, Y.-S. Wu, and S.-C. Zhang. *Topological quantization of the spin Hall effect in two-dimensional paramagnetic semiconductors*. *Phys. Rev. B* **74**, 085308 (2006).
- [Qi08a] X.-L. Qi, T. L. Hughes, and S.-C. Zhang. *Topological field theory of time-reversal invariant insulators*. *Phys. Rev. B* **78**, 195424 (2008).
- [Qi08b] X.-L. Qi and S.-C. Zhang. *Spin-Charge Separation in the Quantum Spin Hall State*. *Phys. Rev. Lett.* **101**, 086802 (2008).

- [Qi11] X.-L. Qi and S.-C. Zhang. *Topological insulators and superconductors*. Rev. Mod. Phys. **83**, 1057 (2011).
- [Rammer86] J. Rammer and H. Smith. *Quantum field-theoretical methods in transport theory of metals*. Rev. Mod. Phys. **58**, 323 (1986).
- [Rammer07] J. Rammer. *Quantum field theory of non-equilibrium states*. Cambridge Univ Pr, 2007.
- [Redlich84] A. N. Redlich. *Parity violation and gauge noninvariance of the effective gauge field action in three dimensions*. Phys. Rev. D **29**, 2366 (1984).
- [Roth09] A. Roth, C. Brüne, H. Buhmann, L. W. Molenkamp, J. Maciejko, X.-L. Qi, and S.-C. Zhang. *Nonlocal Transport in the Quantum Spin Hall State*. Science **325**, 294 (2009).
- [Rothe10] D. G. Rothe, R. W. Reintaler, C.-X. Liu, L. W. Molenkamp, S.-C. Zhang, and E. M. Hankiewicz. *Fingerprint of different spin-orbit terms for spin transport in HgTe quantum wells*. New Journal of Physics **12**, 065012 (2010).
- [Ryu02] S. Ryu and Y. Hatsugai. *Topological Origin of Zero-Energy Edge States in Particle-Hole Symmetric Systems*. Phys. Rev. Lett. **89**, 077002 (2002).
- [Ryu10] S. Ryu, A. P. Schnyder, A. Furusaki, and A. W. W. Ludwig. *Topological insulators and superconductors: tenfold way and dimensional hierarchy*. New Journal of Physics **12**, 065010 (2010).
- [Safi95] I. Safi and H. J. Schulz. *Transport in an inhomogeneous interacting one-dimensional system*. Phys. Rev. B **52**, R17040 (1995).
- [San-Jose08] P. San-Jose, B. Scharfenberger, G. Schön, A. Shnirman, and G. Zarand. *Geometric phases in semiconductor spin qubits: Manipulations and decoherence*. Phys. Rev. B **77**, 045305 (2008).
- [Sato96] H. Sato. *Algebraic Topology: An Intuitive Approach*. American Mathematical Society, 1996.
- [Schmidt11] T. L. Schmidt. *Current Correlations in Quantum Spin Hall Insulators*. Phys. Rev. Lett. **107**, 096602 (2011).
- [Schmidt12] T. L. Schmidt, S. Rachel, F. von Oppen, and L. I. Glazman. *Inelastic Electron Backscattering in a Generic Helical Edge Channel*. Phys. Rev. Lett. **108**, 156402 (2012).
- [Schnyder08] A. P. Schnyder, S. Ryu, A. Furusaki, and A. W. W. Ludwig. *Classification of topological insulators and superconductors in three spatial dimensions*. Phys. Rev. B **78**, 195125 (2008).

-
- [Schnyder09] A. P. Schnyder, S. Ryu, A. Furusaki, and A. W. W. Ludwig. *Classification of Topological Insulators and Superconductors*. AIP Conference Proceedings **1134**, 10 (2009).
- [Schönhammer97] K. Schönhammer. *Interacting fermions in one dimension: The Tomonaga-Luttinger model*. eprint arXiv:cond-mat/9710330 (1997).
- [Schwinger61] J. Schwinger. *Brownian motion of a quantum oscillator*. J. Math. Phys. **2**, 407 (1961).
- [Shankar94] R. Shankar. *Renormalization-group approach to interacting fermions*. Rev. Mod. Phys. **66**, 129 (1994).
- [Simon83] B. Simon. *Holonomy, the Quantum Adiabatic Theorem, and Berry's Phase*. Phys. Rev. Lett. **51**, 2167 (1983).
- [Solinas03] P. Solinas, P. Zanardi, N. Zanghì, and F. Rossi. *Semiconductor-based geometrical quantum gates*. Phys. Rev. B **67**, 121307 (2003).
- [Stormer83] H. L. Stormer, A. Chang, D. C. Tsui, J. C. M. Hwang, A. C. Gossard, and W. Wiegmann. *Fractional Quantization of the Hall Effect*. Phys. Rev. Lett. **50**, 1953 (1983).
- [Ström09] A. Ström and H. Johannesson. *Tunneling between Edge States in a Quantum Spin Hall System*. Phys. Rev. Lett. **102**, 096806 (2009).
- [Ström10] A. Ström, H. Johannesson, and G. I. Japaridze. *Edge Dynamics in a Quantum Spin Hall State: Effects from Rashba Spin-Orbit Interaction*. Phys. Rev. Lett. **104**, 256804 (2010).
- [Sugimoto12] N. Sugimoto and N. Nagaosa. *Spin-Orbit Echo*. Science **336**, 1413 (2012).
- [Sun11] K. Sun, Z. Gu, H. Katsura, and S. Das Sarma. *Nearly Flatbands with Nontrivial Topology*. Phys. Rev. Lett. **106**, 236803 (2011).
- [Swingle11] B. Swingle, M. Barkeshli, J. McGreevy, and T. Senthil. *Correlated topological insulators and the fractional magnetoelectric effect*. Phys. Rev. B **83**, 195139 (2011).
- [Tanaka09] Y. Tanaka and N. Nagaosa. *Two Interacting Helical Edge Modes in Quantum Spin Hall Systems*. Phys. Rev. Lett. **103**, 166403 (2009).
- [Tang11] E. Tang, J.-W. Mei, and X.-G. Wen. *High-Temperature Fractional Quantum Hall States*. Phys. Rev. Lett. **106**, 236802 (2011).
- [Teo09] J. C. Y. Teo and C. L. Kane. *Critical behavior of a point contact in a quantum spin Hall insulator*. Phys. Rev. B **79**, 235321 (2009).
- [Tewari11] S. Tewari and J. D. Sau. *Topological invariants for spin-orbit coupled superconductor nanowires*. arXiv:1111.6592 (2011).

- [Thouless82] D. J. Thouless, M. Kohmoto, M. P. Nightingale, and M. den Nijs. *Quantized Hall Conductance in a Two-Dimensional Periodic Potential*. Phys. Rev. Lett. **49**, 405 (1982).
- [Tomonaga50] S.-I. Tomonaga. *Remarks on Bloch's Method of Sound Waves applied to Many-Fermion Problems*. Progress of Theoretical Physics **5**, 544 (1950).
- [Voit95] J. Voit. *One-dimensional Fermi liquids*. Reports on Progress in Physics **58**, 977 (1995).
- [Volovik88] G. Volovik. *Analog of quantum Hall effect in superfluid ^3He film*. JETP **67(9)**, 1804 (1988).
- [Volovik03] G. E. Volovik. *The Universe in a Helium Droplet*. Clarendon Press, 2003.
- [von Delft98] J. von Delft and H. Schoeller. *Bosonization for beginners - refermionization for experts*. Annalen der Physik **7**, 225 (1998).
- [Wang10] Z. Wang, X.-L. Qi, and S.-C. Zhang. *Topological Order Parameters for Interacting Topological Insulators*. Phys. Rev. Lett. **105**, 256803 (2010).
- [Wang11a] L. Wang, X. Dai, and X. C. Xie. *Frequency domain winding number and interaction effect on topological insulators*. Phys. Rev. B **84**, 205116 (2011).
- [Wang11b] L. Wang, H. Jiang, X. Dai, and X. C. Xie. *Pole expansion of self-energy and interaction effect on topological insulators*. arXiv:1109.6292 (2011).
- [Wang12a] Z. Wang, X.-L. Qi, and S.-C. Zhang. *Topological invariants for interacting topological insulators with inversion symmetry*. Phys. Rev. B **85**, 165126 (2012).
- [Wang12b] Z. Wang and B. Yan. *Topological Hamiltonian as an Exact Tool for Topological Invariants*. arXiv:1207.7341 (2012).
- [Wang12c] Z. Wang and S.-C. Zhang. *Correlated topological superconductors and topological phase transitions via Green's function*. arXiv:1204.3149 (2012).
- [Wang12d] Z. Wang and S.-C. Zhang. *Simplified Topological Invariants for Interacting Insulators*. Phys. Rev. X **2**, 031008 (2012).
- [Wen90] X.-G. Wen. *Topological Orders in Rigid States*. Int. J. Mod. Phys. B **4**, 239 (1990).
- [Wilczek84] F. Wilczek and A. Zee. *Appearance of Gauge Structure in Simple Dynamical Systems*. Phys. Rev. Lett. **52**, 2111 (1984).
- [Witten83] E. Witten. *Global aspects of current algebra*. Nuclear Physics B **223**, 422 (1983).

- [Wu06] C. Wu, B. A. Bernevig, and S.-C. Zhang. *Helical Liquid and the Edge of Quantum Spin Hall Systems*. Phys. Rev. Lett. **96**, 106401 (2006).
- [Xu06] C. Xu and J. E. Moore. *Stability of the quantum spin Hall effect: Effects of interactions, disorder, and Z_2 topology*. Phys. Rev. B **73**, 045322 (2006).
- [Zak89] J. Zak. *Berry's phase for energy bands in solids*. Phys. Rev. Lett. **62**, 2747 (1989).
- [Zanardi99] P. Zanardi and M. Rasetti. *Holonomic quantum computation*. Physics Letters A **264**, 94 (1999).
- [Zee88] A. Zee. *Non-Abelian gauge structure in nuclear quadrupole resonance*. Phys. Rev. A **38**, 1 (1988).
- [Zee95] A. Zee. *Quantum Hall Fluids*. Lecture Notes in Physics **456**, 99 (1995).
- [Zhang01] S.-C. Zhang and J. Hu. *A Four-Dimensional Generalization of the Quantum Hall Effect*. Science **294**, 823 (2001).
- [Zhou08] B. Zhou, H.-Z. Lu, R.-L. Chu, S.-Q. Shen, and Q. Niu. *Finite Size Effects on Helical Edge States in a Quantum Spin-Hall System*. Phys. Rev. Lett. **101**, 246807 (2008).

Acknowledgments

Primary acknowledgments are due to my supervisor Björn Trauzettel from whose peerless professional expertise in general and outstanding physical intuition in particular I could profit a lot during my PhD studies. He enormously stimulated both my scientific and personal development in recent years. With his casual and consultive leadership and inspiring creativity he enabled me to develop my own scientific research interests on the one hand and gave decisive physical input as well as key incentives for fruitful projects on the other hand.

Furthermore, I would like to thank my closest collaborator Patrik Recher for numerous fruitful discussions. From his friendly policy of open doors and tireless willingness to discuss and explain interesting physics, I could benefit significantly. I would also like to acknowledge helpful and interesting discussions with all members of the TP4 group at Würzburg University and with numerous guests and visitors. In particular, I would like to thank François Crépin, Fabrizio Dolcini, Ciao-Xing Liu, Paolo Michetti, Thore Posske, Dietrich Rothe, Joerg Schelter, Pauli Virtanen, and Stefan Walter for countless physical discussions. Generally speaking, the friendly and cooperative atmosphere in the TP4 group provided a perfect environment for both enjoyable and fruitful studies. Cordial acknowledgments are also due to our secretary Nelly Meyer for her absolute helpfulness and for keeping all bureaucratic matters running smoothly which is a highly nontrivial task at a German university.

I am also gratefully indebted to Shou-Cheng Zhang for hosting me during my stay at Stanford University during the winter term 2012 and for explaining so much interesting physics to me. During my stay at Stanford, I could also profit a lot from the scientific expertise of the condensed matter theory group at Stanford, in particular I would like to thank Martin Claassen and Ronny Thomale in this context.

Finally, I would like to thank my girlfriend Mihaela Varnica, my parents Birgit and Wulf Budich, my sister Harriet Budich, and my friends as well as other family members for their unlimited patience and permanent encouragement which, as I am convinced, were crucial contributions to my motivation during my work on this thesis.

List of publications

1. Thore Posske, Chao-Xing Liu, Jan Carl Budich, and Björn Trauzettel.
Exact results for the Kondo screening cloud of two helical liquids.
arXiv:1207.7081 (2012), under review at PRL.
2. Jan Carl Budich and Björn Trauzettel.
 \mathbb{Z}_2 Green's function topology of Majorana wires.
arXiv:1207.1104 (2012), under review at PRL.
3. Tobias Wech, Daniel Stäb, Jan Carl Budich, André Fischer, Johannes Tran-Gia, Dietbert Hahn, and Herbert Köstler.
Resolution evaluation of MR images reconstructed by iterative thresholding algorithms for compressed sensing.
Med. Phys. **39**, 4328 (2012).
4. François Crépin, Jan Carl Budich, Fabrizio Dolcini, Patrik Recher, and Björn Trauzettel.
Renormalization group approach for the scattering off a single Rashba impurity in a helical liquid.
arXiv:1205.0374 (2012), accepted for publication in PRB:RC.
5. Jan Carl Budich, Ronny Thomale, Gang Li, Manuel Laubach, Shou-Cheng Zhang.
Fluctuation-induced Topological Quantum Phase Transitions in Quantum Spin Hall and Quantum Anomalous Hall Insulators.
arXiv:1203.2928 (2012), under review at PRL.
6. Jan Carl Budich, Dietrich Gernot Rothe, Ewelina M. Hankiewicz, and Björn Trauzettel.
All-electric qubit control in heavy hole quantum dots via non-Abelian geometric phases.
Phys. Rev. B **85**, 205425 (2012).
7. Jan Carl Budich, Stefan Walter, and Björn Trauzettel.
Failure of protection of Majorana based qubits against decoherence.
Phys. Rev. B **85**, 121405(R) (2012).

8. Jan Carl Budich, Fabrizio Dolcini, Patrik Recher, and Björn Trauzettel.
Phonon-induced Backscattering in Helical Edge States.
Phys. Rev. Lett. **108**, 086602 (2012).
9. Paolo Michetti, Jan Carl Budich, Elena G. Novik, and Patrik Recher.
Tunable quantum spin Hall effect in double quantum wells.
Phys. Rev. B **85**, 125309 (2012).
10. Jan Carl Budich and Björn Trauzettel.
Local topological phase transitions in periodic condensed matter systems.
Eur. Phys. J. B **85**(3), 94 (2012).
11. Chao-Xing Liu, Jan Carl Budich, Patrik Recher, and Björn Trauzettel.
Charge-spin duality in nonequilibrium transport of helical liquids.
Phys. Rev. B **83**, 035407 (2011).
12. Jan Carl Budich and Björn Trauzettel.
Entanglement transfer from electrons to photons in quantum dots: an open quantum system approach.
Nanotechnology **21**, 274001 (2012).

Curriculum Vitae

Persönliche Angaben:

Name: Jan Carl Budich
Geburtsdatum: 10. November 1985
Geburtsort: Marktheidenfeld
Staatsangehörigkeit: deutsch
Familienstand: ledig

Schulbildung:

09/1995–06/2004: Balthasar Neumann Gymnasium Marktheidenfeld
Abschluss: Abitur

Universitätsbildung:

10/2004–09/2000: Studium der Physik,
Julius-Maximilians-Universität Würzburg
Abschluss: Diplom („mit Auszeichnung“)

seit 10/2009: Doktorand an der Universität Würzburg
unter Leitung von Prof. Dr. Björn Trauzettel

Würzburg, den

.....

(Jan Budich)

Erklärung

Die vorliegende Dissertation wurde am Lehrstuhl für Theoretische Physik IV am Institut für Theoretische Physik und Astrophysik der Fakultät für Physik und Astronomie an der Bayerischen Julius-Maximilians-Universität Würzburg angefertigt unter Betreuung von Prof. Dr. Björn Trauzettel. Hiermit versichere ich, Jan Carl Budich, geboren am 10. November 1985 in Marktheidenfeld, an Eides statt, dass ich die vorliegende Dissertation eigenständig, d. h. insbesondere selbstständig und ohne Hilfe eines kommerziellen Promotionsberaters angefertigt und keine anderen als die angegebenen Quellen und Hilfsmittel benutzt habe. Ich erkläre außerdem, dass die vorliegende Dissertation weder in gleicher noch in anderer Form in einem anderen Prüfungsfach vorgelegen hat, und dass ich außer den mit dem Zulassungsgesuch urkundlich vorgelegten Graden keine weiteren akademischen Grade erworben oder zu erwerben versucht habe.

Würzburg, den

.....

(Jan Budich)